FLOCCULATION STUDIES ON MODEL COLLOIDS USING CHITOSAN

MATTHEW HOWARD ASHMORE

A thesis submitted in partial fulfilment of the requirements of the
The Nottingham Trent University for the degree of Doctor of Philosophy.

September 2000

Abstract

Chitosan, a biodegradable and renewable resource commodity, is a naturally occurring copolymer of poly[β(1→ 4)-2-acetamido-2-deoxy-D-glucopyranose] and poly[β(1→4)-2-amino-2-deoxy-D-glucopyranose], which becomes soluble and positively charged in acidic media and therefore may be used to flocculate anionic dispersions. A series of well-characterised chitosan samples spanning a wide range of molecular weights, having been homogeneously acetylated to produce varying degrees of linear charge density, were used to flocculate "model colloid" polymer latices. Latices were selected to cover a wide range of charge densities and were sized between 85nm and 2.1μm.The optimum flocculation concentrations were identified using both residual turbidity and initial rate methods together with electrophoretic mobility measurements. A charge neutralisation mechanism with an enhancement of rate in comparison to the rate of rapid coagulation indicative of a "charge patch" effect was confirmed, except in the case of the 2.1μm particles. The optimum flocculation concentration of the latter fell below that of rapid coagulation, an effect ascribed to the influence of adsorbed chitosan upon the drainage between particles on close approach. Both molecular weight and degree of acetylation of the chitosans had a small effect upon the optimum flocculation concentration, with efficiency increasing with increase in both molecular weight and linear charge density. Increasing the ionic strength of the dispersion medium broadened the flocculation concentration range and diminished the enhancement of rate produced by the charge patch mechanism. The effects of changing the pH of the dispersion medium were also investigated and it was determined that optimum flocculation dose was increased considerably between pH 3 to pH 7, broadly in line with predictions from pKa calculations. With doses of chitosans in excess of the optimum for flocculation, charge reversal occurred and the cationic latices were rather more stable to electrolyte addition than their anionic precursors and were shown to be electrostatically rather than sterically stabilised.

Acknowledgements

I would like to thank my supervisors, Dr John Hearn for his help, guidance and patience throughout this project and Professor George Roberts for providing his expert knowledge of chitosan chemistry. I am also indebted to the technical staff of the department, especially Mr Arthur Richards and Dr Fran Karpowicz, for their help throughout.

Contents

Chapter 1 Introduction

1.1 Chitosan

1.1.1 Origin

Chitin, which is considered ideally to be poly[β(1→ 4)-2-acetamido-2-deoxy-D-glucopyranose][(1)], is found in abundance in nature in the exoskeletons of insects and crustacean as well as in the cell walls of a few species of fungi. As such chitin constitutes the second most abundant naturally occurring polysaccharide after cellulose. Chitin's idealised structure is shown in Figure(1.1.1b) and it may be observed that the structure is very similar to that of cellulose (Figure(1.1.1a)) with an acetamido group replacing the hydroxyl group at the C-2 position. Chitin is insoluble in most common solvents[(2)] which limits its applications. Chitin's main derivative is chitosan, which is ideally considered to be poly[β(1→4)-2-amino-2-deoxy-D-glucopyranose, shown in figure(1.1.1c). Chitosan is also found naturally but to a much lesser extent. Chitosan's main industrial source is via the alkaline deacetylation of chitin.

In contrast to chitin, chitosan is soluble in dilute solutions of mineral acids as well as a number of organic acids[(3)]. Under such conditions the amine groups present at the chitosan C-2 position become protonated rendering the chain a positively charged polyelectrolyte. Under such conditions therefore, chitosan may be useful in the role of flocculant with none of the problems with biodegradability and presence of toxic monomer associated with synthetic flocculants and with a potentially huge supply of raw material from the seafood processing industries.

(a) Cellulose

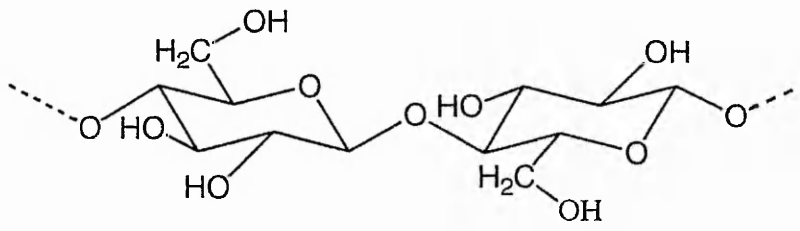

(b) Chitin

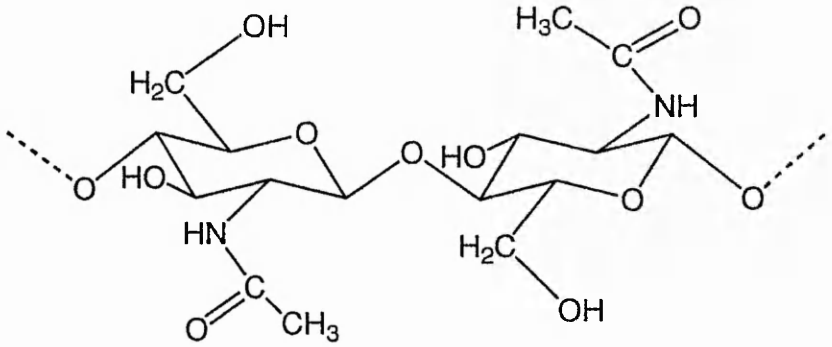

(c) Chitosan

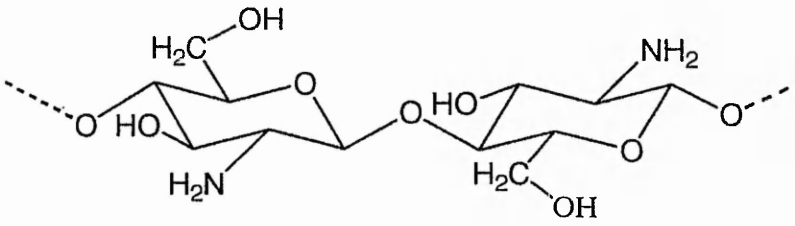

Figure 1.1.1 Idealised structures of Cellulose (a) , Chitin (b) and Chitosan (c)

1.1.2 Nomenclature

Although the terms 'chitin' and 'chitosan' are used extensively in the literature, neither represents a unique chemical structure. In nature chitin does not normally exist as a discrete substance, usually being found complexed with proteins, amongst other agents, in insect and crustacean exoskeletons whilst fungal chitin tends to be complexed with other polysaccharides[4]. Pure, naturally occurring chitin has thus-far only been found in the extra-cellular spines of several diatoms[5]. Thus the pure polymer poly[b-(1-4)-2-acetamido-2-deoxy-D-glucopyranose] is usually only obtained after extensive purification and the need to distinguish between the purified and naturally occurring chitin is apparent. The terms 'Native chitin'[6] and 'chitin-protein complex'[7] have been suggested for the latter to differentiate between the two.

Even given that the term 'chitin' may be used to describe purified native chitin, this in itself does not mean that the discrete chemical entity is poly[β(1→ 4)-2-acetamido-2-deoxy-D-glucopyranose]. The chitin chain will always include some proportion of poly[β(1→4)-2-amino-2-deoxy-D-glucopyranose], 'chitosan' units. Whether this is an artefact of the purification process or a characteristic of the native chitin is uncertain. Conversely, upon deacetylation of chitin to give 'chitosan', complete deacetylation is extremely difficult and so some proportion of chitin is usually present. Therefore it must be recognised that in this context, chitin and chitosan are only idealised structures and in reality particular polysaccharide chains consist of a random co-polymer of these two idealised units. In general, a particular sample is designated arbitrarily as either chitin or chitosan according to its solubility in dilute acid[8], with the latter being soluble.

Many of the desirable properties of chitin and chitosan appear to be dependent upon the relative proportions of the two residues within the polymer chains. In order to characterise a particular fraction of chitin or chitosan, the relative abundance of each ideal unit must be determined and stated in an unambiguous way. To date there is no universally accepted nomenclature for chitin/chitosan. One frequently used method is to quote a fraction as chitin or chitosan, according to solubility in dilute acid, followed by a statement of the mole fraction of acetamido or amino groups at the C-2 position. This method has a wide range of interpretations and generally changes with the researcher. One system suggested by Roberts[9] would be to refer to any sample simply as chitin, followed by a statement of the mole fraction of *N*-acetyl-D-glucosamine units. For example, a sample of pure chitin would be *chitin[1.0],* pure chitosan would be *chitin[0.0]* and a sample of chitin with 50% degree of deacetylation would be *chitin[0.5].* However, as he points out, there are problems with this approach. Firstly, the term chitosan is already in common usage and secondly there are a number of chitinolytic enzymes whose action decreases with decrease in the mole fraction of *N*-acetyl-D-glucosamine units, leading to the potentially confusing situation that such enzymes would have no effect on chitin[0.0] (pure chitosan). Finally there is the large volume of published work using largely uncharacterised fractions, which simply refer to the substrate as 'chitin' or 'chitosan' according to its solubility in dilute acid. Thus it was suggested that the term chitin or chitosan be used according to the sample's solubility in dilute organic acid, followed by the mole fraction of *N*-acetyl-D-glucosamine units stated as above. In the present work, it was decided that the following conventions should be followed. All samples were termed *chitosan* as they were necessarily all soluble in dilute organic acid (aqueous acetic acid exclusively in the study), followed by an indication

of the mole fractionof *N*-acetyl-D-glucosamine residues stated as a mole fraction, 'F_A' (often termed the 'degree of acetylation'). So a sample which contains 90% D-glucosamine units and 10% *N*-acetyl-D-glucosamine units would be designated "F_A[0.10]".

1.1.3 Purification of chitin[10]

1.1.3.1 Introduction

The main commercial sources of chitin at present are the exoskeletons of crustacean, mainly crab and shrimp. In these exoskeletons, the chitin is closely associated with other materials such as inorganic materials (chiefly) $CaCO_3$, proteins, pigments and lipids. There are no standard methods for the extraction of chitin from these materials and many strategies have been adopted. Demineralisation is generally achieved by treatment with HCl and NaOH is used to remove associated protein, though different workers have employed other agents and different orders of treatment. In part, the intended use of the chitin has a bearing on the purification methods employed. For example, some deproteinisation methods may result in partial deacetylation of the chitin, hence if chitin is the ultimate product then these methods are inappropriate, whereas if chitosan is the desired product then partial deacetylation is not a problem. Demineralisation may result in hydrolysis of the polymer chain leading to a reduction in molecular weight.

1.1.3.2 Deproteinisation

By far the most popular method of removing protein from chitin is the use of NaOH, generally approximately 1M and at an elevated temperature. The reaction time has varied enormously in these methods, anywhere between 30 minutes and several days being used. Table 1.1.1 lists some of these studies. Other agents suggested for this step[11, 12] include Na_2CO_3, $NaHCO_3$, KOH, K_2CO_3, $Ca(OH)_2$ and Na_2S.

Deproteinisation of chitin by enzymes has also been studied. In the earliest cases, 'purification bacteria' were employed[11, 12], though Giles *et al*[13] were the first to report the specific use of enzymes for the purification of chitin. This study concentrated on

Material source	NaOH concentration	T /°C	Number of treatments	Total treatment time / h	Reference
Shrimp	0.25M	65	1	1	Wu and Bough[14]
Crab	0.5M	65	1	2	Muzzarelli et al[15]
Crab	1.0M	80	1	3	Mima et al[16]
Crab	1.0M	100	1	36	Shimahara et al[17]
Lobster	1.0M	100	5	60	Hackman[18]
Crab	1.0M	100	3	72	Hackman and Goldberg[19]
Lobster	1.25M	80 - 85	2	1	Blumberg et al[20]
Crab	1.25M	85 - 90	3	1.5 – 2.5	Broussignac[21]
Crab	1.25M	100	1	24	Kuruppaswarmy[22]
Crab	2.5M	Room Temp.	3	72	Whistler and BeMiller[23]

Table 1.1.1 Conditions adopted for the removal of protein from chitin by various workers.

the use of pepsin for deproteinisation and concluded that it offered no advantages over the use of shorter chemical treatments. Broussignac[21] however suggested the use of pepsin or trypsin for deproteinisation if minimal deacetylation of the chitin was required, though no experimental details were offered. Workers have continued to investigate the use of enzymes[24] and bacteria[17] for this purpose but to date none offers complete deproteinisation, even after several hundred hours treatment, and residual protein levels of up to 7% must be removed by more conventional methods.

1.1.3.3 Demineralisation

Generally HCl has been used for demineralisation in the vast majority of studies. Several other acids have been suggested[11, 12] for the purpose including HNO_3, H_2SO_4, CH_3COOH and HCOOH, however to date HNO_3[25] and HCOOH[26] are the only other acids to be used experimentally. The temperature of reaction is usually room temperature in order to minimise chain hydrolysis, though temperatures between 0°C and 100°C have been employed[11, 12]. HCl concentrations have varied from 0.275M[11, 12] to 2M[17,18] and reaction times have varied from several hours[27, 28] to 48 hours[17,18], though these factors have not varied in proportion.

EDTA has also been employed[24, 29, 30] as a non-degradative demineralisation agent for chitin, generally at pH values of 9 or 10.

1.1.4 Deacetylation of chitin

1.1.4.1 Introduction

Formation of chitosan via deacetylation is one of the main uses of chitin. The complete deacetylation of chitin is difficult and generally unnecessary since the material becomes soluble in dilute aqueous acids at a deacetylation of approximately 60% (~F_A[0.4]).

In principle, acid or base hydrolysis may be used to hydrolyse amides but in the case of chitin, acid hydrolysis would also bring about the hydrolysis of the glycosidic links in the chain and hence chain degradation. Horton and Lineback[31] pointed out that the *trans* arrangement of the C(2)-C(3) substituents in chitin increases the resistance of the C(2)-acetamido group to alkaline hydrolysis, hence severe treatments are required to bring about deacetylation in this way. To some extent chain hydrolysis also accompanies alkaline deacetylation and so care must be taken to minimise this effect.

1.1.4.2 Deacetylation by alkali fusion

Deacetylation by fusion with KOH at 180°C has been tried by a number of workers[26, 31 - 37]. Degrees of deacetylation of up to 95% (F_A[0.05]) have been reported [31] but at the cost of a substantial reduction in molecular weight as the final product had a degree of polymerization (DP) of only around 20. An additional purification step involving repeated dissolution of the chitosan in dilute HCl at 50°C may mean that acid hydrolysis was partially responsible for the reduction in DP.

1.1.4.3 Deacetylation with aqueous alkali

This is the usual method of deacetylation, but as yet no standard conditions exist for the process. Generally NaOH and KOH are used, but the use of LiOH, $Ca(OH)_2$ and Na_3PO_4 have also been stated in the literature[11, 12].

Despite a large volume of work in this area, the main conclusions of the first two studies of the alkaline deacetylation of chitin[11, 12] still hold. The main variables stated are alkali concentration, temperature, reaction time, particle size and density. It was found that in order to produce an acid soluble product (chitosan), increasing the alkali concentration decreased the reaction time and temperature required. Furthermore, with an extension of reaction time, F_A tended towards [0.0], this was however at the cost of a considerable decrease in solution viscosity, indicating possible chain degradation and hence reduction in molecular weight.

1.1.4.4 Fully deacetylated chitosan

Generally, alkaline deacetylation of chitin proceeds effectively until the product has an F_A of between [0.35] and [0.25], further treatment has little effect on the F_A whilst the continuing alkaline hydrolysis of the chains leads to further reduction in molecular weight. Mima *et al.*[16] prepared chitosan F_A[0.0] by repeated alkaline deacetylation treatments, interspersed with washing and drying. Domard and Rinaudo[38] employed a repeated alkaline deacetylation, washing and drying regime to produce fully deacetylated chitosan. The deacetylation process was carried out under a nitrogen atmosphere and with the addition of thiophenol to remove oxygen in an attempt to reduce chain hydrolysis. The thiophenol was also claimed to have a catalytic effect in the deacetylation process.

1.1.5 Structure and morphology of chitin and chitosan

1.1.5.1 Structure and morphology of chitin

Of the two polymers, chitin's structure and morphology has been studied most extensively. It has been found that there are two basic polymorphological forms of chitin, termed α-chitin and β-chitin, plus a possible third form termed γ chitin. In each of these three forms, the chitin is formed in sheets and the chains making up any sheet have the same direction.

The most stable form is α-chitin. In α-chitin, the chains in adjacent sheets along the c-axis have an anti-parallel arrangement (↑ ↓). This allows intermolecular hydrogen bonding along the a-axis and c-axis[39, 40], whilst intra-molecular hydrogen bonding occurs along the b-axis (figure 1.1.2). This results in a rigid crystal structure, and thus α-chitin

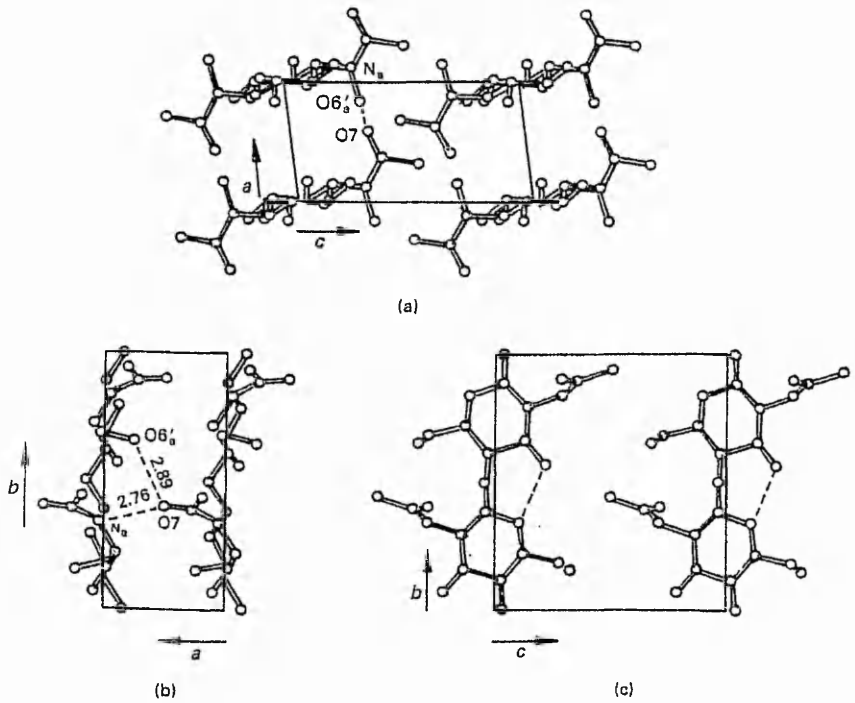

Figure 1.1.2 Crystal structure of anhydrous β-chitin proposed by Blackwell *et al*[40, 44] showing various inter- and intra- chain bonds.

tends to occur where extreme hardness is required. This hydrogen bonding also renders α-chitin non-fusible and severely limits its solubility in many common solvents. Table 1.1.2, below, reproduces the unit cell dimensions determined from several X-ray crystallography studies of α-chitin.

a	b	c	reference
4.76	10.28	18.85	Carlsrom[41]
4.69	10.43	19.13	Dweltz[42]
4.74	10.32	18.86	Minke and Blackwell[39]

Table 1.1.2 Unit cell dimensions (Å) for α-chitin

In contrast, β-chitin has a parallel chain arrangement (↑ ↑) in adjacent sheets which means that intermolecular hydrogen bonding does not occur between sheets. This ensures that the crystal structure is not as tight as α-chitin, and consequently β-chitin tends to occur in nature where a greater flexibility is required. The lack of hydrogen bonding also effects the physical properties of β-chitin so, while it is still not fusible and largely insoluble, it is able to swell in water and it is soluble in 99% formic acid[43, 44]. It has also been reported that β-chitin may be converted to α-chitin upon precipitation from formic acid solution[45] or on treatment with cold 6M HCl[45, 46].

In addition, a third chitin morphology, γ-chitin has been proposed[45] in which two parallel sheets occur for every anti-parallel sheet along the c-axis (↑ ↑ ↓). This is the least stable morphology and is easily converted to α-chitin. Little work has been carried out on γ-chitin and it has been suggested[47] that it may simply be a distorted version of α-chitin or β-chitin rather than a distinct polymorphological form.

1.1.5.2 Structure and morphology of chitosan

The structure and morphology of chitosan is more ambiguous than chitin, and it is only relatively recently, as chitosan's potential uses have multiplied, that such information has been considered useful. The study of chitosan is complicated as there seem to be several different crystalline structures and morphologies. To some extent, this variation

a	b	c	b	crystal type	reference
8.9	10.25	17.0	90°	Orthorhombic	Clark and Smith[25]
4.4	10.30	10.0	90°	Orthorhombic	Samuels[48]
4.46	10.30	8.63	96.3°	Monoclinic	Sakurai *et al*[49]
5.82	10.30	8.37	99.2°	Monoclinic	
8.63	10.30	8.92	96.3°	Monoclinic	Sakurai *et al*[50]
8.37	10.30	11.64	99.2°	Monoclinic	
8.67	10.24	8.96	92.6°	Monoclinic	
8.24	10.39	16.48	90°	Orthorhombic	Ogawa *et al*[51]
8.07	10.34	8.44	90°	Orthorhombic	Cartier *et al*[52]

Table 1.1.3 Unit cell dimensions (Å) for chitosan

may be an artefact of the method of chitosan sample preparation. For example, discrepancies may arise due to F_A and its distribution on the chains and therefore method of deacetylation / re-acetylation, mean molecular weight and its distribution and the method of recovering chitosan from solution, e.g. solvent evaporation, coagulation by alkaline solution, etc. Table 1.1.3 lists the findings of some of these studies.

1.1.6 Dilute solution properties of chitin and chitosan

1.1.6.1 Chitin solvents and solutions

Due to extensive inter- and intra- molecular hydrogen bonding engendering a rigid crystal structure, chitin is found to be insoluble in most common solvents. The best solvents, considered to dissolve chitin without degradation, are N-methylpyrrolidone (MPL)/LiCl and N,N'-dimethyl acetamide (DMAC)/ LiCl, even then, several days stirring at room-temperature are required for dissolution and solubility is inversely proportional to F_A[53]. To date, the latter system has been the solvent of choice in several studies concerning homogeneous synthesis of derivatives, molecular weight determination and preparation of fibres[54].

Both α- and β- chitin have been reported soluble in some hot, concentrated solutions of neutral salts, such as LiCNS, $Ca(CNS)_2$ and calcium halides[55], while Hackman and Goldberg[19] carried out light scattering experiments on a solution of α-chitin in an aqueous, saturated LiCNS solution at room temperature, after dissolving the chitin at 95°C although other workers have found little success with the system[56]. Shirai *et al*[57] suggested that a saturated, methanolic solution of $CaCl_2.2H_2O$ is an excellent solvent for chitin at room temperature, though the usefulness of this system has been questioned by Vincendon and Domard[58].

Chitin is soluble in some concentrated mineral acids such as HCl, H_2SO_4 and H_3PO_4, but not without extensive degradation. Several organic carboxylic acids have been used to dissolve chitin, notably formic, dichloroacetic and trichloroacetic acid. Formic acid has been used to dissolve both α- and β- chitin, though dissolving α–chitin requires at least a 98wt-% solution of the acid, whereas β–chitin requires an 88-90wt-% solution.

Dissolution can take up to three weeks[59]. Dissolution is accompanied by chain degradation[56] and esterification[60], the final solute being O-formylchitin rather than chitin itself. The use of di- and trichloroacetic acid was initially studied by Austin[61]. Of the two, dichloroacetic acid is the more convenient being a liquid at room temperature, but is a less effective solvent producing viscous solutions at low chitin concentrations. Trichloroacetic acid is however a solid at room temperature and demands the presence of a co-solvent, e.g. formic acid.

Several organic solvent systems have been reported, such as dimethyl formamide/N_2O_4[62], hexafluoro-2-propanol[63] and hexafluoroacetone[63], but the solubility of chitin is limited and the latter two have been criticised for being both irritants and toxic[64].

1.1.6.2 Chitosan solvents and solutions

Being basic, chitosan forms salts with acids producing polyelectrolytes whose solubilities depend upon the anion involved as well as chitosan composition and molecular weight. Solutions may be prepared either by formation of the salt, followed by dissolution in water or, more commonly, addition of the acid to a suspension of chitosan in water.

Chitosan is soluble in dilute solutions of common mineral acids, such HCl, HBr, HNO_3, etc but may be precipitated from solutions with increasing acid concentration[26, 65, 66]. Chitosan is insoluble in dilute H_2SO_4, though chitosan sulphate is soluble in hot water. Chitosan does dissolve in concentrated H_2SO_4 but not without sulphation and hydrolysis of the polymer chain[67].

Various studies have investigated the solubilities of organic acid chitosan salts,

Muzzarelli for example produced one of the more comprehensive lists[68], though some authors have published conflicting results.

Salts of monocarboxylic acids, up to hexanoic, are soluble in water, as are the salts of their halogeno- and hydroxy- analogues. Various salts of aromatic carboxylic acids are soluble, depending upon the water-solubility of the acid itself.

Several studies, e.g. Austin and Sennett[69], have described processes for the formation of dry, water-soluble chitosan salts by treating a suspension of chitosan in organic media with the appropriate carboxylic acid.

The only organic solvent system reported for chitosan are mixtures of DMF-N_2O_4[62], although other chitin solvents appear not to have been tried.

Chitosan samples which are soluble in water have also been reported, either by homogeneous deacetylation of chitin[70, 71] or by homogeneous *N*-acetylation[72] to the same level.

1.1.6.3 Solvent compatibility of chitosan

Although chitosan is not soluble in many organic solvents, solutions in aqueous acetic acid will endure the addition of large volumes of polar solvents without displacing the chitosan from solution. Up to 70% v/v of simple alcohols, glycols, acetone and formamide may be tolerated[73], while 2-propanol may be added up to 40% v/v and glycerol up to 80% v/v [74]. In each case, the organic solvent was added to a solution of chitosan in aqueous acetic acid. The viscosity of the solutions was largely unaffected by the addition of the organic solvent except in the case of polyol addition which increased solution viscosity considerably.

1.1.6.4 Acid-Base properties of chitin and chitosan

The dissociation constant K_b, of an amine group is obtained from the equilibrium,

$$RNH_2 + H_2O \rightleftharpoons RN^+H_3 + OH^-$$

Therefore, $$K_b = \frac{[RN^+H_3][OH^-]}{[RNH_2]}$$

and , $$pK_b = -\log K_b$$

similarly, the dissociation constant of the conjugate acid may be determined from the expression,

$$RN^+H_3 + H_2O \rightleftharpoons RNH_2 + H_3O^+$$

Therefore, $$K_a = \frac{[RNH_2]\,[H_3O^+]}{[RN^+H_3]}$$

and , $$pK_a = -\log K_a$$

However, the situation is more complex in the case of polyelectrolytes. Dissociation constants are not in fact constant and vary with the degree of dissociation. The ease of dissociation of a particular $-NH^+_3$ group will be increased by the presence of adjacent $-NH^+_3$ groups, increasing K_a and decreasing pK_a. Hence in the case of chitosan, the pK_a of a particular sample will depend upon the degree of neutralisation of charged groups and on the degree of *N*-acetylation, for samples having the same fraction of $-NH^+_3$ groups neutralised.

Early studies on chitosan appeared not to take this second fact into consideration and hence varying values for the pK_a were reported. e.g., Doczi[75] reported a value of approximately 6.2, while Noguchi *et al*[76] reported a figure of 6.3, and Muzzarelli *et al*[15] found the value to be 6.8. The first workers to take the degree on *N*-acetylation into consideration were Park *et al*[77] who evaluated titration results using the Katchalsky-Spitinik[78] equation,

$$pH = pK_a + n \log [\alpha / (1-\alpha)] \qquad (1.1.1)$$

where α is the degree of neutralisation and n is an empirical parameter related to the free energy change during titration. They concluded that the pKa was 6.1 when $\alpha < 0.72$ and 6.7 when $\alpha > 0.72$.

Domard[79] studied the variation of pK_a as a function of α for chitosan samples with a range of F_A values from [0.0] to [0.25]. While the pK_a of chitosan[0.25] varied little with α (staying approximately 6.5), he found that decreasing the F_A increased the pK_a's dependence on α. For chitosan[0.0], the pK_a increased sharply from approximately 5.3 to 6 as α increased from 0.1 to 0.25, then increased almost linearly towards a pK_a of 6.5 as α tended towards 1 (Figure1.1.4).

1.1.6.5 Electrolyte tolerance

Chitosan is precipitated from dilute hydrogen halide solution upon the addition of a concentrated solution of the same halide[26, 65, 66]. It is the increase in ionic strength rather than the decrease in pH that causes this precipitation. This may be demonstrated simply by the addition of the analogous sodium halide to chitosan in aqueous

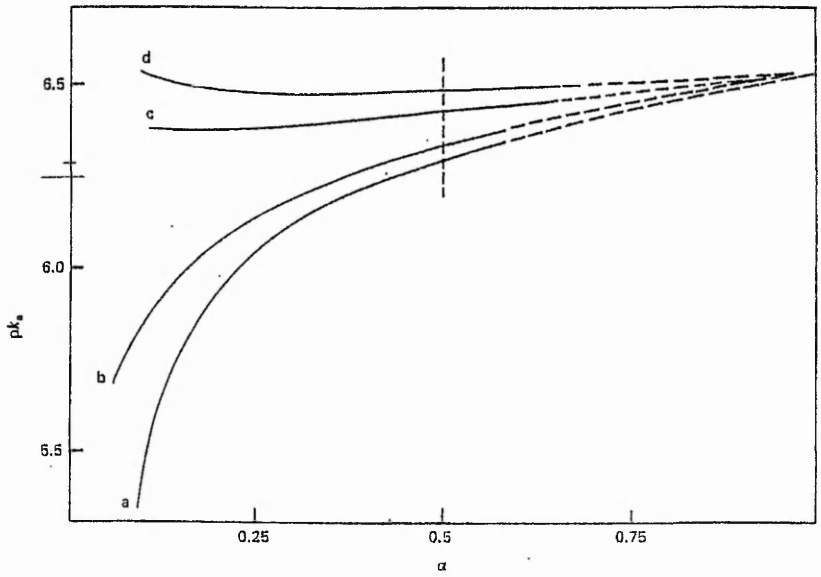

Figure 1.1.3 Variation of pK_a as a function of α for chitosans of different F_A : a) F_A[0.0]; b) F_A[0. 06]; c) F_A[0.19]; d) F_A[0.25] at constant amine group concentration.

acetic acid solution, which produces the same effect. The solid displaced is chitosan hydrohalide, and this may be re-dissolved in water. More complex chitosan precipitates, such as sulphate, phosphate, molybdate and ferrocyanide may be formed in similar fashion.

Precipitation of chitosan from acetic acid solution by complex anions has been put to use, notably in the purification and fractionation of chitosan by formation of chitosan salicylate[75], and in the determination of *N*-acetyl content[80].

1.1.6.6 Formation of polyelectrolyte complexes

The addition of oppositely charged polyelectrolytes is known to produce complexes which generally precipitate out of solution[81, 82]. Katchalsky[83] correlated the point of precipitation with overall charge neutralisation. Terayama[84] suggested that the

stoichiometry of the reaction could be employed to characterise one polyelectrolyte using an oppositely charged polyelectrolyte, the so-called colloid titration. This concept has since been applied to the characterisation of chitosan[71, 85].

1.1.6.7 Solution properties of chitin

^{1}H NMR spectroscopy has been used to show that the C(3′)OH in chitin in DMAc-LiCl solution possesses low values for δ and coupling constant and a relative insensitivity to temperature[86]. This suggested that the C(3′)OH...O(5) intramolecular hydrogen bond found in the chitin's crystalline state persists in solution. Such a bond would cause the chain to be very rigid in solution by restricting rotation around the glycoside bond. Further evidence of the chain's rigidity in solution has been gleaned from viscosity and light scattering measurements[87], though studies on oligomeric chitin in water using ^{13}C NMR spectroscopy[88] seem to indicate a much less inflexible arrangement.

1.1.6.8 Solution properties of chitosan

Once the amine groups have been protonated in acidic solution, chitosan behaves as a typical polyelectrolyte. In the absence of added electrolyte, dilute solutions of a typical polyelectrolyte may be expected to display an aberrant decrease in viscosity number with increasing concentration. This behaviour is ascribed to the decrease in coil dimensions with the increasing electrostatic repulsion at higher polyelectrolyte concentrations. This behaviour has been reported for chitosan by several workers including Van Duin and Hermans[89], Lee[56] and Lyubina *et al*[90]. This effect may be overpowered by the addition of a simple electrolyte to screen the polyelectrolyte charge or even an abnormally high

concentration of acetic acid[91] may result in screening. This results in the more recognised behaviour of increasing viscosity with increasing polyelectrolyte concentration, which is the basis of viscometric molecular weight determination.

1.1.6.9 Chitosan conformation and molecular dimensions

Chitosan would be expected to possess a random coil formation in solution, in common with other β-(1→4)- glucans. A relatively extended conformation would also be expected owing to its rather low chain flexibility. The flexibility of chitosan in solution has been determined by a number of workers[92, 93], and in terms of several different measures of chain[94, 95] stiffness. Whilst most of these studies do not show concordant results, they all do, at least, point towards chitosan being a relatively stiff molecule as expected[96].

1.1.7 Chitosan characterisation

1.1.7.1 Analysis of chitin and chitosan

Whilst the influence of such factors as degree of *N*-acetylation and molecular weight are generally very important especially in adsorption and flocculation behaviour, the use of such data in studies is often neglected. Even in studies where the effects of these variables are taken into account, the full implications of these parameters may not be fully recognised.

1.1.7.2 Degree of *N*-acetylation

The mole fractions of *N*-acetylated and the free amine group are, of course inversely related, and so the level of either may be established by the determination of the

concentration of one.

One must also be aware that the relative distribution of the minor substituent, D-glucosamine in chitin and *N*-acetyl-D-glucosamine in chitosan, may have a bearing upon the behaviour of a particular sample e.g. with regard to solubility.

1.1.7.3 Determination of *N*-acetyl content

(i) Hydrolytic techniques

Acid or alkaline hydrolysis of the *N*-acetyl groups may be used to liberate ethanoic acid, and hence, by determination of acid formed, *N*-acetyl content may be found. Hydrolytic techniques have been used since the first half of this century[97] and still find use with some researchers[98].

(ii) IR spectroscopy

Though Darman and Rudall observed in 1950[99] that the IR spectrum of α-chitin displayed the characteristic bands of hydrogen bonded amide groups at 1655 and 1625 cm^{-1}, their use in determining degree of *N*-acetylation was not proposed until 1977 by Moore and Roberts[100].

The use of IR spectroscopy has several benefits, most noticeably its independence of sample solubility; samples may be prepared as cast films or KBr discs, and independence of sample quantity and purity; internal reference peaks may be employed. Though these advantages may be clear, debate over which peaks should be used as sample and reference peaks still goes on.

Several sample/reference absorbance bands have been proposed: A_{1655} / A_{3450}, A_{1550} / A_{2878}, A_{1655} / A_{2867} and A_{1554} / A_{897}, in conjunction with a variety of baseline corrections. Each system is reported to possess its own merits and limitations, especially in the range of *N*-acetylation values for which it is suitable. It has been suggested that 2878cm^{-1} and 2867cm^{-1} are inappropriate reference peaks[38] as they are subject to interference from the dominant hydroxyl group band at 3450cm^{-1}. The use of the 3450cm^{-1} may also be preferred as reference peak as it is independent of *N*-acetyl content, whereas 2878cm^{-1} and 2867cm^{-1} both arise from C-H band vibrations and therefore are dependant on *N*-acetyl content. However, in the same paper, it is also reported that the A_{1655} / A_{2867} ratio used by Miya *et al*[101] was more reliable for highly deacetylated samples.

More recent studies have favoured the $A_{1655/3450}$ ratio. Baxter *et al* [102] modified this method to use the baseline for the amide I band proposed by Miya *et al*[101]. The FTIR Spectrum of chitosan F_A[0.33]M is shown in figure 1.1.4, included are the baseline corrections used by Baxter *et al*[102]. The N-acetyl content may then be calculated using:

$$\% \text{ N-acetylation} = (A_{1655}/A_{3450}) \times 115 \qquad (1.1.2)$$

Ratajska *et al*[103] chose to use the same two peaks but, however, omitted several of the relevant baseline corrections and the correction factor employed.

(iii) NMR spectroscopy

Hirano and Yamaguchi[104] were the first to determine the degree of *N*-acetylation using NMR spectroscopy by the ratio of N-acetyl methyl protons to methine and methylene protons, the samples being dissolved in DCOOH. Since then, a variety

of NMR methods have been used to determine *N*-acetylation, for example Varum *et al*[105, 106] depolymerised chitosan, then used ^{1}H NMR[105] and ^{13}C NMR[106] to determine degree of *N*-acetylation and distribution of *N*-acetyl groups in the chain. Ratajska *et al*[103] considered solid state ^{13}C NMR to be the reference method in their study of FTIR *N*-acetyl determination methodology.

(iv) Other methods

Other methods have been suggested, based for example on GPC[85], UV[85], first derivative UV[107, 108] and circular dichroism[109] though these are not in general use.

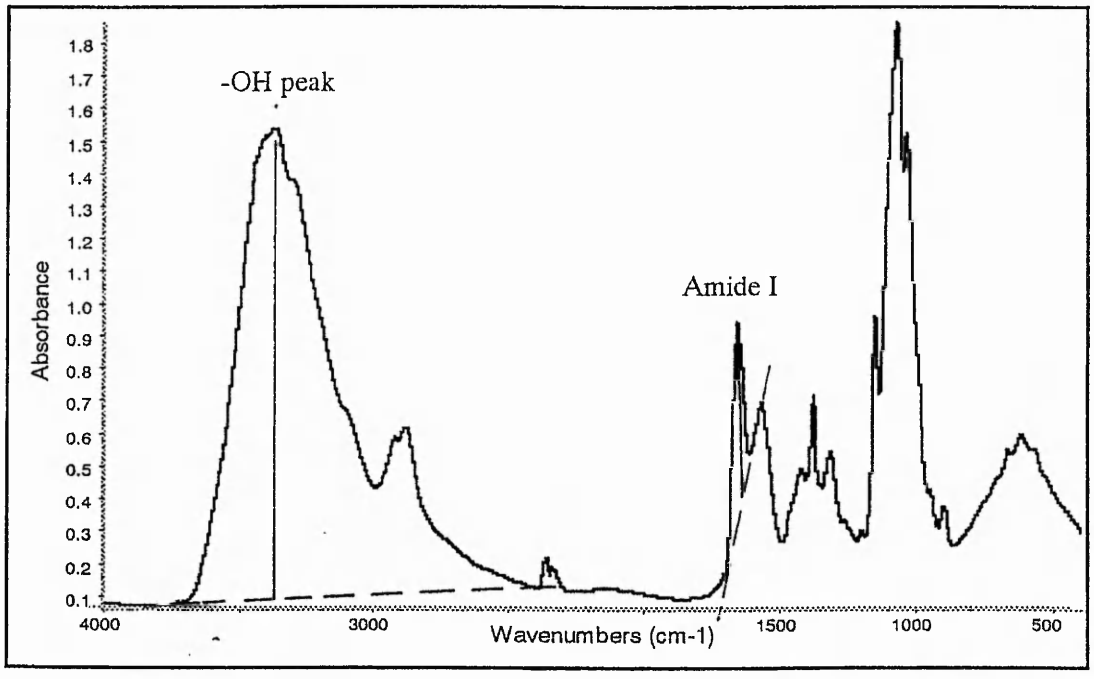

Figure 1.1.4 The FTIR spectrum of chitosan (F_A[0.33]M) showing baseline corrections used by Baxter *et al*[102] and Ratajska *et al*[103]

1.1.7.4 Determination of amine group content

(i) Dye adsorption

The adsorption of certain anionic dyes, notably C.I. Acid Orange 7 and C.I. Acid Red 88 (Figure 1.1.5) onto the protonated amine groups of chitosan has been shown by Maghami and Roberts[110] to have a 1 : 1 stoichiometry irrespective of the solubility of the chitosan sample. A variation on this theme involved the adsorption of picric acid[111] but this remains relatively unused.

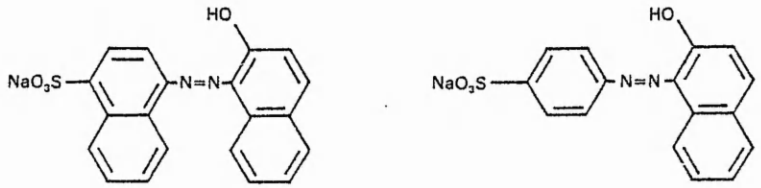

(a) (b)

Figure 1.1.5 Structures of the dyes (a) C.I. Acid Red 88 and (b) C.I. Acid Orange 7.

(ii) Acid – base titration

If chitosan is dissolved in a known excess of acid, typically dilute HCl, the amine group concentration may be determined using a back-titration using, for example, standard sodium hydroxide solution[21], however its precision has been questioned[38] due to chitosan's tendency to precipitate in the neutralisation pH range.

(iii) Metachromatic titration

Metachromatic titration analysis of the amine content of chitosan relies on polyelectrolyte-induced metachromasy in a suitable dye (an anionic dye in this case). If the absorbance of the dye at its λ_{max} is monitored as a function of added polyelectrolyte, the absorbance will be seen to decrease with increasing polyelectrolyte concentration until a minimum value is obtained and further additions of polyelectrolyte will have no effect upon absorbance. The point at which this minimum value is reached represents the point of equivalence between the polyelectrolytes' charged groups ($-NH_3^+$) and the dye anions. Maghami and Roberts[112] found C.I.Acid Orange 7 to be suitable for such an investigation.

(iv) Colloid Titration

Terayama[84] developed the colloid titration technique to analyse one polyelectrolyte using another, oppositely charged polyelectrolyte. It relies on the stoichiometric neutralisation of polycation by known polyanion with some indicator such as Methylene Blue used to show the equivalence point. This method is used by many groups to determine chitosan composition[71, 85] using polyvinyl sulphate potassium (PVSK) as polyanion and Toluidine Blue as indicator.

1.1.7.5 Molecular weight determination

Molecular weight may have a crucial part to play in the flocculation behaviour of chitosan but, as yet, simple, accurate molecular weight determinations remain difficult. The determination of chitosan's molecular weight presents several difficulties. Uneven treatment during deacetylation of chitin may result in the presence of microgels when the ultimate

chitosan is dissolved. Chitosan has also displayed a tendency to aggregate in solution[38, 113]. Rinaudo and Domard suggested[94] that the degree of polymerisation should be quoted rather than the molecular weight average as the latter varies with degree of N-acetylation and the nature of the counter ion, whereas the former does not, however this practice has not been commonly adopted.

Various techniques have been evaluated for the determination of the molecular weight of chitosan including osmometry[38], end group analysis[114] and ultracentrifugation[115] but only light scattering spectrophotometry, gel permeation chromatography and viscometry are found in routine use at present.

(i) Light scattering spectrophotometry

Light scattering spectrophotometry has been used by a number of workers, Domard and Rinaudo[38] for example, but the possibility of overestimation of molecular weight must be recognised due to the tendency of chitosan to aggregate in solution. Van Duin and Hermans[89] first suggested association of the chains in order to explain the apparent increase in M_w with decrease in total ionic strength. As aggregation by hydrogen bonding should decrease with increasing ionic strength, the effect was attributed to the presence of small amounts of divalent ions. The use of de-ionised water gave a reduction in M_w and this was taken as corroborating evidence. Domard and Rinaudo[38] produced direct evidence of aggregation of chitosan chains by observing the increase in scattered light intensity over time after the preparation of the solution. An initial elevation of solution temperature to 50ºC for 2 hours was shown to suppress the rate of increase of scattering. This work suggested aggregate formation characteristic of a crystallisation process. Later studies by Domard and Rinaudo[116] and Muzzarelli *et al*[117] using laser light scattering

spectrophotometry showed no evidence of aggregation with variation in electrolyte concentration over a sodium acetate concentration range of 0.1 - 0.5M and an 80% deacetylated chitosan sample.

Anthonsen *et al*'s static laser light scattering study[113] revealed the presence of concentration dependant aggregates. It concluded that about 5% of the sample had aggregated to give a very high molecular weight. It was therefore concluded that static laser light scattering was not an ideal method for the determination of the molecular weight of chitosan. Although no evidence was obtained to suggest the mechanism of aggregation, the study's results eliminated the possibility of chain association due to bridging by multivalent cations, residual proteins and any influence of the method of degradation. The work finally concluded that the chemical and physical site of interaction was still unknown, though a tentative postulation that the insolubility of consecutive chitin units may lead to association between such areas on chains was mooted.

(ii) Gel permeation chromatography (GPC)

GPC has been employed in a number of studies for the determination of chitosan molecular weight distributions, including the publication of supposedly optimum conditions for the GPC of chitosan[118].

Problems arise in the determination of chitosan's molecular weight due to its cationic charge in acid solution. It is essential that there is no interaction between the polymer being analysed and the gel for the separation process is to occur correctly, consequently electrostatic interaction, both attraction and repulsion must be minimised. Most GPC studies on chitosan[118, 119] do not take account of the fact that GPC gels bear a negative surface charge. Domard and Rinaudo[116] used a silica gel support modified to

bear quaternary ammonium surface groups and added a low molecular weight electrolyte (NH_4OAc) to suppress repulsion between chitosan and gel. It was found that an optimum concentration of NH_4OAc was required (0.05M) for the data to fit the universal calibration plot of Log([η].MW) against V_e (elution volume). A lower concentration of NH_4OAc was found to cause deviation from the plot due to inadequate screening of the cationic surface charges, whilst a greater concentration of NH_4OAc caused deviation due to charge reversal on the chitosan resulting in adsorption on the gel.

(iii) Viscometry

Viscometry is often the most convenient method for the determination of polymer molecular weight but it has the drawback of not being an absolute method. Viscometry relies upon the correlation of limiting viscosity number, [η], with molecular weight values determined by some other, absolute method. The Mark-Houwink equation is then used to relate [η] to molecular weight :

$$[\eta] = K\overline{M}_v^{\alpha}$$

where K and α are constants that are independent of molecular weight over a wide range of molecular weights. They are dependent upon polymer, solvent, temperature and, in the case of polyelectrolytes, concentration and nature of any added electrolyte. These constants must be evaluated from a plot of Log[η] vs. Log $\overline{M}_w$ for a series of different molecular weight polymer samples having narrow molecular weight distributions.

Numerous studies have quoted values for K and α, though a large variation in values for each constant prompted investigation into the effect of F_A on these values. The first such investigation by Maghami and Roberts[112] over an F_A range of 0.0 to 0.40

concluded that K and α were independent of F_A. Wang *et al*[120] found that the value of α increased, while K decreased with increasing F_A. The following equations were quoted for determining each constant :

$$K = 1.64 \times 10^{-30} \times DD^{14.0}$$

and (1.1.4)

$$\alpha = -1.02 \times 10^{-2} \times DD + 1.82$$

where DD is the percentage degree of deacetylation. Anthonsen *et al*[121] reported similar trends in the two values, though with very different actual results :

$$\log K = -0.427 - 3.821 F_A$$

and (1.1.5)

$$\alpha = 0.6169 + 0.759 F_A$$

while Rinaudo *et al*[122] reported results suggesting that α was independent of F_A and equal to 0.76, while K decreased from 0.082 to 0.074 as F_A increase from 0.02 to 0.21.

1.2 Polymer latex as a model colloid

1.2.1 Latex formation

1.2.1.1 Introduction

Polymer latices have been considered as possible model colloids since the early 1960's[123] due to their uniform shape (spherical), size (coefficients of variation of a few percent are easily attained) and manipulation, through polymerisation conditions, of surface characteristics. As such, polymer latices have found applications in calibration of instrumentation, e.g. optical microscopes and ultracentrifuges, as well as being used in

model colloid investigations such as stability[124,125,126], microelectrophoresis [127, 128] and surface conductance [129].

Historically, the first monodisperse latex, 580G Lot3584, was generated by chance at Dow Chemical in 1947. No other 'lots' were anywhere near as uniform. The potential use of the particles as internal standards for electron microscopy was realised[130, 131] and in the early 50's J W Vanderhoff started work to deliberately produce monodisperse latices and not only reproduced 580 G Lot 3584 but also developed the approach of seeded growth[132, 133] to produce a range of larger sizes. Gradually the transition was made from offering free samples to academics to a viable commercial operation. Whilst complete details of the preparative process have never been given for commercial reasons much has been published and much can be deduced.

Dow commercial latices across the size range illustrate the difficulties. Comparing the coefficient of variation of the mean particle diameter CV versus the mean particle diameter, shows that it is more difficult to attain monodispersity at either end of the size range. The CV starts at around 7% for small particles but decreases with increasing diameter down to better than 1% in the 0.5 to 1 micron range but increases again dramatically above 2.5μm rising to 15%. This pattern reflects the use of different polymerisation techniques i.e. emulsion, seeded growth and suspension polymerisation.

1.2.1.2 Emulsion Polymerisation

First considering the basic mechanism of emulsion polymerisation in the presence of emulsifier; monomer, surfactant and initiator are charged into a reactor, which in the laboratory can be a three necked flask or a rotated sealed (beverage) bottle[134], to produce

the separate phases shown in Figure 1.2.1.

The monomer is in three loci as monomer droplets, dissolved in the water and solubilized in the surfactant micelles. Similarly, the surfactant (emulsifier) is present as micelles, dissolved in the water and adsorbed on the monomer droplets. In a free radical addition mechanism the sulphate free radical ion adds monomer units and the hydrophobic chain length increases as follows:

Initiation:

$$S_2O_8^{2-} \xrightarrow{\text{heat}} 2SO_4^{-}\cdot$$

$$2SO_4^{-}\cdot + M \rightarrow SO_4^{-}M\cdot$$

Propagation:

$$SO_4^{-}M\cdot + M \rightarrow SO_4^{-}MM\cdot$$

The oligomeric radicals $SO_4^{-}MMM\cdot$ become surface active when 3 to 5 units long and capable of dynamic exchange with surfactant molecules in micelles. Once in a micelle a radical grows until another radical enters and causes termination. As polymerisation depletes the monomer in the micelle, a supply is maintained by diffusion from the droplets through the aqueous phase to the site of polymerisation. Particle initiation proceeds until all the micelles have disappeared either by capturing radicals and becoming polymer particles or by disbanding to give up their emulsifier to the expanding polymer/water interface.

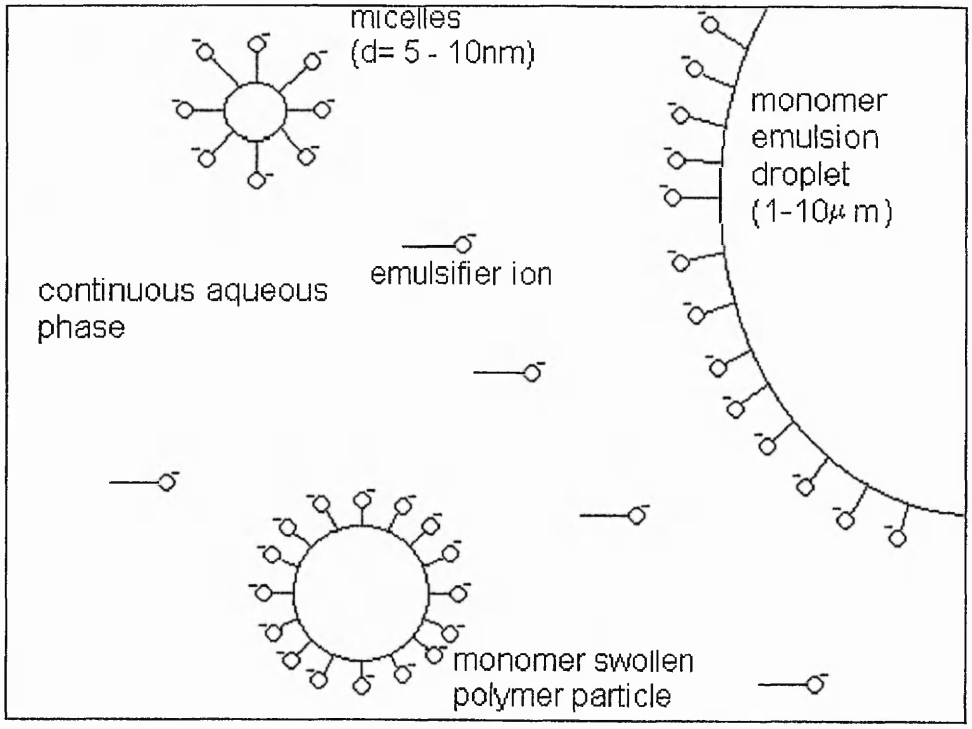

Figure 1.2.1 Schematic diagram of the phases involved in emulsion polymerisation.

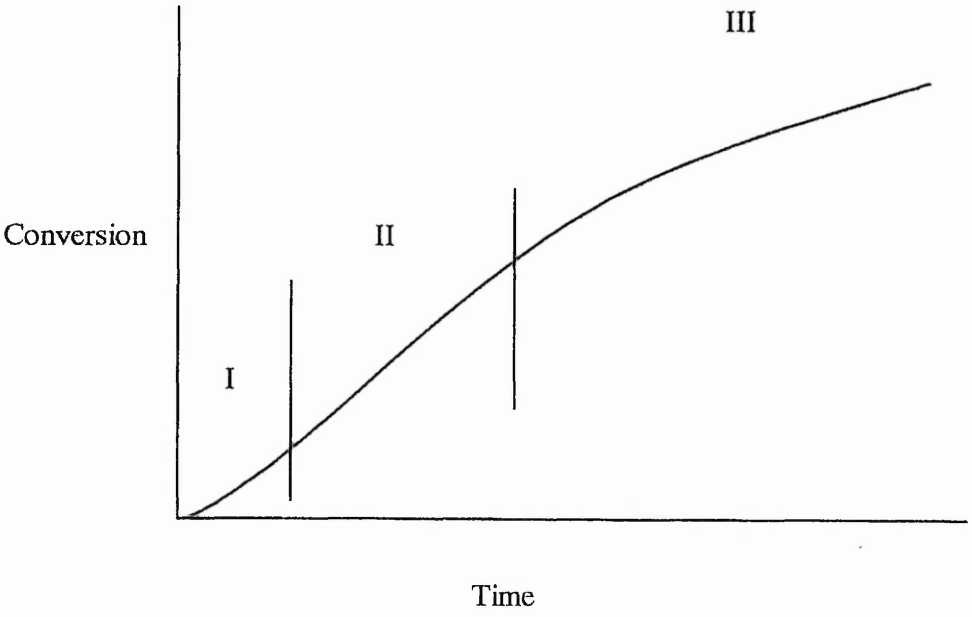

Figure 1.2.2 The three stages of polymer latex particle formation.

The disappearance of the micelles separates the particle initiation stage (interval I Fig 1.2.2) from the particle growth stage (interval II), in which a constant number of particles continue to grow. Once the monomer droplets are exhausted all the monomer is in the particles and the rate decreases in a first order reaction in interval III.. The interval II kinetics follow the classic Smith Ewart theory Case 2 ie: $Rp = [E]^{0.6} [P]^{0.4}$ where P is initiator and E is emulsifier. That growth takes place predominantly in the micelles is ascribed to their greater number density, ie: 10^{18} per ml compared with 10^{12} per ml for monomer droplets and hence higher total surface area than the monomer droplets. Particles in the size range 30nm to 80nm may be produced by emulsion polymerisation.

1.2.1.3 Suspension polymerisation

In the absence of micelles and using a weakly surface active stabiliser and an oil soluble initiator, growth does occur predominantly in the monomer droplets and this is classic suspension polymerisation[135]. Typically millimetre size particles, as used in ion exchange resins, would result but with more strongly surface active stabilisers the droplet size can be reduced to produce the super micron latex particle size range but with the disadvantage mentioned earlier of greater polydispersity. Oil soluble initiators do not contribute to the surface charge on the particles and weaker stabilisation leads to instability during polymerisation, coalescence and increased polydispersity. Whereas particles produced by an accretive growth type of mechanism tend to show a Gaussian distribution of particle size, those produced by attrition/dispersion type of processes produce a log normal distribution.

1.2.1.4 Seeded growth

In the seeded growth process an aliquot of pre-formed latex is added to monomer, water, initiator and emulsifier below its cmc, so that growth takes place at a reduced number density to yield larger product particles. Repeating this process over and over again is not unattractive from the commercial point of view since the intermediate stages are marketable as a range of uniform sizes. The process is good for the control of monodispersity since the growth follows a power law [136, 137]:

$$\frac{dv}{dt} = k_2 D^n \qquad (1.2.1)$$

and relative rate of diameter growth is given by:

$$\frac{1}{D}\left[\frac{dD}{dt}\right] = \left[\frac{2k}{\pi}\right] D^{n-3} \qquad (1.2.2)$$

Thus if $n < 3$ growth will occur on small particles preferentially. Literature reports suggest $n = 2$ for seeded growth[137] so that a self-sharpening tendency is to be expected, i.e.: small particles tend to catch up with large ones, so the CV improves with the 'age' or size of the particles. Above ca. 2.5μm the size starts to broaden again due to coalescence of seed particles and at larger sizes this process was abandoned, until recently[134], in favour of a single step suspension polymerisation but at the cost of a much broader size distribution.

1.2.1.5 Emulsifier-free emulsion polymerisation[138, 139, 140, 141, 142, 143, 144]

Commercially the lower particle number density, resulting from the lack of added stabilising surfactant, is less attractive than conventional emulsion polymerisation but this does lead to larger particle sizes up to 2 μm being produced in a single step.

Nuclei are formed by oligomer aggregation until the particles have a sufficient charge density for stability at the prevailing ionic strength of the medium in line with DLVO theory[145] of colloid stability. The rate of aggregation follows second order kinetics so that in the early stages the particle number density decreases rapidly. W, the Fuchs' stability ratio, increases as the surface charge density increases until the rate of coagulation tends to zero and the reaction then proceeds at constant particle number density.

The final particle size can be controlled systematically [142]:

$$\text{Log } D = 0.238 \left[\frac{\text{Log } [I]\,[M]^{1.723}}{[P]} + \frac{4929}{T} \right] - 0.827 \qquad (1.2.3)$$

where I is the ionic strength and [P] is the concentration of persulphate initiator. In essence, higher temperatures and higher initiator concentrations produce lower molecular weights, so that higher surface charge densities are more quickly reached, to produce more and smaller particles. Higher ionic strength favours fewer large particles and large amounts of monomer allow particles to grow to a larger final size. These reactions do not follow Smith-Ewart (Case 2) kinetics since $n > 0.5$ as several radicals can co-exist in larger particles[146]. Surfactant free latices are very easy to prepare in the laboratory and give a clean product (since there is no added surfactant to remove).

1.2.1.6 Large latex particles by seeded growth

Many applications demand monodisperse latices of larger particle sizes. However, monodisperse latices with sizes greater than 2 μm are not easy to prepare.

A problem of the seeded growth regime is that if the total surface area of seeded polymer is inadequate to mop up all the oligomeric radicals produced, then a secondary crop of smaller particles[130, 137, 147] may be generated. At best this is wasteful and necessitates a size separation process to be used. At fixed % solids, the number density and hence total surface area used decreases with increasing particle size. Above 2.5 μm diameter, particles are sensitive to mechanical shear instability, so that additional surfactant needs to be added to alleviate stability problems. The extra surfactant does however also tend to stabilise secondary nucleation[136, 137, 147]. The operational range of emulsifier concentration gets smaller and smaller with increasing size until at sizes above 1μm it becomes knife-edge[148]. Also, with increasing particle size, there is an increasing tendency for the particles to cream or settle out during polymerisation because of the decreasing intensity of Brownian motion and the density difference between the particles and the aqueous phase. As the polymerisation proceeds, styrene (density 0.905 gm/ml) is converted to polystyrene (density 1.05 gm/ml) and thus the polystyrene latex particles tend to cream at low conversions and to settle out at high conversions. Increasing the agitation rate to offset the creaming-settling tendency often results in the formation of coagulum, because the large particles are sensitive to mechanical shear. The densities of the particles and the aqueous phase can be matched at one end of a reaction by changing the monomer composition (eg: substituting vinyltoluene-t-butylstyrene mixtures for styrene) or by adding electrolytes or non-electrolytes to the aqueous phase. They cannot however be matched at both low and

high conversions because of the continuous change of the particle density. Although successive seeded emulsion polymerisation has not been used to prepare monodisperse latices >2.5μm in large quantity, gram quantities of 3.0 μm and 5.6 μm-diameter latices and microscopic quantities of 12 μm-diameter latex have been prepared by Vanderhoff[149] by recovering the stable residues from polymerisations that produced mostly coagulum.

It was the above considerations which led to polymerisations being carried out on a space shuttle in microgravity[134] in order to minimise stirring to the level required just for heat transfer. Oil soluble initiators, water-soluble inhibitors and a careful choice of stabilizer were needed to avoid secondary nucleation. This was the first commercial product made in space but the extreme cost gave these latices only novelty value as they were impractical for general use, whilst the increase is uniformity of National Bureau of Standards 'space' latices compared with Earth bound formulations was at best marginal.

1.2.1.7 Alternative methods for producing large particles

(i) Dispersion polymerisation (or microsuspension polymerisation) plus separation

The term 'dispersion polymerisation' was defined by Trommsdorff and Schildknecht[150] as a modified suspension polymerisation that produces particles in the 10 μm range. This is the range between suspension polymerisation and emulsion polymerisation. Earlier works by Winslow and Matreyek[151], and later Vanzo[152], can be classified in this category. An extensive study has been carried out by Almog and Levy [153, 154, 155, 156]. The method is similar to a conventional suspension polymerisation except

that a much higher concentration of stabiliser is used. The polymerisation product is usually a polymer dispersion with wide particle size distribution, from several μm to tens or even several hundreds of μm. With subsequent separation methods, such as sieving, elutriation, sedimentation, or centrifugation, a narrower fraction can usually be obtained. The particle size distribution of the separated product is still much wider than those obtained from seeded emulsion polymerisation.

(ii) High-swelling method plus separation

The so-called Ugelstad two-step swelling method[157, 158, 159, 160] also starts from a seed latex. In the first step, a water-insoluble oligomeric compound is incorporated into the seed particles to increase the swellability of the particles. The second step is swelling and polymerisation in situ. The method allows high monomer-polymer swelling ratios (100 - 1000 fold) and hence high particle size build-ups. Monodisperse latexes of 2 to 50 μm have been claimed to be prepared by using this method. Although the method of increasing swellability has been frequently mentioned in publications, no details on the polymerisation process itself have been given. The initiation and stabilisation system used in the polymerisation, the particle size distribution of the product immediately after polymerisation, and the separation methods involved have never been disclosed. It is believed that many small particles are generated along with the large particles during polymerisation and are separated out later.

The Ugelstad enhanced swelling technique revolutionised large particle production with percentage CV's approaching those of the smaller particles ie: ca. 1% but at a price of £2500 per gram, as compared to £40 per gram for the smaller sizes.

1.2.2 Cleaning of polymer colloids

1.2.2.1 Introduction

Model colloids need to be well characterised and an important part of this process is the technique of cleaning. The cleaning process should be capable of removing impurities from both the bulk polymer phase and the suspending medium (usually water), as well as those impurities associated with the particle-suspending medium interface, without affecting the true nature of the latex, e.g., particle size, nature and concentration of surface group functionality, and particle morphology. Dialysis and ion exchange have been employed for many years as cleaning processes, but problems associated with these methods when used for polymer colloids have been identified[161]. Different alternative techniques have been evaluated which include hollow fibre dialysis[162], centrifugation/decantation[163, 164], steam stripping[165, 166, 167, 168, 169], serum exchange[170], microfiltration[171], diafiltration[172, 173], ultrafiltration[174, 175].

The cleaning process can only be properly evaluated after the nature of the impurities have been identified. The major impurities encountered with polystyrene latices, which are probably the most widely studied 'model' sols, have been identified and methods for their removal have been studied by Wilkinson *et al.*[165, 166, 168, 171, 176, 177, 178], El-Aasser[179], Everett *et al.*[167, 180], and others[181, 182], and a summary of these methods is given in Table 1.2.1. The ease of removal of the impurities varies widely; for example, electrolyte material is removed readily by conventional dialysis or ion-exchange, whereas styrene monomer and oligomeric material is only slowly removed by these techniques.

1.2.2.2 Dialysis

(i) Conventional Dialysis.

Typically, dialysis, the traditional technique for cleaning colloidal sols[183], is carried out in Visking dialysis tubing using a ratio of latex to double distilled water of ca 1:20, and with some twenty changes of water occurring over a period of three to four weeks – after which the conductivity of the dialysate usually equals that of the distilled water employed. Thus, it is a slow process, which relies upon the concentration gradient across the membrane as its driving force and it becomes extremely slow when the concentration of impurities is low. For efficient removal the impurity needs to be readily soluble, so that poorly soluble, strongly adsorbed, non-ionic materials would be expected to be desorbed only very slowly[184].

There are major problems associated with the dialysis technique as applied to the cleaning of polymer latices. Not only can material leach out from the tubing, but reactions may occur between impurities in the latex and the components of the dialysis tubing. The technique involves protracted time periods during which post-reaction changes and contamination from external sources (*eg*, bacterial) can occur. Further, the complete removal of unreacted monomer, low-molecular-weight oligomers, reaction by-products and the complete exchange of cations for protons is not achieved. Dialysis, albeit it complemented by other cleaning techniques, is still a widely used procedure[185 - 188].

(ii) Hollow fibre dialysis

Hollow fibre dialysis is faster than conventional dialysis with equilibrium reached in hours rather than weeks or months, but since water is circulated at $40cm^3\ min^{-1}$ some 30 litres of water may be used in cleaning $100cm^3$ of latex. Significant metal cation exchange could occur even when Analar water is used.

Impurity	Location		
	Water phase	Polymer phase	Particle-water interface
Unreacted monomer	✓	✓	✓
Low molecular weight oligomers/polyelectrolyte	✓	✓	✓
Thermally polymerised monomer	✓	✓	✓
By-products of initiation, eg, K^+, H_2SO_4 from potassium persulphate	✓	✗	✓
By-products from monomer, eg, benzaldehyde, formaldehyde and benzoic acid from styrene	✓	✓	✓
Emulsifier	✓	✗	✓
Buffers, eg, sodium bicarbonate	✓	✗	✓
Inhibitors (post reaction additives)	✓	✗	✓
Bacteria and fungi	✓	✗	✓
Dissolved atmospheric gases, eg, carbon dioxide	✓	✗	✓
Material leached from containers, eg, polymers plasticisers, polyelectrolyte	✓	✓	✓

Table 1.2.1 Impurities found in Polymer Latices

1.2.2.3 Ion-exchange.

Vanderhoff and co-workers[181, 189 - 200] developed the use of ion-exchange resins for cleaning polymer latices. This involved developing a procedure for the rigorous purification of the resins. Schenkel and Kitchener[201] and Ottewill[202] had previously reported results

which discouraged the use of ion-exchange resins with colloidal systems due to possible leaching of polyelectrolyte contaminants. The latex surface charge could be altered, perhaps irreversibly, due to the adsorbed polyelectrolyte.

Although Vanderhoff and co-workers have carried out extensive work with ion-exchange resins, especially with regard to cleaning them, many other groups have experienced great difficulties in working with these materials, mainly due to the problems of cleaning prior to use. Ion-exchange resins are effective in removing ionic material and surface-active species, but can be less effective in removing unreacted monomer and polyelectrolyte. Further, since there is direct physical contact between the ion-exchange beads and the latex particles it is possible for materials to be exchanged across this interface – it is known that a certain percentage of latex particles are left adhering to the resin beads after the cleaning process. This may lead to contamination of the latex or removal of material from the surface/sub-surface regions of the latex particles, and to a change in the particle size distribution if it is polydisperse.

1.2.2.4 Centrifugation-decantation.

Several groups of workers[163, 164, 172, 203] have used the technique of centrifugation (typically 25,000 rpm for 45 min) followed by decantation of the supernatant to clean a latex. This technique is repeated until the conductance and surface tension corresponds to that of pure water. The latex can be acid washed *in-situ* to ensure complete exchange of cations for protons.

The main disadvantage of the technique is the problem of redispersion of the sedimented latex. Latices with low concentrations of stabilising groups may be irreversibly

aggregated. The technique is most commonly used to remove water soluble polymer impurity in latices prepared with functional monomer.

1.2.2.5 Steam stripping

Steam stripping is a widely used commercial process for the removal of residual amounts of free monomer. In the laboratory situation, rotary evaporators can be conveniently used. Steam stripping is normally carried out at 353K or less under a reduced nitrogen atmosphere – a volume of steam distillate equal to that of the latex being collected. Although steam stripping is probably the most efficient technique for the removal of both unreacted monomer and low molecular weight oligomers, it can result in the hydrolysis of surface groups. It is not effective in the removal of other impurities. If employed to remove monomer/low molecular weight polymer, it should be followed with one of the other techniques (*eg*, microfiltration) to remove other impurities.

1.2.2.6 Microfiltration/serum exchange/ultrafiltration/diafiltration.

In the processes of microfiltration[171], serum exchange[170, 204] ultrafiltration[174, 175], and diafiltration[172, 173], as in dialysis, the latex is retained by a semi-permeable membrane material, but here hydrostatic pressure is used to force the aqueous phase (serum) through the pores.

The 'microfiltration' technique evaluated by Wilkinson *et al.*[171] employed a Millipore filter (Millipore UK Ltd., Millipore House, Abbey Road, London NW10 7SP, UK) whereas the 'serum exchange' technique evaluated by Ahmed *et al.*[170] employed a Nucleopore filter (Nucleopore Corporation, 7035 Commerce Circle, Pleasanton, Ca 94566, USA).

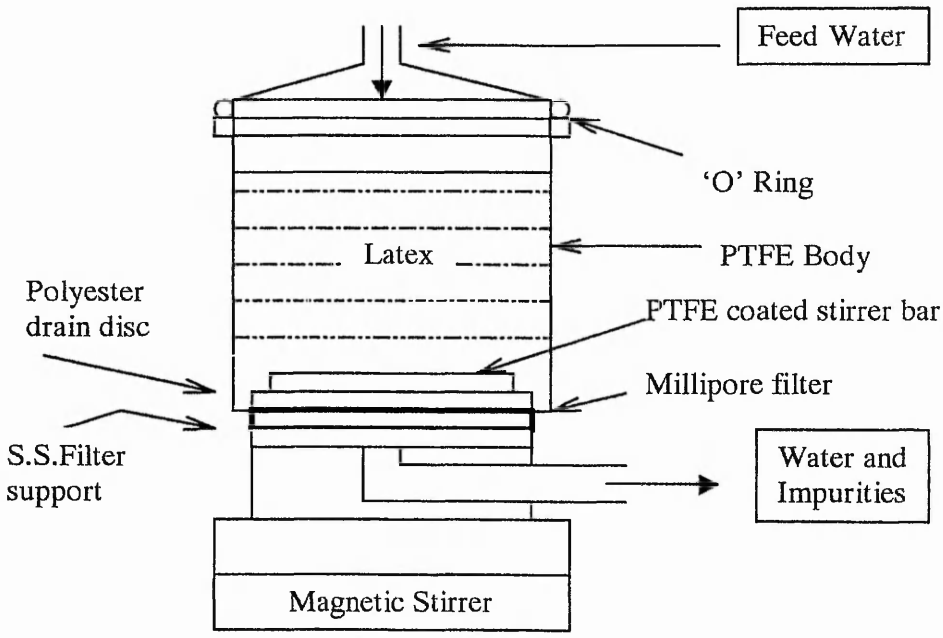

Figure 1.2.3 Construction of cell used for microfiltration of latex

A typical cell design[174] employing a Millipore or Nucleopore filter is shown in Figure 1.2.3. The cell capacity was 80 cm^3 and a standard 47 mm diameter filter was employed (a larger cell could be employed with an appropriately larger filter – up to 293 mm diameter). Prior to use it was disassembled and all parts boiled in double distilled water for 30 min. The unit was then assembled and double distilled water passed through (80 cm^3 hr^{-1}) until the surface tension and conductance were the same as the feed water. This process was then repeated with the filter in position.

The microfiltration/serum exchange technique has several advantages over other methods for the cleaning of latices. It avoids the prolonged preparation associated with the purification of ion-exchange resins, and it permits the rapid removal of adsorbed surface-active agent from the latex, something that may require prolonged periods of dialysis to achieve. Very little water is employed compared with dialysis and, hence, contamination

from trace impurities in the water itself is reduced. The apparatus is also simpler and, hence, cheaper than that required for cross-flow microfiltration/diafiltration or hollow-fibre dialysis. A further advantage of this microfiltration technique is its versatility: apart from cleaning latices, the solids content may be adjusted easily, and a choice of filters of differing composition and construction may be employed to suit varying circumstances.

Although flow rates are high for pure liquids, *eg*, ca 10^4 dm^3 m^{-2} hr^{-1} for a 0.1 μm Nucleopore or Millipore filter at 10 psi (~69 kPa) pressure, this drops rapidly if particulate matter blocks the pores. It is therefore essential to ensure rapid and efficient mixing to prevent this.

This technique has been shown to remove all impurities expected in a polymer latex (refer Table 1.2.1) with the exception of bacteria and/or fungi spores since they will generally be larger than the latex particles. The main drawback of this technique is that latices need to be acid washed to ensure the complete exchange of cations for protons.

Overall a recommended cleaning procedure would involve the use of microfiltration/serum exchange (with an acid wash to ensure complete exchange of cations by protons), steam stripping for removal of residual monomer and efficient sparging with pure nitrogen to remove carbon dioxide.

1.2.3 Characterisation of the latex surface

The determination of the precise nature of the latex particle surface with regard to type, concentration and conformation of end groups, both attributable to the polymer structure, and to the polymer end groups which arise from the initiator (and which may be modified during polymerisation, upon cleaning or storage) or copolymerisable surfactant, has proved extremely difficult and a great deal of literature has arisen dealing with this

aspect alone [181, 142, 168, 173, 176, 180, 205 - 210].

Since the concentrations of functional groups are relatively low compared with the total weight of latex (of the order of μ equivalents gm^{-1}), sensitive analytical techniques are required for their determination. Techniques employed have included x-ray fluorescence for sulphur[199], neutron activation for oxygen and sulphur [211], radiotracer analysis[212], dye partition and dye interaction[213 - 218], soap titration and equilibrium adsorption [219 - 221], IR[222, 223], microeletrophoresis[224, 181], potentiometric titration[223, 225, 226] and conductometric titrations[224, 181, 142]. Of these methods the most commonly used is the conductometric titration for its ease and sensitivity to both strong and weak acids[162].

The typical conductometric titration procedure involves addition of base (usually 0.1 mol dm^{-3} sodium hydroxide), either incrementally by hand from a micrometer syringe or continuously by mechanical means at a constant rate, to the latex dispersion contained in a closed, thermostated and stirred vessel which is flushed with or maintained under a blanket of nitrogen. The conductivity changes are then measured using a sensitive bridge in conjunction with a dip-type cell and recorded either manually at intervals or by continuous output onto a chart recorder or computer.

For a typical strong acid/strong base titration up to the equivalence point $H^+ + X^- + M^+ + OH^- \rightarrow H_2O + M^+ + X^-$, ie some H^+ ions are replaced by M^+ ions and since $\lambda_{H^+} >> \lambda_{M^+}$ the conductance decreases up to the equivalence point.

$$\frac{1}{R} = \frac{A}{1000\ell}\left[C_{H^+}\lambda_{H^+} + C_{M^+}\lambda_{M^+} + C_{X^-}\lambda_{X^-} \right] \qquad (1.2.4)$$

where R is the resistance, A/ℓ is the cell constant, C's are the concentration of the ions indicated having equivalent ionic conductances, λ.

If the initial solution volume is V_a cm^3 and the concentration C°_a mol dm^{-3} and if f is the fraction of acid neutralised by addition of V_b cm^3 of MOH then,

$$C_{H^+} = (1 - f)\, C^\circ_a \left[\frac{V_a}{V_a + V_b} \right] \qquad (1.2.5)$$

$$C_{X^-} = C^\circ_a \left[\frac{V_a}{V_a + V_b} \right] \qquad (1.2.6)$$

and

$$C_{M^+} = C^\circ_a \left[\frac{V_a}{V_a + V_b} \right] \qquad (1.2.7)$$

$$f = \frac{V_b C_b}{V_a C^\circ_a} \qquad (1.2.8)$$

However, since $V_a >> V_b$ (the base is usually chosen at least 10-fold more concentrated than the acid used) then the dilution factor is :

$$\frac{V_a}{V_a + V_b} \qquad (1.2.9)$$

can be approximated to l.

$$\text{hence } \frac{1}{R} = \frac{A\,C^{\circ}_{a}}{1000\ell}\left[\lambda_{H^+} + \lambda_{X^-} + \left[\lambda_{M^+} - \lambda_{H^+}\right]\frac{C_b}{V_a C^{\circ}_{a}}\;V_b\right] \qquad (1.2.10)$$

and a plot of $1 / R$ vs. V_b will be a straight line having a slope α ($\lambda_{M^+} - \lambda_{H^+}$).

Beyond the equivalent point the conductance increases due to the addition of excess OH^- and M^+ ions:

$$\frac{1}{R} = \frac{A\,C^{\circ}_{a}}{1000\ell}\left[\lambda_{X^-} - \lambda_{OH^-} + \left[\lambda_{M^+} - \lambda_{OH^-}\right]\frac{C_b}{V_a C^{\circ}_{a}}\;V_b\right] \qquad (1.2.11)$$

so that a plot of $1 / R$ vs V_b gives a straight line having a slope α ($\lambda_{M^+} + \lambda_{OH^-}$).

The ratio of the slopes of the descending and ascending branches of the titration curve would be expected to be given by,

$$\frac{\lambda_{M^+} - \lambda_{H^+}}{\lambda_{M^+} + \lambda_{OH^-}} \quad (= 1.21) \qquad (1.2.12)$$

with $\lambda_{Na^+} = 50.11$, $\lambda_{H^+} = 349.82$ and $\lambda_{OH^-} = 198.0$ [166].

A small concentration of OH^- and H^+ ions in solution just before and just after the equivalence point respectively make a contribution to the conductance, and were ignored in the derivation of the above equations, and cause a slight curvature near the equivalence point.

If a weak acid is titrated against a strong base then at the very beginning

$$HX + M^+ + OH^- \rightarrow H_2O + M^+ + X^-$$

and the resulting increase in the concentration of X^- decreases the concentration of H^+ by nature of the dissociation equilibrium,

$$HX \rightleftharpoons H^+ + X^-$$

Again a decrease in conductance is observed and the extent of the decrease depends on the pK_a of the weak acid, ie: the higher the pK_a the smaller the decrease for acids of the same concentration. As the titration proceeds the concentration of hydrogen ions is decreased to such a low level that its contribution to the conductance of the solution is negligible. Addition of further MOH adds M^+ and X^- ions and the conductance increases. Once the equivalence point is reached, the curve becomes identical with the strong acid/strong base curve.

End points cannot be accurately determined for acids with dissociation constants in the range 2×10^{-3} to 2×10^{-1} due to the equivalence point lying close to the minimum[227].

In the case of colloidal dispersions, including polymer latices, titration curves of the same general shape are observed but in the case of the strong acid neutralisation branch its slope is depressed 4 – 5 fold due to the limited mobility of counter ions in the electrical double layer[228]. Ratios of slopes of the order of 0.18 to 0.24 have been reported by Vanderhoff[199] for polymer latices and silver iodide sols.

The descending leg is linear when Na^+ counter ions are involved showing that Na^+ and H^+ ions are equivalent in the electrical double layer, but when Ba^{2+} ions are involved the innermost H^+ ions, which contribute least to the conductance, are first replaced by Ba^{2+}

ions and only later are the outermost, faster counter ions replaced so that a curved neutralisation branch results.

Latices show some polyelectrolyte type behaviour. Similar initial conductances may be found for latices having very different surface charge densities and hence equivalence points. Vanderhoff[181] has discussed the concept of the 'apparent degree of dissociation' α of the surface strong acid groups with α becoming smaller as the surface charge density becomes larger. Rice *et al*[229], have discussed the effect in terms of 'counter ion association' and Oosawa[230] in terms of 'counter ion condensation'.

Under the conditions normally employed conductometric titration on latices have been shown to be very reproducible. However, various parameters involved in the procedure have been studied[166]. The volume of latex titrated was varied in the range 10-50 cm^3 at fixed % solids (10%) with 0.1 mol dm^{-3} NaOH and gave end points agreeing to within 5%. The concentration of NaOH was varied in the range 10^{-3} mol dm^{-3} to 1 mol dm^{-3} using 10 cm^3 of latex at 10% solids and gave end points agreeing within 8%. When the % solids was varied from 10% to below 2% using 0.1 mol dm^{-3} NaOH and 10cm^3 sample volume, constant end points were found down to 2% solids but below the results became variable and difficult to interpret. Similar problems in performing titrations at low % solids have been reported by Everett and Gultepe[180] who ascribed irreproducibility of the weak acid end point to adsorbed CO_2 on the particle surface which degassing for 24 hours did not remove. Since gas adsorption experiments[231] on polystyrene latices had indicated that they absorbed CO_2 the effect of exposing a latex to CO_2 prior to titration was investigated. Although the latex was exposed to 1 atmosphere pressure of CO_2, i.e.: a much higher concentration than would ever be encountered on normal storage, it was found that

samples taken at intervals up to two weeks gave constant end points provided that they were well flushed with nitrogen prior to titration and that the end point was in agreement with that obtained prior to deliberate exposure to CO_2. Thus, flushing with nitrogen seems to be adequate for removing CO_2, at least at the % solids (8%) used in this experiment, i.e.well above the 2% solids levels at which irreproducibility had been observed.

Although titration procedures have been shown to be reproducible the titration curves can be difficult to interpret, particularly when low concentrations of weak acids are involved[232]. Thus, whereas strong acids such as hydrochloric can be titrated additively in the presence of a polymer latex which exhibits either strong or weak acid groups, weak acids such as benzoic do not appear to titrate as weak acid either in the presence of strong acid or in the presence of a latex exhibiting strong acid groupings unless their concentration is greater than 10^{-3} mol dm^{-3}. Benzoic acid in concentrations below 10^{-3} mol dm^{-3} had the effect of broadening the titration curves and leading to an apparent increase in the strong acid end point and it was impossible to identify a weak acid end point in order to distinguish the contribution from the benzoic acid.

Everett *et al*[166] have discussed the problem involved in interpreting titration curves where there is no straight line portion between the strong and weak acid end points, eg: for $pK_a < 5$[233]. The weak acid end point can be established if the concentration of the weak acid is greater than 1.5×10^{-2} K_a but if the condition is not met the interpretation in relation to both strong and weak acid is difficult[234]. The same authors also reported problems with the slopes of the ascending legs of titration curves. For dilute solutions of strong acids such as HCl or sulphamic acid the slopes were 15% below the theoretical value whilst for latices the ascending legs varied over ± 30% depending upon the latex concentration, electrolyte

concentration and cleaning procedure and were all substantially lower than for simple acid base titrations. These problems were attributed to adsorption effects.

James[235] concluded, from computer simulations of combined conductometric and potentiometric titration curves for two types of surface site, that if the concentration of either was low or if the difference between ionisation constants was low, then the distinction between surface sites would not be simple. With respect to conductometric titrations it was of note that the simulation suggested that sharper end points could be obtained in the presence of 10^{-3} mol dm^{-3} to 10^{-4} mol dm^{-3} background electrolyte due to the presence of excess Na^+ ions capable of exchanging with the surface protons to form SO_4^- Na^+ type sites.

Potentiometric titrations have been used on latex systems but the titration curves are more difficult to analyse than the corresponding conductometric titration curves[199]. Watillon[236] has described potentiometric titrations, which were completed in about 1 hour with no drift in pH taking place and equilibrium being obtained very quickly upon incremental addition of acid or base. Yates[226] found that after each addition of titrant the pH reached an essentially constant value almost immediately but it was observed that when the suspensions were left for long periods, at high degrees of dissociation, the pH decreased slowly. This was attributed to movement of surface groups to positions more favourable for ionisation. Laaksonen[225] found, using high precision potentiometry and data processing by computer according to the method of Sillen[237], that it was not possible, at least for latices with relatively low surface charges, to make a significant distinction between the effects of COO^- and SO_4^- groups on the binding of hydrogen ions from the small uncertainties in the equivalence point, the concentration of impurities and the diffusion potentials. Due to a

slow attainment of equilibrium, titration times of the order of 16 to 20 hours were employed.

Modern instrumental surface analysis techniques have been surprisingly little used in assessing the effectiveness of cleaning of latices and establishing surface functional group concentration. Weng *et al*[238] have considered XPS (X-ray Photoelectron Spectroscopy) ISS (Ion Scattering Spectroscopy) and SSIMS (Static Secondary Ion Mass Spectroscopy) and found results to be only semi-quantitative.

Whether or not weak acid carboxyl groups are to be expected when potassium persulphate is used as the polymerisation initiator was a matter dispute[162]. Chainey[239] and Kamel[169] showed however that if sodium bicarbonate buffer was used during the polymerisation then acid hydrolysis of sulphate groups to hydroxyl groups was avoided so that their oxidisation to carboxyl groups could not occur.

Whether or not a 'hairy layer' arising from functional end groups at the end of polymer chains being repelled from the particle surface into the aqueous phase causes latex particles to be less than ideal model colloids[240], requires further experimental investigation. Heating polystyrene particles above their *Tg* in a pressure cooker is believed to overcome the problem, by desorption or adsorption of the polymer chains, but hydrolysis of the sulphate groups[241] and particle destabilisation again complicate the analysis. Alternative explanations for the occurrence of anomalous maxima in electrophoretic mobility as a function of ionic strength, other than shear plane expansion as a consequence of the 'hairy layer' have however been proposed[242] including surface conductance effects or preferential ion adsorption. The effects of the 'hairy layer' are likely only to be significant for latices prepared in the presence of a functional co-monomer[243].

1.3 Stability of colloidal dispersions

1.3.1 Electrostatic stabilisation and the DLVO theory

1.3.1.1 Inherent particle properties[244]

The ability of a colloidal dispersion in a liquid medium to resist aggregation and remain in dispersion as discrete, single particles over time and upon changes to the dispersion medium, e.g. changes in temperature, addition of electrolyte, etc., is an important property of a particular dispersion.

The composition of the individual particles in a dispersion can have an important bearing upon its stability. For example, in the case of polymer latex particles, according to the arrangement of the polymer chains, the particles may be crystalline, amorphous, rubbery or glassy, also monomer may be retained by the particles, causing them to be swollen to some extent.

The surface properties of the particles have a significant effect upon the stability of the dispersion. In the case of polymer latices, these are governed by the preparative method employed. Varying the initiator used or the presence of adsorbed or grafted surfactants or polymeric species may give rise to surfaces that are smooth and charged, or possess charged or uncharged "hairy" layers of material.

1.3.1.2 The electrical double layer[244]

In the case of smooth, charged particles, the surface charges are in equilibrium with counter ions in both the inner and diffuse parts of the electrical double layer. Ion exchange techniques may be utilised in order to replace the counter ions in solution with H^+ or OH^- as appropriate. The surface charge density, σ_0, of the latex may then be estimated via conductometric or potentiometric titration (see section 1.2.9). σ_0 may be defined as,

$$\sigma_0 = N_S e v \qquad (1.3.1)$$

where N_S is the number of charged sites per unit area, v is their valency and e is the fundamental charge on an electron (1.6×10^{-19} Coulomb). Often, the surface groups are singly charged, for example SO_4^- or COO^-, and so v is 1. Areas are generally expressed in cm^2 or m^2. Typical values are of the order of μCcm^{-2}.

As a result, the surface has a potential, Ψ_0, relative to the bulk solution. This potential must be offset by an equal amount of opposite charge in the disperse phase in order to ensure electrical neutrality. The presence of charged species on the surface attracts counter-ions from the solution and, conversely, repels co-ions. The surface charge and the diffuse distribution of ions close to the surface is known as the electrical double layer. The inner region is regarded as a layer of hydrated counter-ions, and it's thickness is taken to be one hydrated ion radius δ. The diffuse electrical layer stretches out from this plane to a distance determined by the electrolyte concentration. As well as the surface potential, Ψ_0, the potential at the beginning of the diffuse layer, Ψ_S, is also an important quantity. Generally, considering this model, $\Psi_0 > \Psi_S$, though particles may possess a diffuse layer only, in which case $\Psi_0 = \Psi_S$. In general, the diffuse electrical layer determines colloid stability, though the inner layer may become more pertinent in

close-range interactions.

A Boltzmann equation may be used to represent the distribution anions and cations in the diffuse layer. For low potentials (Ψ_S < 25mV), a first approximation for the potential at a distance x from the surface may be obtained from the equation[245]

$$\Psi_x = \Psi_S \exp(-\kappa x) \quad (1.3.2)$$

and, for a spherical particle of radius R, at a distance r from the centre of the particle,

$$\Psi_r = \Psi_S R/r \exp[\kappa(R-r)] \quad (1.3.3)$$

It is clear that the fall of potential with distance from the surface is exponential and the parameter κ determines this rate of fall, which may be related to the electrolyte concentration by

$$\kappa^2 = 2 n_0 v^2 e^2 / \varepsilon_r \varepsilon_0 kT \quad (1.3.4)$$

where n_0 is the number of each type of ion in the bulk phase per unit volume, v is the valency of the ions (assuming a symmetrical electrolyte), ε_r is the relative permittivity of the solution phase and ε_0 is the permittivity of free space. k is the Boltzmann constant and T the absolute temperature.

κ has the dimensions of reciprocal length, and a distance of $2/\kappa$ from the surface gives a useful approximation of the extension of the electric field from the surface. Hence, the electric fields of two approaching particles begin to overlap at a distance of $4/\kappa$. For example, in a solution of a 1:1 electrolyte of concentration 10^{-5} mol dm^{-3}, $1/\kappa$ = 100nm, and so electrostatic interaction would begin at a separation of approximately 400nm, whereas in a 0.1mol dm^{-3} solution, $1/\kappa$ is just 1nm.

The theoretical quantity Ψ_S is difficult to determine; however a similar quantity, zeta-potential, may be determined from electrokinetic experiments. For example, the

electrophoretic mobility, u, may be determined by either micro-electrophoresis or moving boundary methods[128]. The zeta-potential, ζ, may then be determined using the expression

$$u = \frac{\varepsilon_r \varepsilon_0 \zeta}{\eta} f(\kappa R, \zeta) \qquad (1.3.5)$$

where η is the viscosity of the medium and $f(\kappa R, \zeta)$ is a numerical value obtained from the literature[128, 246, 247]. Many of these important quantities may be represented schematically (Figure 1.3.1).

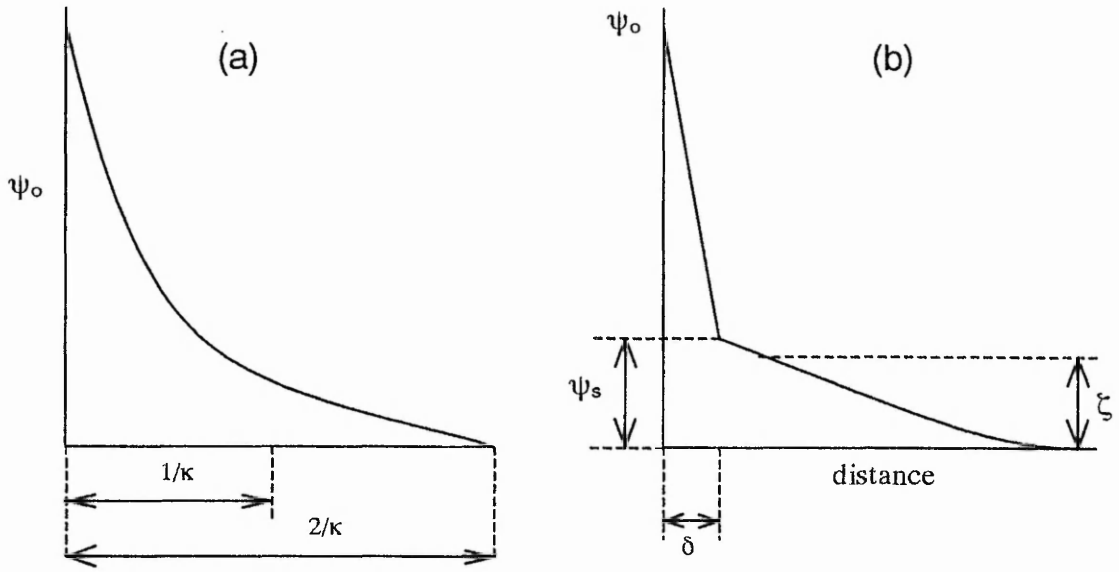

Figure 1.3.1 (a) diffuse electrical double layer (b) inner layer plus diffuse layer.

1.3.1.3 Electrostatic interaction between two surfaces

As two particles approach, repulsion will be experienced when the diffuse counter-ion layers begin to overlap at a separation of $4/\kappa$. The interaction between two flat plates is much easier to study than between spheres. When two plates, with the same diffuse double

layer potential Ψ_S, interact, the excess osmotic pressure, P, may be determined from the expression[128]

$$P = 64\, n_0\, kT \left[\frac{\exp(ve\,\Psi_S / 2\,kT) - 1}{\exp(ve\,\Psi_S / 2\,kT) + 1} \right]^2 \exp(-\kappa h) \qquad (1.3.6)$$

here h represents the separation of the plates. This relationship demonstrates the dependence of the interaction upon Ψ_S and on the ionic strength of the dispersion medium through n_0 and κ.

The analogous equation determining the force of interaction, F_{el} between a flat surface and a sphere of radius, R, for the condition $h > 2/\kappa$ may be written

$$F_{el} = \frac{2\,\pi\, R\, 64\, n_0\, kT}{\kappa} \left[\frac{\exp(ve\,\Psi_S / 2\,kT) - 1}{\exp(ve\,\Psi_S / 2\,kT) + 1} \right]^2 \exp(-\kappa h) \qquad (1.3.7)$$

which also represents the equivalent geometry of the interaction between two cylinders of radius R. This equation has been tested experimentally[248, 249]. F_{el} may be measured using a transducer and the surface separation, h, may be determined using a multiple beam interferometer[250]. Figure 1.3.2 represents plots of $\ln[F_{el} / 2\pi R]$ obtained in 10^{-3} and 10^{-2} mol dm^{-3} potassium chloride. Rearrangement of equation (1.3.7) gives,

$$\frac{\ln F_{el}}{2\pi R} = \frac{\ln\, 64\, n_0\, kT}{\kappa} \left[\frac{\exp(ve\,\Psi_S / 2\,kT) - 1}{\exp(ve\,\Psi_S / 2\,kT) + 1} \right]^2 (-\kappa h) \qquad (1.3.8)$$

and so κ may be obtained from the gradient of the line and, since the electrolyte concentration is known, Ψ_S may be calculated from the intercept. Table 1.3.1 provides a summary of the results obtained, together with some calculated values.

Experimental and theoretical values proved to be reasonably concordant at distances of separation $h > 2/\kappa$ and therefore the electrostatic repulsion, and hence stability, is dependant upon the overlap of the diffuse double layers of particles. The values of Ψ_S have also been shown to be similar to measured values of zeta-potential[251].

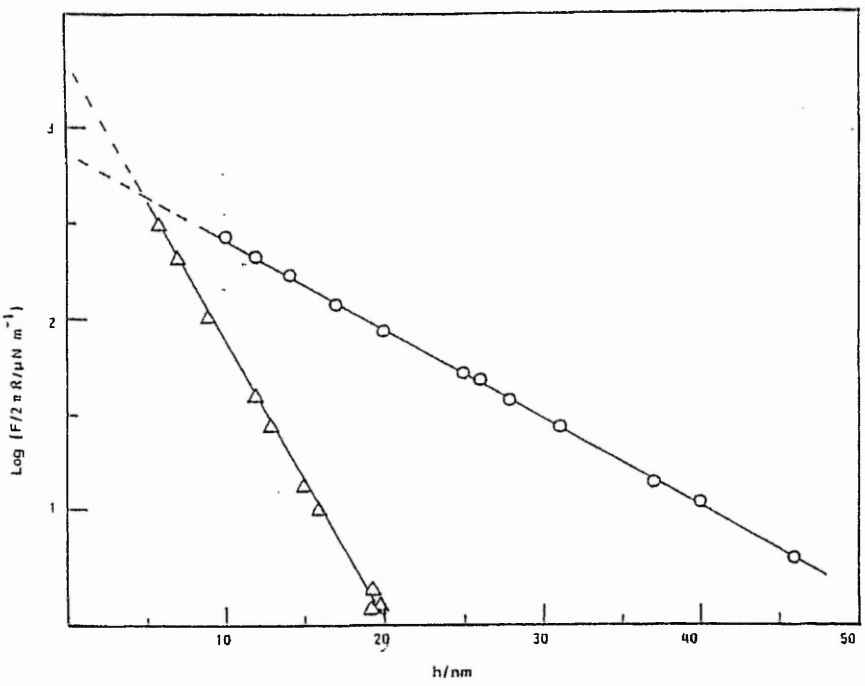

Figure 1.3.2 Ln[F_{el} / $2\pi R$] versus h for mica surfaces in potassium chloride solution (mol dm-3); (O) 10^{-3}, (△) 10^{-2}.

Potassium Chloride Concentration / mol dm^{-3}	$(1/\kappa)$ / nm experimental	$(1/\kappa)$ / nm calculated	Ψ_S / mV experimental
10^{-4}	32.0	30.40	80
10^{-3}	9.6	9.62	84
10^{-2}	3.5	3.04	79
10^{-1}	1.2	0.96	89

Table1.3.1 Determination of Ψ_S and κ by direct and experimental methods

By integration of the force of repulsion between two flat plates with respect to distance, we can obtain an expression for the potential energy of electrostatic repulsion,

$$V_R = \frac{64\, n_0\, kT}{\kappa} \left[\frac{\exp(ve\,\Psi_S / 2\,kT) - 1}{\exp(ve\,\Psi_S / 2\,kT) + 1} \right]^2 \exp(-\kappa h) \qquad (1.3.9)$$

For spherical particles, several expressions may be used according to the value of κR,

for $\kappa R < 3$,

$$V_R = 4\,\pi\,\varepsilon_r\,\varepsilon_0\,\Psi_S^2\,R^2 \exp(-\kappa h) \qquad (1.3.10)$$

for $10 < \kappa R < 3$, Reerink and Overbeek[252] suggested the expression,

$$V_R = 4.36 \times 10^{20}\, \varepsilon_r\, \varepsilon_0 (kT)^2 \left[\frac{\exp(ve\,\Psi_S / 2\,kT) - 1}{\exp(ve\,\Psi_S / 2\,kT) + 1} \right]^2 \exp(-\kappa h) / v^2 \qquad (1.3.11)$$

and for $\kappa R > 10$,

$$V_R = 2\,\pi\,\varepsilon_r\,\varepsilon_0\,\Psi_S^2\,R \ln[1 + \exp(-\kappa h)] \qquad (1.3.12)$$

1.3.1.4 Attractive interactions between surfaces

An approximate expression for the potential energy of attraction, V_A, between two "thick" flat plates of material 1 immersed in a liquid of material 2 may be written[245, 253],

$$V_A = - \frac{(A_{11}^{1/2} - A_{22}^{1/2})^2}{12 \pi h^2} \qquad (1.3.13)$$

where A represents the Hamaker constant appropriate to the particular material. A may be obtained from the expression,

$$A = 3 \pi^2 h_p \nu_0 \alpha_E^2 q^2 /4 \qquad (1.3.14)$$

in which h_p represents Planck's constant, ν_0 is the dispersion frequency, α_E is the electronic polarisability and q is the number of atoms (or molecules) per unit volume.

Expression (1.3.13) may lead to an approximate expression for the case of two spherical particles[253],

$$V_A = - \frac{(A_{11}^{1/2} - A_{22}^{1/2})^2 R}{12 h} \qquad (1.3.15)$$

$(A_{11}^{1/2} - A_{22}^{1/2})^2$ may be regarded as the composite Hamaker constant for the particular system and may be replaced by the symbol A_C.

1.3.2 The effects of dissolved polymer on dispersion stability

The effect of polymer adsorption on colloid stability is much more complex than that of simple electrolytes. Unlike the latter's charge destabilising effect, polymers may produce stabilising or destabilising effects depending upon the nature of both the polymer and particle, the relative amounts of each and even upon such factors as the method of mixing and the nature of the dispersion media. Non-adsorbing polymers may even effect the stability of a particulate dispersion and these are generally known as depletion effects (flocculation and stabilisation).

1.3.2.1 Polymer adsorption

It may be assumed that to some extent, any polymer may adsorb on any surface. This is because, generally speaking, at any moment in time there are many points of contact between polymer and surface and so only a small binding energy is needed per polymer repeat unit for the polymer to remain in contact with the surface, effectively irreversibly[254]. In practice, adsorption onto a surface may be unfavourable if the polymer's affinity for the surface is no greater or less than its affinity for the solvent. For example, the adsorption of a negatively charged polymer onto a negatively charged surface is unfavourable due to electrostatic repulsion. Other factors however may facilitate adsorption. e.g. in the above case, multivalent metal cations may anchor the polymer to the surface[255].

In general it must be assumed that adsorption is irreversible with respect to dilution[255]. This irreversibility may be important, as the adsorption behaviour will also depend upon the history of the system. Therefore, for example, the procedure of polymer

adsorption is important.

After the initial stages of the adsorption of a polymer onto a particle, the main contribution to the amount of polymer adsorbed (Γ_p) is made up of polymer segments not directly adsorbed onto the surface, rather they extend into the solution in the form of loops and tails (Figure 1.3.3) while the chain is anchored to the particle by relatively few segments.

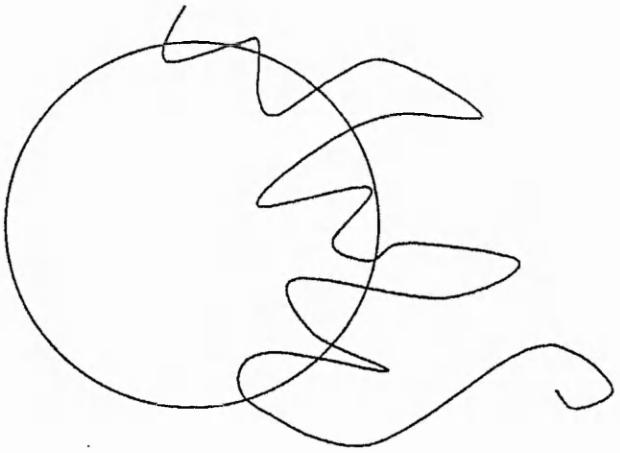

Figure 1.3.3 The adsorption of polymer onto a particle producing loops and tails extending into the solution.

Γ_p increases with decreasing solvent quality as in a poor solvent, the segments are less likely to become solvated and more likely to pack closely together.

1.3.2.2 Colloid stabilisation due to adsorbed polymers

Colloid stability may be increased due to the effects of one or all of the following:

- A decrease in the van der Waals' forces of attraction.
- An increase in the electrical repulsion between particles.
- The introduction of a steric component to repulsion.

When a polymer is acting to stabilise a system, it is often termed 'protection'.

The *polymeric* nature is not essential in any of the stabilising mechanisms, indeed relatively small molecules, most notably surfactants, produce similar effects. Polymers however produce some of the most marked effects due to the greater depth of the adsorbed layers produced.

1.3.2.3 Effect upon electrical interaction between particles

Clearly polymers will have greatest effect in this respect if they contain ionised groups (i.e. they are polyelectrolytes). If the polymer carries the opposite charge with respect to the particle, for example a positively charged chitosan molecule interacting with a negative polystyrene particle, then the polymer acts to decrease the electrical repulsion between colloidal particles until flocculation results. This effect will be discussed presently. When polymer and particle carry like charges, repulsion is increased and the stability of the dispersion is increased. Anionic polymer and particle systems are the most commonly encountered, and the effect in this case has been explained at least qualitatively in terms of the DLVO theory[256]. Even a non-ionic polymer may effect electrical interaction and consequently stability, though obviously to a much lesser extent. The most significant effect in this case is the physical displacement of counter ions from the Stern Layer[257]. Hence the diffuse layer is shifted further from the particle and, for a given inter-particle distance, the overlap between neighbouring particle's diffuse layers would increase, increasing repulsion and therefore stability. However, non-ionic polymers may also act to decrease colloidal stability by a process known as 'sensitisation', which is usually brought about by a reduced surface charge e.g. by displacement of water from the surface in aqueous media.

1.3.2.4 Effect on van der Waals' forces of attraction

The effect of adsorbed polymer on the van der Waals' forces is somewhat complex. Vold[258] postulated that adsorption of polymer onto colloidal particles works to *increase* attraction due to van der Waals' forces thereby *decreasing* colloidal stability. If the distance between the centres of adjacent spheres, R_c, is held constant then the addition of polymer to the surfaces of the spheres will reduce the inter-particle distance between the surfaces, h , and hence in general will lead to increase in the van der Waals' forces. This effect though is now rarely thought to contribute significantly to the stability of a given system.

It is of greater relevance to consider the case where the inter-particle distance, h, is held constant with increasing polymer adsorption. This consideration means that the centres of the original spheres become progressively further apart with increasing polymer thickness. Since the adsorbed material usually possesses a much lower Hamaker Constant than the original spheres, the van der Waals' forces of attraction are progressively reduced with increasing polymer layer thickness. This "*Core Spacing Effect*" was examined by Osmond[259] in a reappraisal of Vold's work.

1.3.2.5 Steric stabilisation

The effects of increased electrical repulsion and decreased van der Waals' attraction forces are not always sufficient to explain the increased stability of a given colloidal dispersion due to the adsorption of a polymer. The stabilising effect may also be attributed to an additional interaction known as "*Steric Repulsion*" or "*Steric Stabilisation*". Steric stabilisation arises from interaction between adsorbed polymer layers and is generally explained via one of two mechanisms.

(i) Compression

Upon collision between two polymer-coated particles, the adsorbed polymer layers may compress. This restriction of the polymers causes a decrease in entropy, and in turn a corresponding increase in free energy, and hence repulsion.

(ii) Interpenetration

Upon collision, the adsorbed polymer layers overlap. This means that the concentration of polymer segments between the particles is increased. This may lead to repulsion or attraction depending upon the nature of the polymer-solvent interaction (see below).

Of the above mechanisms, *Interpenetration* is more likely to predominate, probably with some degree of compression inherent in it.

In general, particle-particle repulsion due to steric stabilisation is maximised when the disperse phase is a good solvent for the stabilising polymer chains. In this case overlap of the polymer layers is undesirable as the chains 'prefer' to be in the solvent environment and overlap of polymer layers hence leads to an increased free energy of the system and so repulsion. In this case, polymer layer compression would be relatively unimportant as a stabilising process as particles would not approach close enough for a significant degree of compression to occur. If the quality of the solvent is progressively lowered by change in temperature or by addition of particular solutes then the surface free energy of interaction may be lowered. The point at which polymer segments can mix with no increase in surface free energy is known as the *THETA CONDITION* and the corresponding solvent composition or temperature is prefixed by θ. At this point, there is still some degree of

stabilisation due to polymer compression. Beyond the Theta condition, mixing of polymer segments is favoured leading to attraction between surfaces, this process being known as '*incipient*' flocculation, as the solvent quality of the disperse phase towards the adsorbed polymer is reduced further.

The above arguments rely only on a simplified situation, i.e. that of terminally adsorbed polymer chains, and also simplify matters by assuming a uniform polymer segment density over the surface of the particle[260]. More complex arguments, including segment density functions[261], seem to compare favourably with the limited experimental data available[262]. Napper et. al.[263] reported that steric stabilisation of this type is effective in disperse phases of considerably worse than the θ condition, although the reason for this was not immediately obvious. In practical cases, for the adsorbed polymer layers to produce effective stabilisation, they must be of sufficient thickness to prevent particles from approaching close enough for van der Waals' forces to become significant. A well solvated polymer layer may be considered to have a Hamaker constant comparable with the dispersion medium implying that it acts only as a steric barrier[264]. In general, four factors must be considered when dealing with the stability of such polymer-coated particles.

(i) The size of the particles.

(ii) The (effective) Hamaker constant of the particles.

(iii) The thickness of the adsorbed layer.

(iv) The solvation of the adsorbed polymer.

Figure 1.3.4 shows schematically for a given particle size, Hamaker constant and a well solvated polymer layer of thickness Δ, the qualitative effect of adsorbed polymer layer thickness (where V_A is energy of attraction and V_T is the total interaction energy). Considering the effect of particle size, in general, for an adsorbed layer thickness Δ, van der Waals' attraction at inter-particle distance 2Δ increases with increasing particle size. The apparent need for thicker stabilising layers for larger particles has been shown experimentally[264].

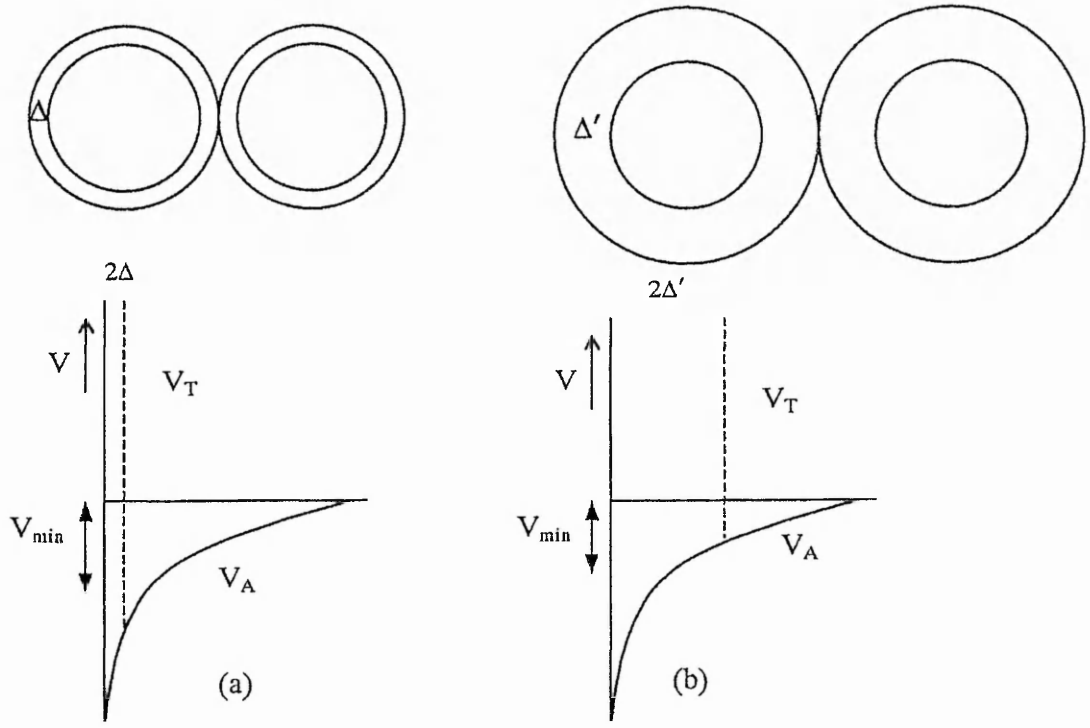

Figure1.3.4 The effect of adsorbed polymer layer thickness on attraction between particles

If the adsorbed layer is relatively thin, as in Figure 1.3.4 (a) above, then the particles may approach close enough to be held in a deep van der Waals' energy minimum i.e. the dispersion is unstable. In the case of Figure 1.3.4 (b), for a much deeper layer, thickness Δ′, protection against flocculation is much more complete. For polymer layers of a depth intermediate between these extremes, the particles may be held in a shallow

van der Waals' minimum, i.e., unstable but relatively easy to re-disperse. This may well be more desirable over (b) in a practical system as it produces a weakly flocculated structure, which is easy to re-disperse by agitation. Unflocculated systems, represented by case (b), tend to sediment producing a compact layer of particles, which is often difficult to re-disperse.

Steric stabilisers are particularly useful in non-aqueous systems where charge stabilisation is not effective. In aqueous systems they are useful at high particle concentrations. Electroviscous effects mean that these types of dispersions are generally very viscous. Addition of electrolyte alleviates the problem but of course also causes particle aggregation. Steric stabilisation means that electrolyte addition may be tolerated and dispersions with high solid content may be utilised without the limitations that high viscosity imposes.

1.3.2.6 Polymeric flocculants

Polymeric flocculants tend to be simple, high molecular weight homopolymers or random copolymers and are often polyelectrolytes. Early examples of polymeric flocculants included alginates and gelatine, some of which are still widely used. Latterly however these naturally derived flocculants have been largely superseded by synthetic polymers, which can offer advantages such as higher molecular weights and the control of chemical and physical properties. However, due to the use of polymeric flocculants in the water and food industries, one major concern is the potential toxicity of a synthetic polymer. In general, the polymers themselves have toxicities low enough to render them irrelevant. However synthetic polymers may contain significantly high proportions, up to several percent,

of unreacted monomer, which presents a greater health risk. Potable water grades of flocculants are required to contain less than 0.05% monomer[257]. Of course use of natural polyelectrolytes such as chitosan and other cellulose-based flocculants circumvents this problem. Naturally derived flocculants also avoid problems of non-biodegradability.

Anionic, cationic, non-ionic and amphoteric flocculants may be employed according to the nature of the dispersion conditions and properties but, however, these factors may not preclude the use of a particular flocculant. La Mer[265], for example, studied the flocculation of an anionic silica suspension by both anionic and cationic flocculants. Destabilisation of the system generally required the addition of a greater quantity of anionic flocculant than cationic flocculant. It was reported that whilst the anionic polymers were only effective flocculants at molecular weights above approximately 10^6, cationic polymers with molecular weights down to few thousand were capable flocculants.

Many polyelectrolytes contain weakly ionic groups such as carboxyl or tertiary amine, so that the pH of the media effects the charge density and hence flocculation behaviour (and also solubility). Polyelectrolytes that contain more strongly ionic groups, such as quaternary ammonium or sulphate groups, tend to be less sensitive to pH effects.

Accurate characterisation of the polyelectrolyte is essential if the precise flocculation process is to be understood. Size and shape of the molecule in solution is of obvious importance. Light scattering and viscosity measurements are often used in molecular mass determination, however these are not always trustworthy depending upon the shape of the polymer in solution. Determination of the linear charge density is also of great importance.

A particular problem with many such molecules, especially higher molecular mass polymers, is that they are difficult to dissolve and many may require vigorous agitation, but chain scission may result if the agitation proves too vigorous. Another problem with higher molecular mass polymers is 'ageing' effects in solution, for example by the slow disentangling of polymer chains[266].

1.3.2.7 Modes of flocculation

The flocculation of colloidal dispersions by polyelectrolytes may follow one of three generally recognised mechanisms: *Inter-particle Bridging*[267], *Charge Neutralisation*[268, 269, 270, 271] or *Depletion Flocculation*[272], or aggregation may be brought about by a combination of several of these processes.

(i) Bridging flocculation

Bridging flocculation was perhaps the earliest mechanism of flocculation proposed, and has been invoked in descriptions of aggregation in systems by both neutral polymers and polyelectrolytes bearing the same charge as the dispersion. Ruehrwein and Ward[273] suggested in 1952 that flocculant molecules may be of comparable size to colloidal particles and hence one polymer molecule adsorbs onto the surface of more than one particle thereby bridging them. This idea was extended by Michaels[274] in a study of the flocculation of silt and clay suspensions by polyacrylamide polymers to include the effects of molecular weight and charge density of the polyelectrolyte, and in doing so determined that particular values were important in the optimisation of flocculation. The inference made was that increasing the charge density causes the folded polyelectrolyte chain to expand due to charge repulsion thereby forming a more effective bridge, but as charge density is increased it becomes

less favourable for the negatively charged chain to adsorb onto the negatively charged particle. Therefore some intermediate point is reached where the charge density is optimised for flocculation. Michaels' paper also proposed that an optimum flocculant concentration might be reached after which flocculation efficiency falls off. This corresponds to re-stabilisation of the particles as they become saturated with flocculant and eventually steric stabilisation is effected.

La-Mer and co-workers extended the work to other polymer-particle systems[265] and came to broadly similar conclusions concerning the optimisation of flocculation behaviour. La-Mer's work also sought to surpass these simple conclusions with an attempt to develop a quantitative theory for bridging flocculation. La-Mer considered that bridging efficiency was related to the *fractional coverage*, f, of the particle's surface by polymer segments. The work concluded that as areas of the particle's surface were required to be vacant for bridging to take place, then the optimum condition for flocculation occurred when the term: f(1-f) was at a maximum, i.e. f = 0.5, 'half surface coverage'. However, the precise meaning of the term 'half surface coverage' is ambiguous as it depends upon the nature and configuration of the adsorbed polymer.

For bridging flocculation to occur, the affinity of polymer for particle should not be too strong, ensuring that a relatively small proportion of segments are attached and so leaving the majority of the polymer's chain to form loops and tails extending away from the particle. Even a small number of adsorbed segments should ensure irreversible adsorption. In general, oppositely charged polymers are adsorbed too strongly to affect equilibrium bridging flocculation and different mechanism of flocculation must be considered (see section 1.3.2.7 (ii) below).

For charged particles to be bridged in this way, then the loops and tails of the adsorbed flocculant molecule must stretch over a distance greater than the distance over which electrostatic repulsion operates. This distance may generally be assumed to be twice the diffuse layer thickness for the particles[275]. This situation is of course dictated by the ionic strength of the solution. In the case of non-ionic flocculants, flocculation efficiency may be simply increased by increasing ionic strength, thereby compressing the double layer[276,268]. More complex behaviour is observed when a polyelectrolyte is used[257], as the ionic strength not only affects the double layer of the particle, but also screening of the charge on the polyelectrolyte may result in a less extended chain and hence less efficient bridging. If the ionic strength is modified using multivalent counter-ions then, in the case of like polymer/particle charges, sensitisation (attachment of like charged polymer to particle by a counter ion "bridge") will be increased and hence increase the tendency toward inter-particle bridging.

(ii) Particles and polymer of opposite charge

Polymers bearing a charge opposite to that present on the particles tend to interact too strongly for simple bridging to dominate. Such polyelectrolytes are believed to be strongly adsorbed to the surface and lie in a relatively flat configuration[271], close to the surface rather than extending into the media, a conclusion which has been used to discount bridging as a mechanism in such cases[271]. Polyelectrolytes are quantitatively adsorbed onto oppositely charged sols, at least up until the point of flocculation[277,270], which suggests that a simple charge neutralisation mechanism, as may be expected with salts or surfactants, may be in operation. Gregory[269] however pointed out several difficulties with this conclusion.

Firstly, it was observed that the critical flocculation concentration of a polymer in a particular system was unaffected by the molecular weight of the polymer and secondly, a greater flocculation rate was displayed than that of simple coagulation. Bridging was discounted as there was a significant increase in flocculation rate over rapid coagulation rate, even when the polymer in question was of a molecular weight too low to produce significantly large loop dimensions for efficient bridging. Additionally, the molecular weight of the polymer had relatively little effect upon the optimum flocculation rate. These effects were instead explained via a "*Charge-Patch*" mechanism[271]. Considering the average distance between adjacent charges on the surface of a particle and on a flocculant molecule, the charges on the flocculant were found to be much closer together. Therefore when a flocculant molecule is adsorbed, it may be assumed that all the charges it possesses are not discharged, setting up a region, or patch, of opposite charge on the surface (Figure1.3.5). Coulombic attraction between oppositely charged patches on adjacent particles would then explain the increased flocculation rate over simple coagulation whilst the system overall is electrically neutral. The range of this extra attractive force should decrease with increasing ionic strength, due to charge screening, until the flocculation rate is no higher than the coagulation rate produced by simple electrolyte or surfactant. Under these conditions, the breadth of the flocculation region should also increase as simple coagulation plays an increasing role around the region of instability.

(iii) Depletion effects

Regions of instability and re-stabilisation may also be conferred at much higher flocculant concentrations by non-adsorbing polymer in solution[272]. These are known as depletion flocculation and stabilisation respectively and are generally explained in terms of osmotic effects produced by the flocculant in solution. For chitosan however at the concentrations that would be required to produce these effects, up to $1gl^{-1}$, the viscosity of the system is so great that it renders its part in a practical study impracticable.

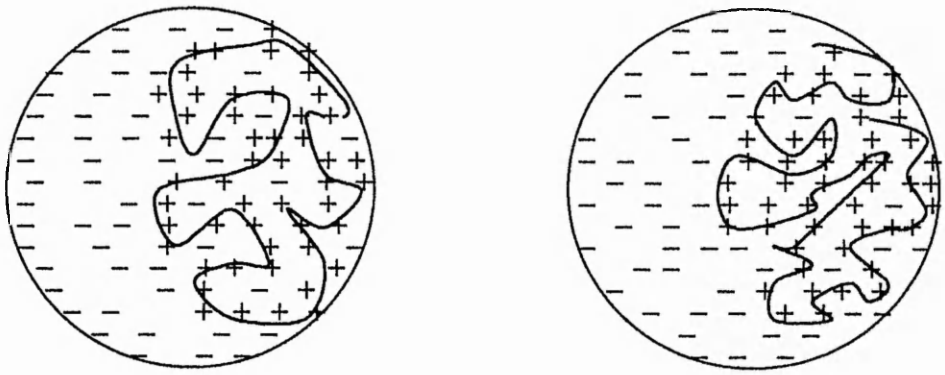

Figure 1.3.5 The formation of oppositely charged patches on the surface of latex particles

1.3.3 Techniques for assessing the state of a dispersion

1.3.3.1 Introduction

Estimating the extent of flocculation or coagulation depends on measuring some suitable property of either the total system (for example light scattering, rheology or electrical conductivity), or the supernatant above the aggregates (e.g. light scattering), or of the aggregates themselves (e.g. sedimentation rate or volume). Measurements may be taken after some arbitrary time or continuously as a function of aggregation time to form kinetic studies[269, 278, 279]. Rate constants probably form the best basis for comparison of aggregation conditions. Absolute rate constants may be obtained from particle counting techniques such as optical and electron microscopy, Coulter, ultramicroscopic techniques and centrifugal particle counters. Comparative rate constants may be obtained by other methods, notably light scattering. It may be argued that the large open structured aggregates formed in flocculation render light scattering studies invalid, though data obtained at the beginning of the flocculation process, i.e. that representing the formation doublet, triplets etc, may still be useful for simple comparison[268].

1.3.3.2 Particle counting

(i) Microscopic methods

Absolute rate constants may be determined by methods that can provide data on the total concentration of all aggregates or the individual concentration of each aggregate size as a function of aggregation time. Direct techniques, such as optical and electron microscopy, may be time consuming, though it is possible to automate the process.

However, the use of electron microscopy is impeded by any tendency of the particles to aggregate, or aggregates to break up, upon evaporation of the solvent.

(ii) Zone sensing particle counters

Indirect particle counting methods tend to be less tedious. For example, Coulter counters[280] can count around 10^4 particles per second. Their operating principle is based on monitoring the electrical resistance of an electrolyte solution, passing through an orifice. When a particle passes through the orifice, the resistance is affected and a voltage pulse is observed. As most particles' resistance can be assumed to be infinite compared to the electrolyte, the size of the pulse may be related to particle volume. They do however have the disadvantages of being limited to dispersions of particle sizes generally in excess of 1μm, or requiring large dilutions (to around 10^6 particles per ml) and requiring the presence of electrolyte to increase electrical conductivity of the dispersion. Both these latter factors may of course alter the state of the dispersion themselves. One other potential problem is that aggregates may be disrupted on passing through the orifice. This has been refuted by Schyluk and Smith[281] who claimed that flocs in their system were strong enough to withstand this. If aggregates do break up during their passage through the orifice, then the sum of the volumes of the smaller particles formed should be the same as that of the original aggregate and so, as they pass through orifice together, they should produce a pulse equivalent to that of the original aggregate. More troublesome may be the breakage of flocs in the elongational flow field immediately before the orifice, which would then imply that several smaller pulses would be observed.

The use of the Coulter technique in the study of aggregation kinetics was first reported by Matthews and Rhodes[282, 283] in which they considered the coagulation of latex particles.

1.3.3.3 Light scattering

Light scattering methods may be used to monitor aggregation without disturbing the system. Although absorption of the incident light may be involved, and even utilised industrially, it is often more useful to consider wavelengths at which only scattering takes place.

(i) Turbidity[284]

The simplest and one of the most widely used techniques is the comparison of turbidities. All solutions scatter light, and therefore appear turbid, to some extent (the Tyndall effect), but in colloidal solutions this is notably pronounced. The turbidity of a system may be represented by,

$$I / I_0 = \exp(- \tau L) \qquad (1.3.16)$$

where I and I_0 are the transmitted and incident light intensities respectively, L is the sample path length and τ is the turbidity. The turbidity τ of a system is dependent upon the nature and size of the particles and the particle concentration.

So, comparing the flocculation in a set of systems may be achieved by comparing the turbidity at some set wavelength after an arbitrary period of time. However, the change in turbidity with particle size may not be uniform[285], unless spherical aggregates

are formed, as the scattering behaviour of the aggregates becomes more complex. Problems may also occur as large flocs begin to sediment out of the light beam. For these reasons, aggregates in the system may be deliberately removed by centrifugation[163, 276] then, assuming that only singlet particles remain dispersed, the turbidity of the supernatant may be used as a measure of unflocculated particles. The definition of the residual turbidity at which the system is considered to be flocculated is somewhat arbitrary, but if reasonable flocculation time-scales and centrifuge speeds are chosen, the boundary between aggregated and unaggregated systems should be clearly defined.

While absolute rates can only be obtained for particles where Rayleigh theory applies (i.e. of a particle size much smaller than the wavelength of light) the initial increase in turbidity displayed by an aggregating systems may be used to compare aggregation rates with rates of rapid coagulation and, hence, derive stability ratios. Rapid mixing techniques are required in aggregation studies, e.g. the stopped-flow technique[276,286,].

(ii) Static light scattering techniques

As well as monitoring the light transmitted through a dispersion, measurement of the intensity, polarisation and angular distribution of light scattered provides information on the state of the dispersion.

For particles much smaller than the wavelength of light (<10%), Rayleigh theory may apply. From Rayleigh theory, equation (1.3.17) may be derived which shows that the light

$$\frac{I_\theta}{I_0} = \frac{1}{r^2}\left[\frac{8\pi^4 a^6}{\lambda^4}\left[\frac{m^2-1}{m^2+2}\right]\right]^2 (1+\cos^2\theta) = \frac{R}{r^2} \qquad (1.3.17)$$

scattered by a particle varies as the sixth power of particle size (a) and the square of the particle volume. Hence, in a flocculating system, if the total particle volume remains constant, the scattered light intensity should increase with increasing mean particle size. However the small particle sizes required for the theory to hold limit the practical application of Rayleigh theory.

(iii) Photon Correlation Spectroscopy (Dynamic Light Scattering techniques)[287, 288]

The intensity of laser light scattered by particles moving under Brownian motion fluctuates producing a speckled pattern. These fluctuations are dependant upon particle speed and hence the diffusion coefficient, D, of the particles. D may then be related to particle diameter by the Stokes-Einstein equation.

The technique may be known as photon correlation spectroscopy (PCS), quasi-elastic light scattering (QELS) as well as dynamic light scattering (DLS) and may be used to estimate particle sizes up to several microns in diameter[288] and has been used to study the rates of coagulating latex dispersions[289, 290], as well as several inorganic dispersions[291, 292].

1.3.3.4 Settlement rate, sediment volume and filtration

As a flocculating system settles, a clear boundary is formed between the flocs and the supernatant above. The rate of change of boundary height with time may be used as a

measure of the extent of flocculation. Empirical equations relating boundary height to time have been produced[293].

In contrast to stable dispersions, which tend to sediment to form close-packed structures of low volume, the sediment of aggregated systems is much less dense and so may provide useful information about the state of aggregation. The sediment volume, measured after some appropriate time period, may be used to compare different aggregation regimes, though the time-scales involved in reaching equilibrium may be prohibitive.

A simple procedure of sieving out flocs and coagulum may be employed, however La Mer *et al*[293,294] devised a system where the flocs themselves, supported on some substrate, were employed as the filter bed and the filtrate was then re-passed through the bed. Generally speaking, they found that greater degrees of flocculation commanded shorter refiltration times.

1.3.4 Kinetics of aggregation

Smoluchowski[330] considered a dispersion of identical spherical particles which aggregated to give n_i particles of size i, n_j particles of size j, etc, where n is the number of particles per unit volume and the size is the number of primary particles in the aggregate. Aggregation was considered to be a second order process with a rate of collision proportional to the concentration of colliding species.

The number of collisions in unit time per unit volume is given by,

$$J_{ij} = k_{ij} n_i n_j \qquad (1.3.18)$$

For k-fold aggregates where k = i + j. The rate of change of concentration is given by[285],

$$\frac{dn_k}{dt} = \underbrace{\frac{1}{2} \sum_{i=1}^{i=k-1} k_{ij} n_i n_j}_{\text{Formation}} - \underbrace{n_k \sum_{i=1}^{\infty} k_{ik} n_i}_{\text{Loss}} \qquad (1.3.19)$$

The factor ½ is included to avoid counting each collision twice. For perikinetic aggregation, brought about by Brownian motion, Smoluchowski calculated the rate of diffusion of spherical particles i towards a fixed sphere j. In the steady state,

$$J_i = 4 \pi R_{ij} D_i n_i \qquad (1.3.20)$$

Where R_{ij} is the collision radius taken as the sum of the particle radii.

$$\text{When } k_{ij} = \frac{2kT}{3\mu} \frac{(a_i + a_j)^2}{a_i a_j} \qquad (1.3.21)$$

where μ is the viscosity of the dispersion medium.

$$\text{If } a_i \approx a_j, \quad \text{then } (a_i + a_j)^2 / a_i a_j \approx 4 \qquad (1.3.22)$$

$$\text{And so } k_{ij} = \frac{8kT}{3\mu} \qquad (1.3.23)$$

i.e. k_{ij} is independent of particle size.

Considering only the early stages of aggregation, the rate of change of the singlet population can be calculated from the right hand term only in equation (1.3.19) giving the loss of singlets,

$$\left[\frac{dn_1}{dt}\right]_{t\to 0} = -k_{11} n_1^2 \qquad (1.3.24)$$

or, for total particle concentration,

$$\left[\frac{dn_T}{dt}\right]_{t\to 0} = \frac{-k_{11} n_1^2}{2} \qquad (1.3.25)$$

and this can be integrated to give,

$$n_T = \frac{n_0}{1 + k_a n_0 t} \qquad (1.3.26)$$

where $k_a = 4kT / 3\mu$

The half life for aggregation will occur when $t = T_{1/2} = 1 / k_a n_0$ (1.3.27)

Or:

$$n_T = \frac{n_0}{1 + t / T_{1/2}} \qquad (1.3.28)$$

This equation assumes that all k_{ij} values are constant and that all particles including aggregates are spherical. The equation is regarded as an acceptable approximation if the diffusion coefficient for aggregation decreases at about the same rate as the collision radius of aggregation grows.

The concentration of individual aggregate types are given by,

$$n_1 = \frac{n_0}{(1 + t / T_{1/2})^2} \quad (1.3.29)$$

$$n_2 = \frac{n_0(t / T_{1/2})}{(1 + t / T_{1/2})^3} \quad (1.3.30)$$

$$n_k = \frac{n_0(t / T_{1/2})^{k-1}}{(1 + t / T_{1/2})^{k+1}} \quad (1.3.31)$$

For orthokinetic aggregation in a uniform laminar shear field with a rate of shear G, Smoluchowski showed that

$$k_{ij} = 4/3\ G(a_i + a_j)^3 \quad (1.3.32)$$

and in this case there is great dependence of the rate constant on particle size and constant k_{ij} is not valid beyond the very early stages of aggregation. For aggregation at constant volume fraction (ϕ):

$$\frac{n_T}{n_0} = \exp\left[\frac{-4\ G\ \phi\ t}{\pi}\right] \quad (1.3.33)$$

i.e. a first order process.

1.4 Chitosan as a flocculant

1.4.1 Adsorption of chitosan from solution

1.4.1.1 Adsorption on cellulose

The adsorption of chitosan onto a number of substrates has been considered. Interest in the use of chitosan, and chitosan derivatives, in papermaking has led to studies of adsorption onto cellulose

In water, cellulose acquires an anionic surface charge[295] and so electrostatic interaction between this and the chitosan's cationic charge may be a dominant factor in adsorption. Allen *et al*[296] were the first to point this out and went on to correlate the amount of chitosan adsorbed to the charge density on the surface of the cellulose samples. This conclusion was supported by Domszy *et al*[297] who found a linear relationship between the degree of *N*-acetylation and the amount of chitosan adsorbed, the amount adsorbed increasing with decreasing degree *N*-acetylation.

Domszy *et al*[297] also measured the amount of methylene blue (C.I. Basic Blue 9), a cationic dye, which was displaced from the anionic sites of a carboxyl-containing cellulose on displacement by chitosan. The results, surprisingly, indicated that approximately only one amine group in every 800 is directly involved in electrostatic interactions with the carboxyl groups on the cellulose, and this data was used to suggest that adsorption occurred to give a large loop conformation.

The effects of added electrolyte on the adsorption of chitosan on cellulose have been reported. Rippon[298] reported that the amount of adsorbed chitosan was unaffected by an addition of 0.34mol dm^{-3} NaCl. However, Domszy *et al*[299] observed an initial increase in adsorbed amount, followed by a decrease with increasing NaCl concentration.

The initial rise in adsorption was attributed to a reduction in the hydrodynamic radius of the chitosan coils due to charge-screening, thus allowing a greater surface area contact between the chitosan and cellulose chains. The adsorbed amount subsequently decreased with increasing electrolyte concentration due to a reduction of electrostatic interaction between the cationic chitosan and anionic cellulose by charge screening and also because of increasing competition for anionic sites on the cellulose surface between the $-N^{+}H_3$ and the Na^{+} ions. The lack of change in Rippon's[298] results may be attributed to an approximate balancing of the above effects.

1.4.1.2 Adsorption on inorganic materials

Kaolin and other clay dispersions have been used, to some extent, to study the adsorption and flocculation behaviour of chitosan and chitosan derivatives. While several workers have studied purely flocculation behaviour (see later) only Domard *et al*[300] have produced a major study of the actual adsorption process. The study is concerned with the equilibrium adsorption isotherms of four chitosan samples as well as a quaternized derivative, N,N,N-trimethylchitosan[0.05]chloride on kaolin at pH4 and pH6, as well as studying the flocculation behaviour by several techniques. The adsorption isotherms showed that the amount of unmodified chitosan adsorbed increased with increasing pH regardless of molecular weight or degree of deacetylation and at pH6 the adsorption isotherm for all these samples failed to level off. This was attributed to a decrease in linear charge density with increasing pH. Molecular weight was also shown to be a factor, an increase in molecular weight, characterised by intrinsic viscosity, being shown to increase adsorption on kaolin for chitosan fractions of roughly equivalent composition. However, the

importance of the degree of acetylation was found to be in agreement with the results for adsorption onto cellulose, i.e. adsorption decreased with increasing acetyl content. This was attributed to the presence of acetyl derivatives being an unspecified, unfavourable factor. Other factors however may have influenced the result, notably the unsuitability of using intrinsic viscosity as a direct expression of the molecular weight of chitosan (see later). The quaternized derivative, which was relatively unaffected by pH, showed only a slight increase in the amount of polymer adsorbed when changing from pH4 to pH6. This, it was suggested, may simply be attributed to a slight increase in negative charge on the surface of the kaolin as pH was increased.

Claesson and Ninham[301] studied the adsorption of chitosan on mica via surface force measurements. They report that, at an acetic acid concentration of 0.01wt% (pH ~3.8), chitosan (FA ~[0.05]) added an extra repulsive force to the system, ascribed to steric effects from a thin (7-8Å) chitosan layer as two mica plates were brought together. On re-separation of the plates, an extra attractive force was observed which was attributed to the formation of polymer bridges when the plates were close together. On replacing the solution with chitosan free 0.01 % acetic acid there was observed a small degree of desorption of chitosan from the surface, shown by a slight fall in the repulsive forces measured, though the desorption process was brief and effectively completed in under an hour. Increasing the pH to 4.9 (by addition of NaOH) had little effect, but at pH6.2, measurements indicated the reduced protonated charge on the chitosan balanced the charge on the mica resulting in forces consistent only with van der Waals' forces being operative. Increasing the pH to 9.1 displayed a repulsive effect attributed to an increase in the mica surface charge density and

to a steric contribution due to swelling of the chitosan layer. Replacing the solution with 0.01% acetic acid again resulted in a return to (approximately) the original measured forces, indicating that there was very little desorption throughout the experiment. The results were interpreted in terms of adsorbed layer structure. At low pH values, the chitosan chains were said to adopt a very flat conformation. Increasing the pH forced the adsorbed layer to adopt a more compact structure up to pH6.2, due to its increasing hydrophobic nature pushing the chains together. Increasing pH beyond this made the structure less compact.

1.4.1.3 Adsorption on organic dispersions

Chitosan' s potential as a flocculant for organic dispersions in waste-water systems is well documented[302,303,304, 305]. Most studies centre upon the optimisation of the system involved rather than the underlying principles involved, though a study by Wu and Bough[14] concluded that the extent of deacetylation and molecular weight distribution , measured by HPLC, were the important parameters governing chitosan's effectiveness, though the optimum conditions varied with the waste-water system involved.

1.4.2 Chitosan flocculation

Although chitosan and certain derivatives have been used as flocculants to a small extent for a number of years, notably in Japan and Scandinavia, very little fundamental work has been carried out on the flocculation behaviour of chitosan. Most studies involve simple jar-test comparisons with other flocculants. For example, Kawamura[305] reported that chitosan was as effective, if not more so, than comparable synthetic flocculants especially in particularly turbid waters, though the actual composition of the chitosan sample was not

stated and the molecular weight merely quoted as approximately 10^6. More detailed studies carried out by Zhuo et al[306] and Huang and Chen[307] have centred upon the effect of chitosan on the stability of clay suspensions. The former of these was concerned with the effect of chitosan on the zeta-potential of bentonite suspensions over a range of F_A values, whilst the latter was concerned with the effect of one uncharacterised chitosan fraction on the residual turbidity of bentonite and kaolinite suspensions. Both these studies' general conclusions were that inter-particle bridging was the predominant mechanism with charge neutralisation playing a small contributory role. Huang and Chen also reported that the effect of pH was relatively unimportant over the range pH4 - 9. Domard, Rinaudo and Terrassin[300] studied the adsorption behaviour of a series of relatively well-defined chitosan fractions onto kaolin dispersions. From adsorption isotherms they concluded that chitosan adsorption increases with molecular weight and with increased degree of deacetylation. Ultimately they concluded that the adsorption was electrostatic in nature at pH4, when the chitosan is protonated to give its cationic polyelectrolyte form and kaolin possess a net negative charge. Increasing the pH lessens this effect and the conclusion is that hydrogen bonding becomes more important in the adsorption mechanism. From the flocculation study, it was concluded that the flocculation range is slightly increased between pH4 and pH6. Inter-particle bridging is stated as the mechanism of aggregation and there is passing mention to the formation of loops and tails with increasing molecular weight which would be consistent with a bridging mechanism. Various studies by Domard and co-workers[308, 309, 310] have centred upon the effect of chitosan on the stability of lipid solutions, generally undecylenic acid, which tend to conclude that a charge neutralisation destabilisation mechanism, presumed to be the charge-patch mechanism, was at work.

A more recent study concentrated on the effect of chitosan on the stability of gold sols at varying pH's[311]. The study concluded that chitosan flocculated the system via a combined charge-neutralisation / inter-particle bridging mechanism. This conclusion can be partially rationalised by considering that the extremely small particle sizes (~ 20nm) increased the scope for bridging. The effect of pH was reported to be the increase of optimum flocculation concentration by an order of magnitude in increasing the pH from 4 to 6.

1.5 Aims of the Present Work

To use a well characterised system in order to elucidate the mechanism of particle flocculation by chitosans. To this end, highly deacetylated chitosans of different molecular weights will be homogeneously reacetylated to varying degrees and characterised. These will then be used to flocculate well-characterised model colloid latex particles of varying sizes and surface charge densities.

2.1 Materials

2.2.1 General Materials

- All water used was double distilled from an all Pyrex apparatus.
- Acetic acid was GPR grade (99.5%) supplied by BDH, Poole, Dorset, UK.
- Sodium Chloride SLR grade(99.6% after drying), methanol AR grade, ammonia SLR grade (0.88, 35% NH_3), sodium acetate SLR grade (>99%) and CTAB AR grade (>99%), potassium persulphate SLR(>97%)- recrystalised twice from double distilled water, were supplied by Fisher Scientific, Loughborough, Leics., UK.
- Styrene (Aldrich 99%), distilled under reduced pressure to remove stabiliser.
- Sodium dodecyl sulphate (Fluka >98%).

2.1.2 Chitosan

- Chitosan samples designated as being 'oligomeric, 'medium molecular weight' and 'high molecular weight', subsequently coded O, M and H, were supplied by Professor GAF Roberts of the Department of Fashion and Textiles at the Nottingham Trent University.
- C.I. Acid Orange 7 (Orange II; 4-(2 hydroxy-1-naphthylazo) benzene sulphonic acid sodium salt C.I. No. 15510), (>90%), laboratory reagent grade (used without further purification) and acetic anhydride (>98%) were supplied by Sigma Aldrich, Poole, Dorset, UK.

2.2.2 Latices

2.2.2.1 In-house latices

- 85nm latex was prepared by emulsion polymerisation of styrene with potassium persulphate initiator and sodium dodecyl sulphate emulsifier used without further purification.
- 2250nm latex was prepared by emulsifier free emulsion polymerisation of styrene with potassium persulphate initiator.

Details of latex preparation are given in section 2.2.4.2.

2.2.2.2 Interfacial Dynamics latices

- Surfactant free polystyrene latexes with diameters of 350nm (Product Number: 1-300 Batch Number: 401-1), 400nm(Product Number: 1-400 Batch Number: 2-63-46.186,1) and 2100nm (Product Number: 1-2000 Batch Number: 780) were obtained from the Interfacial Dynamics Corporation, Portland, Oregan.

2.2 Methods

2.2.1 Preparation of chitosan

2.2.1.1 Medium and high molecular weight chitosan samples

The 'medium molecular weight' and 'high molecular weight' chitosan samples were prepared as follows:

The starting material was initially dissolved in 0.1M acetic acid and filtered through polyester monofilament to remove insoluble impurities and swollen gel particles. The material was then precipitated by addition of methanol/0.880 ammonia to pH 8. The precipitated chitosan was then washed with double distilled water until neutral to litmus.

The neutral chitosan was then steeped in methanol twice and then in ether overnight twice, filtering between each, then dried under vacuum at 40°C.

2.2.1.2 Oligomeric chitosan

The oligomeric chitosan, supplied as the hydrochloride salt, was neutralised in methanolic ammonia, washed with ether and dried under vacuum at 40°C.

2.2.2 Homogeneous *N*-acetylation of chitosan

Chitosan, F_A[0.02]M starting material (4g) was weighed and placed into a 1 litre stoppered conical flask and then dissolved in 400ml of 0.1M acetic acid. A methanolic solution of acetic anhydride was prepared such that 10ml contained a 1:0.1 molar ratio chitosan amine groups:acetic anhydride. The required volume of acetic anhydride solution was pipetted into a 500ml measuring cylinder and made up to 400ml with methanol. This solution was added to the chitosan solution with continuous stirring and stirred for a further 20 minutes before being transferred to a water bath at 25°C for 24 hours. After removal from the water bath, the chitosan was reprecipitated by addition of methanol/0.880 ammonia solution to pH8. The material was then filtered through polyester monofilament, washed with water until neutral to litmus and twice steeped in methanol overnight then filtered, twice steeped in ether and filtered, before drying under vacuum at 40C. Chitosan with degrees of acetylation between F_A[0.02] and F_A[0.57] were prepared by this method.

2.2.3 Characterisation of chitosan

2.2.3.1 Thermogravimetric analysis

5mg of sample was placed in a platinum crucible and introduced into a Stanton Redcroft TG 760 series thermobalance. The temperature was increased from ambient to 110°C at a rate of 5°C per minute. The temperature was held at 110°C until the mass of the sample was constant. Comparing the initial mass of the sample with the final constant, mass allows the mass due to solvent (water or methanol) to be determined.

2.2.3.2 Determination of N-acetyl content

(i) Dye Adsorption

The method for dye adsorption by chitosan was based on the procedure developed by Maghami and Roberts [110].

A 5 x 10^{-3}M ($1.75gl^{-1}$) solution of C.I. Acid Orange 7 in 0.1M acetic acid was prepared. 0.05g of chitosan was accurately weighed and placed in each of three clean, dry 250ml Quickfit conical flasks. 100ml of dye solution was pipetted into each flask plus a fourth, control flask containing no polymer. All flasks were then stoppered and placed in a water bath at 60°C for 20 hours.

After 20 hours, the contents of each flask were filtered through glass wool to remove the polymer residue and allowed to cool. Each test solution was then diluted by a factor of 100 and the control diluted by a factor of 200 with 0.1M acetic acid. The amount of dye adsorbed by the chitosan was then be determined by comparing the test solution with the control solution, via UV absorption at 484nm, and subsequently the *N*-acetyl

content assessed, based on the 1:1 stoichiometry between protonated amine groups and the negatively charged groups on the dye.

(ii) Metachromatic titration

The method of metachromatic titration of chitosan was based upon the procedure developed by Gummow and Roberts[312].

Chitosan (0.1g) was accurately weighed and dissolved in 1 litre of 0.1M acetic acid. 0.18g of C.I Acid Orange 7 was dissolved in 1 l of 0.1M acetic acid to give a solution of approximately $5x10^{-4}$M. A range of chitosan solutions was prepared as follows: 10ml of the dye solution was pipetted into each of a number of volumetric flasks (100ml) followed by approximately 40ml of 0.1M acetic acid. Varying volumes of the chitosan stock solution, over the range of 1ml to 20ml were then added to each flask. Each flask was then made up to the mark with 0.1M acetic acid and the solutions mixed gently by repeated inversion of the flasks. A further, control flask containing no chitosan was also prepared. The absorbance of each solution was measured at 484nm in 1cm cells against a blank of 0.1M acetic acid. The absorbances were then plotted against the volume of chitosan solution added in order to determine the equivalence point, from which chitosan concentration at that point and finally N-acetyl content may be determined.

(iii) Infrared spectroscopy

Films were prepared from 0.5% solutions of chitosan in 0.01M acetic acid by casting on glass plates and drying overnight at room temperature. These were steeped in methanolic ammonia to convert them from the acid salt to the free amine form, washed thoroughly with

distilled water, then methanol, dried overnight at 60°C under vacuum and stored in a vacuum dessicator. Spectra were obtained using a Nicholet Magna 750 FTIR spectrophotometer. The degree of N-acetylation was calculated from the absorption band ratio $A_{\text{amide peak}} / A_{\text{reference peak}}$. The method proposed by Baxter[102] was used i.e. the ratio A_{1655} / A_{3450} was determined using a line drawn from 4000cm^{-1} to 2500cm^{-1} as the baseline for the hydroxyl group band and one drawn from 1800cm^{-1} to 1600cm^{-1} as the baseline for the Amide I band from which the degree of N-acetylation was calculated using:

$$\% \text{ N-acetylation} = (A_{1655} / A_{3450}) \times 115$$

This procedure has been found[102] to give good agreement with results from dye adsorption for degrees on N-acetylation up to 55%

2.2.3.3 Molecular weight

The molecular weight of each chitosan sample was determined by visometry in order to check that no degradation of the polymer occurred during reacetylation. The method followed was that described by Wang, Bo, Li and Qin [120]. A range of standard chitosan solutions was prepared in 0.2M acetic acid/0.1M sodium acetate solution.

Viscosity measurements of the polymer solutions and pure solvent were carried out using an Ubbelohde viscometer at 30°C ± 0.05°C in a thermostated water bath. The flow times of the solutions enabled the intrinsic viscosity [η] to be determined for each solution.

The intrinsic viscosity was then be related to molecular weight by use of the Mark-Houwink equation:

$$[\eta] = K M_v^{\alpha}$$

where K and α are constants dependant upon the nature of polymer, solvent and temperature but independent of molecular weight. K and α were calculated using the equations determined in the above study:

$$K = 1.64 \times 10^{-30}. DD^{14.0}$$

$$\alpha = -1.02 \times 10^{-2}. DD + 1.82$$

where DD is the percentage degree of deacetylation of the chitosan sample.

2.2.4 Latices

2.2.4.1 Interfacial Dynamics latices

The latices supplied by Interfacial Dynamics were prepared by surfactant-free emulsion polymerisation. Tables 2.1.1 to 2.1.3 summarise particle diameter, solids content, number density, charge density and area per charged group for each latex. Particle diameters were determined using Transmission Electron Microscopy (TEM) and charge content was determined using conductometric titration. Conductometric titration further revealed that surface charges were due to sulphate groups, with a negligible contribution of carboxyl groups to total surface charge.

Mean Diameter	0.35 μm (Coefficient of Variance = 6.0%)
Solids	8.4 ± 0.1 g $100ml^{-1}$
Number density	3.5×10^{12} particles per ml
Charge content	0.6 μ Eq g^{-1}
Area per charged group	4734 $Å^2$ per group

Table 2.1.1 Summary of information on 350nm Interfacial Dynamics Latex

Mean Diameter	0.40 μm (Coefficient of Variance = 3.8%)
Solids	8.4 ± 0.1 g $100ml^{-1}$
Number density	2.4×10^{12} particles per ml
Charge content	5.0 μ Eq g^{-1}
Area per charged group	474 $Å^2$ per group

Table 2.1.2 Summary of information on 400nm Interfacial Dynamics Latex

Mean Diameter	2.1 μm (Coefficient of Variance = 1.8%)
Solids	8.1 ± 0.1 g $100ml^{-1}$
Number density	1.6×10^{10} particles per ml
Charge content	2.4 μ Eq g^{-1}
Area per charged group	186 $Å^2$ per group

Table 2.1.3 Summary of information on 2100nm Interfacial Dynamics Latex

2.2.4.2 85nm latex

(i) Preparation

The 85nm latex was prepared by emulsion polymerisation of styrene using sodium dodecyl sulphate as emulsifier and doubly recrystallised potassium persulphate as initiator.

The polymerisation was carried out at a temperature of 40°C and stirred with a PTFE stirrer blade at 300rpm for 4 hours. The resulting latex was dialysed extensively to remove all electrolyte and desorbable emulsifier. After acid washing in 0.1M HCl, the latex was again dialysed and finally equilibrated with double distilled water, by microfiltration.

Photon correlation spectroscopy showed the latex to be monodisperse with a mean diameter of approximately 85nm.

(ii) Titration of latex

The number of sulphate and carboxyl groups present on the surface of the dialysed latex may be assessed by conductometric titration with sodium hydroxide solution.

25ml of latex solution was pipetted into a thermostated 100ml beaker at 25°C± 0.05°C, also placed in the beaker were a conductivity cell and a temperature probe and the solution was stirred using a magnetic stirrer. Nitrogen gas was initially bubbled through the solution and the system was allowed to equilibrate for 30 minutes. The nitrogen gas was then allowed to play over the surface whilst the solution was titrated with 0.1002M sodium hydroxide solution dispensed from a syringe equipped with a Vernier scale. The conductance reading for each addition was then plotted against cumulative volume in order to determine the end point for each acid group.

(iii) Percent solids determination

The percentage of latex solids present in the dispersion was determined by drying 5ml of the dispersion at 60°C, under vacuum, to constant mass.

2.2.4.3 2250nm latex

A latex of particle diameter approximately 2250nm was prepared by surfactant free emulsion polymerisation via a seeded growth approach[144]. The polymerisation was carried out in two stages. Firstly a seed latex with a particle diameter of approximately 1000nm was prepared in a four-necked 1litre flask from 450cm^3 water, 60cm^3 styrene, 0.124g potassium persulphate and 0.7g of sodium chloride. This was stirred via a glass rod / half-moon PTFE stirrer blade at 250rpm for 24 hours. The latex was then filtered through glass wool to remove coagulum, checked for approximate size by TEM and dialysed overnight to remove excess initiator and sodium chloride.

2250nm latex was subsequently prepared by adding 26ml of the 1000nm seed latex to 690cm^3 water, 80cm^3 styrene, 0.347g potassium persulphate initiator, 0.125g of sodium bicarbonate and 1.025g of sodium chloride. Again the polymerisation was carried out for 24 hours with a stirrer speed of 250rpm. The resulting latex was filtered through glass wool to remove coagulum, dialysed extensively to remove excess potassium persulphate and sodium chloride, and steam stripped to remove excess styrene. It was then acid washed and equilibrated with double distilled water, by microfiltration.

The approximated size of the latex particles was determined by TEM to be 2.25μm.

2.2.5 Flocculation experiments

When preparing and using solutions of cationic materials, all vessels were conditioned with the aggregant under investigation to allow for losses by adsorption on to the walls[221, 313], i.e. the vessels were first equilibrated with a solution of the desired concentration which was then discarded and replaced with a new solution at the desired concentration. This procedure was carried out twice before each flocculation or coagulation experiment was carried out.

2.2.5.1 Aggregation of 85nm latex

(i) PCS measurements

A comparison of the flocculation range produced by each chitosan sample, plus the coagulation range of CTAB was achieved by measuring mean particle diameter after some arbitrary flocculation time (12 minutes).

A 1:2500 dilution of the original 85nm latex dispersion, diluted with double distilled water, was prepared for use in aggregation experiments.

2ml of diluted 85nm latex solution was pipetted into a PCS cell. Added to this was 0.5ml of a modifier solution designed to modify the flocculation conditions, eg sodium chloride solution was added to alter ionic strength. To this was added 0.5ml of flocculant or coagulant solution using a 500μl syringe. The needle of the syringe was ground flat. The flocculant or CTAB solution was added smoothly to ensure good mixing of the contents of the cell. The PCS run was then initiated. Four runs of three minutes each were carried out on each sample, the last of these measurements being taken as the result (This ensured the particle diameter was determined over a sufficient time interval, 3 minutes, whilst the data for the earlier measurements was not included in the mean diameter.).

Plots of mean particle diameter against flocculant or CTAB concentration could then be prepared to indicate flocculation range.

Dynamic light scattering estimates of particle size are not considered accurate at particle sizes above several microns[288], even for spherical particles. It was therefore considered that the plotting of measured values of particle diameter in greatly aggregated dispersions was too inaccurate to be relevant and so an arbitrary cut off point of 1μm was chosen as the maximum reported floc size in flocculated systems.

(ii) Initial rates

Initial increases in turbidity of the aggregating dispersion were used as a comparison of the initial rates of flocculation and coagulation[269].

The initial rates of increase in turbidity of 85nm polystyrene latex dispersion upon aggregation were estimated by following the increase in absorbance at 550nm using a UNICAM 8720 UV/VIS spectrophotometer in kinetics mode.

2ml of 85nm latex dispersion was placed in a 1cm UV/VIS cell. 0.5ml of an appropriate modifier solution was added to this in order to alter the solution conditions. For example, sodium hydroxide or acetic acid solution to alter pH, sodium chloride solution to alter ionic strength or water.

The cell was placed in the UV/VIS spectrophotometer, and 0.5ml of coagulant (NaCl) or flocculant solution was added smoothly using a 500μl syringe, the lid was closed and the run initiated.

Absorbance versus time rate curves were recorded over several minutes and subsequently plotted. The initial gradient of the curves, $\Delta A/\Delta t$ was determined graphically.

The ratio of initial flocculation rate to maximum initial coagulation rate was plotted against polymer concentration, expressed in terms of the concentration of moles of chitosan amine groups per litre, and hence positive charge added.

2.2.5.2 400nm latex

The stock latex was diluted 0.5ml : 500ml with double distilled water to produce a suitable test dispersion.

(i) Residual turbidity

1ml of the latex dispersion was pipetted into a 2.5ml micro-centrifuge tube together with 0.25ml of the appropriate modifier solution. 0.25ml of flocculant or CTAB solution was added smoothly using a 500μl syringe. (The tubes were initially made up with 1ml of double distilled water instead of the latex dispersion and left overnight. After draining and drying, the flocculation experiment was carried out twice, followed by rinsing and draining before the actual experiment was carried out in order to ensure the surface of the tubes were properly conditioned.). The tube was then capped, inverted five times to ensure good mixing, and left overnight. The tubes were then centrifuged at 1000rpm for 5 minutes. Supernatant from each tube was transferred to a 1cm cell and the absorbance of the solution determined at 550nm. Supernatant absorbance at 550nm was plotted against chitosan amine group concentration to produce a flocculation range.

(ii) Initial rates

As with the 85nm latex dispersion, the initial increases in turbidity of the aggregating dispersion was used to compare the initial rates of flocculation and coagulation[269].

The initial rates of increase in turbidity of 400nm polystyrene latex solution were determined manually from rate curves produced in the same fashion as those for the 85nm dispersion.

(iii) Electrophoresis

0.5ml of latex dispersion and 0.5ml of 0.1M acetic acid were pipetted into a 15ml Pyrex tube. Xml of chitosan solution was introduced by syringe after (9-X)ml of 0.05M acetic acid had been added in order to stop any flocculation. Electrophoretic mobilities were determined using a Coulter Delsa 440SX zeta potential analyser.

2.2.5.3 350nm latex

The supplied latex dispersion was diluted 0.34 ml to 500ml with double distilled water to produce a suitable test dispersion.

(i) Residual turbidity

Residual turbidity studies on the 350nm latex were carried out in analogous fashion to those involving the 400nm latex; again the absorbance at 550nm was plotted against chitosan amine group or CTAB concentration to produce a flocculation range.

(ii) Initial rates

Again, as with the 400nm latex, initial rates of flocculation and coagulation were compared using the initial increases in turbidity upon addition of aggregant to the dispersion.

The initial rates of increase in turbidity of 350nm polystyrene latex dispersion upon aggregation were estimated by following the increase in absorbance at 550nm using a UNICAM 8720 UV/VIS spectrophotometer in kinetics mode.

(iii) Electrophoresis

Electrophoretic mobility measurements on the 350nm latex were carried out in the same way as for the 400nm latex.

2.2.5.4 2100nm latex

A 1/10 dilution of the supplied Interfacial Dynamics dispersion was prepared to form a stock solution for flocculation experiments.

(i) Residual singlets method

Stock solutions of approximately 1 x 10^{-5} moles dm^{-3} chitosan amine group were accurately prepared in 0.05M acetic acid solution for a range of chitosan samples.

Test solutions were made up in 15ml Pyrex screw-top sample tubes, after preparation similar to previous flocculation experiments, as follows; the desired volume of chitosan solution was pipetted into each tube to form a range typically between 0.5 to 1.5ml of chitosan solution. Sufficient 0.05M acetic acid was pipetted into the tube to make it up to 9ml, 0.5ml of 0.1M acetic acid was also added to ensure a 0.05M acid concentration overall. Finally, 0.5ml of latex solution was added smoothly from a 500μl syringe. The cap was then replaced and the tube inverted gently five times to ensure adequate mixing.

After 24 hours, the number of remaining singlets in each solution was determined as follows;

A 50ml volumetric flask and a 50ml Pyrex beaker were thoroughly rinsed with Isoton electrolyte solution. The flask was then overfilled with Isoton and the contents transferred to the beaker. The singlet particle count of solution was determined using a Coulter Multisizer. This measurement was used as a blank.

The sample tube was gently inverted several times in order to re-suspend settled particles. 50μl of suspension was then removed from the tube and made up to 50ml in the 50ml volumetric flask using the Isoton from the beaker. Any excess Isoton was then discarded from the beaker and replaced with the 50ml of diluted suspension. The number of singlets in this solution was then determined using the Multisizer, and the total number of latex singlet particles taken to be this figure minus the earlier blank measurement. The concentration of chitosan amine groups was plotted against residual singlet counts to produce flocculation ranges.

(ii) Initial rate measurements

The initial rate of flocculation was determined as follows. The appropriate volume of flocculant was placed in the tube followed by enough 0.05M acetic acid to make it up to 9ml. 0.5ml of 0.1M acetic acid was then added to compensate for the latex solution. Finally, 0.5ml of latex solution was introduced smoothly from a 500μl syringe with a flat needle point, a stop clock was started, and the tube was inverted five times to gently mix the contents. Monitoring of coagulation was carried out in analogous fashion with 1M sodium chloride solution replacing the flocculant solution and double distilled water replacing acetic acid.

Immediately after mixing, a 50μl sample of the solution was taken using an auto pipette and transferred into a 50ml volumetric flask and made up to the mark with a sample Isoton whose blank had already been determined (see Residual Method).

Determinations of singlet particle numbers in solution were carried out at regular intervals for several hours.

Later experiments, involving rolling the tubes to determine orthokinetic aggregation rate, were prepared, sampled and tested in the same fashion.

Further methods involved the use of a two-portion mixing method[270] as it was suspected that, in the rate experiments already carried out, the time required for sufficient adsorption of flocculant onto the latex surface may have been greater than the particle collision frequency and thus the observed rate of flocculation may have been less than the true maximum rate. In this method of the optimum amount of F_A[0.02]M chitosan required for flocculation, as determined by the previous method, was added to *half* the quantity of latex, followed by 0.5ml of 0.1M acetic acid and sufficient 0.05M acetic to make the test solution up to 9.5ml in total. This solution was then left for 24 hours to equilibrate in order to produce a chitosan restabilised latex dispersion. 0.25ml of bare latex dispersion was then added and the flocculation rate studied as before.

(iii) Electrophoresis

Electrophoretic mobility measurements were carried out as for the 400nm and 350nm dispersions. In the case of the 2100nm latex, the final test dispersion (latex plus aggregant) was allowed to equilibrate for 30 minutes to ensure complete adsorption of polymer onto particles.

2.2.5.5 Electrophoretic mobility determination of 2250nm latex

The electrophoretic mobility of the in-house prepared 2250nm latex in the presence of chitosan and CTAB was studied using the Rank Bros. Particle Microelectrophoresis Apparatus Mark II.

All glassware was conditioned with the appropriate solution of chitosan or CTAB prior to each determination.

20ml of latex solution was added briskly to 20ml of chitosan or CTAB solution, and the resulting solution was left overnight to equilibrate.

After addition of the solution to the flat electrophoresis cell, the electrodes were insterted, taking care that no air bubbles were included. Mobility measurements were carried out by timing the particles over ten squares of the eyepiece graticule (the graticule was calibrated by comparison with a microscope slide on which a distance of 1mm was divided into 100 divisions. This led to a calibration of 52 microns / square on the graticule.). Measurements on each sample were carried out on ten separate singlets in each, in both directions by reversing the polarity of the electrodes, and at both stationary layers in order to determine a mean particle velocity for each sample.

2.3 Instrumental Theory

2.3.1 Photon correlation spectroscopy theory[288]

2.3.1.1 Introduction

Photon Correlation Spectroscopy (PCS) provides a means to determine the diffusion coefficient shown by small particles in solution due to random thermal (Brownian) motion. The speed, and hence, diffusion coefficient, of the particles can be directly related to particle size (eg: if a particle is large in relation to the solvent molecules, then the laws of motion imply that the imparted movement will be small in comparison to a particle closer in size to the solvent molecule). Therefore a knowledge of the diffusion coefficient, together with the solution viscosity and temperature, allows the derivation of the particle radius, by means of the Stokes-Einstein relationship.

$$r_h = \frac{kT}{6 \pi \eta D} \qquad (2.3.1)$$

where:

r_h = hydrodynamic particle radius;
k = Boltzmann constant;
T = temperature;
π = pi (3.14 ....);
η = viscosity;
D = diffusion coefficient.

(The use of the above equation implies conditions of ideality, such as an infinitely dilute solution, and spherical particles of a monodisperse nature. The result is statistical in that it applies to a population of particles rather than a single particle).

The diffusion coefficient of individual particles cannot be determined, therefore, P.C.S. uses a photomultiplier tube to count photons (ie: intensity) in the light scattered

from a dilute population of particles illuminated by a laser beam. This coherent source of light is scattered by the samples' particles as a whole, but because of the Brownian motion, the intensity fluctuates with time: with the fluctuations dependent upon particle speed. When the oscillating electric field in the laser beam passes through the particle sample, oscillating dipoles are induced in the polarizable particles that act to radiate the light in all possible directions. If the particle size is small compared to the wavelength (λ) of light (eg: $< \lambda/10$), then radiation of equal energy is scattered to all angles and is said to be isotropic. This is the common Rayleigh-Gans-Debye scattering phenomenon. If the particle size is close to that of the wavelength of light (λ = 623.8 nm for He-Ne laser) then the radiation is dependent upon the angle between the incident and scattered beam. This is Mie scattering.

Although the light source is in phase, the scattered light, when viewed as a whole, will be of constant mean intensity (ie: constant photon counts as a function of time) but incoherent. If the detector however, is focused on only a small area (ie: the size of a *speckle* in the fluctuating intensity, eg: < 0.1mm) then the phase is maintained. This is known as coherent detection, and the fluctuating intensity with time is observed. (Incoherent detection would be seen using a wider aperture, such that the fluctuations in intensity are averaged out).

The correlator acts on the fluctuating intensity signal to determine the diffusion coefficient. For an infinitely small time period, the fluctuating intensity will appear to show no change such that there is complete correlation between the two near-instantaneous frames of events. As the time interval between sampling the intensity signal is increased (ie: the time between the event frames increases) then the greater will be the change in intensity and hence the less will be the correlation between the two signals.

The correlation function between any two signals V1(t) & V2(t) can be expressed by:

$$G_{12}(\tau) = \lim \int V1(t)V2(t + \tau)\, dt \qquad (2.3.2)$$

Where $G_{12}(\tau)$ = cross correlation between the two signals for a time delay τ. i.e., it is the integral of the product of the two signals with the one signal shifted in time. The process of correlation between a signal and a delayed version of itself is the procedure known as auto-correlation, and may be represented by,

$$G_{11}(\tau) = \int V1(t)V1(t + \tau)\, dt \qquad (2.3.3)$$

This applies to continuous (analogue) systems. For digital systems (where time and signal amplitude are quantised) the integral is changed to a summation. The discrete auto-correlation function at delay time xT is thus defined as,

$$G(xT) = \sum_{x=1}^{k} V1(t)V1(t + xT) \qquad (2.3.4)$$

The rate modulated (ie: the pulse frequency is proportional to the amplitude of the analogue signal such that as the signal varies so will the pulse frequency) photomultiplier output is thus cyclically integrated over short periods of time (sampling time) and stored in the channels of the correlator. A comparison of the incoming intensity signal with a history of the previous signals gives rise (for a monodisperse sample) to an exponential decay function (ie: the incoming intensity signal is multiplied with the stored intensity at an array of stored times delayed with respect to the most recent signal). The resulting values of this multiplication of current and historical signals are then added to the

accumulated correlation coefficient at each delay time: the latest signal being added to the historical record whilst the oldest is lost; the remainder being shifted through one sample time. This process is shown schematically in Figure 2.3.1.

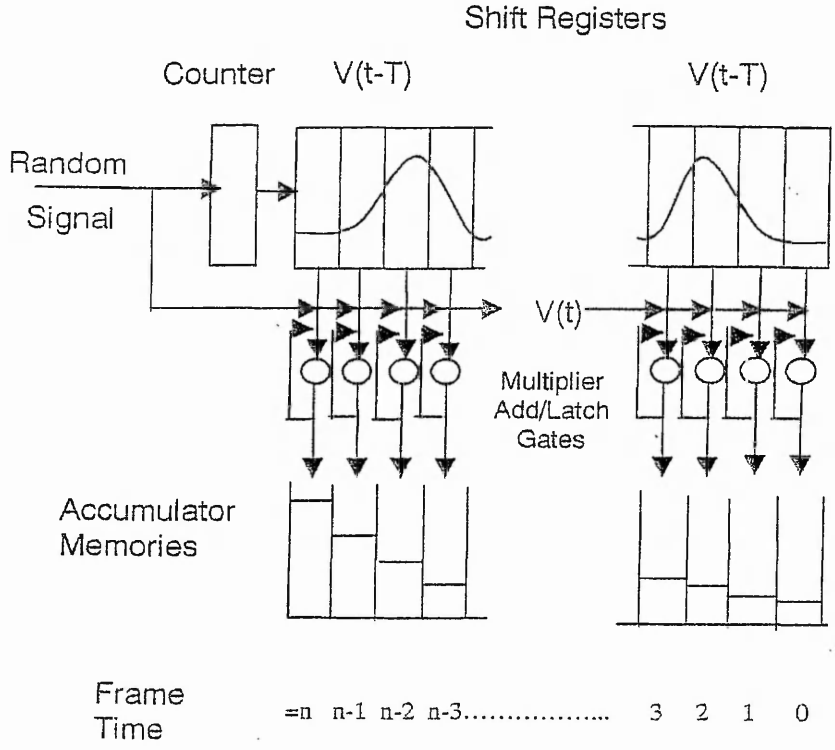

Figure 2.3.1 Schematic demonstrating the processing of the intensity signal to give a decay in correlation with time.

It should be noted that the longer the sampling interval period, the greater the probability of large counts per sample. If the sample time is too long, all of the signal information will be within one single sample that will thus give poor resolution. If the interval is too short, the resolution will be too great and only a small section of the information will be examined. Ideally, the optimum sample time allows the signal range to be spanned by all of the correlator channels.

The correlator multiplication is implemented in practice by successive additions as the incoming signal is passed down the add/latch gates. For each pulse at the input, the content of each delay (shift) register is added to the sum in its corresponding accumulator. The partial sum, (being given by equation (2.3.5)) accumulated per sample time is equal to the number of input pulses multiplied by the 8-bit representation held in a particular delay element.

$$\text{Partial sum} = V(t)V(t - xT) \qquad (2.3.5)$$

The actual photon count rate is determined by the photomultiplier dead time, or the time for recovery following a count. The dead time is typically 50 ns. The accuracy of the calculations is determined by the number of correlator channels: in the case of the Malvern Zetasizer, 64 channels at 8-bit precision.

The maximum rate of addition of the incoming signal is limited by the number of (correlator) computer clock cycles per sample (fixed in the design of the instrument).

The correlation coefficient at a particular time delay is the accumulated sum over k samples. The experimental time is the time to perform k samples and it is statistically advantageous to repeat the experiment accumulating the results within the correlator.

A digital correlator is a suitable device for removing background noise from a signal, as might result from analogue to digital conversion. For rate modulated experiments, analogue to digital conversion is not used, however, noise is generated by the photomultiplier tube. The detection process of a photomultiplier tube is a Poisson probability function, therefore giving a Poisson random pulse train.

In a typical PCS experiment particle motion will give a scattered electric field, incident on the photomultiplier tube, which is constantly changing with time and whose intensity is proportional to the square of the electric field strength.

For simple diffusion of a system of compact, monodisperse particles, the autocorrelation function takes the form of an exponential decay function:

$$C(\tau) = (n)^2 (1 + B \exp[-2\Gamma\tau]) \qquad (2.3.6)$$

where: $C(\tau)$ is the decay function (of delay time), (n) is the mean intensity (number of photons) per unit time, B is the optical constant, τ is the delay time and Γ is given by,

$$\Gamma = D_\tau q \qquad (2.3.7)$$

where D_τ is the diffusion coefficient and q is the wave vector. The slope of a semi-logarithmic plot of the decay (equation (2.3.6)) thus equates to the diffusion coefficient, which then allows the particle radius to be determined from the aforementioned Stokes-Einstein equation. It should be noted that the decay is never a true exponential, as in equation (2.3.6), due to polydispersity of the sample leading to a number of overlapping exponential decay functions. The semi-log plot is thus never linear, and hence, deviations in the linearity provide a means to measure sample polydispersity.

2.3.1.1 Sample preparation and Zetasizer operation

Before experimental samples were measured for particle diameter, the PCS apparatus was tested for correct operation (eg: tested for correct optical alignment, and for contamination of the constant temperature sample-bath water: both of which could lead to possible erroneous results) by measuring the size of a 'standard' latex (Malvern AZ55 electrophoretic standard) of known particle size (ie: 317nm).

Samples were prepared by diluting a latex, with double distilled water, until slightly turbid. The Zetasizer 3 displays an indication, on a sliding scale, of the ideality of sample

dilution. Too great a concentration leads to false results due to inter-particle back-scatter on the photomultiplier, whilst too dilute a concentration provides insufficient scattering intensity for a measurement to be made.

The PCS data is interpreted by the Zetasizer depending on the initial instrument set-up. The two main methods are the 'cumulants method' and the 'exponential sampling method'. Similarly, which of the two light scattering theories is used (Rayleigh {for small particles with respect to the wavelength of light} or Mie {for larger particles}), is also dependent on the initial instrument settings.

The cumulants method gives only a measure of the 'z-average mean' particle size and a measure of the sample polydispersity (the z-average mean size is defined by Malvern as "The mean particle size weighted by the amount of light scattered by each size of particle in the sample".). This method is used when the sample distribution width is not known such that an estimated value of one is entered when setting up a measurement (an estimated value can be set to shorten the experimental time by reducing the range over which analysis is made. A value of one causes the instrument to work over the whole of its range). The analysis fits the logarithm of the PCS correlation function to a polynomial series,

$$F(t) = A + Bt + Ct^2 + \ldots \text{etc} \qquad (2.3.8)$$

where:

- F(t) logarithm of the correlation function.
- A when divided by 100, gives the % merit.
  Typically 30%, but dependent on photomultiplier aperture size; this relates to the signal to noise ratio;
- B initial slope, which gives the z-average mean size.
- C when divided by B^2 gives the value of the polydispersity of sample (<0.05indicates good monodispersity).

The z-average mean calculated by this method is always presented no matter which of the two methods of analysis is used.

As stated above, if the sample distribution width is set to one, the instrument defaults to a cumulants fit. This fits a log-normal distribution to the z-average mean and Gaussian peak, centred on the modal value, independent of whether the distribution is monodisperse or not. The exponential method of analysis requires the input of an estimated sample size distribution (eg: as measured using the cumulative method). This is then used to resolve more complex distributions. Least squares analysis is used to determine the mix of chosen sizes that provide the best fit between the experimental data and the correlation function calculated from the mixture. The method iterates the result sixty times, reducing the difference between the experimental and calculated correlation functions.

The chosen sizes form a geometric series, using twenty-four size classes. The computer chooses the mean during initial sample checking. The ratio of the largest size to the smallest size is defined by the sample distribution width. This can either be set manually or left at a value of one such that the machine chooses a suitable value. If too large a width is chosen, some classes will remain empty. If too small a width is chosen, the analysis will be false in that the data will not fit the chosen classes. A symptom of this is a multimodal distribution in a monodisperse sample, and a large increase in the value of the 'fit'. (The fit is the value given by the least squares error of the difference between the experimental and calculated data ie: a minimum in the fit value indicates the best fit). Once taken, the experimental data can be re-analysed using a different distribution width. It is thus usual to start with a large distribution width and to reduce the value to give a better resolution. The ideal width distribution leaves just one or two empty classes at either end of the calculated size distribution.

The light scattering theories used, can be either Rayleigh-Gans-Debye or Mie. The former is used if no value of particle refractive index is set (ie: if the value is left at zero), and makes the assumption that the particle refractive index is the same as the liquid refractive index (this approximation is less valid for turbid latices than for polymer solutions). Mie theory is used when a value other than zero is set for the particle refractive index. (Mie theory also demands an imaginary refractive index. This is an absorption factor and, as such, is more applicable to blue objects that will absorb the red laser light).

2.3.2 The Coulter counter

2.3.2.1 General principle

This instrument was originally developed by W.H. Coulter[314] for counting blood cells. It has since been used to measure many systems eg: inorganic powders, polymer latices, emulsion and dust samples in air[315]. The Coulter principle[316] is shown schematically in Figure 2.3.2. Particles dispersed in an electrolyte solution are caused to flow through a small aperture on either side of which are two immersed platinum electrodes. A small electrical current passes between the electrodes through the aperture. Each particle passing through the aperture displaces a volume of electrolyte equal to its own volume and thus changes the electrical resistance between the electrodes. This produces a voltage pulse of short duration, which has an amplitude proportional to the particle volume.

When the top tap is opened, a controlled external vacuum initiates the liquid flow from the beaker through the aperture and unbalances the mercury manometer. When the top tap is closed, the system is isolated and the sample flow is continued by the siphoning action of the mercury. The advancing mercury column contacts the start and stop probes between which the electronic counter is activated. The probes are placed a fixed distance

apart so that counting occurs within a constant volume. The voltage pulses are amplified and fed to a threshold circuit, which has an adjustable threshold level. A pulse is counted if it reaches or exceeds this threshold level. By taking a series of counts at selected threshold values, a distribution of particle number versus size is generated. Integration under this curve gives the total number of particles.

2.3.2.2 Relationship between particle size and electrical response[315]

It is assumed that the aperture is a cylinder of length l_{ap} and diameter d_{ap}. Within this region the current density is uniform. The random passage of individual particles is considered to be evenly distributed through the aperture cross-section. Figure 2.3.3 shows (a) the passage of a particle through the orifice and (b) a cylindrical element of the aperture and particle of thickness $\delta 1$.

The resistance of this aperture element without a particle present is:

$$R_0 = \rho_f \, \delta l / A_{ap} \qquad (2.3.9)$$

When a particle is present the total resistance is that of two resistors in parallel, assuming that the particles acts as a pure resistor, i.e. there are no capacitance effects.

$$R_1 = \left[\frac{A_{ap} - A_p}{p_f \delta 1} + \frac{A_p}{p_p \delta 1} \right]^{-1} \qquad (2.3.10)$$

where A_{ap} and A_p are the cross-sectional areas of the cylindrical aperture and the particle, respectively; p_f and p_p are the resistivities of the fluid and the particle.

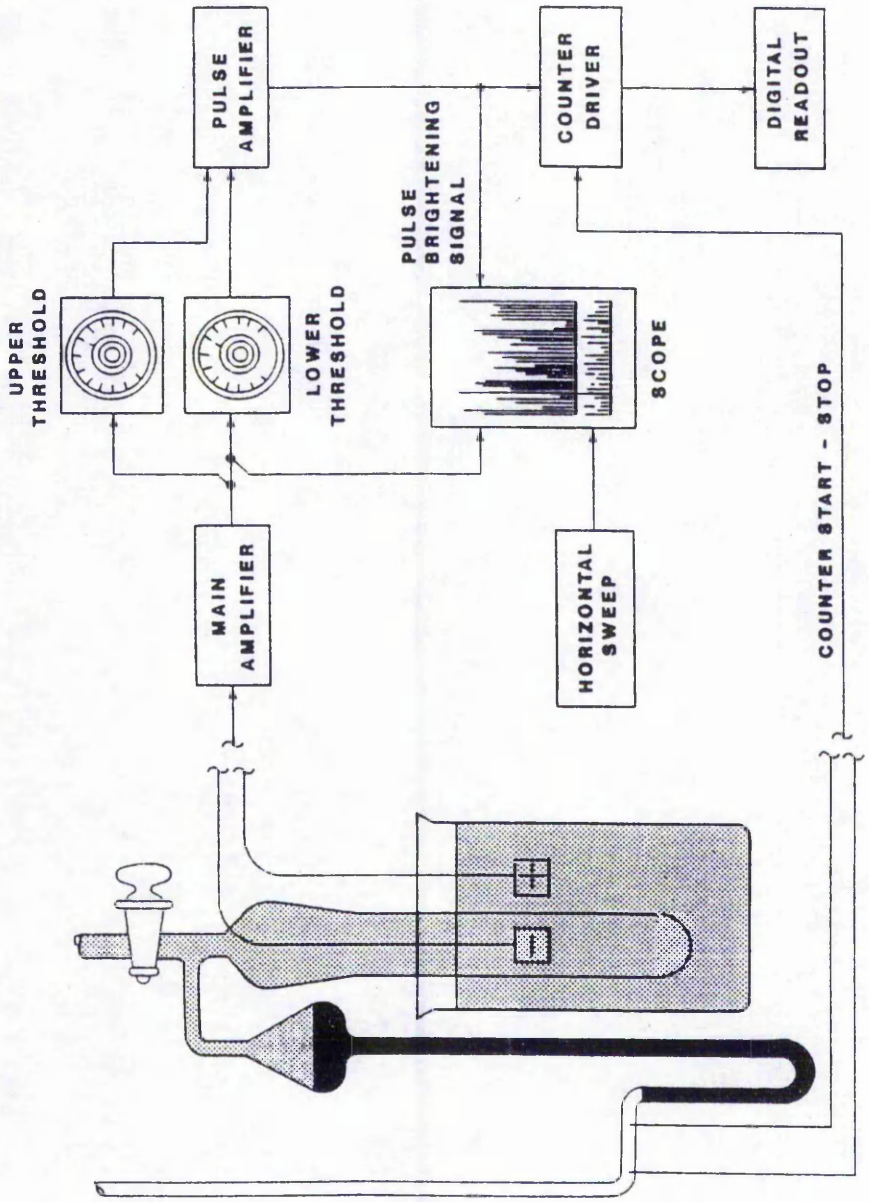

Figure 2.3.2 Schematic representation of the Coulter principle[315]

Therefore, the resistance change due to the presence of the particle is,

$$\Delta R = R_1 - R_0 = \frac{\rho_f A_p \delta 1}{A_{ap}^2} \frac{1 - \rho_f}{\rho_p} \left[1 - \left[1 - \frac{\rho_f}{\rho_p} \right] \left[\frac{A_p}{A_{ap}} \right] \right]^{-1} \qquad (2.3.11)$$

Assuming that the particle has an infinite resistivity ie: no current flows through the particle itself, the ratio ρ_f to ρ_p will be very small and hence equation (2.3.11) may be simplified to give,

$$\Delta R = \rho_f A_p \delta 1 / A_{ap}^2 [1 - A_p/A_{ap}]^{-1} \qquad (2.3.12)$$

Equation (2.4.12) may be rewritten in terms of the particle, d_p, and aperture, d_{ap}, diameters as,

$$\Delta R = 4 \rho_f d_p^2 \delta 1 / \pi d_{ap}^4 [1 - d_p^2 / d_{ap}^2]^{-1} \qquad (2.3.13)$$

The Coulter Counter measures an equivalent sphere diameter, d_s, which has an equal volume to this cylindrical particle. Thus the length and diameter of the cylindrical element are given by:

$$\delta 1 = \alpha d_s \quad \text{and} \quad d_p = \beta d_s$$

where α and β are constants such that for equal volumes $1.5\alpha = 1 / \beta^2$. Therefore equation (2.4.13) becomes:

$$\Delta R = 4 \rho_f d_s^3 / \pi d_{ap}^4 [1.5 - d_s^2/\alpha d_{ap}^2]^{-1} \qquad (2.3.14)$$

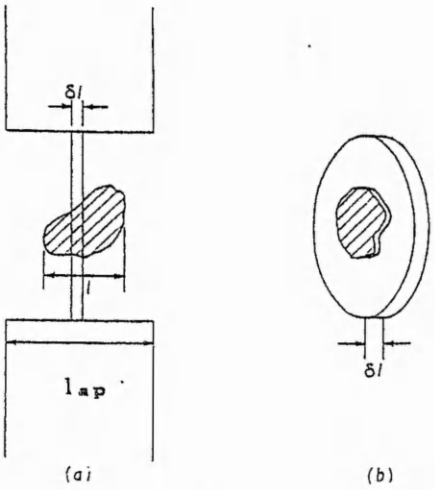

Figure 2.3.3 The passage of a particle through the orifice[317].
(a) particle passing through the orifice (b) an element of the particle and the orifice.

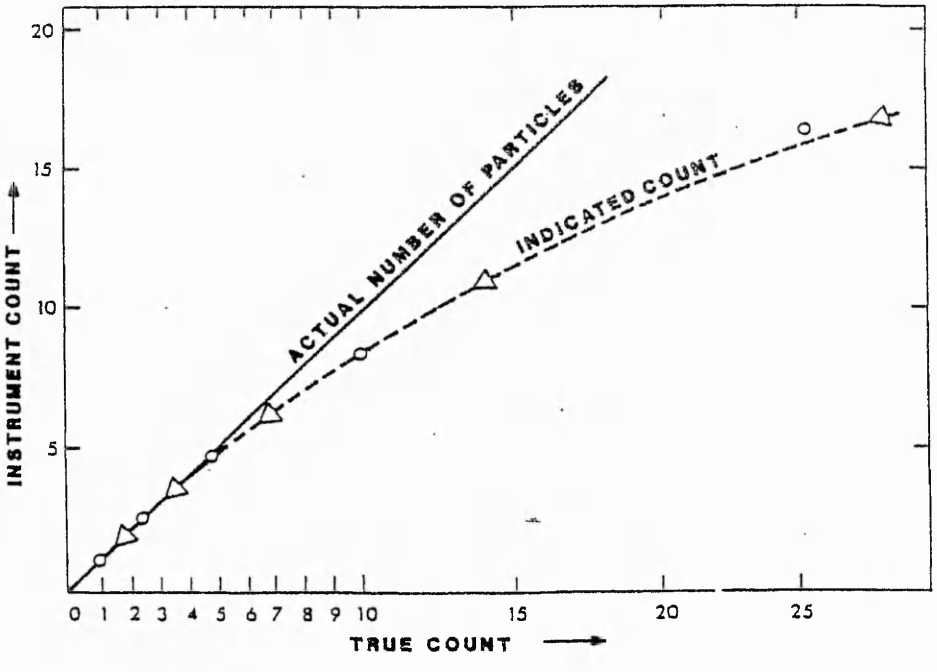

Figure 2.3.4 The effect of coincidence on the total count

The response is thus directly proportional to the particle volume except as modified by the last term in the denominator. This effect is limited because aperture blockage may occur if d_s/d_{ap} exceeds 0.5. For aqueous electrolytes and non-conducting particles, deviation from volumetric response has proved to be negligible due to two factors:

i) A larger particle causes a greater increase in the current density; hence electrical heating in the rest of the aperture occurs and the resistivity of the electrolyte is lowered momentarily.

ii) The factor α is probably only slightly greater than one especially for larger particles which are more likely to have irregular shapes and thus become 'feathered' to align with the flow stream.

2.3.2.3 The coincidence correction[315, 317, 318]

If the particles traverse the aperture individually perfect data would result. In practice, the probability of multiple passage or coincidence should be corrected for. The primary coincidence effect results in the total count being lowered as shown in Figure 2.3.4. Mattern[319] considered that the aperture had a critical volume, Figure 2.3.5A, within which two or more cells cannot be resolved as individual pulses. Figures 2.3.5B and C show schematically how the pulse height and width vary for two coincident particles separated by different distances as they pass through the critical volume. A continuum of pulse heights and widths is observed.

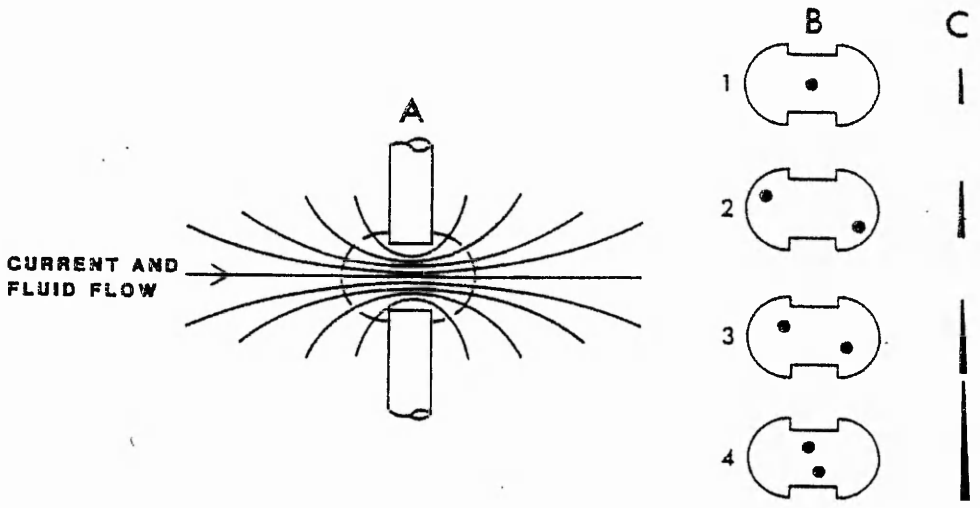

Figure 2.3.5 A)Schematic view of the coincidence effect including the critical volume (broken lines), B) several different aperture events and C) resulting pulses.

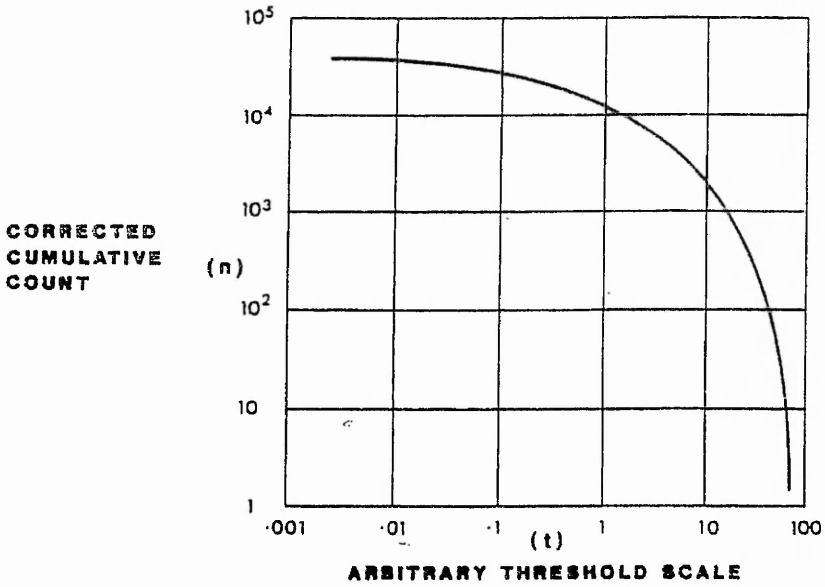

Figure 2.3.6 Calibration of the threshold scale

The coincidence loss due to the presence of doublets, triplets etc may be expressed as a Poisson distribution. If the average number of particles in this critical volume of suspension is m, then:

The probabilities of a) no cells in this critical volume $P_o = e^{-m}$; b) of one cell $P_1 = m\, e^{-m}$ and c) of n cells $P_n = m^n/n!\, e^{-m}$. Since the total probability $\sum P_n = 1$, then the theoretical ratio of instrument count to actual number of cells passing through the aperture is:

$$\sum P_n / \sum n P_n = 1 - P_o /\{1 - P_o + (P_2 + 2P_3 + \ldots (n-1)P_n \ldots \} \qquad (2.3.15)$$

This ratio deviates from unity because a doublet encountered within the critical volume will register as half its actual number. Coulter Electronics have used the following relationship between the true count N and the observed count n:

$$N = n + p\, n^2 \qquad (2.3.16)$$

where the coincidence correction p is given by:

$$p = 2.5\, (d_{ap} / 100)^3\ (500 / v) \times 10^{-6} \qquad (2.3.17)$$

where v is volume of suspension monitored for each count (μl). The factor 2.5 was determined experimentally using a 100μm aperture and v = 500μl. When the coincidence correction[320, 321, 322] is below 15% and the number of particles counted is of the order of 10,000, equation (2.4.16) may give an accuracy of better than 1%.

Secondary coincidence occurs when two particles, which individually give rise to pulses below the threshold level, collectively give rise to a single pulse above the threshold level. For this to arise, the particles must be of similar size (which must be close to the

threshold limit) and also in close proximity. Practically, secondary coincidence may be minimised by making sure that the coincidence correction is less than 10%.

2.3.2.4 Calibration of the threshold scale

The threshold scale is proportional to the pulse height and relates the electrical response to the particle volume (or size). It may be calibrated using suitable calibration particles which have a known volume concentration and a particle size distribution such that substantially all of the particulate mass is accounted for ie: there are only a few particles at the upper size limit (half the aperture diameter). Repeat counts are taken at various threshold levels and corrected for coincidence. The graph of cumulative frequency versus relative particle volume is shown in Figure 2.3.6. Integration of this curve gives,

$$V_p = k_d^3 \sum (\Delta n)\, t \qquad (2.3.18)$$

Where V_p = total particle volume in the sensing zone volume (ml)

k_d^3 = volume proportionality factor

Δn = count increments read from the integration curve

t = average values of the threshold

If the volume or mass of the suspension is known from measurements by a pipette and balance then,

$$k_d^3 = \{1 / \sum (\Delta n)\, t\} \cdot \{ v\, W_1 / V_s\, p_1 \} \qquad (2.3.19)$$

where v = sensing zone counting volume; V_s = total suspension volume;

W_1 = total mass of the particles and p_1 = particle density

This is the mass calibration method where the threshold scale is correlated with the particle volume such that $k_d^3\ t = \pi/6\ d^3$.

Therefore, the relationship between particle size and threshold is given by,

$$d = k_d\ t^{1/3}$$

where k_d = diameter calibration constant and d = particle diameter.

In practice, the calibration constant is determined for each electrolyte and aperture tube. Since the resistivity ratio of the fluid to the particle is usually very small, a single calibration factor will service for many materials.

2.3.2.5 Improvements for narrow particle size distributions by hydrodynamic focusing or electronic pulse editing

It was assumed in section 2.3.2.2 that a particle passing through the orifice generated a rectangular-topped pulse independent of its position relative to the aperture ie: the electric field within the sensing zone was uniform. Allen[317] reported distorted pulses, which might be caused by coincidence effects and also variable residence time within the orifice.

Grover[323] conducted theoretical and experimental studies of the pulses generated in the orifice region. The potential field in and around the orifice was calculated and was shown to be dense at the inlet and outlet edges. Particles travelling near to the walls pass through two regions of high potential gradient and generate M-shaped pulses.

For narrow particle size distributions, the non-axial passage of some latex particles through the aperture may lead to either a skewed distribution towards coarser sizes or to a falsely recorded second population[324]. One method of obtaining the true size distribution

is to "focus" the particle suspension so that it flows along a stream-line through the aperture[325]. This is achieved by applying Bernoulli's principle to generate flow using a hydro-dynamically-focused (HDF) aperture. One end of an inlet tube ("director") is placed very precisely in the aperture region so that the pressure drop across its end causes the suspension to flow down the central stream-line of the aperture. Practical problems with this method include establishing a consistent and correct pressure drop at the director exit. Also a low exit velocity may affect the response (calibration constant) of the instrument. Therefore, HDF apertures have only been used for low-density materials eg: cells or for small ultra-narrow latex distributions.

Alternatively, a conventional aperture is combined with electronic pulse editing to reduce the variance of the pulse height spectrum. In the Coulter C256 multi-channel analyser (MCA), the shapes of the pulses from streamlines near the aperture walls are distinguished from those nearer the centre and are rejected. It may also remove coincident pulses and aperture thermal and base-line noise[326]. The number of pulses edited out is a function of the particle and aperture diameters and hence the relative proportions of a mixture of two narrow size distributions, which are widely spaced apart, will be less accurate than that obtained by focused flow methods. In focused flow all the pulses are counted and the relative proportions of the components may therefore be accurately assessed.

2.3.2.6 The Coulter Multisizer

The Coulter Multisizer[327] is shown in Figure 2.3.7. This instrument[325] incorporates both high resolution and a wide particle size range. A working range of 2 to 60% of the aperture diameter is achieved through the use of a multistage high performance amplification system that can accurately reproduce pulse heights and shapes while having

minimum response to unwanted noise. This range is subdivided into 256 channels or size classes. In most Multi Channel Analysers the spacing of the channels is fixed by the design of the threshold circuit which measures the height of each pulse from the amplifier. The Multisizer particle pulse converter allows certain ranges, or channel spacings, to be selected as the most appropriate for particle size analysis. A high resolution analysis may be obtained by selecting a "window" of observation anywhere within the FULL range. Two levels of windowing are provided which each has a minimum width of 10% of the previous scale. The FULL range offers a choice of windowing ie: NARROW range offers a choice of linear by diameter, volume or surface area; the second windowing level ie: WINDOW uses the channel spacings previously selected for NARROW. The increased resolution of a particle size distribution in going from FULL to NARROW to WINDOW range[328] is shown in Figure 2.3.8.

The Multisizer is microprocessor controlled, and data accumulated as number of particles per channel may be rapidly converted to give size distributions. The instrument is menu-driven and the instrument may be set up automatically. The optimum aperture current and gain combination for each aperture size and electrolyte resistance may be automatically selected by the Multisizer or selected manually. The procedure for calibrating the x-axis on the Multisizer screen is shown in Figure 2.3.9. (Diameter scaling is usually used for the x-axis but volumes or surface areas are also possible). The two cursors are made to coincide with the modal size of a calibration latex measure on NARROW range. An algorithm calculates the calibration constant for a given aperture diameter from which the size scale of the diameter axis is computed by the microprocessor. The boundaries of the FULL size range are calculated to be as close a possible to 2% and 60% of the aperture diameter for either linear or logarithmic size scales. The calibration constant and the other set-up information is stored in battery-backed memory. A blank

subtract facility enables background counts to be recorded and subtracted from the current analysis. This may also be used to subtract an earlier reference distribution. Statistical analysis of the results and further data processing may be carried out using the Accucomp software on the attached computer.

2.3.2.7. Calculation of statistical size distributions[327]

The Accucomp computer program uses the following equations to calculate the particle size distribution statistics. On the FULL range with linear diameter scaling along the x axis, the diameter at the right hand edge of any channel X is calculated from:

$$d = k_d X / J (I G)^{1/3} \qquad (2.3.21)$$

Where J = number of channels in use, I = aperture current and G = aperture gain

The size at the left-hand edge of midpoint of any channel may be calculated by substituting X - 1 or X - 0.5 for X in equation (2.4.21). With logarithmic diameter scaling along the x axis, the maximum size that can measured on FULL range, d_{max}, may be found by substituting X = 256 in equation (2.4.21). The logarithmic channel spacing is such that when J = 256 the diameter halves every 50 channels down ie: the log step ratio $i = 2^{1/50}$ ≈1.01396.

The diameter is therefore calculated from:

$$d = d_{max}\ i^u \qquad (2.3.22)$$

where U = 256 [(X/J) - 1]

The diameters may be converted to areas or volumes if required. Similar calculations may be used for the NARROW and WINDOW ranges except that the channel

spacings will be different depending on the range set by the cursors experimentally. The various arithmetic mean diameters that may be calculated are given in Table 2.3.1. The median and modal diameters are also calculated.

Name	Symbol	Mathematical Expression
Number mean	d_{10}	$\bar{X}_1 = \sum (f\, d_{mid}) \;/\; \sum f$
Number-surface mean (Area-weighted mean)	d_{20}	$\bar{X}_2 = \sum \frac{(f\, A_{mid})}{\sum f} = \sum \frac{(f\, d_{mid}^2)}{\sum f}$ 1/2
Volume-number (Volume-weighted mean)	d_{30}	$\bar{X}_3 = \sum \frac{(f\, V_{mid})}{\sum f} = \sum \frac{(f\, d_{mid}^3)}{\sum f}$ 1/3
Surface-Volume mean (Sauter mean)	d_{32}	$\bar{X}_{32} = (f\, d_{mid}^3) \,/\, (f\, d_{mid}^2)$
Volume-weight moment mean; (Weight-average particle size)	d_{43}	$\bar{X}_{43} = (f\, d_{mid}^4) / (f\, d_{mid}^3)$

Table 2.3.1 Equations Used to Calculate the Mean Diameters:
X = arithmetic mean diameter; f = channel contents eg: the frequency or number of particles or the percentage by weight in each channel d_{mid}, A_{mid} & V_{mid} are the diameter, area and volume at the midpoint of the respectively spaced channels.

More information about the particle size distribution may be generated by taking moments about the mean. The second moment, μ_2, gives the variance:

$$\mu_2 = \sigma^2 = \sum [f(\bar{x} - x)^2] / \sum f \qquad (2.3.23)$$

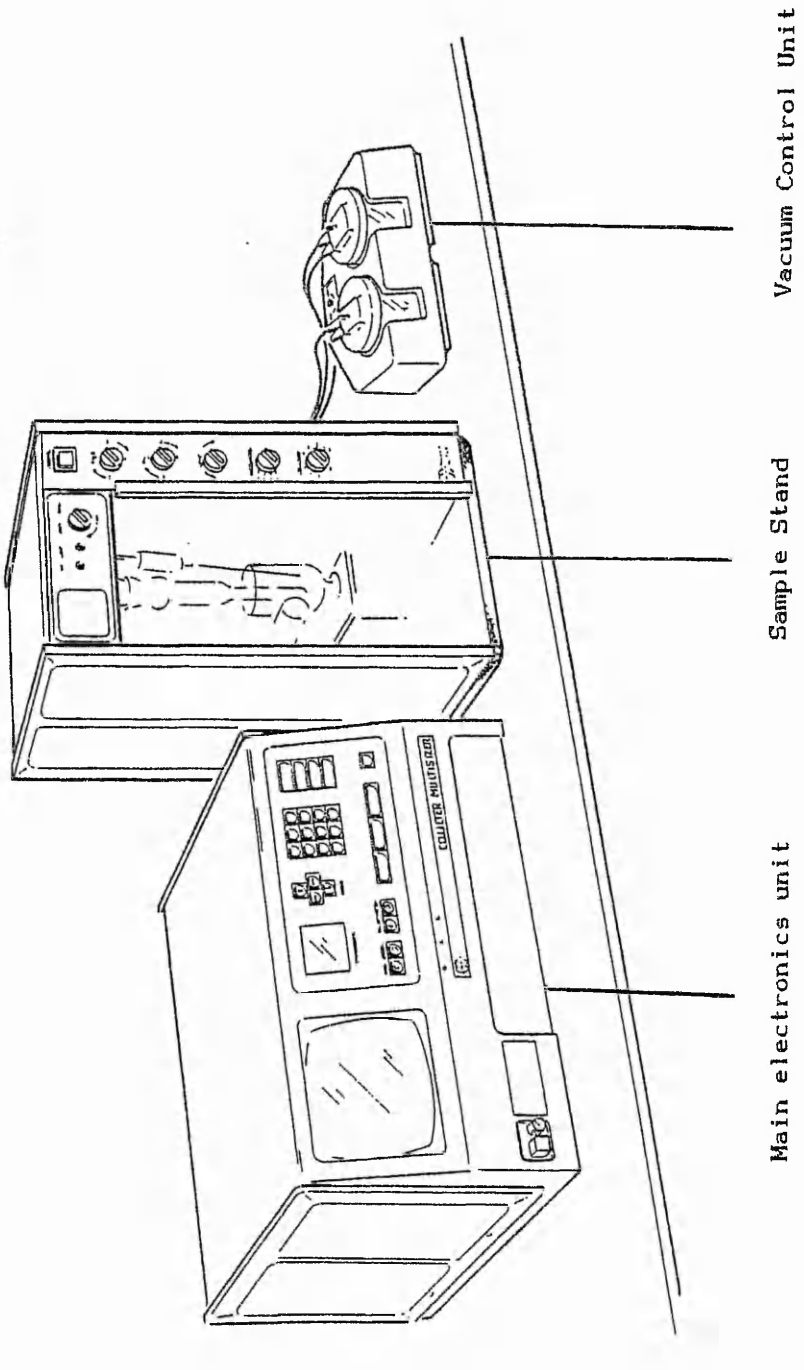

Figure 2.3.7 The Coulter Multisizer.

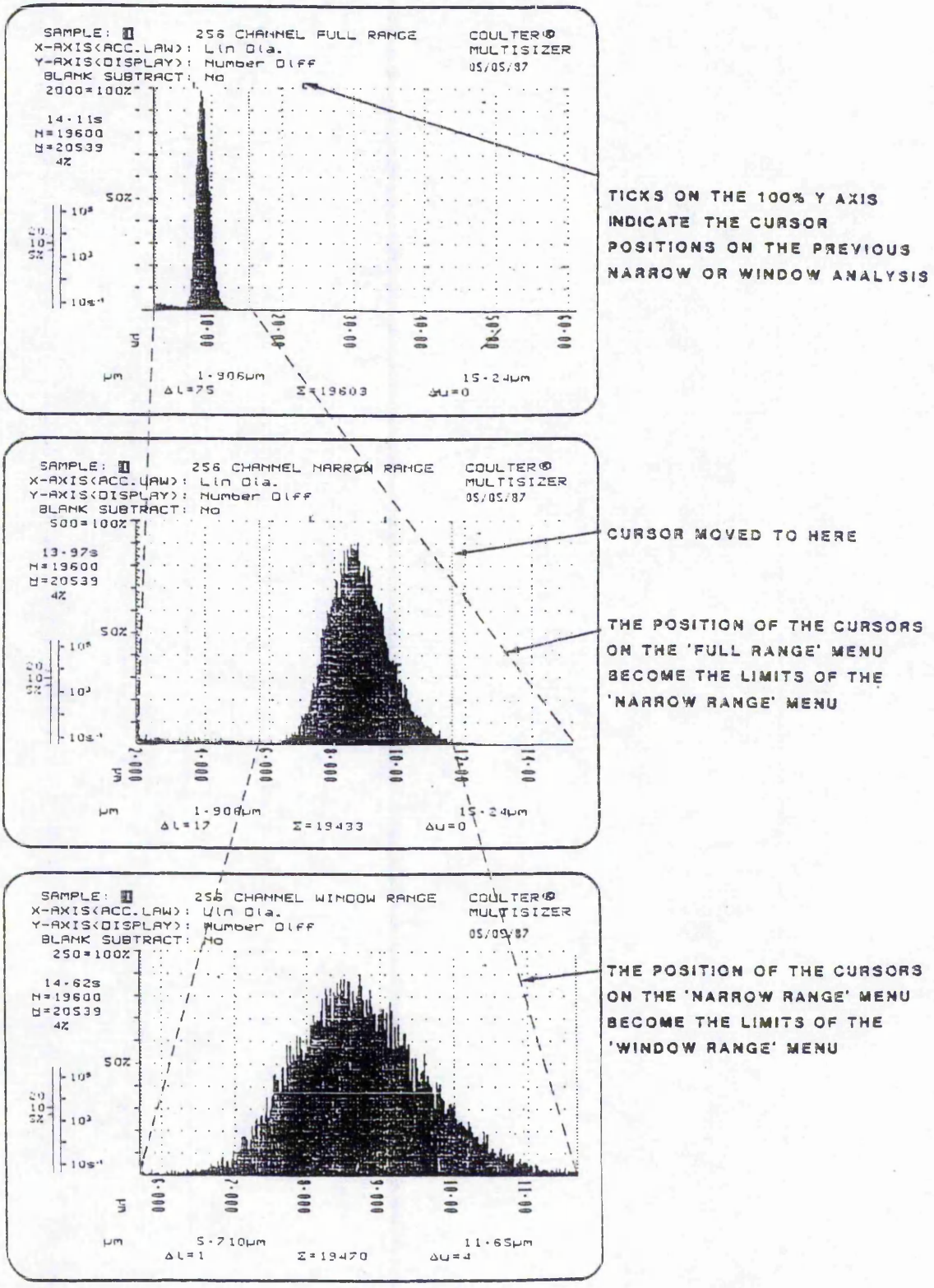

Figure 2.3.8 Particle size distributions on Full, Narrow and Window ranges.

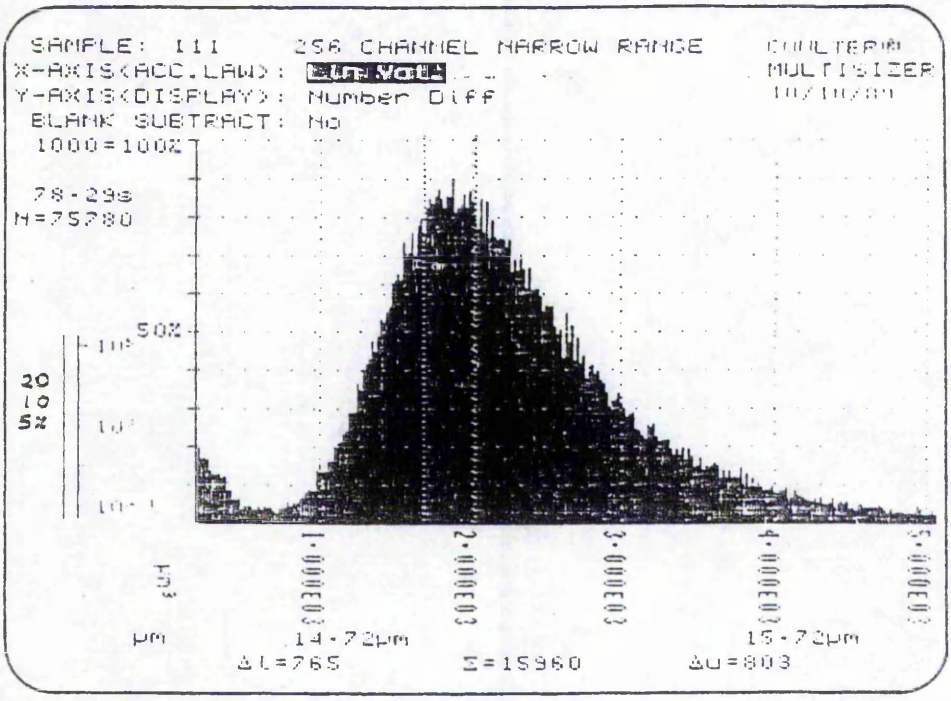

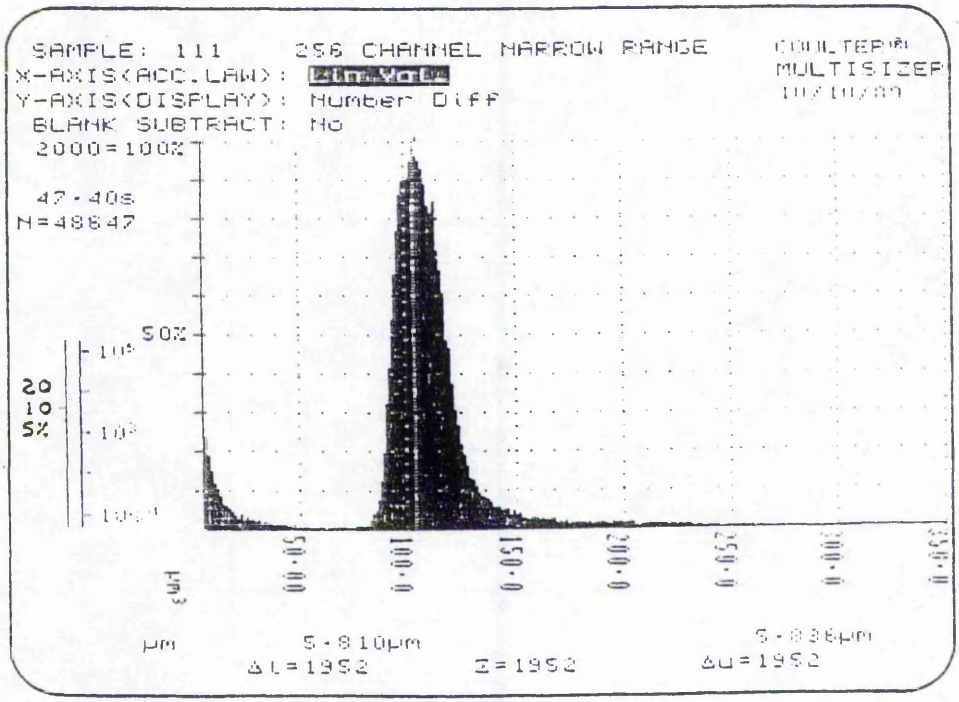

Figure 2.3.9 Calibration procedure for the diameter axis.

The standard deviation, σ, is the positive root of the variance and provides a measure of the "breadth" of the distribution.

$$\sigma = [\sum \{f (\bar{x} - x)^2\} / \sum f]^{1/2} \qquad (2.3.24)$$

The coefficient of variation, which is a dimension-less percentage, may also be used:

$$cv = 100\ \sigma / \bar{x}$$

The skewness, g_1, is calculated from the third moment, $\mu 3$, and is a measure of the symmetry of the distribution function.

$$g_1 = \mu_3 / \sigma^3 = \sum [f(\bar{x} - x)^3] / \sigma^3 \sum f \qquad (2.3.25)$$

There are three possible cases:

a) $g_1 = O$ symmetrical ie: Normal or Gaussian distribution

b) $g_1 < O$ negatively skewed ie: long tail to the left or low x side

c) $g_1 > O$ positively skewed ie: long tail to the right or high x side

the kurtosis, g_2, which measures the degree of "flattening" of the distribution may be calculated from the fourth moment, μ_4.

$$g_2 = \{\mu_4 / \mu_2^2\} - 3 = \{ \sum [f (\bar{x} - x)^4] / \sigma^4 \sum f \} - 3 \qquad (2.3.26)$$

When $g_2 = 0$, the distribution is normal; $g_2 > 0$, it is tall and slim, and $g_2 < 0$, it is squat.

The normal or Gaussian distribution[318] is defined by the equation,

$$Y = \{1 / \sigma \sqrt{(2\pi)}\} \exp [- (\bar{x} - x)^2 / 2 \sigma^2] \qquad (2.3.27)$$

Skewed distributions may be given by the log-normal distribution,

$$Y = \{1 / \ln \sigma_g \sqrt{(2\pi)}\} \exp [- (\ln x - \ln x_g)^2 / 2 \ln^2 \sigma_g] \quad (2.3.28)$$

Where x_g and σ_g are the geometric mean and standard deviation

$$\ln x_g = \sum \ln x f / \sum f \quad (2.3.29)$$

when the log diameter scaling is selected, the geometric mean is automatically generated[327].

2.3.2.8 Using the Coulter counter to measure latex particle sizes

Wilkinson *et al*[329, 335, 336] used the Coulter Counter model ZB coupled to a channelyzer C1000 to monitor the particle size distribution and number density of mono-disperse polystyrene-divinylbenzene latices of 2.14, 4.86 & 9.60μm diameters over long time periods (up to 3 years) under a variety of conditions, e.g. 4°C to 40°C, exposure to sunlight, freeze-thaw cycles and elevated ionic strength. These were to be adopted by European Community Bureau of Reference (BCR) as standard reference particles. When adsorbed surfactants and a bactericide were present, no change in the mode of the particle size distribution was observed for any of the latices. The quality of the cap seals on the storage vials however influenced the change in particle number density by evaporative loss of water.

It was shown that the size distribution of these uniform latices were broadened somewhat, despite the use of editing facilities and a long ratio orifice tube, when compared with results from hydrodynamic focusing and the optical microscope certified results which were superimposable. Interestingly, although the Channelyzer had an edit on/off facility even with "edit off" some pulse editing appeared to take place since a lower count was always recorded by the Channelyzer than the counter itself.

Number counting techniques such as the Coulter counter should be useful in determining the flocculation kinetics provided that the flocs remain stable when subjected to high shear through the orifice. Matthews and Rhodes[283] used a ZB counter to study the coagulation kinetics of monosized latices of 0.714μm, 1.099μm and 1.857μm diameter. A good correlation was found between the experimental results and the Smoluchowski theory for rapid coagulation[330]. The results were affected by sedimentation only for the largest particle size latex. Slow rotation of the samples was a suggested solution to the problem. When using mixtures of particle sizes it was noted that the larger particles produced a high noise level at settings which corresponded to the small ones so complicating the analysis[331].

2.3.3 Particle electrophoresis[332]

2.3.3.1 Introduction

Electrophoresis is the motion of a liquid borne particle in an applied electric field. This phenomenon is also called "particle electrophoresis" or "microelectrophoresis" to distinguish it from the more widely known "gel electrophoresis".

In the simple particle electrophoresis measurement apparatus (Rank Bros, Cambridge, UK) the sample is contained in a capillary tube of total volume less than 10ml, immersed in a thermostat bath. The electrical field is applied at the ends and the central part of the tube is a capillary of either circular or rectangular cross-section. Particles are illuminated with white light and viewed at right angles i.e. ultra-microscopic illumination in the case of a cylindrical cell. Dark field illumination from the back of the apparatus, which shines a hollow cone of light directly at the microscope objective, is used in the case of the rectangular cell. None of that light can pass into the objective directly. It must be scattered by a particle before it will be intercepted. When viewed through the microscope,

the suspended particles appear as pinpoints of light (like stars) and when the field is applied they all move with essentially the same velocity. The speed is measured by timing their progress against an eyepiece graticule (that is, a rectangular grid which sits in the eye-piece of the microscope).

A potential of about 60-70 V is applied to the (platinum or palladium) electrodes which are about 5-10cm apart. The field strength is determined by measuring the effective distance between the electrodes, by comparing the conductivity of a salt solution in the electrophoresis cell with the value obtained in a standard conductance cell. Fields of the order of 10 V cm^{-1} are normal. The resultant velocity divided by the applied electric field yields the mobility, *U*:

$$U = V/E \qquad (2.3.30)$$

Where : V = the electrophoretic velocity

E = the applied electric field

2.3.3.2 Stationary levels

The walls of the electrophoresis cell are generally charged in the presence of solvent (negative for water), this will lead to a streaming of the oppositely charged solvent near the walls towards the appropriate electrode. This electro-osmotic streaming velocity would be uniform across the cell were it not for the reverse flow at hydrostatic equilibrium. The combination of these two opposing flows leads to a situation where the solvent itself is only stationary at well-defined levels in the cell. The observed velocity of the particle at this point is equal to its own electrophoretic velocity when measured at these 'stationary levels'.

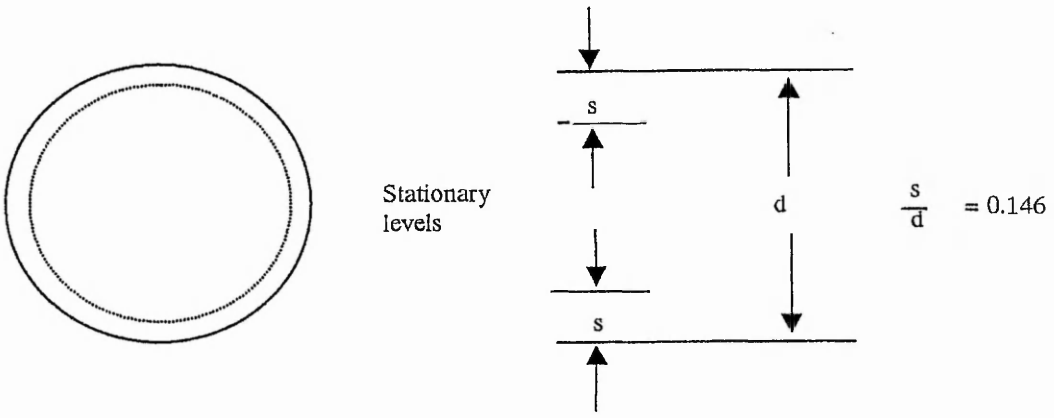

Figure 2.3.10 - Stationary level location in cylindrical cells.

The reverse flow is according to Poiseuilles law[333]:

$$V_L = V_{E.O.} - c(a^2 - r^2) \qquad (2.3.31)$$

Where V_L is the liquid velocity at a distance r from the centre of the tube of radius a and c is a constant. For zero overall liquid transport:

$$\int_0^a V_L (2\pi r).dr = 0 \qquad (2.3.32)$$

Solution of these expressions gives $c = 2V_{E.O.} / a^2$ so that:

$$V_L = V_{E.O.} \frac{2r^2}{a^2} - 1 \qquad (2.3.33)$$

The stationary level (ie: $V_L = 0$) is therefore located at r = 0.707a or 0.146 of the internal diameter of the cell.

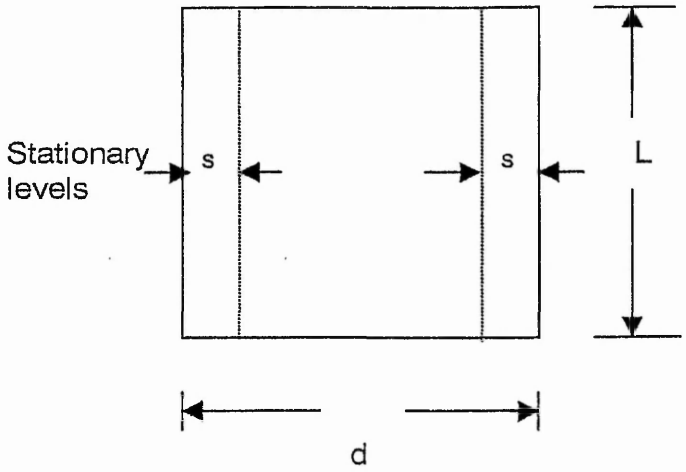

$$s/d = 0.5 - [0.0833 + 32d/\pi^5 L]^{0.5}$$

Figure 2.3.11 - Stationary level location in flat cells.

Calculation of the stationary levels for flat cells is much more complex. The location depends upon the width to thickness ratio given in the following table:

1 / d	S / d
∞	0.211
50	0.208
20	0.202
10	0.194
5	0.177

Table 2.3.2 Width to thickness ratios for calculation of stationary levels

The flat cell provided with the Rank Bros apparatus had 1/d = 5 (10mm x 2mm), ie: stationary levels at 0.177x d.

The microscope method suffers from many disadvantages:

1) The method is very slow, tedious and time-consuming.
2) Only a few particles can be followed and timed.
3) It yields results of low statistical significance.
4) Particles smaller than 0.1 μm are invisible unless the particle's refractive index is greatly different from that of the suspending liquid (eg: TiO_2 in water). For particles with a refractive index close to that of the suspending liquid (eg: gum agar in water and many important biological systems), even a 1μm particle cannot be measured.
5) There is a bias toward the more easily visible particles.

More recently developed automated techniques, e.g. DELSA discussed below, overcome the problems of operator fatigue and vast numbers of particles may be analysed improving statistical significance.

2.3.4 Doppler electrophoretic light scattering analysis (DELSA)[334]

2.3.4.1 Introduction

Electrophoretic light scattering, or ELS, makes direct velocity measurements of particles moving in an electrical field. The methodology is loosely analogous to the determination of the speed of a moving object by radar, whereby the velocity is obtained by measuring the Doppler shift (or frequency change) of microwave radiation reflected by the object. The ELS technique measures electrophoretic mobility by analysing the Doppler shift of laser light scattered from a moving particle electrophoresing in liquid.

The Doppler frequency shift resulting from a transmitter and receiver moving with a relative speed V is given by,

$$\Delta v = V v_o / c \qquad (2.3.34)$$

Where: Δv = Doppler frequency shift

V = speed of receiver relative to transmitter

v_o = frequency of transmitted wave

c = velocity of transmitted wave

In the DELSA 440, moving colloidal particles radiate scattered laser light (transmitter) and the light is detected by fixed photodiodes. The Doppler shift in this scattering measurement depends on the scattering angle according to:

$$\Delta v = 2nV \sin(\theta/2)/\lambda o \qquad (2.3.35)$$

Where: θ = scattering angle

n = index of refraction of the medium

λo = wavelength of light in vacuum.

From equation (2.3.35), it should be noted that the Doppler frequency shift is linear with $\sin(\theta/2)$. Hence, the frequency shift measured is reasonably linear with scattering angle for small scattering angles. The analyser makes Doppler frequency shift measurements simultaneously at four different scattering angles. These angles are 7.5, 15, 22.5 and 30°.

The result of a measurement on a colloid system is shown in figure 2.3.12. The intensities of scattered light from all angles are normalised. This is done to emphasise that line widths are strongly dependent on scattering angle.

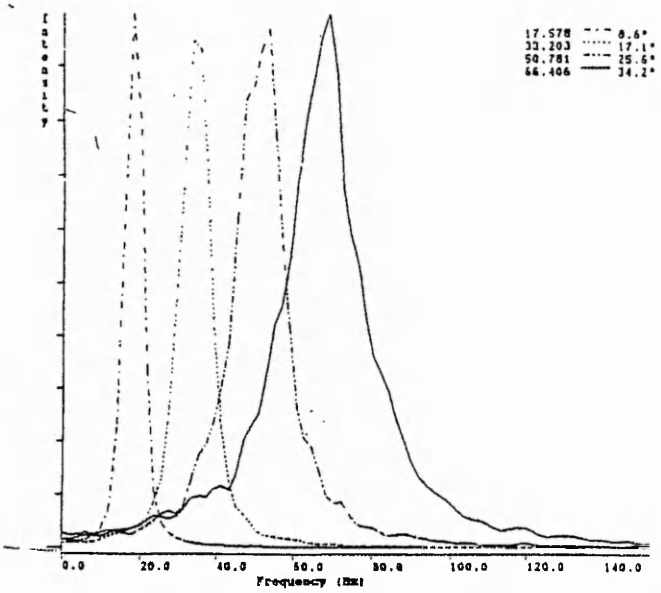

Figure 2.3.12 The Doppler frequency shift at different detection angles

Frequency shifts can range from zero (for a particle at rest) up to 1000Hz. Combining equation (2.3.34) and (2.3.35), a simple result for the mobility is obtained:

$$U = \Delta v \lambda_o / 2nE\sin(\theta/2) \qquad (2.3.36)$$

Where: U = electrophoretic mobility

Δv = Doppler shifted frequency

λ_o = laser wavelength in vacuum

n = index of refraction of the continuous medium

θ = scattering angle

E = electric field

Figure 2.3.13 shows the mobility results from simultaneous measurement at four different angles. The angles of detection displayed are the actual detection angles after the mechanical detection angles have been corrected for the refractive index of the media.

Since the He-Ne light has a frequency of about 6.0×10^{14} Hz, measurements of frequency shifts ranging from zero to several hundred Hz might be expected to present insurmountable problems because of the difficulty in measuring small differences between

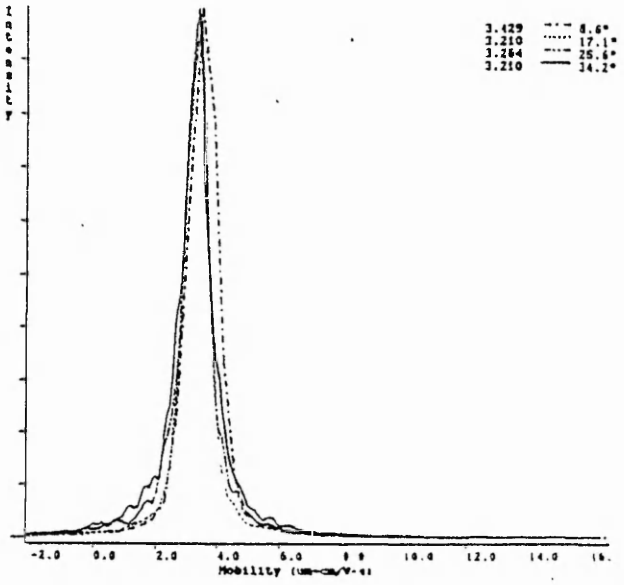

Figure 2.3.13 Display of the electrophoretic mobility of a system detected simultaneously at four different scattering angles.

large quantities. This is not the case, as is explained with the help of Figures 2.3.14 and 2.3.15.

Figure 2.3.14 is a schematic diagram of the optical system used in the DELSA 440 system. Although only one scattering angle and one detector is shown, in the system there are four detectors and four reference beams. The laser beam has some of its light scattered by the colloidal system shown between the electrodes. Most of the light passes straight through the system with some small portion of the total scattered light incident on the photo-detector shown. The reference beam is generated from the original laser beam and hence coherent with it.

These two beams, one Doppler shifted by a small amount due to the motion of the particles, and the other, the reference beam, which is not Doppler shifted, are mixed at the surface of the photo-detector. The result of this mixing is shown in Figure 2.3.14. The upper trace (A) is that of two high, but slightly different, frequency laser beams

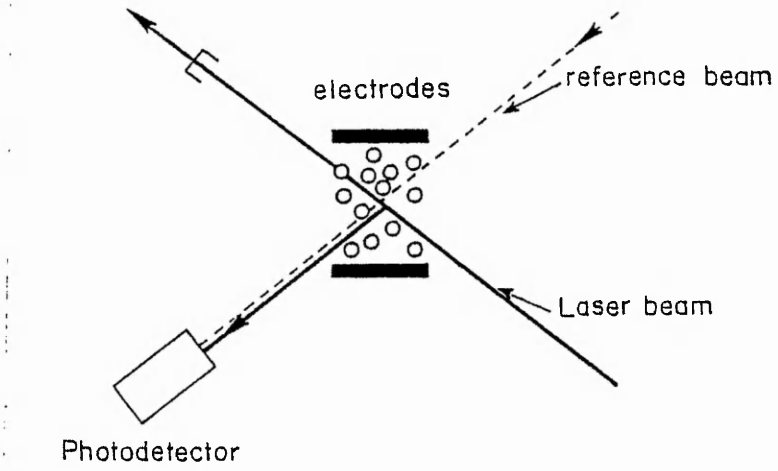

Figure 2.3.14 Schematic diagram of the optical system used in the DELSA 440 instrument

superimposed. The lower trace (B) shows the result of this superimposition. This is a particular example of the principle of heterodyning. The photo-detectors cannot follow the high incident light

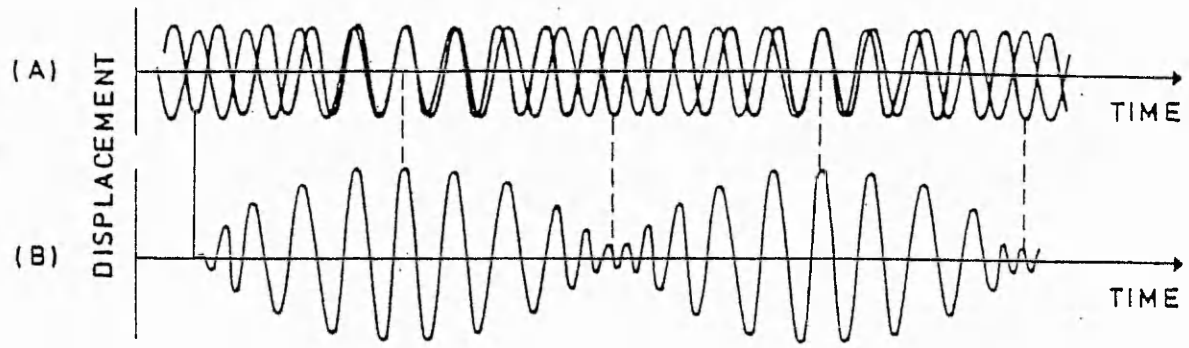

Figure 2.3.15 Schematic representation of the mixing of the reference beam with the Doppler-shifted sample beam

frequency, but they are easily capable of detecting the so-called "difference frequency" or the "beat frequency" shown as the long wavelength modulation in the bottom trace.

This then explains, in a simple way, why it is possible to detect frequency shifts as small as one part in a hundred hundred million.

The outputs of the four photo-detectors are dampened sinusoidal signals. The power spectra of the dampened sinusoidal signals are found by first passing each of the four signals into a separate 256-channel autocorrelator. The power spectra are then obtained by computing the Fourier transforms of the autocorrelation functions. The four 256-point power spectra obtained from a single measurement constitute a much higher resolution result than is obtainable from any other instruments of this kind.

Figure 2.3.12 shows that the line width of the measured frequency spectra increased with increasing scattering angle. The magnitude of the increase in line width, in fact, provides considerable information about the colloidal system being measured. The ability to make simultaneous measurements at several scattering angles is therefore an extremely critical feature, which permits a more complete characterisation of a sample, as is explained below.

Consider a collection of colloidal particles with identical electrophoretic mobility, with negligible Brownian motion. In this limiting case, the power spectrum would be four very narrow peaks separated in frequency according to Equation (2.4.35). Actual spectral peaks have considerable line width. The main causes of line width broadening are:

1) Brownian motion (for particles less than one micrometer)

2) A distribution of electrophoretic mobilities

The scattering vector magnitude (K) is a useful quantity in discussing line width broadening, where K is given by:

$$K = 4\pi n \sin(\theta/2)\lambda_o \qquad (2.3.37)$$

Line width broadening due to Brownian motion is related to K by:

$$\text{Line width} = DK^2/\pi \qquad (2.3.38)$$

Where: $D = kT/6\pi\eta r$

Thus, the line width broadening due to Brownian motion increases quadratically with scattering angle according to K^2.

Line width broadening due to the distribution of electrophoretic mobilities (ie: a population of particles having electrophoretic mobilities different from one another), is directly proportional to the breadth of the distribution and increases linearly with the scattering angle. A plot of the angular dependence of a spectral peak's line width allows one to separate the normally intermixed effects of Brownian motion and distribution width. Since the Brownian motion increases a spectral peak's line width by the square of K compared to the linear increase in line width due to the breadth of the electrophoretic mobility distribution, the shape of the line width versus scattering angle plot will be quadratic if the primary source of broadening is Brownian motion versus linear if the distribution breadth is the main source of broadening.

Separation of the two sources of spectral peak broadening is more important than it might at first seem. Without such a separation, a measurement of electrophoretic mobility at a single angle provides information only about the peak position. The shape of the peak, being attributable to either of the two effects, cannot be interpreted with a single angle

measurement. Simultaneous, multiple angle measurements allow peak shapes to be interpreted even in spectra which contain several peaks. In certain cases, a DELSA 440 multi-angle measurement can be used to separate multi-modal distributions of electrophoretic mobilities while in the same measurement obtaining the size of the particles in each of the electrophoretic mobility populations.

2.3.4.2 Mobility and zeta-potential

Particle electrophoretic mobilities are useful for characterising particle surfaces including the surfaces of organisms such as bacteria, viruses and blood cells. The nature of the surface charge can be investigated by studying the dependence of electrophoretic mobility on factors such as pH, ionic strength, addition of surface-active agents and treatment with specific chemical reagents, particularly enzymes.

It is mobility that is the fundamental parameter derived from the electrophoretic experiment, which should always be reported. Zeta potentials are often derived from mobilities as a measure of colloid stability. In estimating the double-layer repulsive forces between particles, it is usually assumed that Ψ_δ is the operative potential and that the ζ potential (calculated from electrophoretic mobilities) is identical.

Electrokinetic theory involves both the theory of the electric double layer and that of liquid flow, and is quite complicated. For curved surfaces the shape of the double layer can be described in terms of the dimension-less quantity 'κa', which is the ratio of radius of curvature to double-layer thickness. When κa is small, a charged particle may be treated as a point charge. When κa is large, the double layer is effectively flat and may be treated as such.

The Hückel equation (small κa)

$$u_E = \frac{\zeta\varepsilon}{1.5\eta} \qquad (2.3.39)$$

where ε is the permitivity of the electrolyte medium and η is the viscosity.

The Hückel equation is not likely to be applicable to particle electrophoresis in aqueous media; for example, particles of radius 10^{-8} m suspended in a 1-1 aqueous electrolyte solution would require an electrolyte concentration as low as 10^{-5} mol dm^{-3} to give κa = 0.1. The equation, however, does have possible applicability to electrophoresis in non-aqueous media of low conductance.

The Smoluchowski equation (large κa)

$$u_E = \frac{\zeta\varepsilon}{\eta} \qquad (2.3.40)$$

This equation can be used accurately for larger particles such as emulsion droplets and biological cells.

2.3.4.3 The Henry Equation

Henry[335] derived a general electrophoretic equation for conducting and non-conducting spheres, which takes the form,

$$u_E = \frac{\zeta\varepsilon}{1.5\,\eta}\,[1 + \lambda F(\kappa a)] \qquad (2.3.41)$$

where F(κa) varies between zero for small values of κa and 1.0 for large values of κa, and $\lambda = (\kappa_0 - \kappa_1)/(2\kappa_0 + \kappa_1)$, where κ_0 is the conductivity of the bulk electrolyte solution and

κ_1 is the conductivity of the particles. For small κa, the effect of particle conductance is negligible. For large *κa* the Henry equation predicts that λ should approach -1 and the electrophoretic mobility approach zero as the particle conductivity increases; however, in most practical cases, 'conducting' particles are rapidly polarised by the applied electric field and behave as non-conductors.

For non-conducting particles (λ = ½) the Henry equation can be written in the form:

$$u_E = \frac{\zeta \varepsilon}{1.5\,\eta} f(\kappa a) \qquad (2.3.42)$$

where f (*κa*) varies between 1.0 for small κa (Hückel equation) and 1.5 for large κa (Smoluchowski equation) (see Figure 2.3.16). Zeta potentials calculated from the Hückel equation (for *κa* = 0.5) and from the Smoluchowski equation (for κa = 300) differ by about 1 percent from the corresponding zeta potentials calculated from the Henry equation.

The ions in the mobile part of the double layer show a net movement in a direction opposite to that of the particle under the influence of the applied electric field. This creates a local movement of liquid which opposes the motion of the particle, and is known as *electrophoretic retardation*. It is allowed for in the Henry equation.

2.3.4.4 Relaxation

The movement of the particle relative to the mobile part of the double layer results in the double layer being distorted, because a finite time (relaxation time) is required for the original symmetry to be restored by diffusion and conduction. The resulting asymmetric mobile part of the double layer exerts an additional retarding force on the particle, known as the *relaxation effect*, and this is not accounted for in the Henry equation.

Relaxation can be safely neglected when κa is either small (<ca.0.1) or large (>ca.300), but it is significant for intermediate values of κa especially at high potentials and when the counter-ions are of high charge number and/or have low mobilities.

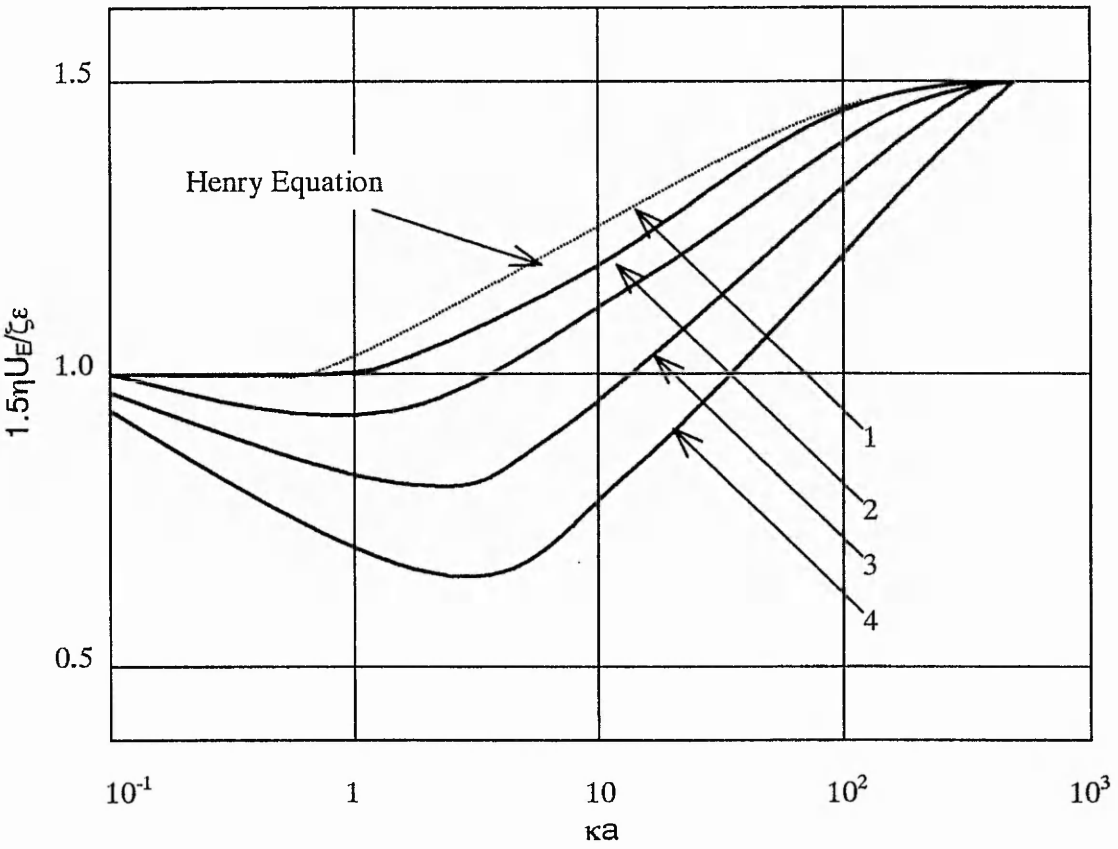

Figure 2.3.16 Electrophoretic mobility and zeta potential for spherical colloidal particles in 1-1 electrolyte ($\Lambda_+ = \Lambda_- = 70\ \Omega^{-1}\ cm^2\ mol^{-1}$). The curves refer to $e\zeta/kT$ = 1, 2, 3 and 4 (ie: ζ/mV = 25.6, 51.2, 76.8 and 102.4 at 25°C). [After P.H. Wiersema, A.L. Loeb and J.Th.G. Overbeek, *J Colloid Interface Sci* **22**, 78 (1966)].

Wiersema, Loeb and Overbeek[337] have derived equations, which allow for retardation, relaxation and for surface conductance in the mobile part of the double layer, and have solved them numerically by computer.

Thus, although the simplifying assumption that the Smoluchowski treatment will suffice for larger particle sizes, for particles in the colloidal size range κa values of 1-100 are likely to be appropriate and it can be seen from Figure 2.3.16 that errors in zeta potential may be considerable. When polyelectrolytes are adsorbed on particle surfaces, the location of the shear plane becomes uncertain and the value of conversion of mobilities to zeta particles becomes doubtful[335].

2.3.5 Laser diffraction particle size analysis

The Coulter LS230 laser diffraction instrument allows accurate particle size analysis across a wide range (0.04mm – 2000mm) by combining conventional laser diffraction with a patented Polarisation Intensity Differential Scattering system(PIDS). The scatter pattern differences from polarised light are large for small particles so as well as particle size determinations to the order of nanometers, the PIDS system also allows the resolution of multimodal size distributions.

3.1 Chitosan

3.1.1 Introduction

The flocculation behaviour of any polyelectrolyte may depend critically on its linear charge density and molecular weight. A high linear charge density on a polyelectrolyte of opposite sign to the dispersion surface charge would imply a very flat configuration[271] when adsorbed on a particle's surface, lessening the probability of bridging and increasing the likelihood of a charge neutralisation mechanism predominating. The molecular weight of the polymer is important if a bridging mechanism is in operation as longer chains imply that bridging is more effective. Modelling the charge patch mechanism, Kasper[271] reported that the adsorption density i.e. the ratio of weight of polymer per patch to area of patch, is proportional to the molecular weight raised to the power one third. Thus increasing molecular weight would be expected to increase efficiency of patches. It has also been reported that flocculation of a negatively charged dispersion by cationic polyelectrolytes can occur while the particles still carry a significantly negative charge[338]. This may be due to both bridging and charge neutralisation playing a role in the flocculation mechanism[339].

3.1.2 TGA

The presence of water or methanol (from washing stages) in the final sample would cause inaccuracies in the dye adsorption and metachromatic titration results, ultimately giving a low result for degree of deacetylation (F_D) and hence a high F_A. The amount of water or methanol present was determined by thermogravimetric analysis (TGA). The sample was heated to 110°C over a period of 22 minutes and held at that temperature until the sample

remained at constant weight. Several typical plots of mass (g) against time (s) are displayed in Figure 3.1. The overall mass of water or methanol in each sample, expressed as a percentage by weight, is displayed in table 3.1. It can be seen that, in general, each sample contains several percent water/methanol by weight, none have been dried completely by the vacuum oven treatment. The additional mass was taken into account in all, subsequent calculations, concentrations of chitosan stated are based on the amount of actual chitosan added after the water/methanol content has been subtracted.

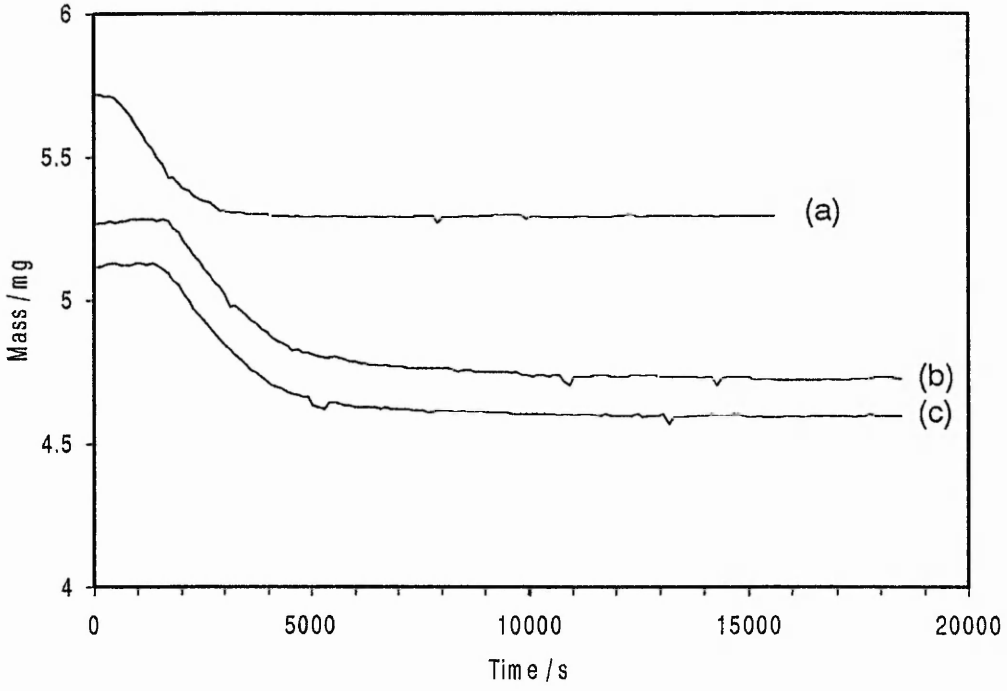

Figure 3.1.1 Plots of mass versus time for chitosan samples (a) F_A[0.57]M, (b) F_A[0.17]H and (c) F_A[0.02]M held at 110°C

Sample	Mass loss on TGA /%
Oligomer	10.41
1	9.89
2	11.65
3	7.53
4	5.62
5	13.53
6	7.36
1H	10.38
2H	6.11

Table 3.1.1 The percentage of water or methanol present in each chitosan sample

3.1.3 Degree of Acetylation

As stated in section 3.1, the flocculation behaviour of chitosan may depend strongly upon the linear charge density of the sample. In a chitosan sample, the linear charge density is determined by the fraction of polymer units bearing amine (chitosan) rather than amide (chitin) groups. This is generally expressed as degree of *N*-acetylation (fraction bearing amide groups) or degree of deacetylation (fraction bearing amine groups).

The degree of acetylation was determined in three ways: dye adsorption, metachromatic titration and FTIR. However, for reasons to be subsequently discussed the dye adsorption determination was found to give the most reproducible results and therefore these were results used. The FTIR and metachromatic titration possess inherent problems

and so, in this study, they were employed purely as checks on the dye adsorption method on several of the chitosan samples.

3.1.3.1 Dye Adsorption Results

The mole fraction of deacetylated groups (F_D) was determined using the method by Maghami and Roberts[110], as recounted in section 1.1.7.4 . When heated under reflux, there is a 1:1 stoichiometry between protonated amine groups on the polymer chain with a suitable anionic dye, in this case Orange II. Comparison between the concentration of dye in a solution containing chitosan and a blank sample containing no chitosan allows the calculation of the number of moles of dye removed from the solution by the chitosan and hence the number of moles of chitosan units in the polymer sample. This means that the degree of deacetylation (F_D) can be calculated, and the degree of acetylation, F_A is then given by $(1 - F_D)$.

Such determinations were carried out at least ten times on each crushed chitosan sample and the results displayed in table 3.1.2.

3.1.3.2 Metachromatic Titration Results

The degrees of acetylation of several samples were determined by Metachromatic Titration, the results of these are displayed in Table 3.1.3.

Figure 3.1.2 shows a typical titration plot (determined for F_A[0.14]M).

In general, those samples analysed by metachromatic titration gave F_A values which correlated well with the results obtained dye adsorption, with only F_A[0.33]M varying by more than 0.02.

Sample	Molecular Weight	Acetylated Fraction	Designation
Oligomer	Oligomer	0.021 ± 1.07 %	**F_A[0.02]O**
1	Medium	0.019 ± 1.32 %	**F_A[0.02]M**
2	Medium	0.079 ± 1.73 %	**F_A[0.08]M**
3	Medium	0.141 ± 1.47 %	**F_A[0.14]M**
4	Medium	0.240 ± 2.26 %	**F_A[0.24]M**
5	Medium	0.329 ± 1.56 %	**F_A[0.33]M**
6	Medium	0.570 ± 3.57 %	**F_A[0.57]M**
1H	High	0.172 ± 0.52%	**F_A[0.17]H**
2H	High	0.382 ± 1.64%	**F_A[0.38]H**

Table 3.1.2 degree of acetylation of chitosan samples determined by dye adsorption

Sample	F_A (mole fraction), Determined by Metachromatic Titration	F_A (mole fraction), Determined by Dye Adsorption
F_A[0.14]M	0.157 (±3.53%)	0.141 (±1.47%)
F_A[0.33]M	0.276(±1.73%)	0.329 (±1.56%)
F_A[0.17]H	0.161 *	0.172 (±0.52%)
F_A[0.38]H	0.382(±2.66%)	0.382 (±1.64%)

* - based on a single result

Table 3.1.3 degree of acetylation of chitosan samples determined by metachromatic titration

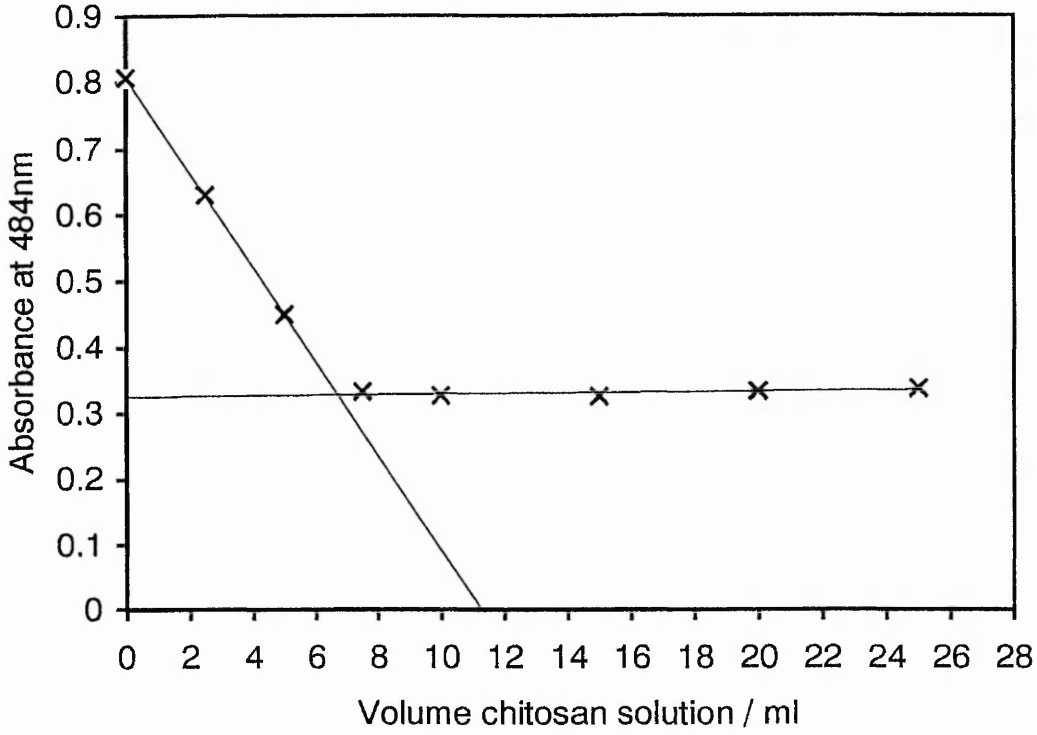

Figure 3.1.2 Example of metachromatic titration plot for F_A[0.14]M

3.1.3.3 FTIR Results

Initially, the chitosan samples were presented as KBr discs, however it proved difficult to crush the samples sufficiently using a ball mill and the resolution of the spectra were consequently too poor to be used (Figure 3.1.3). Instead, the degree of acetylation of each sample was determined according to the method described by Baxter *et al*[102], using films cast from acetic acid solution. Figure 3.4 shows a comparison of several spectra obtained in order to pick out the relevant peaks. Figure 3.1.5 shows a spectrum obtained for chitosan F_A[0.33]M including the baseline corrections

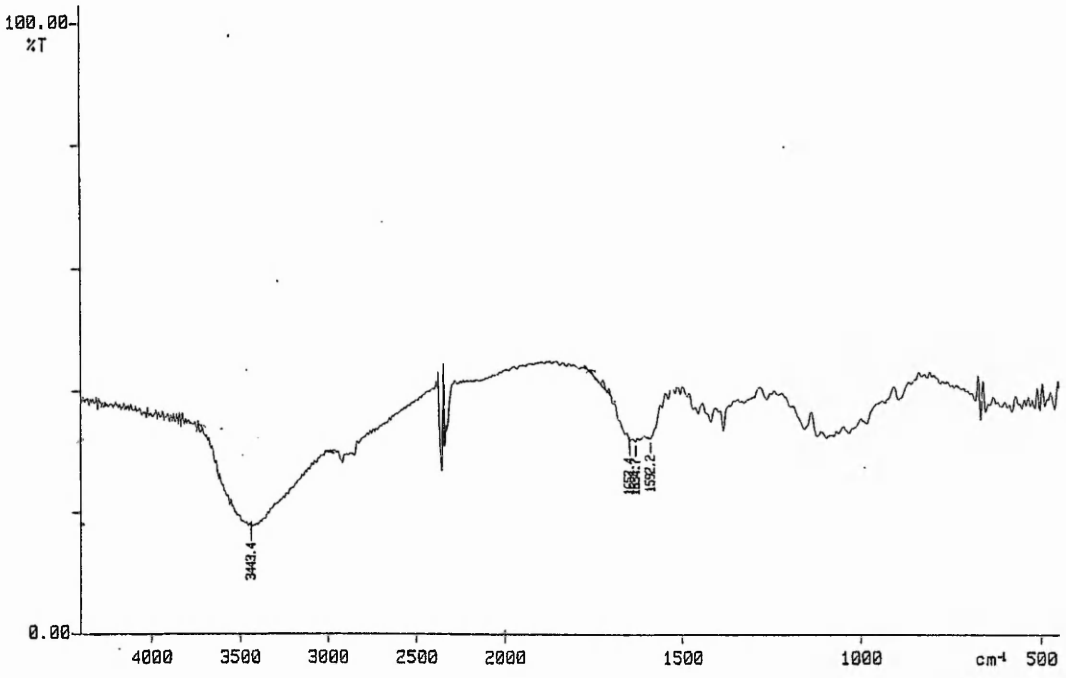

Figure 3.1.3 FTIR spectrum of chitosan (KBr disk)

outlined by Baxter *et al*[102]. The degree of acetylation (quoted as a percentage) was than determined using the relationship,

$$F_A\,(\%) = \frac{A_{1665}}{A_{3450}} \times 115$$

(These may then be displayed as mole fractions by dividing the figure by 100%.)

Table 3.1.4 displays the results obtained.

Generally, it can be seen that there is poor agreement between FTIR and dye adsorption results. F_A[0.02]O did not produce a suitable film and so could not be analysed in this way. Of the rest of the samples analysed by this method, only F_A[0.02]M and F_A[0.14]M agree well with the dye adsorption results, though the error range of these samples is large.

Sample	F_A (mole fraction), Determined by FTIR	F_A (mole fraction), Determined by Dye Adsorption
F_A[0.02]M	0.026 (±15.85%)	0.019 (±1.32%)
F_A[0.14]M	0.171 (±8.74%)	0.141 (±1.47%)
F_A[0.33]M	0.482 (±6.08%)	0.329 (±1.56%)
F_A[0.17]H	0.261 (±6.32%)	0.172 (±0.52%)
F_A[0.38]H	0.432 (±7.78%)	0.382 (±1.64%)

Table 3.1.4 Degrees of acetylation determined by FTIR

3.1.3.4 Comparison of the three methods

Comparing the results from the three methods of F_A determination, it can be seen that the dye adsorption and metachromatic titration results agree reasonably well, while the FTIR results show poor agreement. Of the three methods, the dye adsorption and metachromatic titration methods give the narrowest error ranges, generally no more than several percent, while FTIR gives much wider error ranges. This may be in part due to the ease of each method. The dye adsorption method lends itself to a large number of simultaneous determinations and so a much larger sample of results may be analysed. The metachromatic titration is much more labour intensive, one such determination taking a similar amount of time to up to six dye adsorption determinations, however it requires much less sample and so may be useful when the amount of sample is limited. The metachromatic titration method however possesses drawbacks, which may compromise accuracy and precision. As pointed out by Baxter *et al*[102], the dye used for the determination, Orange II (Acid Orange 7) has a tendency to aggregate in concentrated

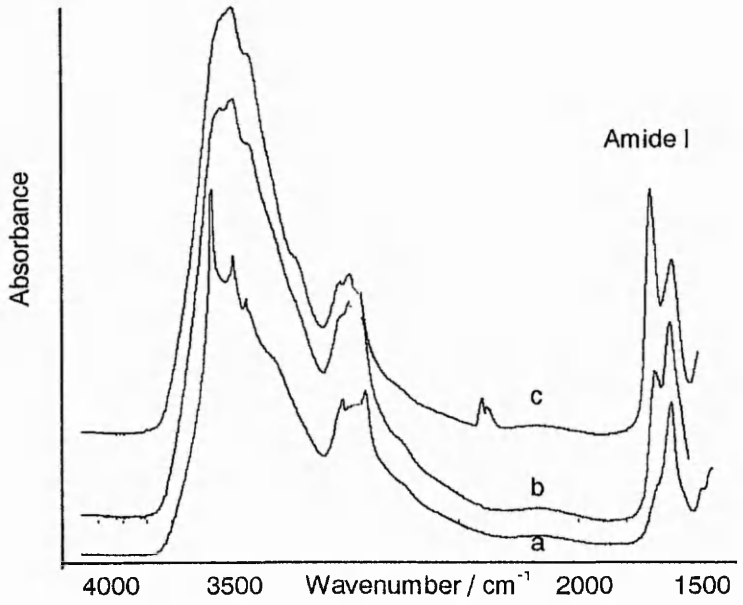

Figure 3.1.4 Examples of spectra of F_A [0.02], [0.14] and [0.33] showing variation of the amide I band

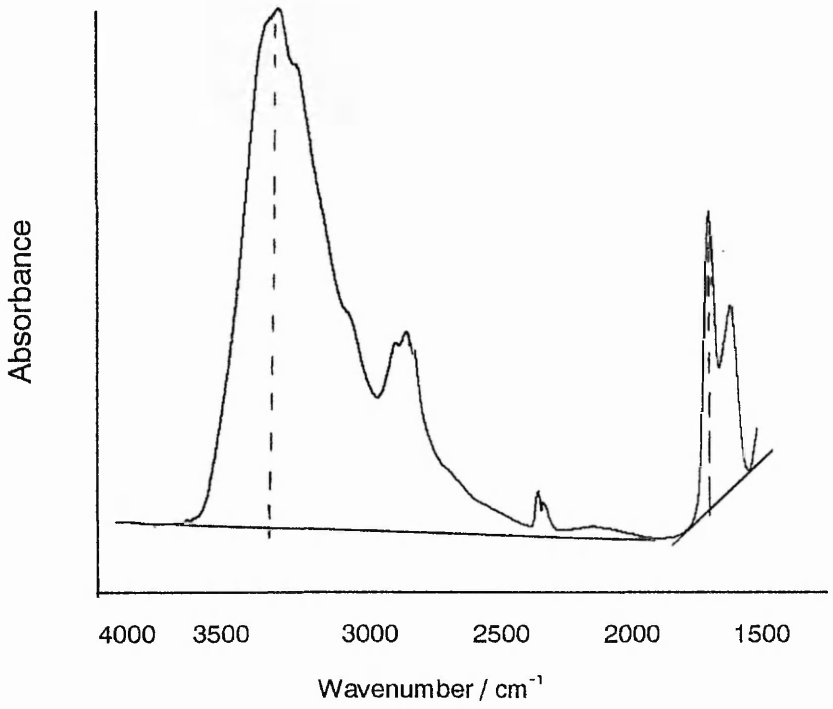

Figure 3.1.5 FTIR spectrum of chitosan F_A[0.33]M showing baseline corrections used in the determinations

solution over time, aggregates which remain in solution even after several dilution steps. This behaviour is characterised by a fall in absorption at the λ_{MAX}. This means that, potentially, if the dye solutions are not freshly prepared, the concentration of dye solutions could appear lower than they actually are. Should aggregation occur however, the use of the same stock solution for both blank and samples should help to mitigate this effect. The dye adsorption method, despite utilising the same dye, should not suffer inaccuracy because of this since all samples are refluxed for 24 hours which prevents the dye aggregating (Baxter *et al*[102]).

The FTIR method uses the absorbance of the amide I band at 1655cm^{-1} to estimate the concentration of the amide in a solid sample. The hydrogen bonded OH stretch peak at 3450 cm^{-1} is used as an internal reference peak as this band is unaffected by the acetylation reaction and should therefore remain constant. It is implicitly assumed that the films produced are completely free of water and methanol from the film casting stage, any water or methanol present in the film will add to the OH_{3450} peak. However, it is apparent from the preparation of the chitosan samples that complete removal of water and methanol from the samples is not guaranteed by the vacuum drying stage. Any residual water or methanol in the film will increase the absorbance of the 3450 cm^{-1} band causing an error in the estimation of the degree of acetylation. Figure 3.1.6 shows a TGA result for a film prepared from the F_A[0.83]H sample. It can be seen that approximately 10% of the mass of the film is lost on drying at elevated temperatures. This loss of mass may be made up of water or methanol from the casting stage which, if unaccounted for, would increase the absorbance of the OH stretch peak at 3450cm^{-1}, and thus causing a reduction in the observed amide concentration. The relative effect of water and methanol on the peak height may not be equal, for example water possesses two hydroxy groups to methanol's one implying that IR response for this band may be greater. This means that simply allowing for the mass loss

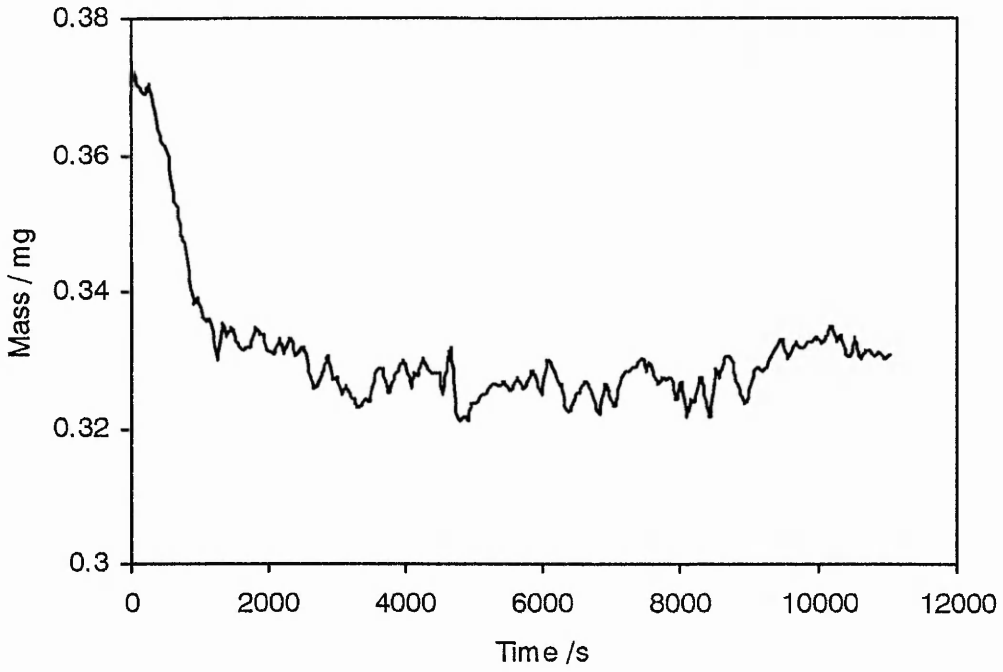

Figure 3.1.6 TGA plot showing mass loss with time for F_A[0.83]H chitosan sample heated to 110°C.

indicated by TGA would not be enough to produce an accurate level of acetylation. In order to produce a reliable result it may be necessary to use more aggressive drying conditions such as elevated temperatures and replacing silica gel with agents such as P_2O_5.

3.1.4 Molecular weight determination

The molecular weight of the flocculant may have an important bearing on its effectiveness as a flocculant. Also, determination of the molecular weight of the samples would help to show that no degradation of the polymer chains occur as a consequence of the reacetylation reaction. Table 3.1.5 sets out the results measured and calculated from a viscometry study of chitosan samples of several different degrees of acetylation, all the medium molecular weight samples being prepared by the reacetylation of the original F_A[0.02]M chitosan sample. The determinations were carried out using an Ubbleholde viscometer according to the method by

Wang *et al*[120]. The determined molecular weight for each of the medium molecular weight samples is plotted against acetylation degree in Figure 3.1.6 (upper unbroken line). Assuming that the initial estimate of molecular weight of F_A[0.02]M is correct (at 5.09 x 10^5), then it is a simple matter to calculate the increase in molecular weight that the addition of a number of acetyl groups will imply. This figure for each sample is also displayed on Figure 3.1.7 (represented by the upper broken line). Similarly, the degree of polymerisation may be calculated for the samples by dividing its determined molecular weight by the average repeat unit weight, represented by the lower pair of unbroken (experimental) and broken (theoretical) lines. If the chitosan chains are not degraded during reacetylation, then the DP should remain constant throughout the range of samples.

Sample	[η]	M	DP
F_A[0.02]O	6.05	1.90×10^3	12
F_A[0.02]M	548	5.09×10^5	3142
F_A[0.08]M	611	5.27×10^5	3205
F_A[0.14]M	573	6.03×10^5	3614
F_A[0.26]M	474	8.07×10^5	4615
F_A[0.33]M	835	1.92×10^6	1.1×10^4
FA[0.17]H	932	1.12×10^6	6661

Table 3.1.5 Intrinsic viscosities of chitosan solutions and calculated quantities

Observing Figure 3.1.7, it can be seen that the pattern of increasing molecular weight deviates from the expected straight line. Indeed the measured molecular weight appears to increase almost exponentially with F_A. If the value of DP of each sample is considered, it can be seen that, instead of remaining constant, these results imply that DP

increases with increasing F_A. These two points indicate that the viscometry parameters employed are unreliable. Indeed, Wang himself has since cast doubt this method[340] along with several other recently proposed viscometry methods. Using similar arguments combined with evidence from an ultracentrifugation study of molecular weight, which showed DP to be constant with degree of acetylation, it was concluded that there were, as yet, no reliable viscometric methods for the determination of the molecular weight of chitosan. This may be in part ascribed to the association of chitosan chains in solution[89, 113] which may be due to a crystallisation process[38] or to the presence of small concentrations of multivalent ions[89, 19]. This effect would increase with increasing F_A as an increasing number of amide groups would necessarily imply an increasing number of amide groups situated adjacently on a chain.

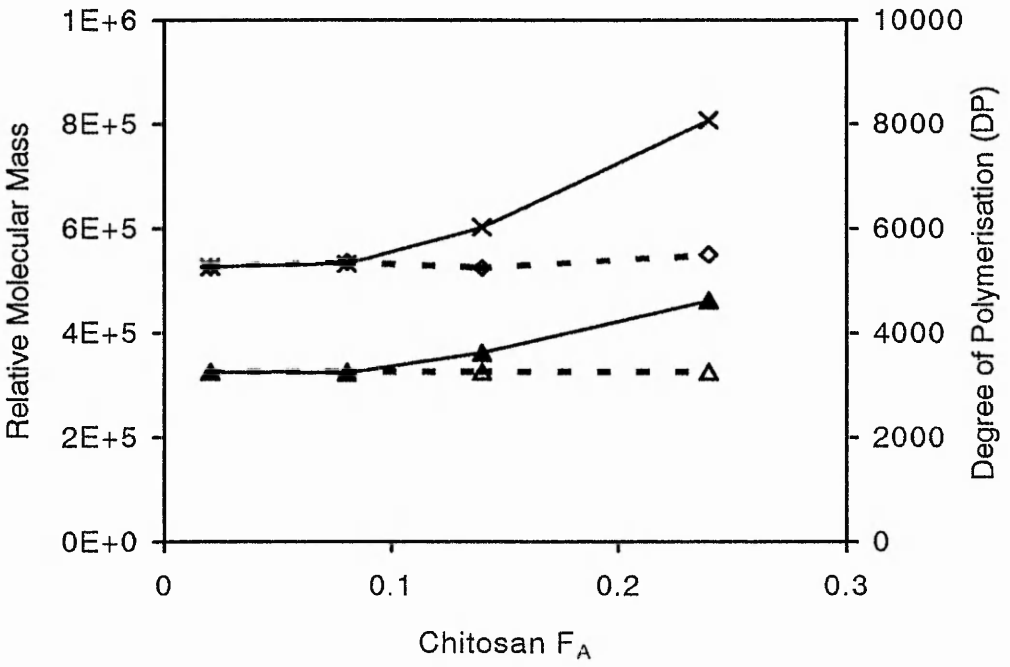

Figure 3.1.7 Plot of calculated molecular weight (upper curves) and DP (lower curves) against F_A, according to Wang *et al*'s[120] method, for a range of chitosan samples.

Although Wang *et al's*[340] conclusions about the validity of viscometric methods were broadly similar to the present study's, the [η] of a sample possessing a degree of acetylation quoted as F_A[0.02] and studied under identical conditions to those used here, was determined to be very similar to the F_A[0.02] sample used in this study indicating that it possessed a similar molecular weight. The molecular weight of the F_A[0.02] in Wang *et al's* study was determined by ultracentrifugation studies to be approximately 2.5×10^5 (DP ~ 1545), and so it may be reasonably assumed that the molecular weight of sample used in the present study is of the same order.

Comparing the [η] values of the F_A[0.14]M and F_A[0.17]H indicates that the molecular weight of the "high molecular weight" samples may be approximately 33% greater than the "medium molecular weight" samples.

The oligomeric sample, F_A[0.02]O was found to possess an intrinsic viscosity of 6.05 which gives, using Wang's method[120], a molecular weight of 1.9×10^3 and a DP of 12.

3.2 Latices

3.2.1 In-house latices

3.2.1.1 85nm Latex

(i) Size, Percent Solids and Number Density

Mean particle diameter, determined by PCS = 85nm

Solids content in original latex = 6.67% w/v

Number density in flocculation experiments = 1.97×10^{14} particles cm^{-3}

(ii) Titration of the Latex

The latex was titrated conductometrically against 0.1002M sodium hydroxide solution. Figure 3.2.1 shows the titration of the acid washed latex.

The end-points for both sulphate and carboxyl groups may be found,

(a) Strong Acid (sulphate)

= 0.39ml of 0.1002M NaOH = 2.339×10^{-5} Eq g^{-1}

(b) Weak Acid (carboxyl) = (0.555-0.39)

= 0.165ml of 0.1002M NaOH = 9.94×10^{-6} Eq g^{-1}

Total anionic surface groups

= 0.555ml of 0.1002M NaOH = 3.333×10^{-5} Eq g^{-1}

Using the end points of both the strong and the strong plus weak acid groups would give the following concentrations of charge at the dilution used, in the flocculation experiments.

(i) Strong acid groups 4.16×10^{-7} eql^{-1} surface groups

(ii) Strong + Weak acid groups 5.92×10^{-7} eql^{-1} surface groups

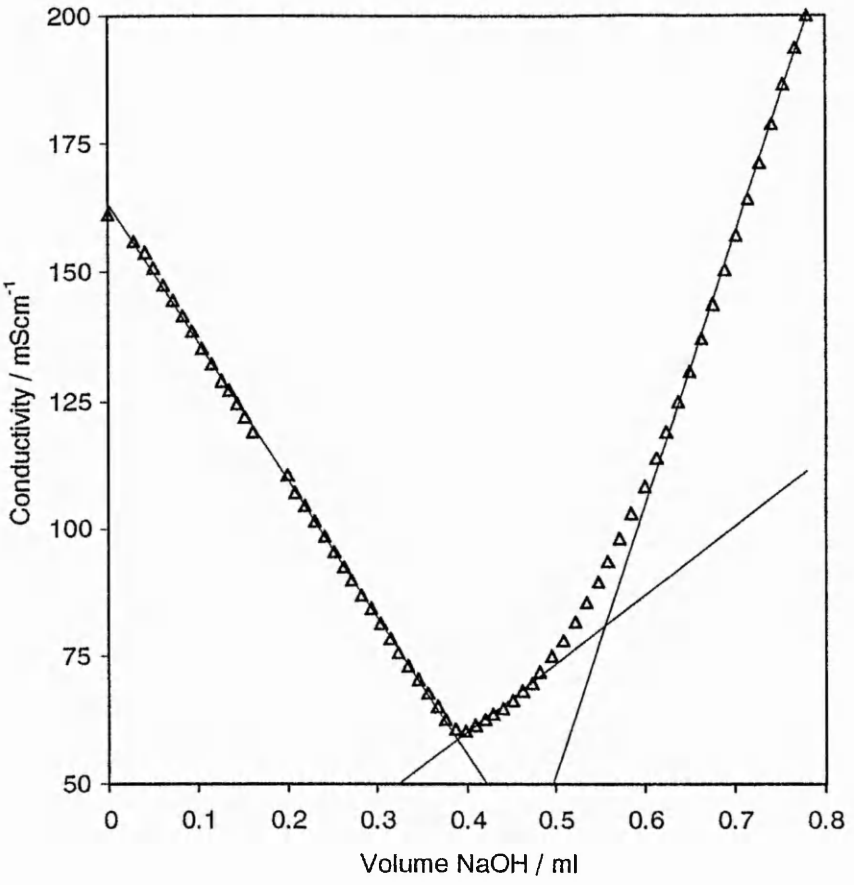

Figure 3.2.1 Conductometric titration curve for 85nm latex titrated against 0.1002M sodium hydroxide solution.

A repeat titration of this latex gave the sulphate surface charge concentration as 3.87 eq L^{-1}, an error of just under ±4% and the total surface charge concentration as 6 $x10^{-7}$ eq L^{-1}, an error of less than ±1%.

3.2.1.2 2100nm Latex

Unfortunately, the 2100nm in-house prepared latex was accidentally destroyed by freezing before it could be titrated, however, a small amount of cleaned latex was left and this was the subject of an electrophoresis study using the Rank Electrophoresis apparatus.

3.2.2 Interfacial Dynamics Latices

Mean diameter, solids content, particle number density, charge content per gram and area per charge group for each of the latexes obtained from the Interfacial Dynamics Corporation are reproduced in Section 2.2.4.1 In the following Sections, the

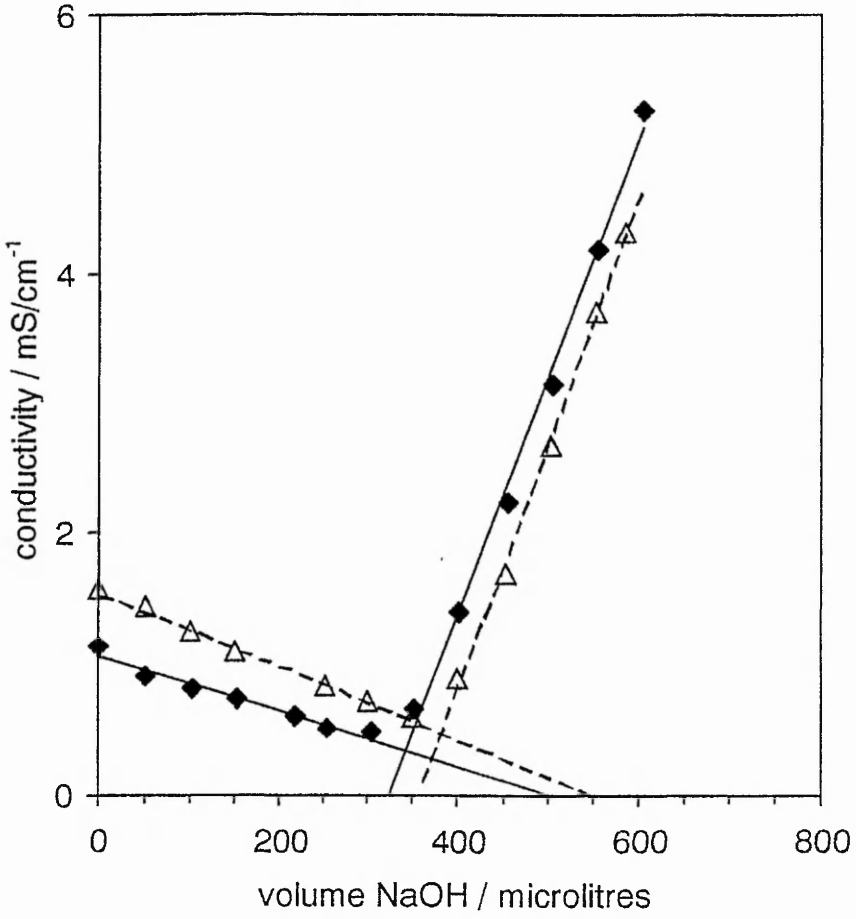

Figure 3.2.3 Repeat conductometric titrations of the 400nm Interfacial Dynamics latex

conductometric titration plots of conductivity versus charge group concentration, expressed in terms of volume of titrant or μEq g^{-1}, are here reproduced for the 400nm latex. It may be observed from figure 3.2.3 that the presence of carboxyl groups is not apparent and may therefore be regarded as negligible. Two repeat titrations of the

400nm latex are displayed in figure 3.2.3 in order to give an idea of experimental error, this was estimated to be approximately ± 4%.

3.3 Conclusions

It is clear that complete removal of all solvents from the "dry" chitosan samples is important or that the residual solvent levels should be known accurately, so that allowance can be made for them.

The dye adsorption method for determining degree of acetylation of chitosans proved more reliable and reproducible than the metachromatic titration technique whilst completely solvent free samples are required in order for FTIR to be a useful technique.

Viscometric methods for molecular weight characterisation of chitosan are clearly unsatisfactory at this stage of their development. Degrees of polymerisation which would be expected to remain constant, vary dramatically. The problem lies in the fact that chitosans are not homopolymers for which K and α would remain constant but rather each copolymer composition (degree of acetylation) would require unique values. Fortunately in this work accurate molecular weight values are not needed in charge group stoichiometry calculations, rather the knowledge that a wide range of molecular weight samples have been employed is all that is required and this can be judged from intrinsic viscosities, without conversion to molecular weights.

The conductometric titrations of the 'sulphate only" latices from Interfacial Dynamics confirm, at least in the case of the 400nm and 2μm particles, that there is no discernible weak acid group contribution to a highly reproducible end point. The problems experienced with the very low surface charge 300nm latex particles are discussed later.

4.1 85nm Latex Flocculation Results and Discussion

Dynamic light scattering was used to identify the flocculation concentration range for each flocculant or coagulant. Once the latex started to aggregate, an increase in the mean particle size was readily apparent. Figure 4.1 shows the mean size of particles, flocculated with F_A[0.02]M, after a series of three minute intervals up to twelve minutes and again after 24 hours. The peak height increases as the floc size increases and the shoulder of the peak becomes better defined, although the range is essentially unchanged after 3 minutes. It was decided that results would be taken after 12 minutes. PCS is a less effective measuring technique for particles above 1μm as the influence of Brownian motion becomes less pronounced[288]. Reliably reproducible sizes were obtained by accumulating the data over 4 runs lasting 120 seconds. Slow data accumulation in this way makes the technique unsuitable for a kinetic study. The final reported data was accumulated over the last three minutes of a 12-minute run, and in subsequent determinations, any particle sizes measured above 1μm were arbitrarily reported as being equal to 1μm.

Figures 4.2, 4.3, and 4.4 show how chitosan samples with different linear charge densities (degrees of acetylation) behave as flocculants. In can be seen that the concentration of flocculant required to effect aggregation is increased with decreasing charge density. If chitosan flocculates the system via inter-particle bridging, it may be expected that linear charge density would be largely unimportant, as polymer bridges require few points of attachment. If, on the other hand, chitosan flocculates this system via a charge neutralisation mechanism then, as less cationic charge is being added per unit

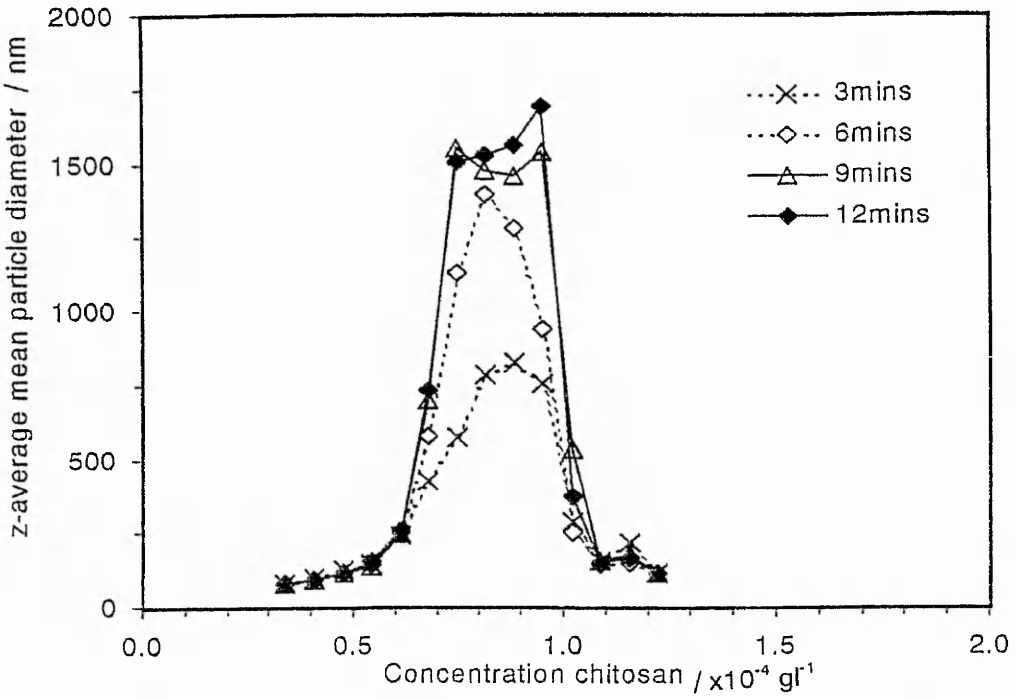

Figure 4.1 The variation in particle diameter of the 85nm latex with time for a range of added chitosan concentrations.

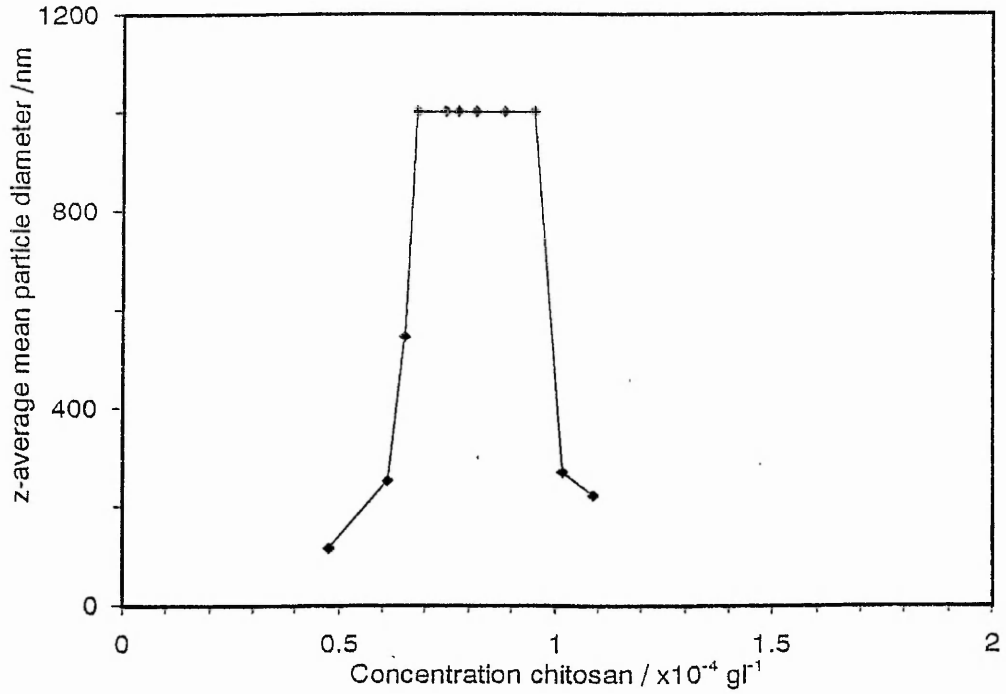

Figure 4.2 Flocculation of the 85nm dispersion with time using F_A[0.02]M chitosan

mass with samples of lower charge densities, more flocculant is needed to provide the optimum level of charge. Furthermore, if inter-particle bridging were the predominant mechanism then the critical flocculation concentration should be strongly dependent upon the molecular weight of the flocculant. The higher the molecular weight the lower the optimum flocculant concentration and vice versa. Figure 4.5 shows the effect of F_A[0.17]H on the system and it is apparent that the critical flocculation concentration is not significantly different from the medium molecular weight chitosan F_A[0.14]M. Figure 4.6, which depicts the behaviour of F_A[0.38]H, again shows little difference from the medium molecular weight sample F_A[0.33]M. Both of these results argue against bridging being the operative mechanism of aggregation. Furthering this argument, if bridging is the predominant mechanism, the oligomeric sample (DP ≈ 12, RMM ≈ 10^3) should display by far the worst flocculation efficiency as the loops and tails required to bridge adjacent particles would be so much shorter than the those produced by the other samples. On the other hand, if charge neutralisation dominated, then the optimum flocculation concentration should be no different from that for the F_A[0.02]M sample. Figure 4.7 shows that, although the range of the oligomer is slightly narrower, both peaks are centred at approximately $8x10^{-5}gl^{-1}$, indicating the charge neutralisation mechanism rather than bridging.

If some form of charge neutralisation mechanism is occurring, then a comparison of the concentrations of anions and cations available in the flocculating system should make this clear. For the anionic latex a simple form of charge neutralisation, analogous to coagulation by a suitable cationic surfactant such as cetyl trimethyl ammonium bromide, would result in optimum flocculation at a point when the concentration of the oppositely charged ions on the particle surface and on the flocculant was equal. In the "electrostatic patch" mechanism suggested by Kasper[271] and by Gregory[269] for flocculation by an

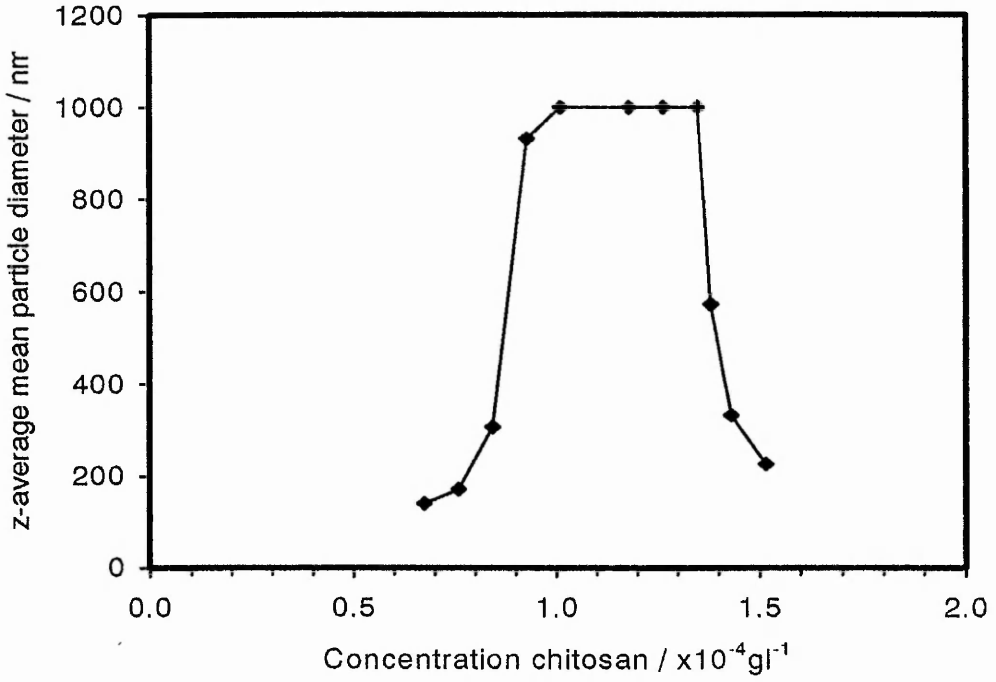

Figure 4.3 Flocculation of the 85nm dispersion using F_A[0.14]M chitosan

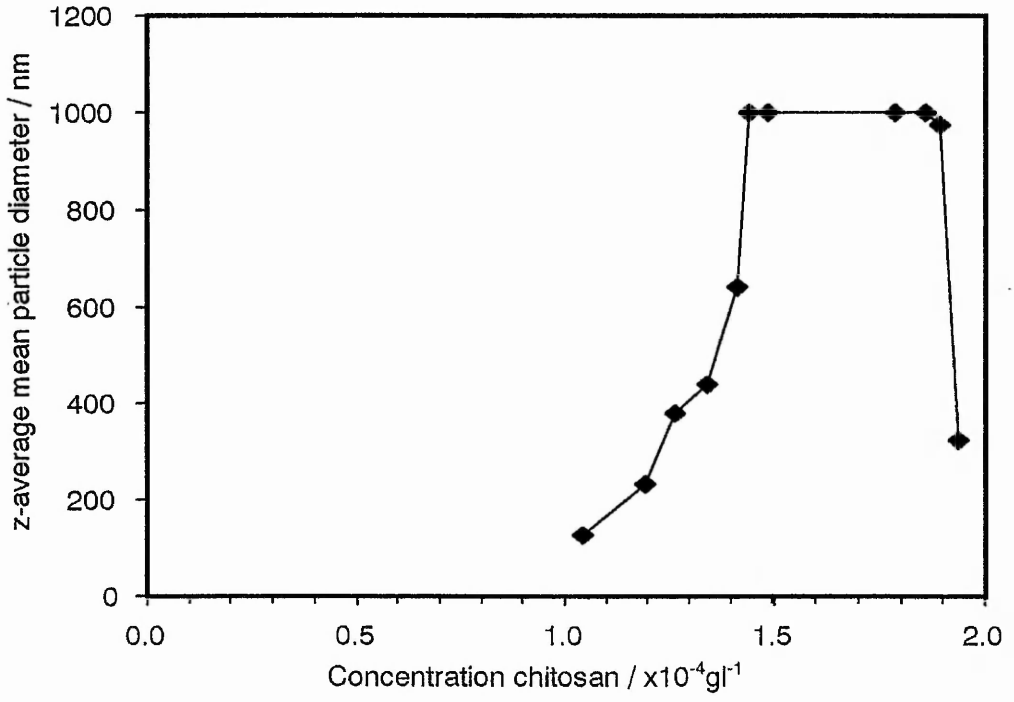

Figure 4.4 Flocculation of the 85nm dispersion using F_A[0.33]M chitosan

oppositely charged polyelectrolyte, the critical flocculation concentration occurs around the point of charge neutralisation.

Figure 4.8 shows the flocculation range for the chitosan sample F_A[0.02]M with the flocculant concentration plotted in terms of the concentration of amine units in the flocculating system. As described earlier, the charge due to the latex surface was determined by conductometric titration (see section 3.2.1.1). As carboxyl as well as sulphate groups may contribute to the surface charge of this latex, it is necessary to assess whether the weaker carboxyl groups (pK_a 4.5) will be dissociated under the conditions of the experiment. The stronger sulphate groups ($pK_a < 2$) should be dissociated at any pH relevant to this study. At the acetic acid concentration used (0.1M, pH 2.9) it would be expected that the surface carboxyl groups, pK_a 4.5, may be partially ionised. An electrophoresis study of carboxylated latices (Hearn *et al*[184]) suggested that about 10% dissociation would be expected at this pH which gives a likely charge of 4.3 $x10^{-7}$ mol dm^{-3}. Shubin *et al*[341] have suggested that the adsorption of a polycation on to a charge regulating surface increases the dissociation of weak acid groups.Shinoda and Nakajima[342] have proposed, for hydroxyethyl chitosan [0.38] at pH 3.5 interacting with carboxyl groups in hyaluronic acid, a low linear charge density polyelectrolyte, that about 70% of the NH_3^+ groups had been electrically neutralised through induced dissociation of the carboxyl groups. It may therefore be uncertain what proportion, between 10% and 70%, of the carboxyl surface groups contribute to the overall surface charge of the dispersion. However, as flocculation peak for F_A[0.02]M in Figure 4.8 is centred midway between the concentration of sulphate groups (4.16 x 10^{-7}mol dm^{-3}) and the total concentration of sulphate plus carboxylic acid groups (5.92 x 10^{-7}mol dm^{-3}) it may be assumed that approximately 50% of the carboxylic acid groups are ionised on flocculation. So, generally speaking, a charge neutralisation mechanism is indicated to be at work in this system.

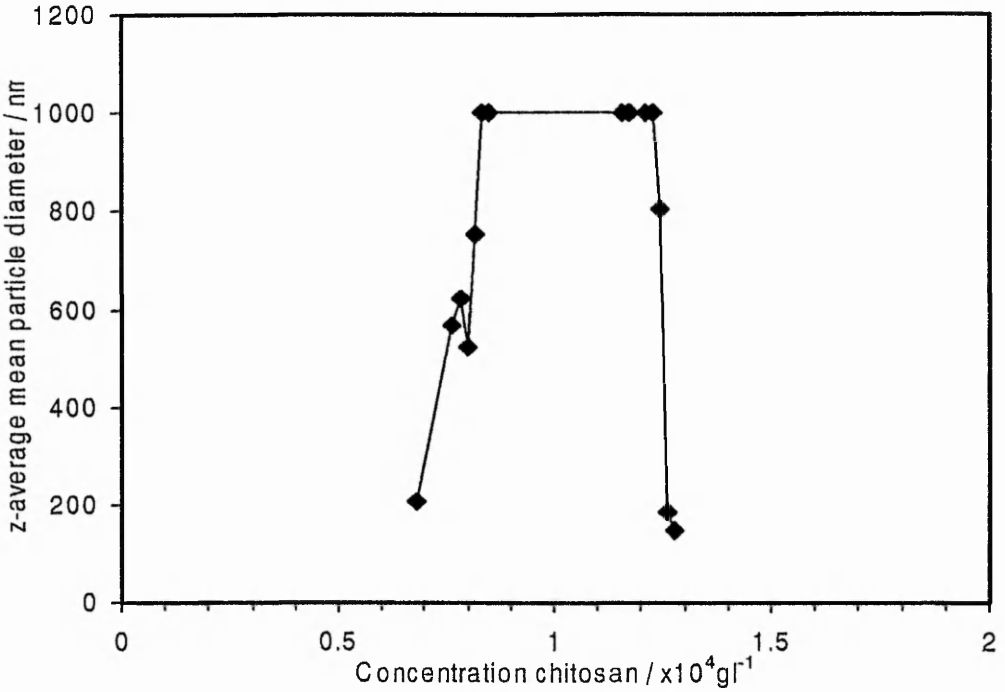

Figure 4.5 Flocculation of the 85nm dispersion using F_A[0.17]H chitosan

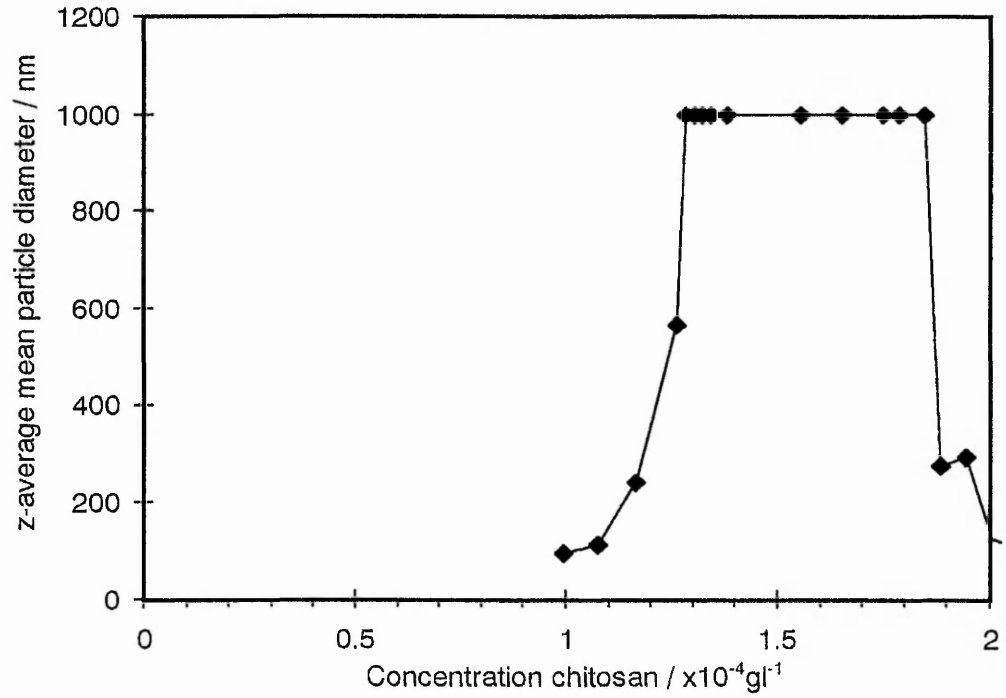

Figure 4.6 Flocculation of the 85nm dispersion using F_A[0.38]H chitosan

Figure 4.9 illustrates the coagulation behaviour of CTAB with this system. If it can be assumed that a 1:1 stoichiometry between dissociated surface acid groups and CTA+ ions exists at the coagulation point[221, 270], this data suggests that the charge neutralisation point occurs at a CTAB concentration of around 6 x 10^{-7}mol dm^{-3} indicating that a significant proportion of the carboxyl species may well be dissociated. However some degree of equilibrium may exist between CTA+ ions on the surface and in solution, implying that a slight excess of CTA+ over the anionic surface charges would be required in the solution before flocculation occurred. Whatever the finer points of the mechanism, this data strongly suggests a charge neutralisation mechanism rather than a bridging mechanism is in operation in this system.

To distinguish between simple charge neutralisation, analogous to coagulation by CTAB, and the electrostatic patch model, it is necessary to determine the rates of aggregation. Coagulation by indifferent electrolyte results in aggregation solely through van der Waals' forces of attraction once the electrostatic repulsion in the system is effectively removed, therefore any analogous mechanism should be marked by a similar rate, though it may be slightly elevated[279] due to factors such as the increased collision radius of the CTAB coated particle, or an increase in the hydrophobic effect. The electrostatic patch model for polyelectrolyte induced flocculation may be distinguished by a marked elevation of aggregation rate over the rate of simple coagulation. This is due to Coulombic attraction between oppositely charged patches on adjacent particles. Gregory also reported[269] that increasing the ionic strength in the system brought about a decrease in the rate elevation, tending towards the rate of rapid coagulation, and a broadening of the flocculation range. The former of these effects was attributed to increased screening of the charges on polymer and particle bringing about a reduction in electrostatic attraction between patches.

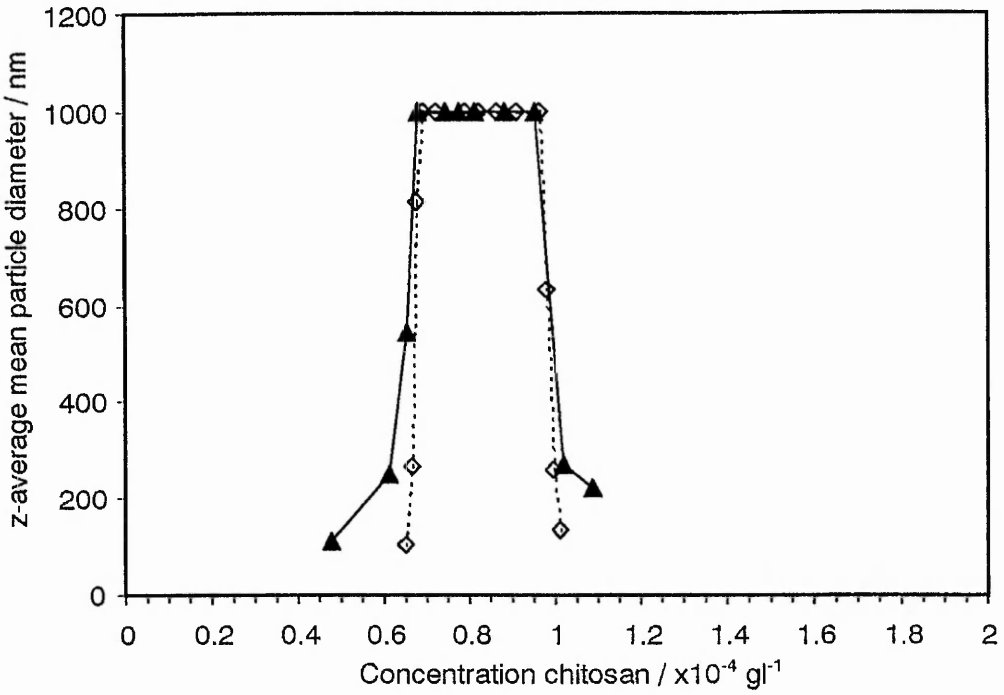

Figure 4.7 Comparison of the flocculation ranges displayed by F_A[0.02]O (◇) and F_A[0.02]M (▲).

The latter is simply due to the destabilisation of latex particles with partially neutralised surface charges. Figure 4.10 shows the variation in initial rate of flocculation, relative to rapid coagulation with 1M NaCl, in the system with concentration of F_A[0.02]M. The system displays a marked elevation of approximately 40% over rapid coagulation indicating the increased attraction inherent in the electrostatic patch mechanism. Figure 4.11 shows the broadening effect of increasing ionic strength on the flocculation range, an increase in the width of the flocculation range may also be taken as an indication of the electrostatic patch mechanism[269].

If the results obtained for the flocculation ranges of chitosan samples of varying degrees of acetylation are compared in terms of equivalents of charge added to the system, the results shown in Figures 4.12 and 4.13 are obtained for samples F_A[0.14]M and FA[0.33]M respectively. These samples also flocculate the system around the point of

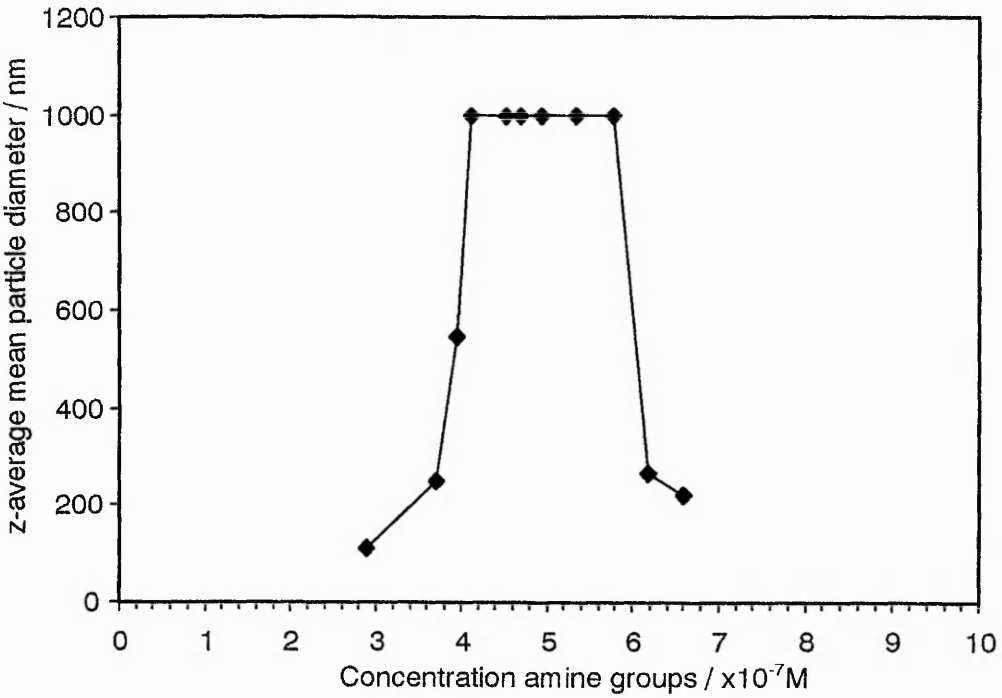

Figure 4.8 The flocculation range for the F_A[0.02]M chitosan / 85nm latex system redisplayed with concentration plotted in terms of amine group concentration (equal to the concentration of molar equivalents of charge when protonated).

charge neutralisation, however there appears to be a trend towards higher flocculation concentrations with increasing acetylation (i.e. decreasing linear charge density.). Chitosan undergoes changes in physical properties with increasing acetylation degree, which may help to account for this behaviour. The more acetylated chains are not only needed in greater numbers to produce the necessary charge because of their lower linear charge densities, they are also stiffer, more linear chains as a consequence of intra-molecular hydrogen bonding (Figure 4.14) and are less able to configure themselves to match the template set by the charges on the latex particle surface.

The behaviour of the oligomeric sample F_A[0.02]O shown if Figure 4.8 helps to discount the bridging mechanism when compared to higher molecular weight samples as it

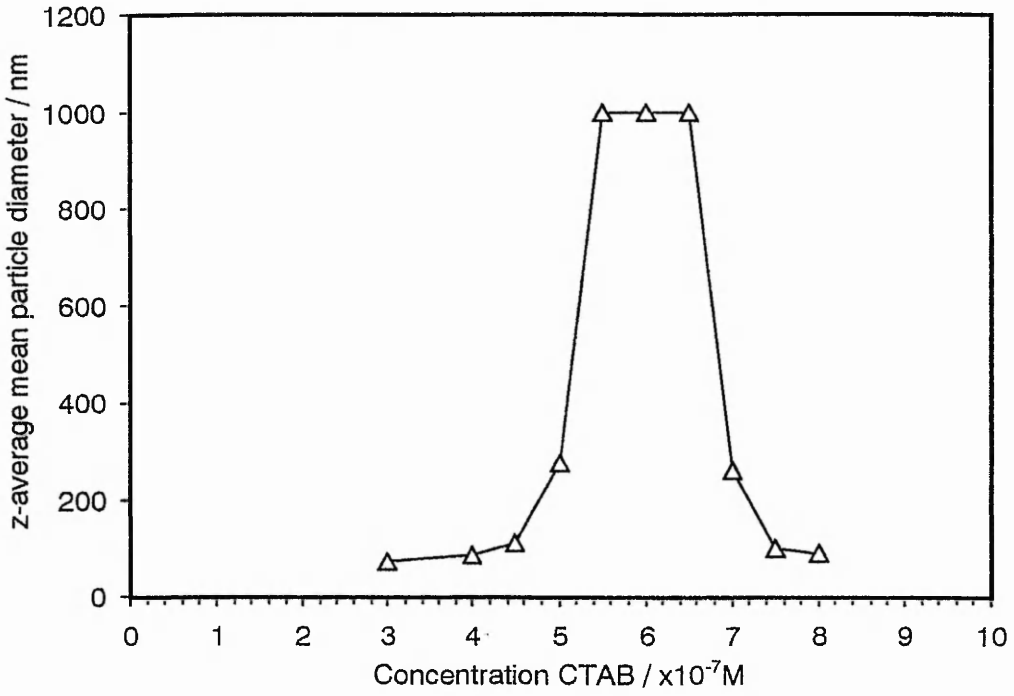

Figure 4.9 The coagulation range displayed by CTAB

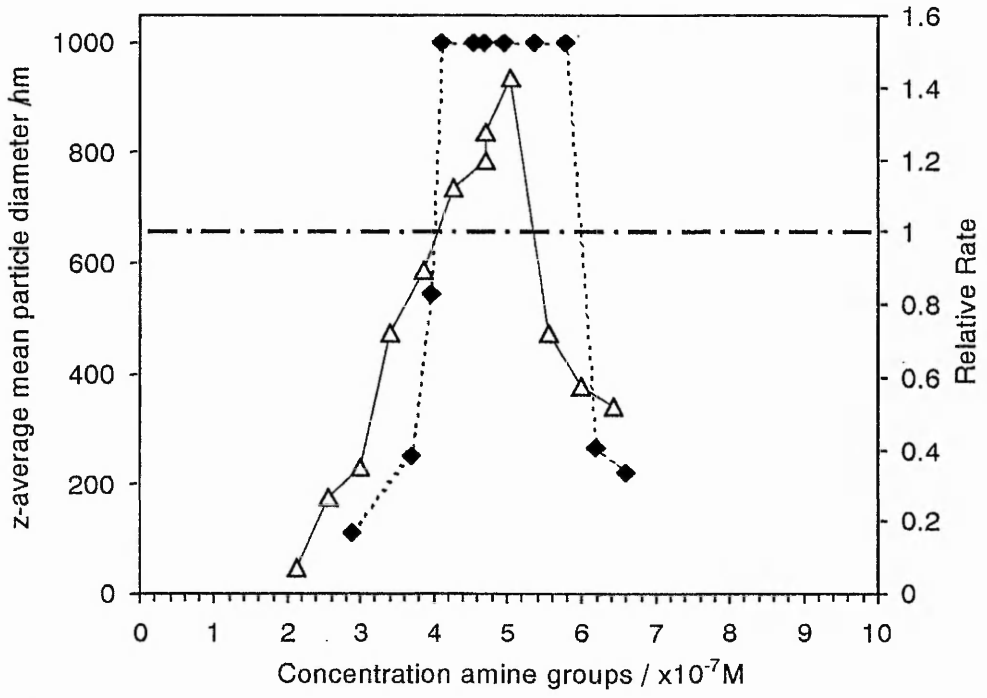

Figure 4.10 The rate of flocculation of 85nm latex by F_A[0.02]M chitosan relative to rapid coagulation (△) across the flocculation range determined by PCS (◆).

shows that, rather than requiring a higher dosage than other samples to effect flocculation, due to the formation of shorter and therefore less efficient bridges, it actually displays an optimum flocculation concentration (in terms of cationic charge) comparable to that of the F_A[0.02]M sample, indicating that charge neutralisation is more likely. Plotting concentration in terms of amine concentration as with the other samples would help to clarify whether charge neutralisation is the key effect. Figure 4.15 redisplays Figure 4.8 in terms of amine concentration and it shows F_A[0.02]O flocculates the 85nm system at an amine concentration equivalent to that for F_A[0.02]M i.e. at approximately the point of charge neutralisation. Considering the higher molecular weight chitosan samples in Figure 4.16 and 4.17, flocculation occurs again at an amine concentration of around 5 x 10^{-7}mol dm^{-3}. Imposing an arbitrary measure of peak position and width would help to compare the behaviour of these samples more easily. Table 4.1 sets out the peak position, in terms of concentration of amine groups at the onset of flocculation (lower limit), at the centre of the peak, at the upper limit of flocculation and the resulting peak width, all at the point at which the mean particle diameter = 500nm. The choice of error range is difficult to make in

Aggregant	Lower Limit / x10^{-7}M	Peak Centre / x10^{-7}M	Upper Limit / x10^{-7}M	Peak Width / x10^{-7}M	Error Range / x10^{-7}M
CTAB	5.06	5.81	6.55	1.49	4.92 – 5.55
F_A[0.02]O	4.02	5.13	6.28	2.26	5.04 – 5.43
F_A[0.02]M	3.97	5.00	6.10	2.13	5.03 – 5.44
F_A[0.14]M	4.45	5.88	7.22	2.77	5.02 – 5.45
F_A[0.33]M	5.21	6.26	7.34	2.13	5.02 – 5.46
F_A[0.17]H	3.68	4.94	6.19	2.51	5.07 – 5.40
F_A[0.38]H	4.34	5.45	6.60	2.26	5.02 – 5.46

Table 4.1 Flocculation peak positions and widths produced by aggregants with 85nm dispersion, total surface groups at this concentration equals 5.92x10^{-7}EqL^{-1}.

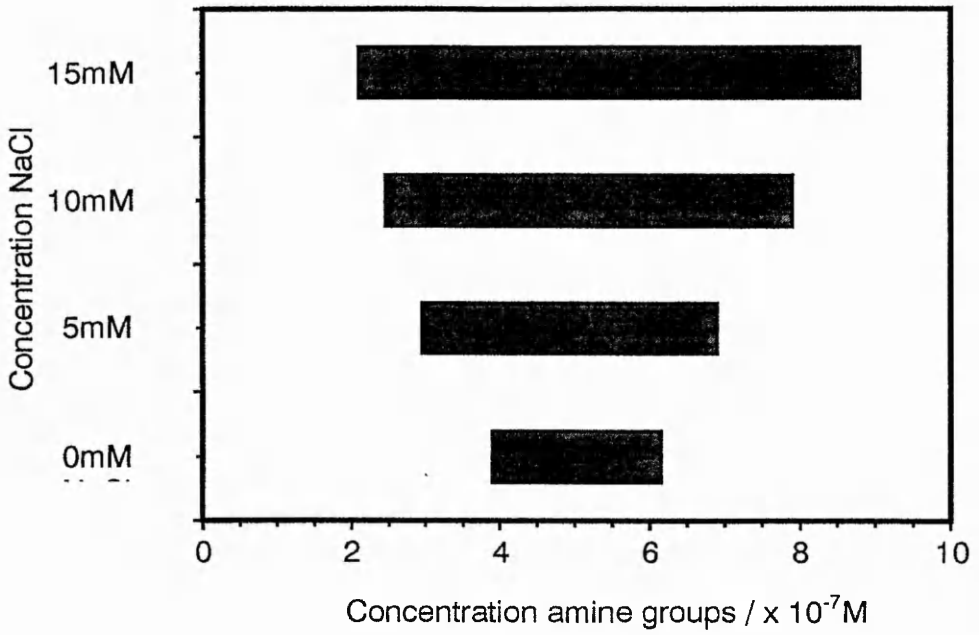

Figure 4.11 The broadening effect of ionic strength on the width of the flocculation range of F_A[0.02]M chitosan, measured by PCS.

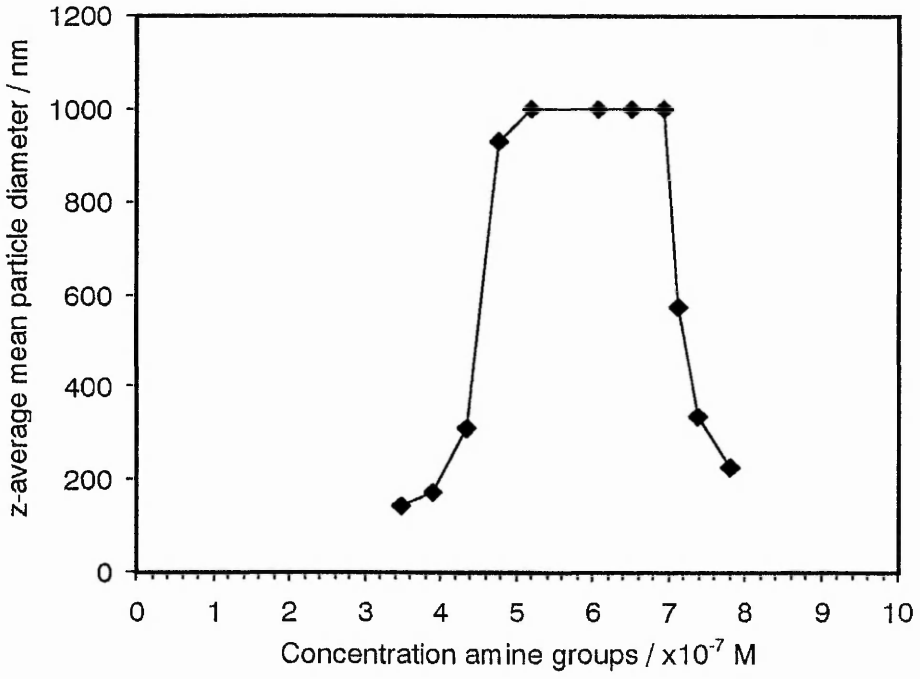

Figure 4.12 Flocculation of 85nm latex by F_A[0.14]M chitosan

view of the uncertainty in the extent of ionisation of the carboxyl groups. The choice was made on the basis that the oligomeric sample produced flocculation at the point of charge neutralisation for other latices subsequently studied. Several of the quantities displayed in Table 4.2 may be seen more easily in Figure 4.18. The trend towards higher amine concentration with increasing F_A is clearly illustrated. Also apparent are the coincident ranges of F_A[0.02]O and F_A[0.02]M. The oligomeric sample's flocculation range is slightly narrower than the medium molecular weight sample, in line with the observations of other studies[269, 270], as the flocculation mechanism tends towards simple coagulation with the reduction in molecular weight due to the patches formed being smaller and more dispersed across the particle surface.

Turning to the higher molecular weight samples, as with the medium molecular weight samples, an increase in required amine concentration with degree of acetylation is observed, but the effect is not as pronounced as with medium molecular weight samples, indicating an increasing efficiency with increasing molecular weight. This may result from the increased density of adsorbed patches[271] and therefore their efficiency in the flocculation mechanism is increased by molecular weight.

So, the flocculation of the 85nm system by chitosan appears to follow a charge neutralisation mechanism and, for the F_A[0.02]M sample at least, it may be concluded that the electrostatic patch mechanism is in operation.

As some doubt may surround the role played by the carboxyl groups in the charge neutralisation of this system, in further studies latices were chosen where carboxyl functionality could be considered negligible.

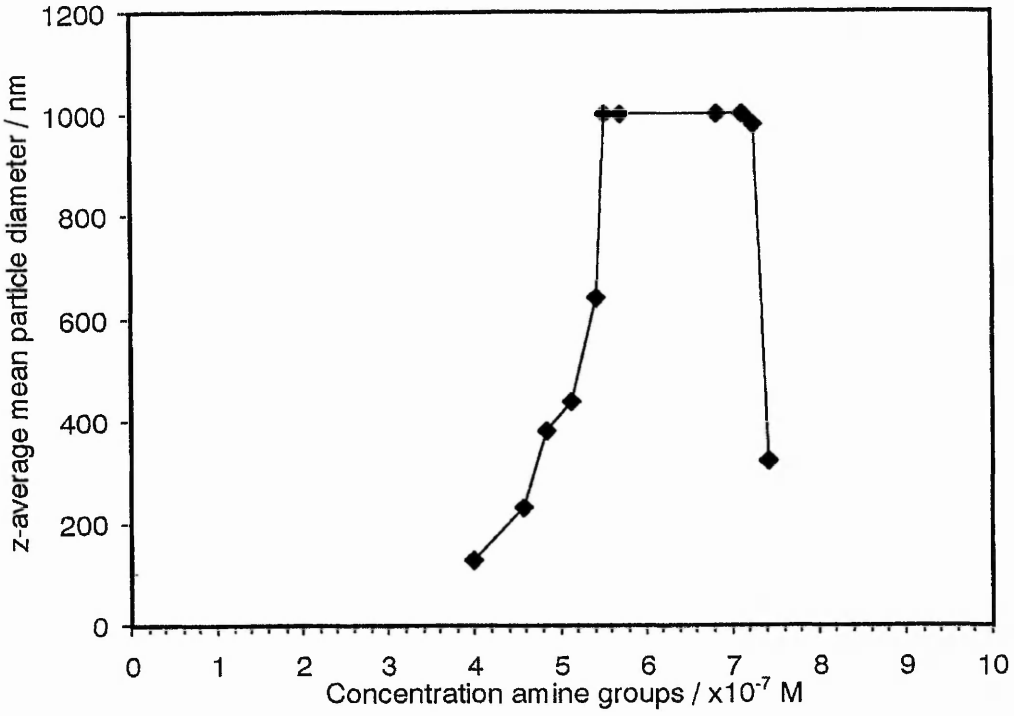

Figure 4.13 Flocculation of 85nm latex by F_A[0.33]M chitosan

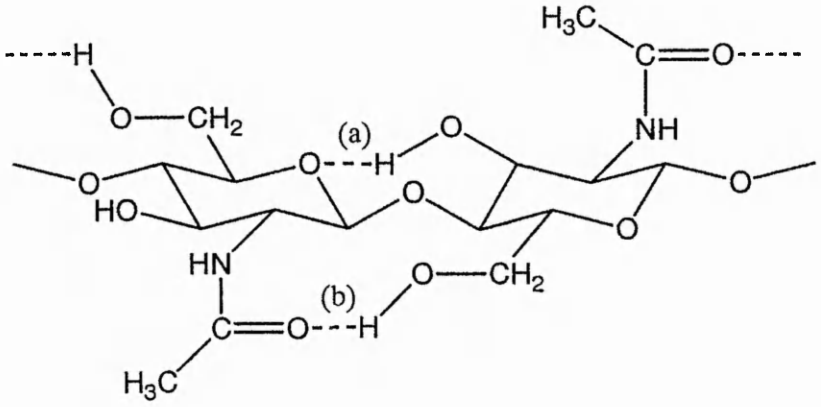

Figure 4.14 Intramolecular Hydrogen bonding between adjacent chitin units causing chain stiffening

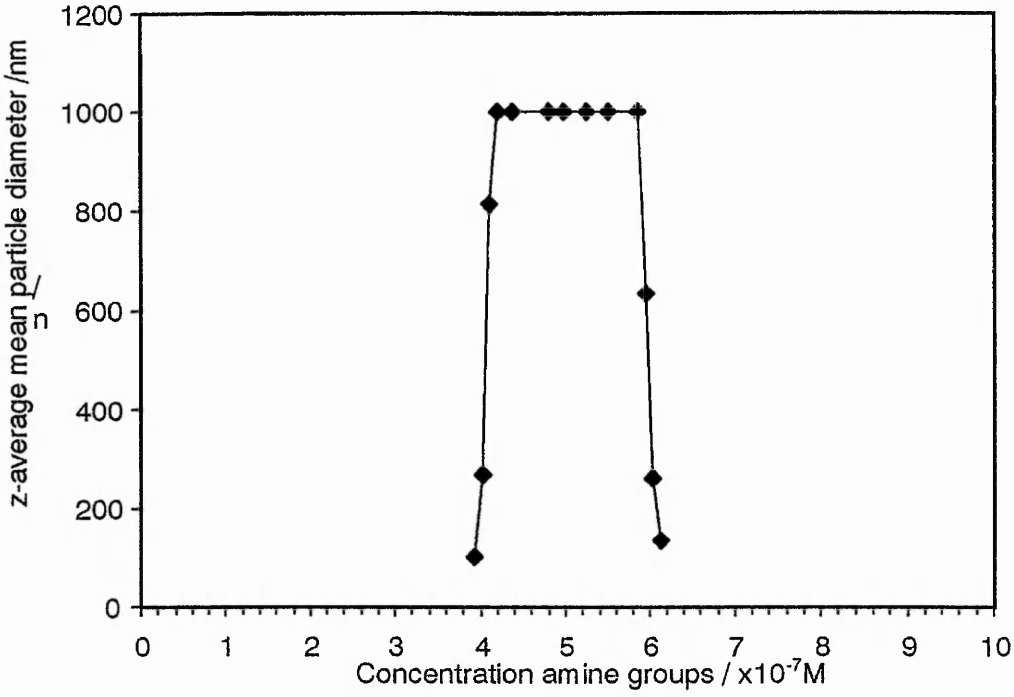

Figure 4.15 Flocculation of 85nm latex by F_A[0.02]O chitosan

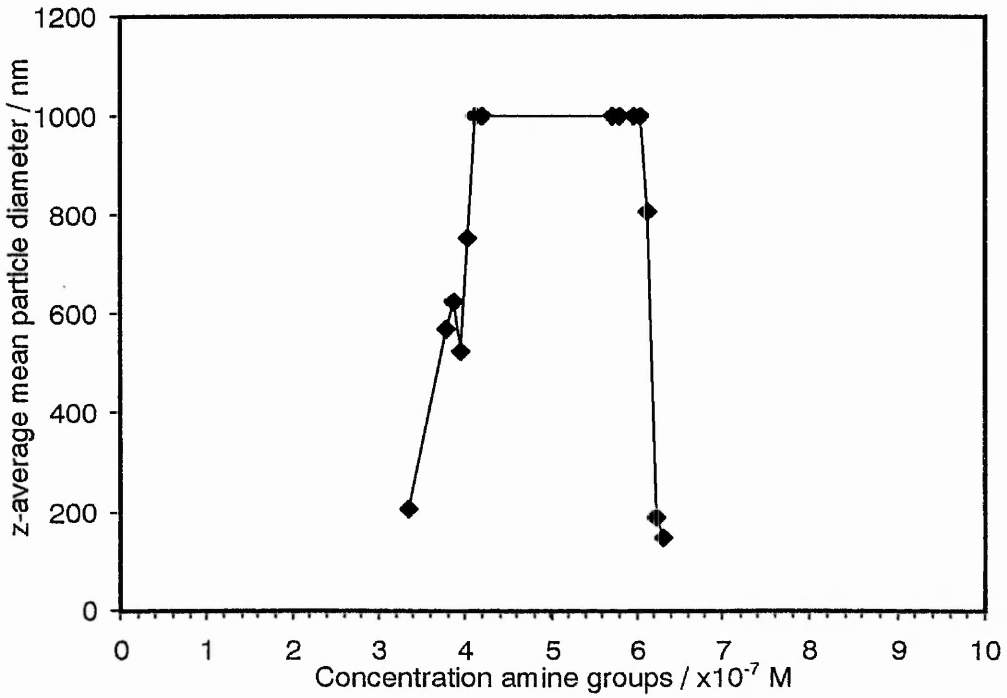

Figure 4.16 Flocculation of 85nm latex by F_A[0.17]H chitosan

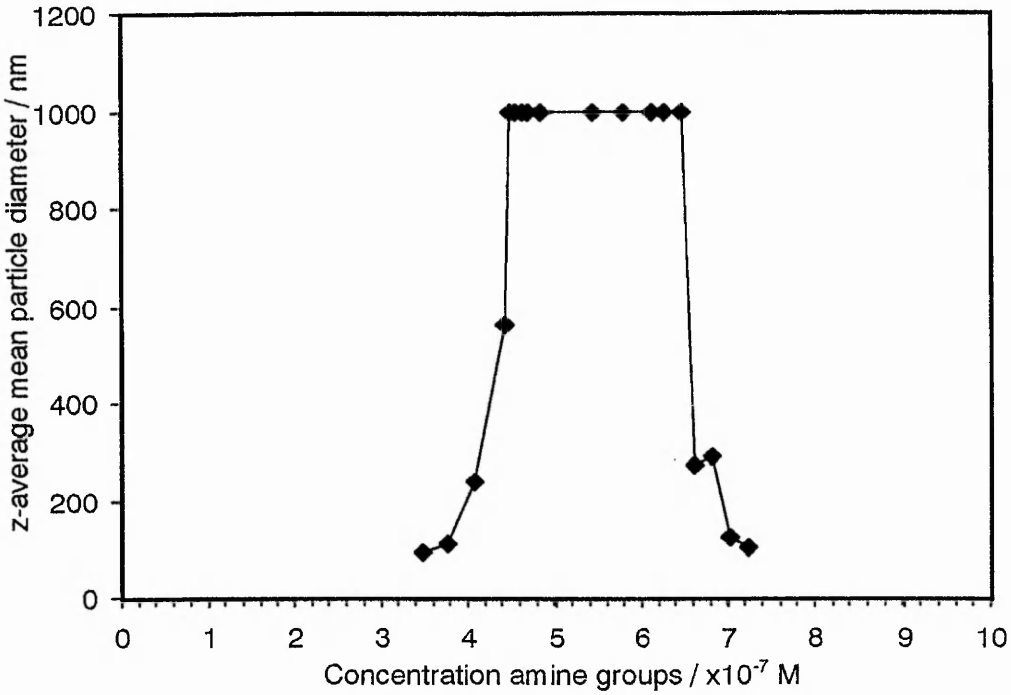

Figure 4.17 Flocculation of 85nm latex by F_A[0.38]H chitosan

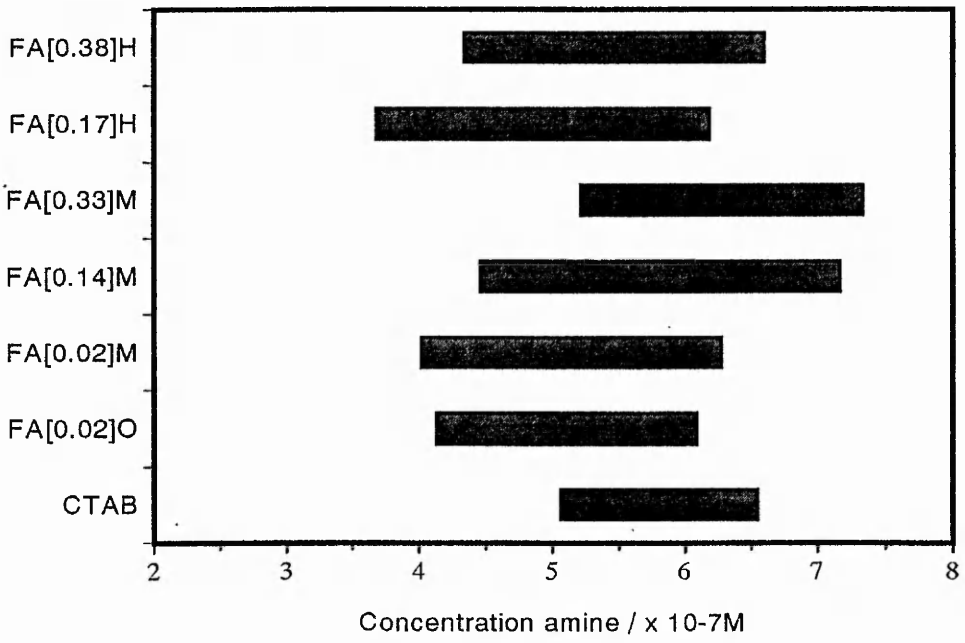

Figure 4.18 Flocculation peak positions and widths produced by various aggregants with 85nm dispersion

4.2 400nm Latex

4.2.1 Flocculation at constant acetic acid concentration

The Interfacial Dynamics (ID) latices are produced by surfactant-free emulsion polymerisation and therefore circumvent the problems of removing excess emulsifier before use. They are effectively stabilised by sulphate groups only as carboxyl groups, if present at all, should account for a negligible proportion of the total surface charge (see Figure 3.2.3, section 3.2.2.2). The sulphate groups have a $pK_a < 2$ and are therefore dissociated over a wide pH range. Under the general flocculation regime therefore, at an acetic acid concentration of 0.05M, approximately pH3, the surface groups should be fully ionised and any instability will be solely due to added coagulant or flocculant.

Figure 4.20 shows the results of adding F_A[0.02]M and F_A[0.57]M to the 400nm ID latex, with concentration of chitosan in gl^{-1}. Again it may be seen that the greater the acetylation degree, the larger the critical flocculation concentration. Figure 4.21 displays the flocculation range with respect to amine concentration for F_A[0.02]M. If we compare this to the anionic surface charge due to the latex (5.6×10^{-7} equivalents l^{-1}), we can see that the flocculation occurs around the point of charge neutralisation. This may be seen more clearly if the flocculation range is plotted against the ratio of amine:sulphate groups as in figure 4.22. This figure suggests that the critical flocculation concentration is reached while the particles are still slightly negative. This behaviour has been noted before in different charge-neutralisation flocculation systems[346], though this has been ascribed to a bridging component within the mechanism. Comparing this with initial rate data in figure 4.23, it can be seen that the flocculation range suggested by both methods is in good agreement indicating that the mixing regime in the initial rate experiments is adequate.

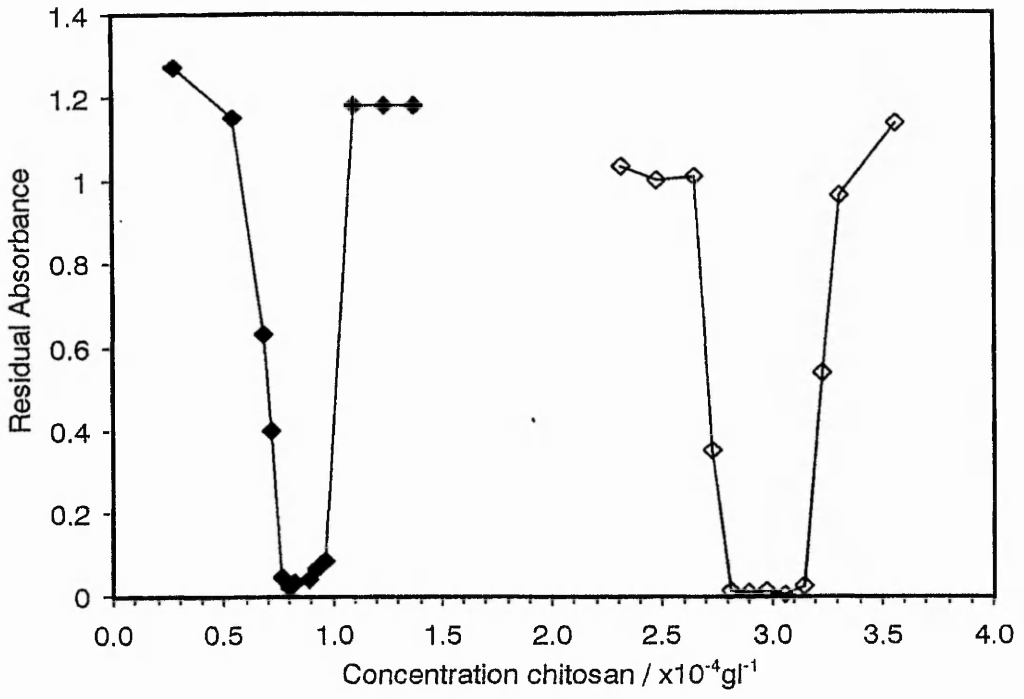

Figure 4.20 The flocculation of 400nm latex using F_A[0.02]M (◆) and F_A[0.57]M (△), concentration in terms of gl^{-1}.

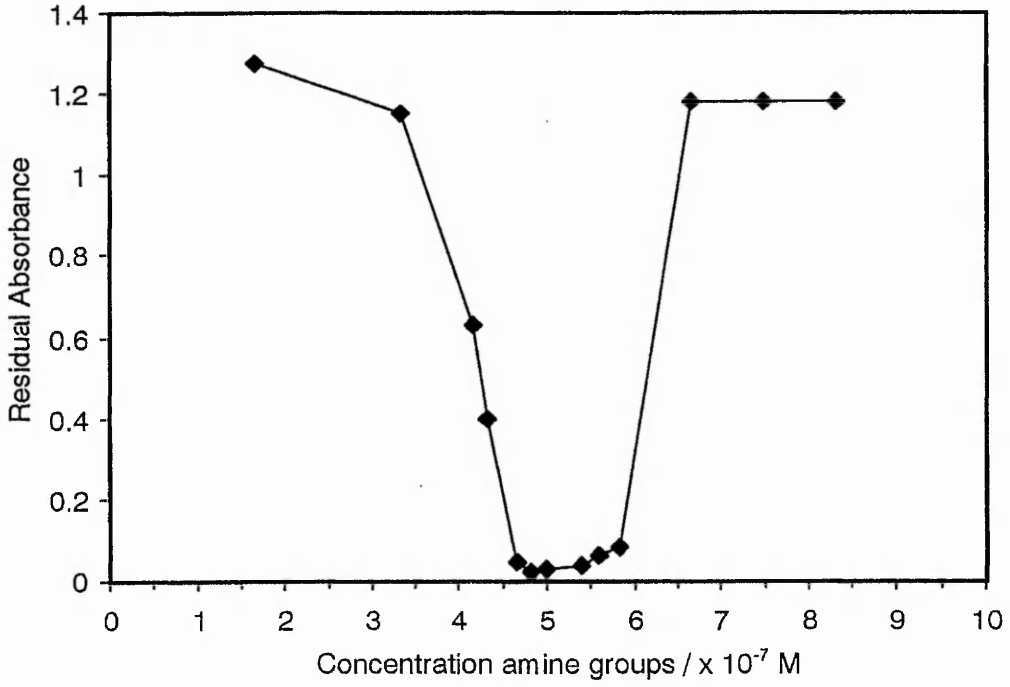

Figure 4.21 Flocculation of 400nm latex using F_A[0.02]M, concentration in terms of moles dm^{-3} of amine groups added.

The actual peak rate of flocculation, displayed relative to rapid coagulation rate, is again elevated, indicating that for this system something other than simple charge neutralisation is in operation. The apparent elevation in rate is slightly less than in the 85nm system, 30% in this case while of the order of 40% for the 85nm system, and lower than those reported by other workers for different systems and flocculants[269, 270] in distilled water. The latter comparison may be explained in part by the prevailing conditions of ionic strength due to the acetic acid that screens the charges on latex and polyelectrolyte thereby reducing attraction.

Figure 4.24 shows the effects of increasing ionic strength upon the flocculation of the 400nm system by F_A[0.02]M chitosan. If the flocculation is due to the attraction of oppositely charged patches, then as the ionic strength of the disperse phase is increased, the observed elevated rate of flocculation should decrease towards the rate of simple coagulation as the added electrolyte increasingly screens the charges, reducing Coulombic attraction. As can be seen from figure 4.24, the rate of aggregation in the system decreases with increasing sodium chloride concentration and the rate becomes essentially constant at around the rate of rapid coagulation.

Figure 4.25 shows the coagulation of the 400nm system by CTAB. It can be seen immediately that the range of the flocculation region, measured by both techniques, lies at a ratio (CTA+ : sulphate) greater than 1. Assuming all glassware is sufficiently equilibrated, this indicates a partition may exist between surface and aqueous phase. The optimum rate of coagulation by CTAB shows a small elevation above the rate of rapid coagulation by simple electrolyte of just a few percent, an effect which has been observed previously[270], this may be attributed to an increase in the collision radius or an increase in hydrophobic interaction.

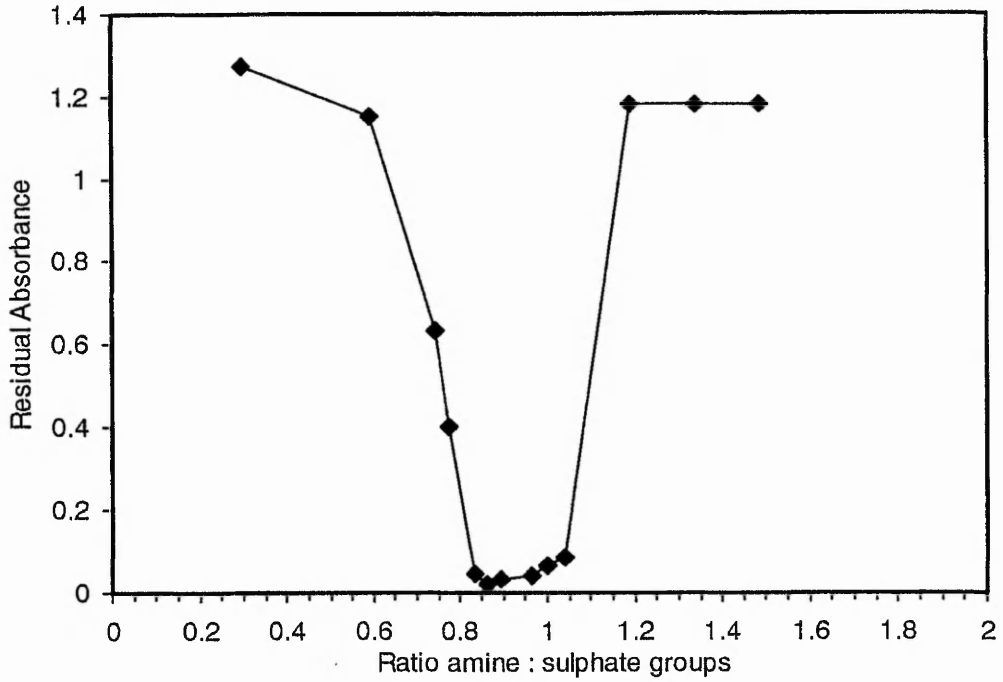

Figure 4.22 Flocculation of 400nm latex using F_A[0.02]M, re-plotted in terms of the ratio of amine : sulphate groups in the system.

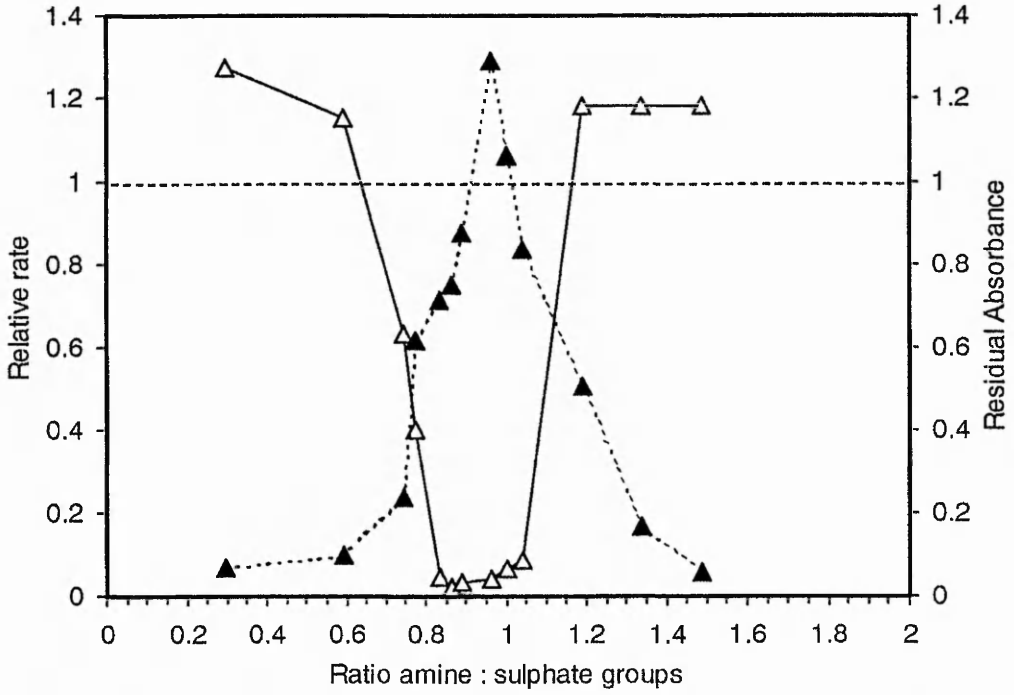

Figure 4.23 Flocculation rate (relative to coagulation rate) (▲) and residual turbidity (△) versus ratio of amine to sulphate groups in the system produced by F_A[0.02]M chitosan.

Figure 4.26 represents flocculation by F_A[0.02]O. Flocculation is at the point of charge neutralisation, implying that the increase in efficiency in flocculation by F_A[0.02]M, whose flocculation peak centre lies at an amine:sulphate ratio of 0.93 compared to 1.01 for the oligomer, is due to its polymeric nature. It also displays a much narrower flocculation range which is line with other comparisons of polymer / oligomer flocculation[269, 270]. The enhancement in aggregation rate in this case appears to be somewhat less than that of F_A[0.02]M but, at approximately 15%, it is still noticeably greater than that produced by CTAB.

The residual turbidity study of the 400nm latex / F_A[0.02]O system appears to show that a much larger proportion of singlet particles remain after flocculation by the oligomer compared with the medium molecular weight sample. In fact, this was due to the flocs formed by the oligomer being much more delicate than those of the medium molecular weight sample, the formers large flocs were more easily re-dispersed as smaller flocs during the removal of the supernatant for analysis. So, although a large reduction in molecular weight appears to have little effect on the flocculation process, it may have more profound effects on the strength of the flocs produced.

Figures 4.27 to 4.29 show the effects of degree of acetylation on flocculation of the 400nm system. Again, as with the 85nm system, the flocculation region appears to be pushed towards higher ratios with samples of decreasing charge density. All these systems display an initial flocculation rate that is elevated above that of simple coagulation, though this elevation decreases with increasing F_A (see later).

The efficiency of flocculation by the higher molecular weight samples appears unaffected by the level of acetylation (Figures 4.30 and 4.31), both samples displaying flocculation ranges around the point of zero charge.

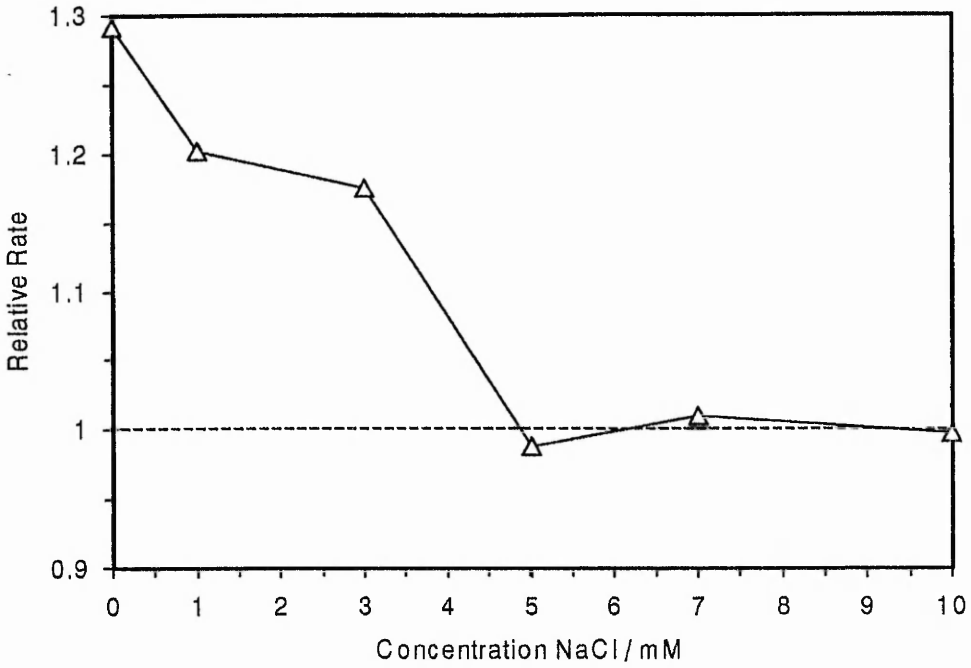

Figure 4.24 The decrease in flocculation rate with increasing ionic strength for the 400nm latex / F_A[0.02]M chitosan system.

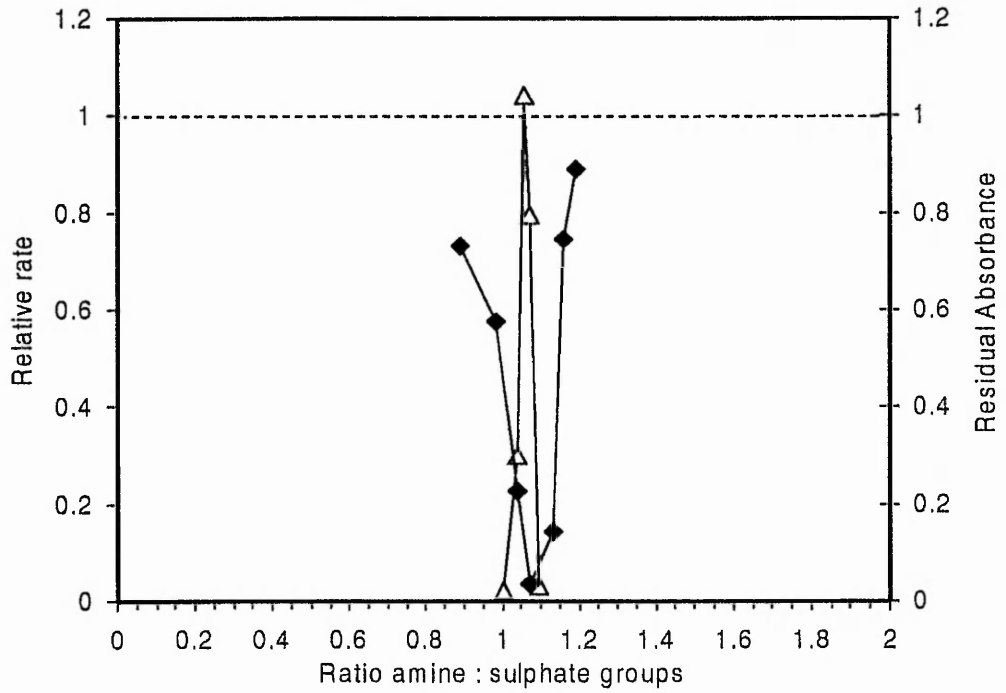

Figure 4.25 Coagulation rate (△) and residual absorbance (◆) of the 400nm latex using CTAB.

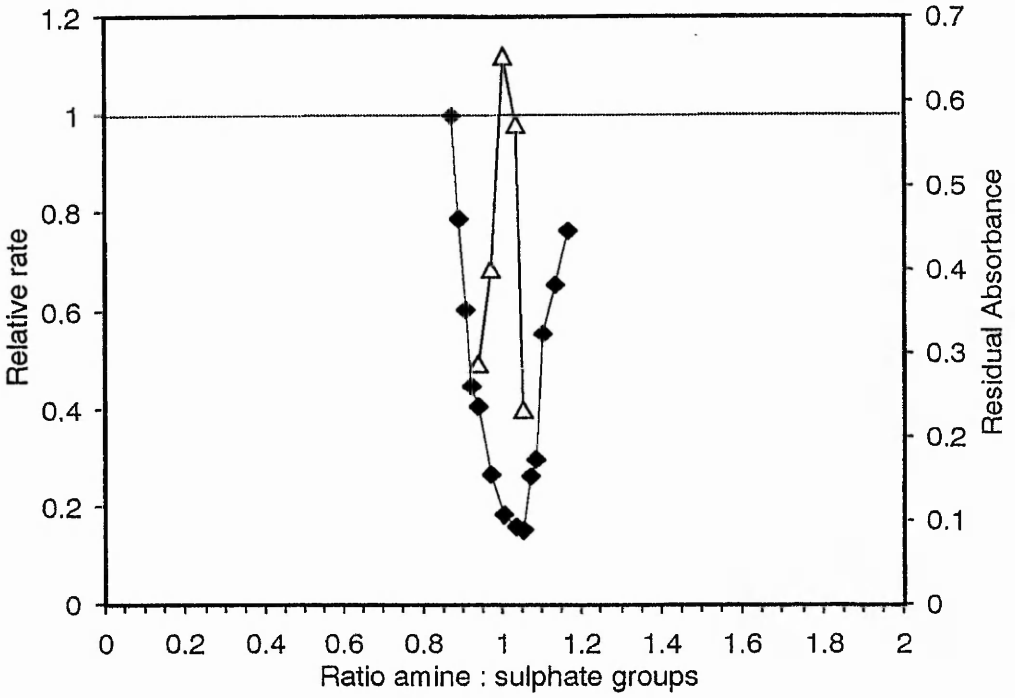

Figure 4.26 Flocculation rate (△) and residual absorbance (◆) of 400nm latex using F_A[0.02]O.

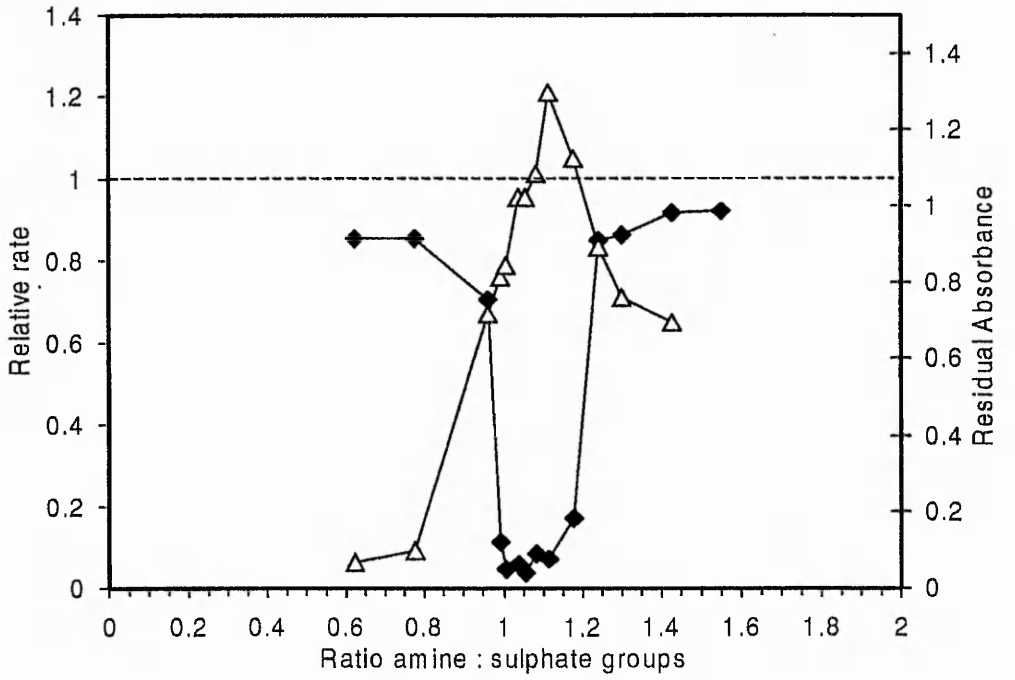

Figure 4.27 Flocculation rate (△) and residual absorbance (◆) of 400nm latex using F_A[0.14]M.

Table 4.2 shows a summary of the results for the residual turbidity studies involving the 400nm latex, including the lower and upper ratio limits, the peak centre and peak width all determined at 0.5 absorbance units along with the error range, assuming a 1:1 stoichiometric ratio between amine and sulphate, considering errors in latex charge, delivery of solutions and acetylation degree of chitosan. Also displayed is the ratio at which the maximum initial rate is observed.

Figure 4.32 represents peak position and width for each of the flocculants and CTAB set out in Table 4.2 in the residual turbidity studies of the 400nm latex.

Aggregant	Lower Limit	Peak Centre	Upper Limit	Peak Width	Max. Rate	Error Range
CTAB	1.00	1.08	1.15	0.15	1.05	0.94 – 1.06
F_A[0.02]O	0.90	1.01	1.09	0.16	1.01	0.93 – 1.07
F_A[0.02]M	0.76	0.93	1.09	0.33	0.97	0.93 – 1.07
F_A[0.14]M	0.97	1.10	1.23	0.26	1.11	0.93 – 1.07
F_A[0.33]M	1.01	1.03	1.24	0.25	1.12	0.93 – 1.07
F_A[0.57]M	1.12	1.23	1.34	0.16	1.28	0.91 – 1.09
F_A[0.17]H	0.85	1.00	1.14	0.29	1.06	0.94 – 1.06
F_A[0.38]H	0.89	1.02	1.14	0.25	0.96	0.93 – 1.07

Table 4.2 Depiction of the concentrations (in terms of ratio of amine : sulphate groups) of various quantities determined from Residual Turbidity studies of flocculants and CTAB with 400nm latex dispersion. All quantities, except ratio at which the maximum rate occurred, were determined at 0.5 absorbance units.

Figure 4.32 clearly illustrates several points. Firstly, CTAB shows a slightly greater ratio than 1 is required for flocculation, indicating that there may be a partition effect between surface and solution. The oligomer displays a narrow range centred almost precisely on a ratio of one indicating charge neutralisation. The F_A[0.02]M range is shown to be much wider than that produced by the oligomer, tending towards flocculation while the dispersion is still negatively charged overall. The trend in increasing optimum flocculation

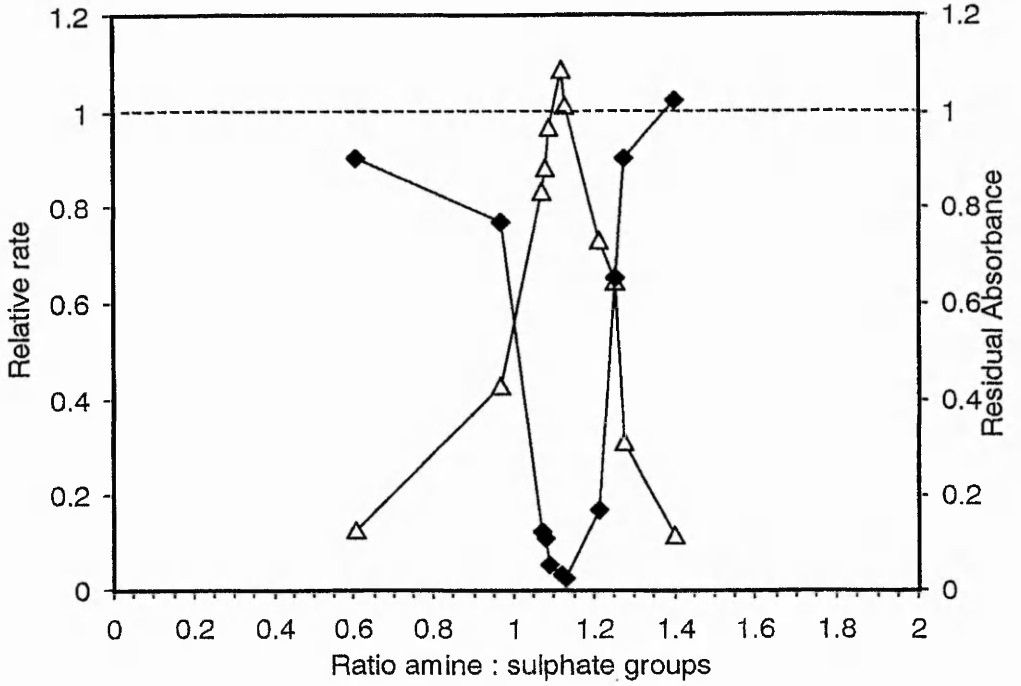

Figure 4.28 Flocculation rate (△) and residual absorbance (◆) of 400nm latex using F_A[0.33]M.

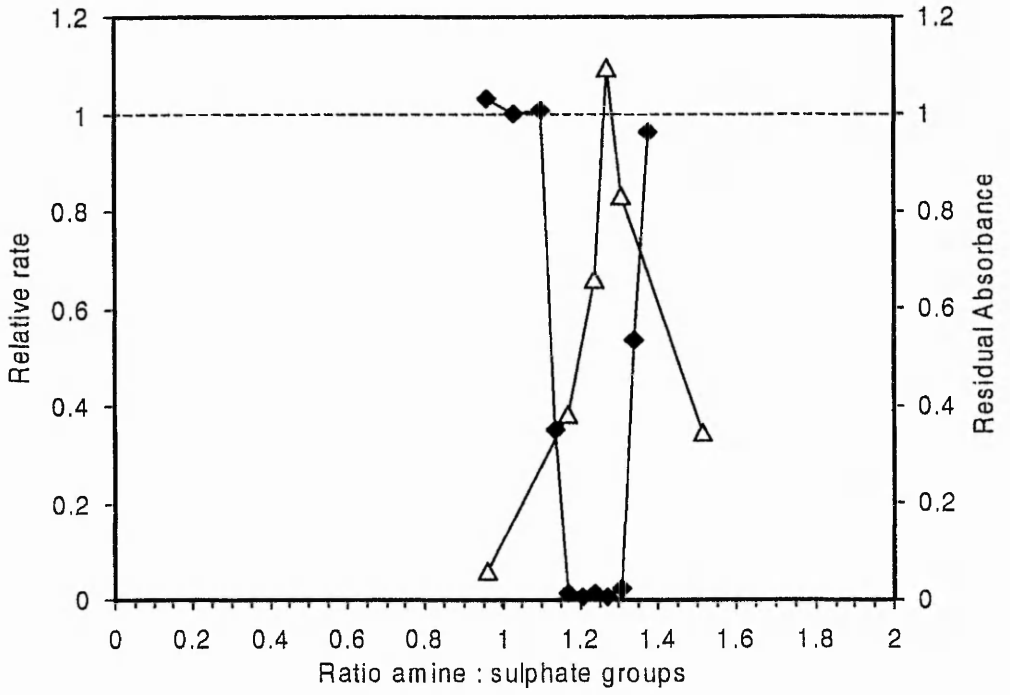

Figure 4.28 Flocculation rate (△) and residual absorbance (◆) of 400nm latex using F_A[0.57]M.

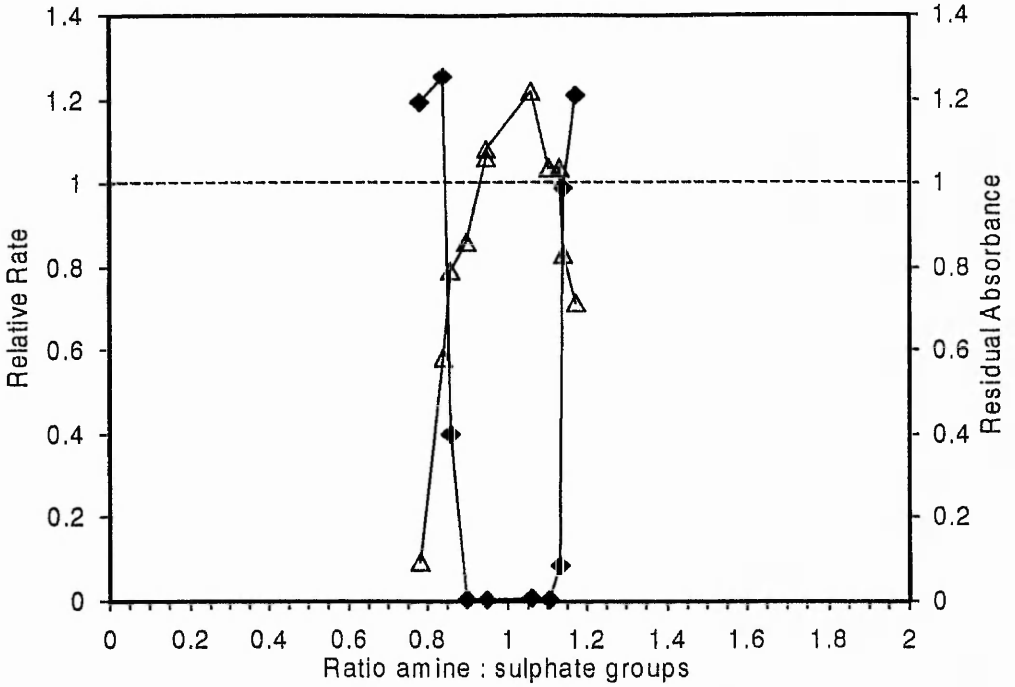

Figure 4.30 Flocculation rate (△) and residual absorbance (◆) of 400nm latex using F_A[0.17]H.

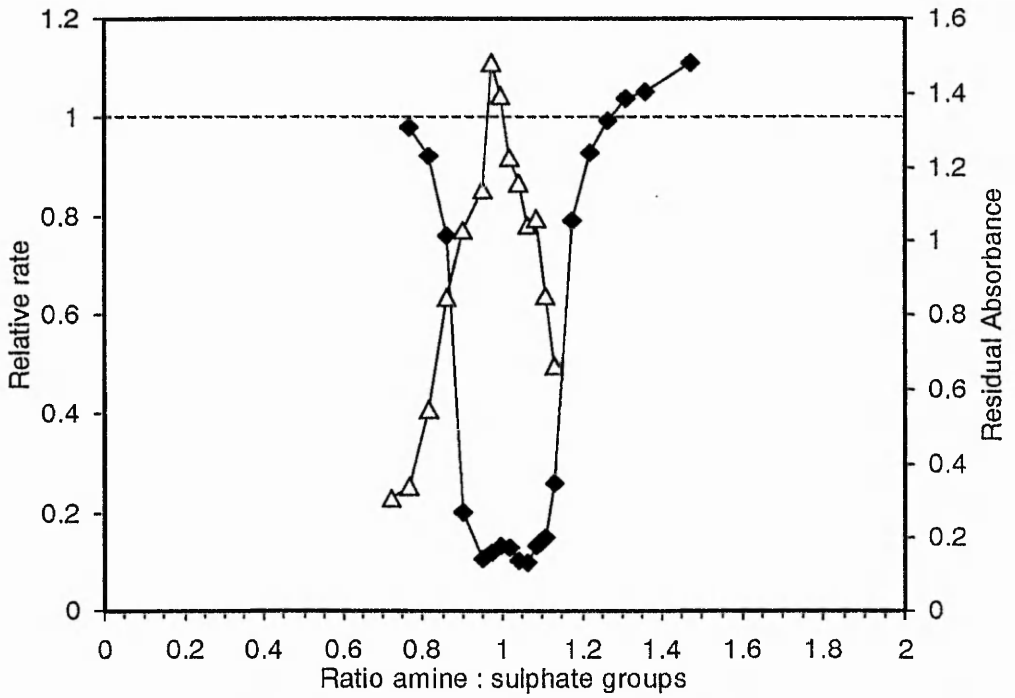

Figure 4.31 Flocculation rate (△) and residual absorbance (◆) of 400nm latex using F_A[0.38]H.

concentration (by whichever method, e.g. minimum concentration, peak centre etc.) may be clearly observed, as can the return towards 1:1 stoichiometry displayed by the higher molecular weight samples. Although the flocculation ranges of these latter samples coincide, the lower concentration limit is higher for the F_A[0.38]H sample perhaps indicating that the increasing concentration with increasing F_A effect may also be displayed if higher F_As were studied.

The maximum observed rates (relative to coagulation) are presented in Table 4.3. All these systems display an elevated aggregation rate, though not to the same extent as F_A[0.02]M, and (seem to) show decreasing elevation with increasing acetylation degree.

Aggregant	Apparent Rate Elevation (%)
CTAB	5
F_A[0.02]O	15
F_A[0.02]M	30
F_A[0.14]M	21
F_A[0.33]M	9
F_A[0.57]M	10
F_A[0.17]H	22
F_A[0.38]H	11

Table 4.3 Elevation in aggregation rate over rapid coagulation

Elevation in flocculation rate over coagulation rate of higher molecular weight samples seems to be of a similar magnitude to that for analogous medium molecular weight samples. The oligomeric samples rate elevation is somewhat less than the F_A[0.02]M sample's. In all, it appears that rate elevation decreases with increasing F_A, due to the reduction in linear charge density, hence reduction in cationic patch charge density and therefore coulombic attraction towards negative patches on other particles. Molecular weight seems

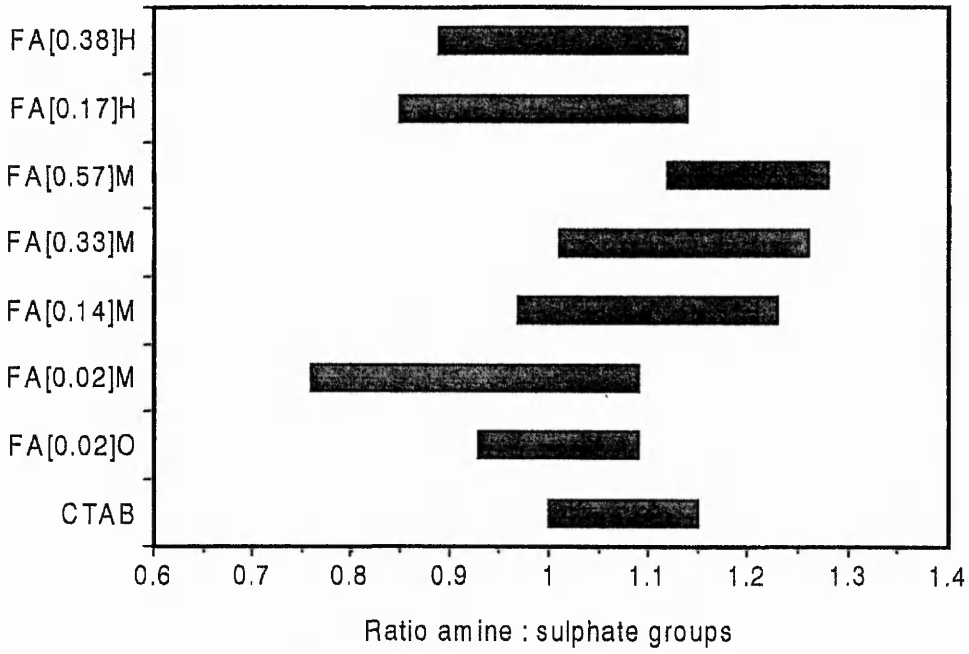

Figure 4.32 Relative peak positions and widths determined for various flocculants and CTAB produced in the aggregation of the 400nm dispersion.

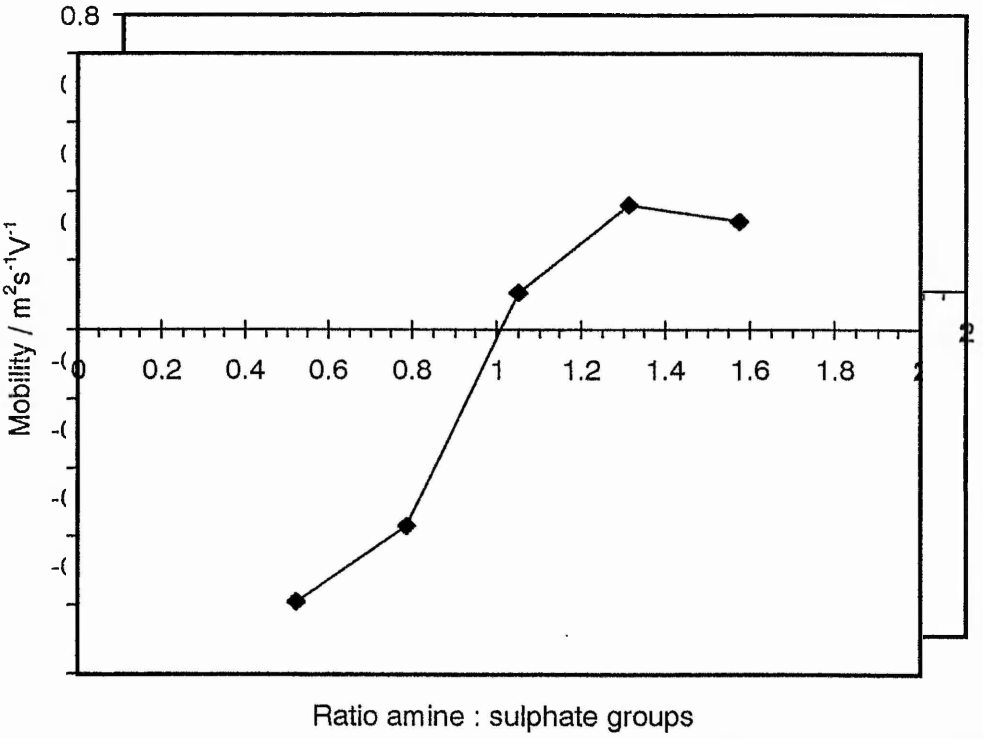

Figure 4.33 The electrophoretic mobility of the 400nm latex in the presence of F_A[0.02]M.

to have less of an effect, with comparable medium and high molecular weight samples giving similar results for maximum rate, though the oligomeric sample shows a decline in maximum rate compared to F_A[0.02]M as the mechanism begins to resemble simple coagulation.

Electrophoretic mobility data, plotted against amine:sulphate ratio, for the F_A[0.02]M / 400nm system is displayed in Figure 4.33. The system displays zero mobility around the point of charge neutralisation (1:1 ratio) which confirms that the critical flocculation concentration occurs around the point of charge neutralisation.

Figure 4.34 shows the electrophoretic mobility data for the system upon the addition of F_A[0.57]M chitosan. The point at which the mobility is zero occurs at a ratio of 1.15, again indicating that a charge neutralisation mechanism is likely. A result above 1:1 stoichiometry would not be unexpected in view of the flocculation result which suggest that the stiffer-chained, more acetylated chitosan sample may be less efficiently adsorbed.

4.2.2 Effects of changing pH on flocculation

One of the major considerations if chitosan is to be used practically as a flocculant is its behaviour under different conditions of pH[300, 305, 307, 308, 311, 354]. Figures 4.35, 4.36 and 4.37 represent the effect of increasing pH on flocculation by the chitosan samples F_A[0.02]M, F_A[033]M and F_A[0.57]M respectively.

At pH3, the equilibrium,

$$-NH_3^+ + H_2O \rightleftharpoons -NH_2 + H_3O^+$$

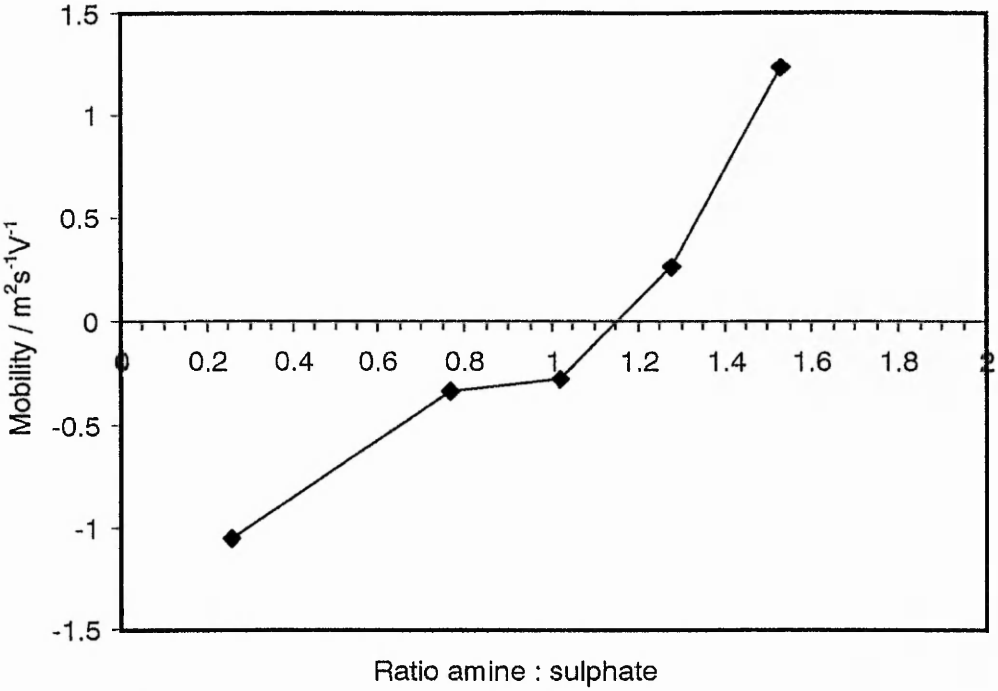

Figure 4.34 The electrophoretic mobility of the 400nm latex in the presence of F_A[0.57]M.

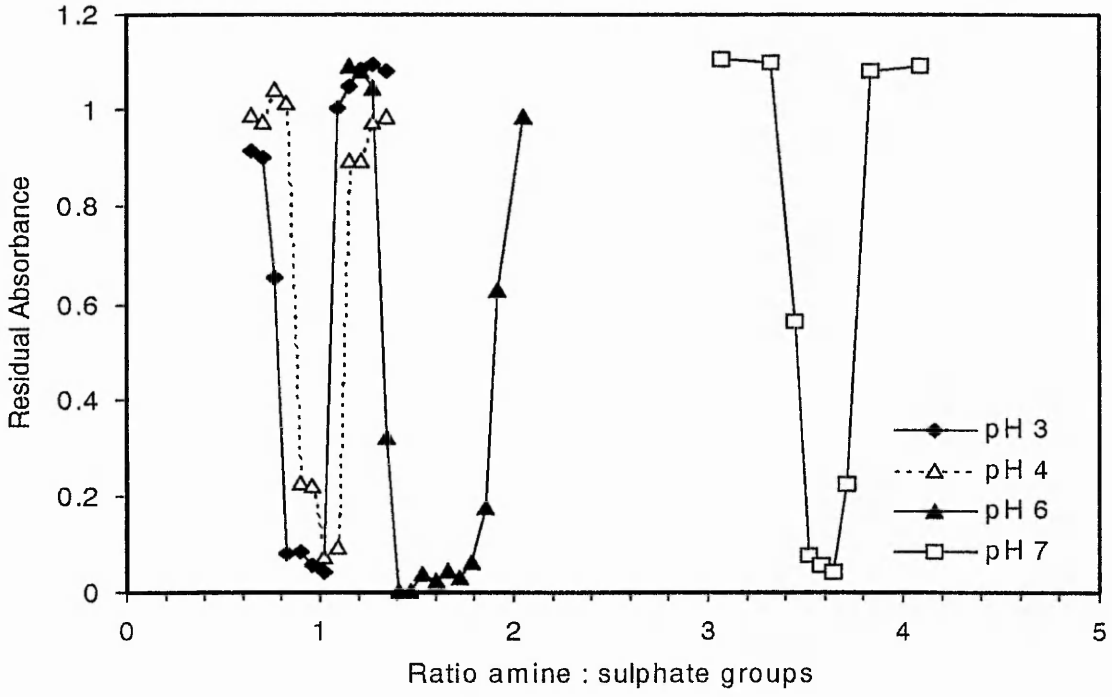

Figure 4.35 The effect of pH on the critical flocculation concentration of the F_A[0.02]M chitosan in the 400nm latex system.

lies predominantly (99.97%) to the left. The acid dissociation constant for polyelectrolytes is not actually constant since, for example, the ease of dissociation of the conjugate acid group $-NH_3^+$ will be increased in the presence of similar adjacent groups thereby increasing K_a and decreasing pK_a. If however pK_a is approximated constant at 6.5[79, 94] then using the Katchlasky's equation[78],

$$pK_a = pH + \log\{(1-\alpha) / \alpha\}$$

it may be predicted that at pH5, the association will be largely unchanged at 97%, implying that only 3% more polyelectrolyte would be required, while at pH 6, 76% association would mean that a third ([100/76]-1) more flocculant would be required over that at pH 3. At pH 7, a four-fold increase in flocculant concentration would be required to produce the same concentration of protonated amine groups as at pH 3.

It can be seen from Figures 4.35, 4.36 and 4.37 that the chitosan samples from across the soluble range of compositions are affected by increasing pH. This is at odds with studies of chitosan flocculation in other systems, for example Demarger-Andre and Domard[308] reported that pH had little effect on the flocculation of undecylenic acid micelles by chitosan, Pinotti *et al*[354] reported that pH had no significant effect on chitosan flocculation of model food emulsions while Huang and Chen[307] found that pH had little effect on flocculation of kaolinite and bentonite suspensions. It is interesting to note that in many of these cases, pH effects the surface charge of the dispersion as well as the charge on the chitosan. Tsar'kova and Lopatina[311] noted an increase in the required chitosan concentration for flocculation of gold sols, though little quantitative data was reported. In this study it was observed that, in general, the required concentration of chitosan (expressed in terms of the ratio of amine:sulphate groups) increases with increasing pH. The measured values are not predicted accurately by the calculated values above, though they are in qualitative accord. Superficially, the shift in flocculation range with pH for each sample

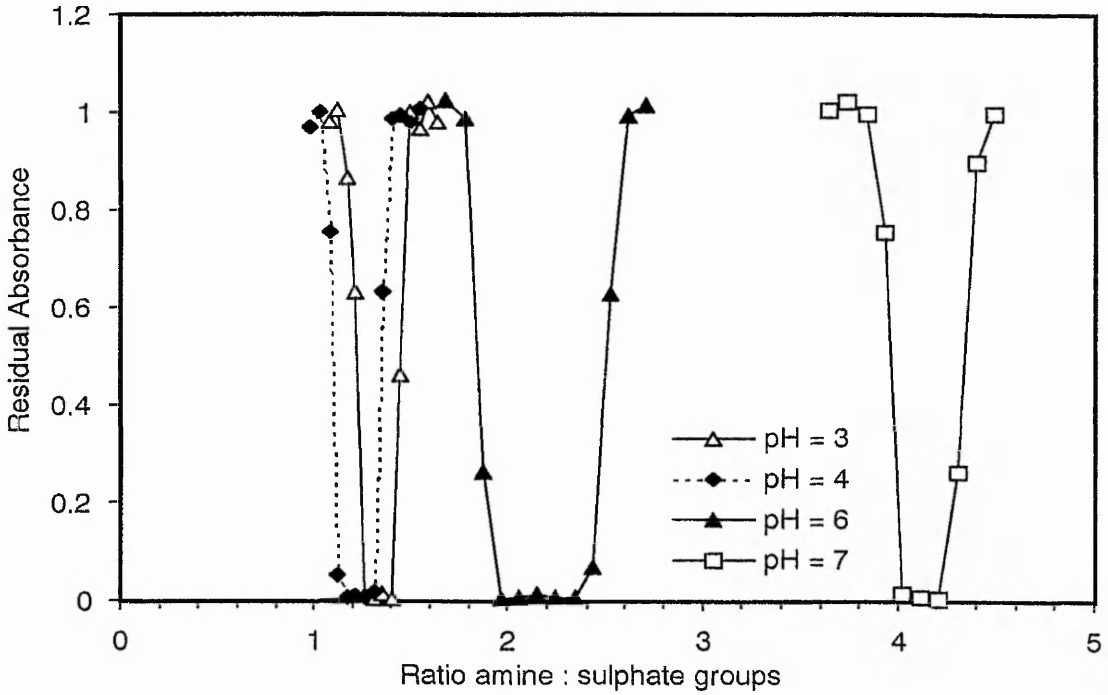

Figure 4.36 The effect of pH on the critical flocculation concentration of the F_A[0.33]M chitosan in the 400nm latex system.

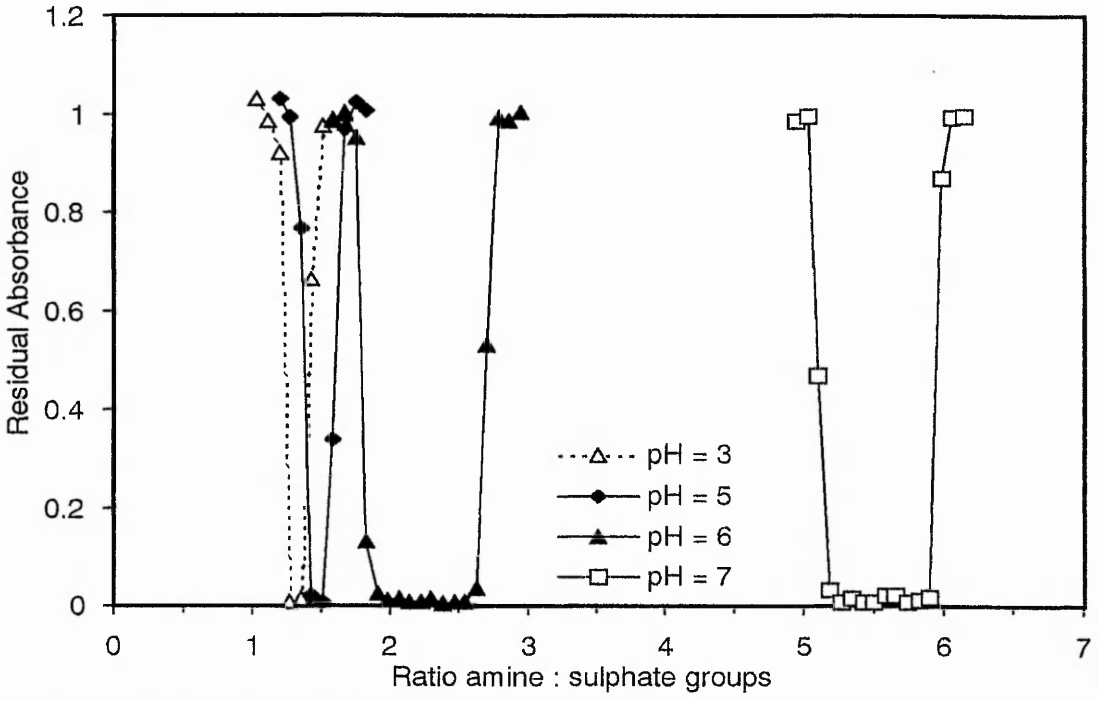

Figure 4.37 The effect of pH on the critical flocculation concentration of the FA[0.57]M chitosan in the 400nm latex system

is relatively similar, with approximately 10% more amine groups required on raising the pH from 3 to 5, an extra 70 – 80% at pH 6 and 300 – 400 % at pH 7.

4.2.3 Stability to coagulation

As may be observed from previous figures, an excess of chitosan leads to a region of restabilisation, this may be the result of one of several effects depending upon the nature and the adsorbed configuration of the polymer. If adsorption leads to the open, looped configuration associated with inter-particle bridging then excess polymer would lead to steric stabilisation. If however the adsorption is achieved via the attraction of opposite charges on polyelectrolyte and particle and the adsorption configuration is consequently relatively flat, then the stability of the dispersion observed on the addition of excess polyelectrolyte is generally due simply to the reversal of particle surface charge. The incidence of steric stabilisation is usually marked by a large increase in the tolerance of the dispersion to added 1:1 electrolyte, for example up to sodium chloride concentrations of the order of several moles dm^{-3}[347]. In the case of charge reversal however, as the overall surface charge is of a similar level to that of the original latex, there is generally only a minor change in dispersion stability.

In order to determine the relative stability of chitosan-protected 400nm latex, a portion of the latex was exposed to a level of F_A[0.02]M chitosan corresponding to twice that which would bring about flocculation. Figures 4.38 and 4.39 represent particle size analysis of the bare 400nm latex and the chitosan-protected 400nm latex respectively using a Coulter LS particle size analyser. It may be observed that the addition of chitosan to the system has resulted in little discernible aggregation, which would be characterised by doublet, triplet etc. peaks in figure 4.39.

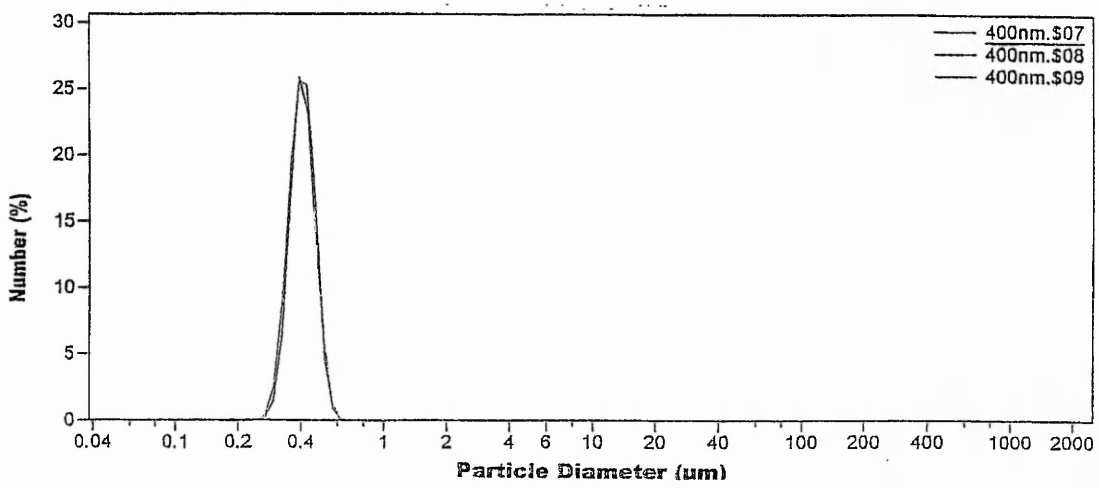

Figure 4.38 Particle size determination of 400nm latex using the Coulter LS instrument.

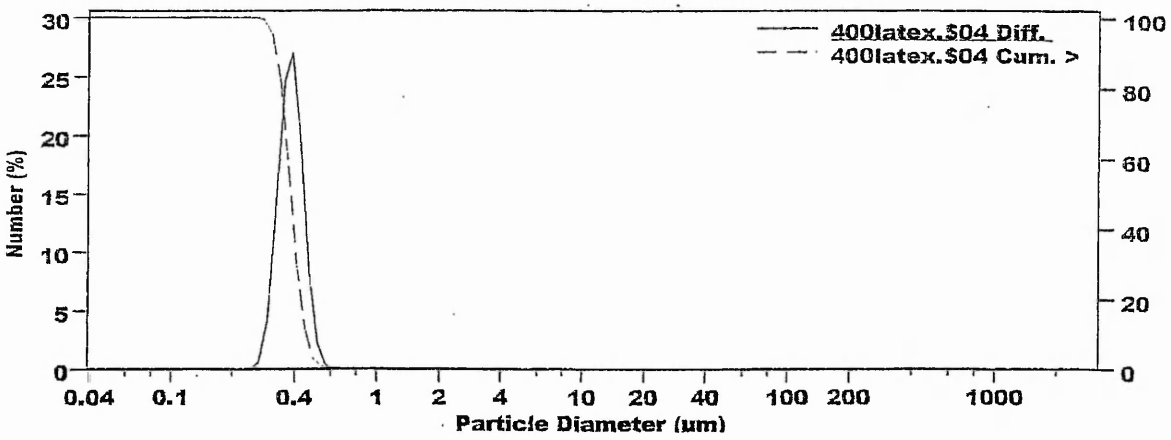

Figure 4.39 Particle size determination of F_A[0.02]M chitosan protected 400nm latex using the Coulter LS instrument.

Figure 4.40 shows the effects of the addition of increasing concentrations of sodium chloride to the 400nm system, without chitosan 'protection', in coagulation rate determination experiments similar to the flocculation rate determinations for this latex. The Stability Ratio W, generally defined as k_2^0/k_2 where k_2^0 is the rate constant for diffusion controlled (rapid) coagulation and k_2 is a second order rate constant for slow coagulation, was estimated by dividing the maximum observed coagulation rate by the coagulation rate produced by each sodium chloride concentration. $Log_{10}W$ was then plotted against sodium chloride concentration to give figure 4.40. It can be seen that the transition from slow to rapid coagulation for this latex occurs at a sodium chloride concentration of approximately 0.25M. Figure 4.41 shows a repeat of this experiment using the chitosan protected latex. In this case, the change from slow to rapid coagulation occurs at around 0.4M NaCl, a relatively small increase in stability over that of the bare latex which points towards a charge inversion restabilisation mechanism entailing a relatively flat adsorbed polymer configuration.

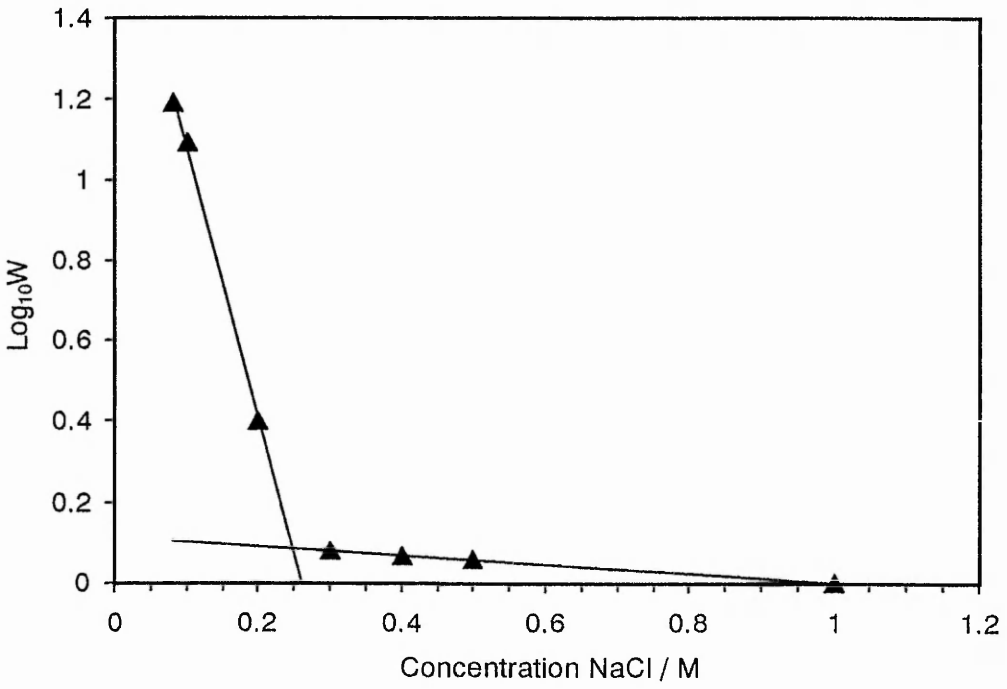

Figure 4.40 Stability of bare 400nm latex to added electrolyte (NaCl)

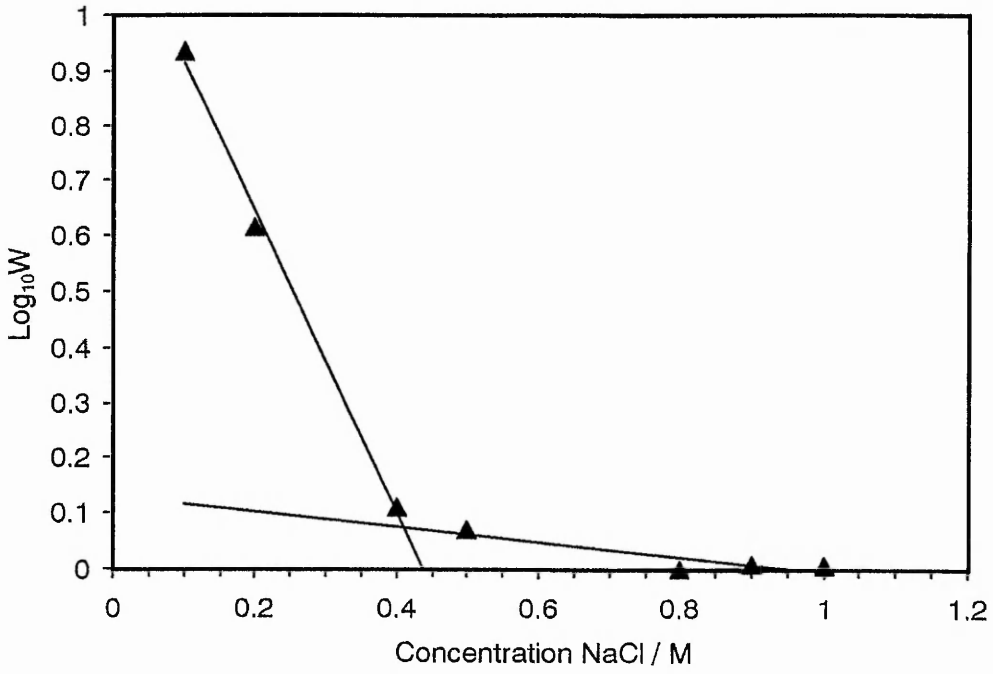

Figure 4.41 Stability of F_A[0.02]M chitosan protected 400nm latex to electrolyte addition.

4.3 2.1μm latex results and discussion

4.3.1 Residual singlet population

Figure 4.42 represents a determination of flocculation range for the F_A[0.02]M / 2.1μm system in a method analogous to the Residual Turbidity method employed for the 400nm particles. In this case, instead of an estimation of the turbidity of residual singlets after a period of flocculation, a Coulter Counter was used to directly measure the number of singlets in the flocculated system. The number of singlets (the number of singlets detected in the 500μl sample volume is reported, effectively the sample undergoes a 2000 fold dilution from sample tube to count) is then plotted against cation : anion ratio as before to produce the flocculation range after an arbitrary time frame (in this case, 24 hours). Figure 4.42 shows that, for F_A[0.02]M, the critical flocculation concentration is again at a ratio of approximately 1, suggesting that the largest particles in the study are also flocculated by charge a neutralisation mechanism. Figure 4.43 compares this data with the electrophoretic mobilities of particles over the same range of ratios. It can be seen that the point at which the particles have zero mobility again lies at a ratio of approximately 1, and corresponds roughly to the centre of the residual singlets peak. This observation provides further evidence for the charge neutralisation conclusion. In addition to the electrophoresis data determined using the Coulter Delsa instrument, further evidence comes from a small study which had earlier been carried out using the Rank electrophoresis apparatus using a sample of 2.25μm diameter soap free latex prepared in-house. Unfortunately no data concerning the surface charge on this latex was obtained before it was accidentally destroyed, however the electrophoretic mobility of the latex in the presence of a variety of CTAB and chitosan-amine concentrations (using F_A[0.02]M) was determined and the results displayed in Figure 4.44. As can be seen, the concentrations of cations at which the system has zero mobility

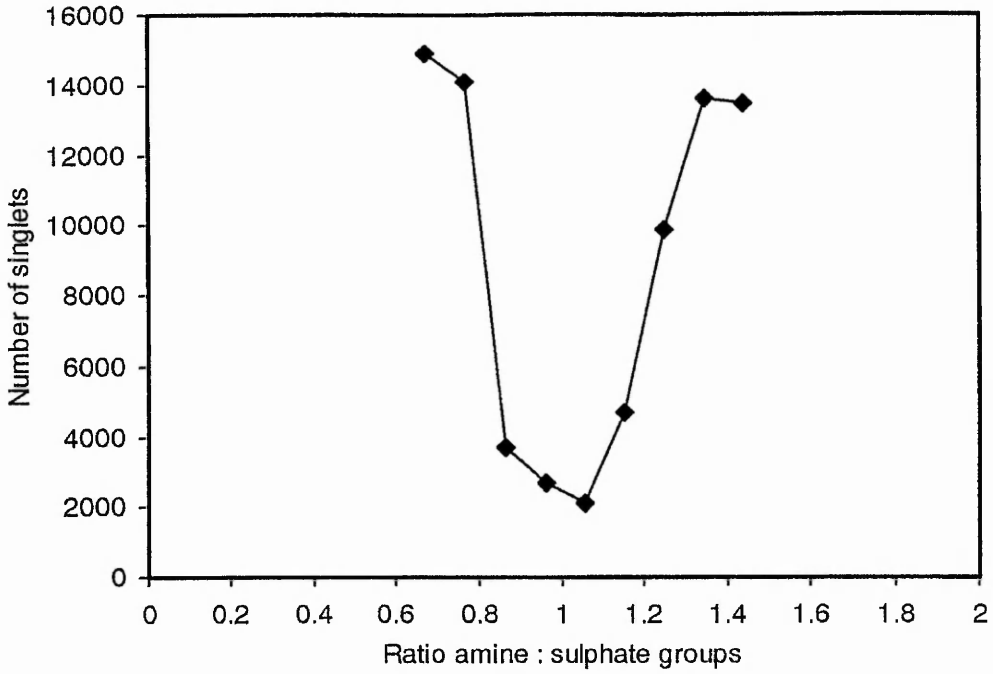

Figure 4.42 The residual singlet population of 2.1μm latex after flocculation by F_A[0.02]M chitosan.

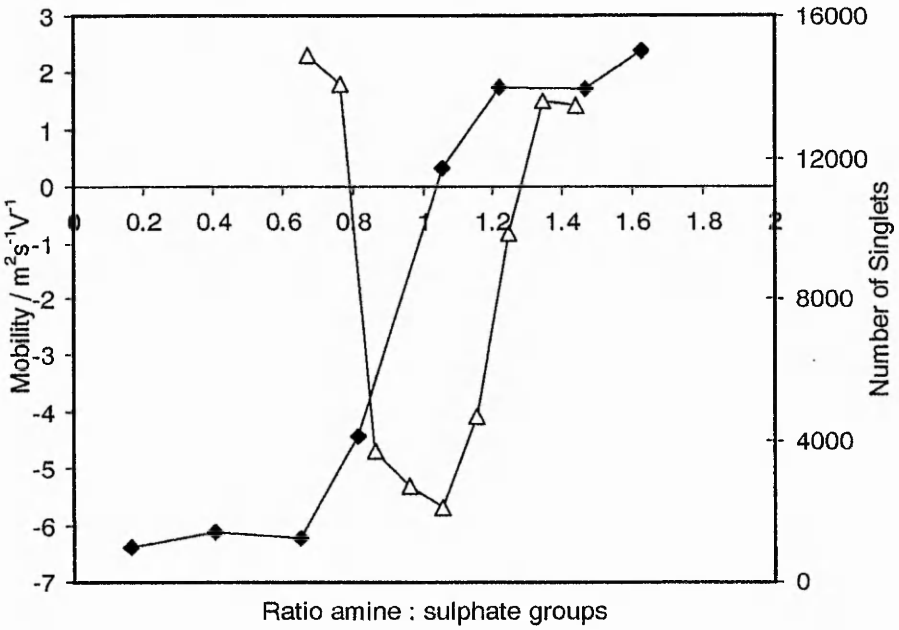

Figure 4.43 The residual singlet population of 2.1μm latex after flocculation by F_A[0.02]M (△) chitosan compared with the latexes electrophoretic mobility (◆) over the same range.

is similar in each case, between 1 x 10^{-6} and 5 x 10^{-6}M, with CTAB requiring the higher concentration which may possibly be due to a partition effect between surface and solution.

Returning to the results for the 2.1μm I.D. latex, Figure 4.45 shows the residual singlet peak for the oligomeric, F_A[0.02]O, chitosan and this again agrees with the medium molecular weight observation that flocculation occurs at amine : sulphate ratio of 1, i.e. indicating charge neutralisation.

Figures 4.46 and 4.47 represent the flocculation ranges for the F_A[0.14]M and F_A[0.57]M samples, whilst figure 4.48, represents the high molecular weight F_A[0.17]H sample. Table 4.3 summarises some of the information from these figures, lower limit, peak centre and upper limit of flocculation as well as peak width (in terms of ratio amine : sulphate groups) at an arbitrary value of 10000 singlets (approximately half peak height) to show a general comparison of the flocculation ranges, whilst Figure 4.49 re-plots these in graphical form. From figure 4.49, the overlap of the peaks of the oligomeric sample and F_A[0.02]M can be clearly seen and, from Table 4.3, the difference in peak width produced by the two samples can also be observed. Figure 4.49 shows clearly the trend towards higher required ratios with F_A of the medium molecular weight samples, as does the peak

Flocculant	Lower Limit	Peak Centre	Upper Limit	Peak Width	Error Range
F_A[0.02]O	0.92	0.97	1.02	0.10	0.93 – 1.07
F_A[0.02]M	0.80	1.03	1.26	0.46	0.93 – 1.07
F_A[0.14]M	1.01	1.24	1.48	0.47	0.93 – 1.07
F_A[0.57]M	1.06	1.43	1.80	0.74	0.91 – 1.09
F_A[0.17]H	0.79	1.03	1.26	0.47	0.94 – 1.06

Table 4.3 Comparison of peak limits, centre and width for flocculants with 2100nm Interfacial Dynamics latex at 10000 singlets.

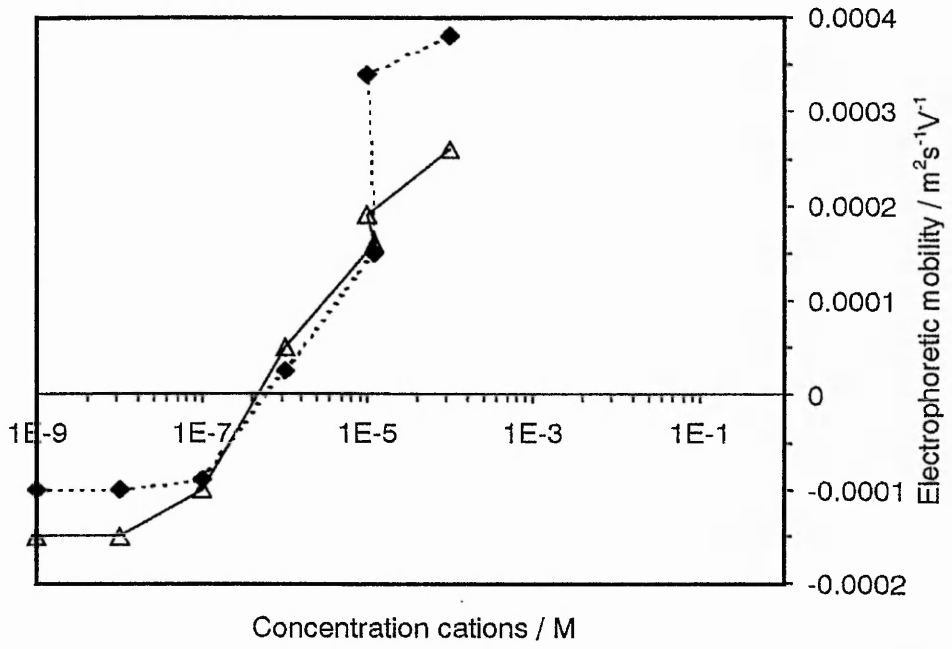

Figure 4.44 The electrophoretic mobility of the 2250nm latex in the presence of CTAB (◆) and F_A[0.02]M (△).

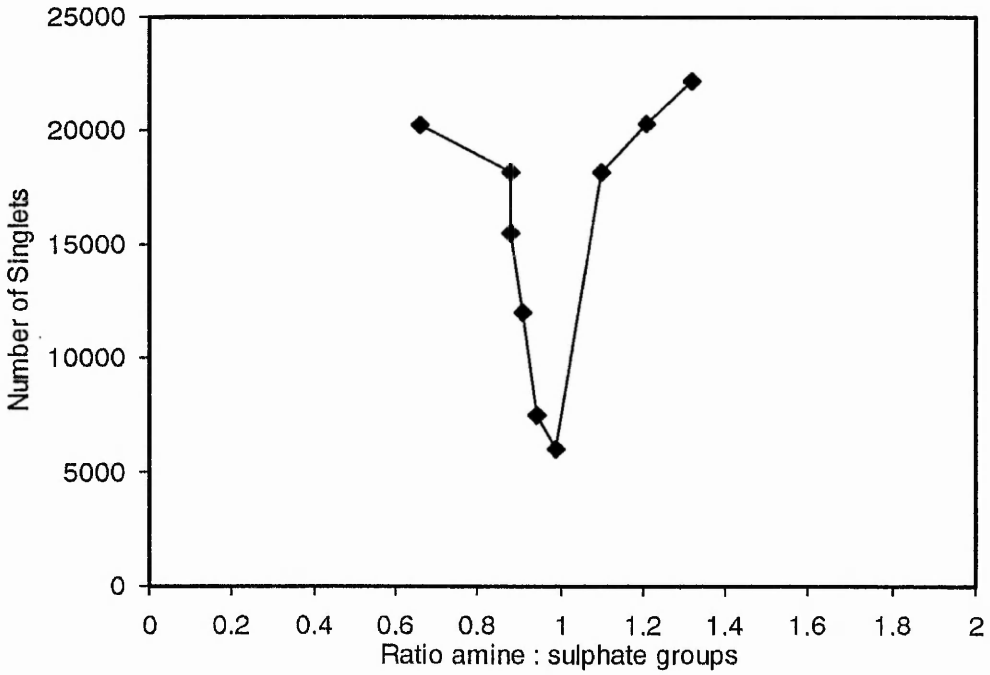

Figure 4.45 The residual singlet population of 2.1μm latex after flocculation by F_A[0.02]O chitosan.

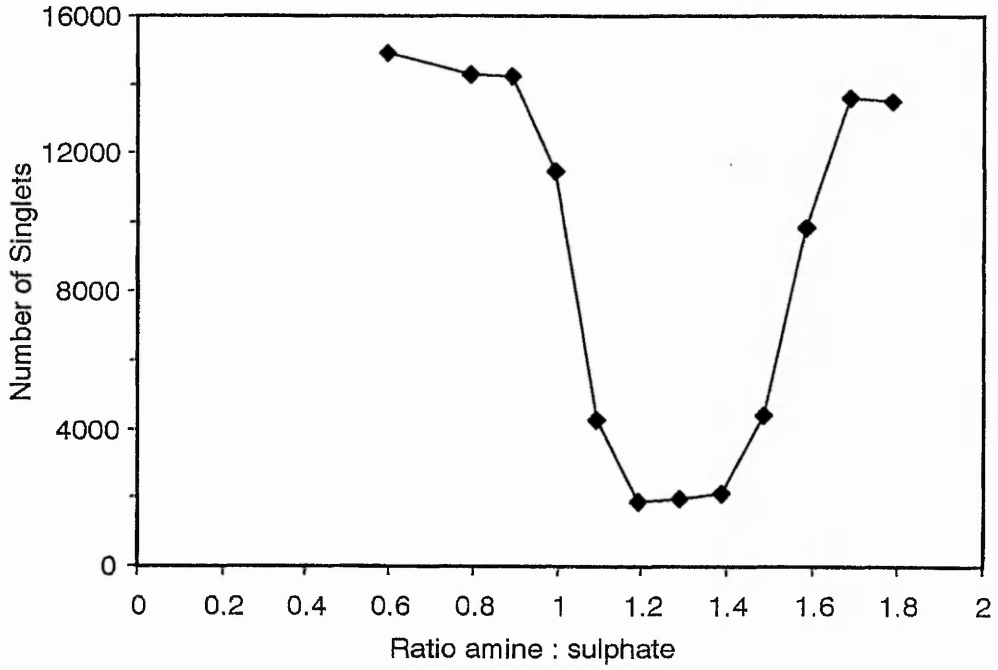

Figure 4.46 The residual singlet population of 2.1μm latex after flocculation by F_A[0.14]M chitosan.

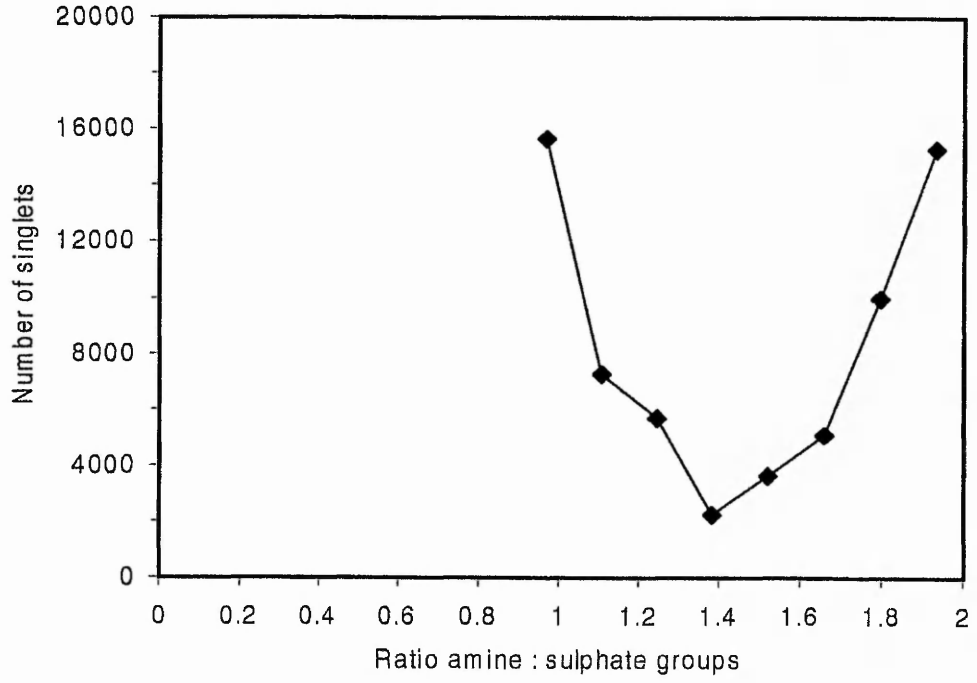

Figure 4.47 The residual singlet population of 2.1μm latex after flocculation by F_A[0.57]M chitosan.

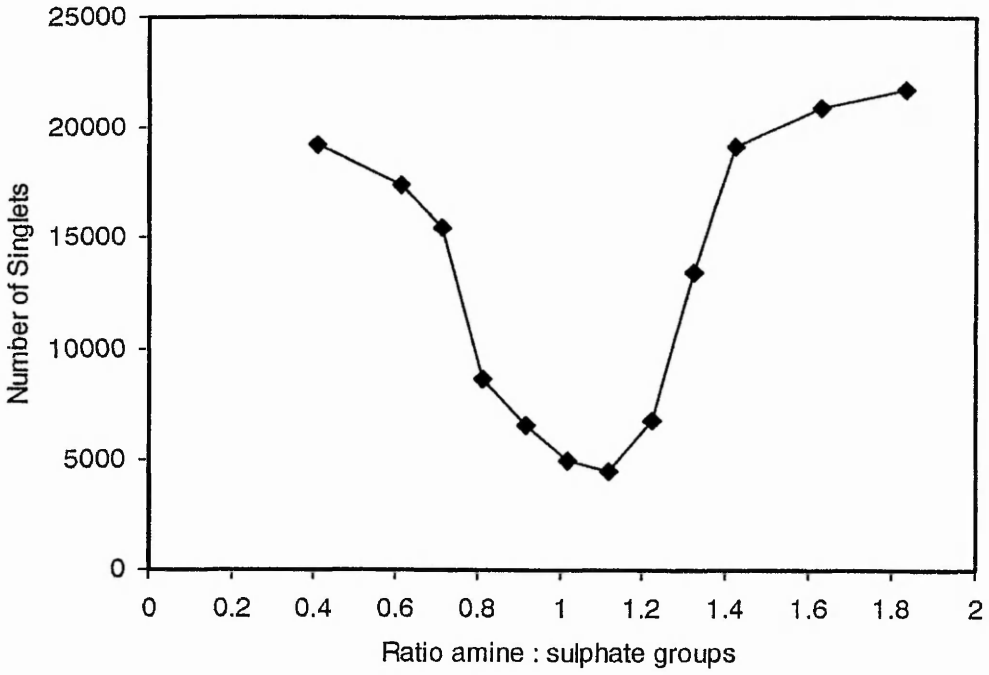

Figure 4.48 The residual singlet population of 2.1μm Interfacial Dynamics latex after flocculation by F_A[0.17]H chitosan.

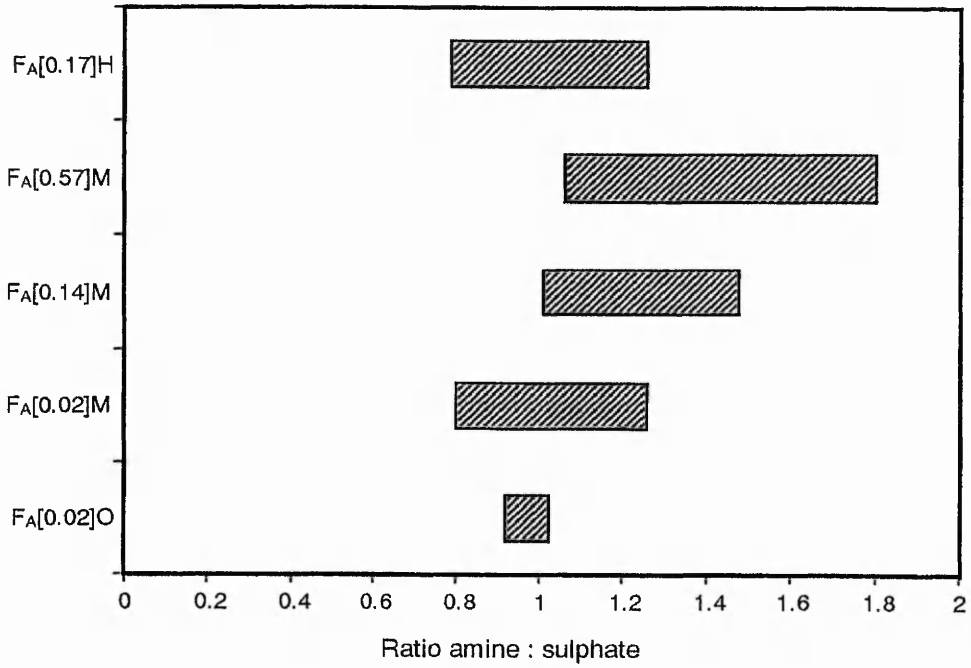

Figure 4.49 Comparison of the peak widths and positions at 10000 singlets of the flocculation ranges of the samples F_A[0.02]O, F_A[0.02]M, F_A[0.14]M, F_A[0.57]M and F_A[0.17]H with the Interfacial Dynamics 2100nm latex.

centre information in Table 4.3.This latter parameter appears to show again a rough correlation between increased required dose and F_A. Both Table 4.3 and Figure 4.49 clearly illustrate the return of the higher molecular weight sample to a 1:1 stoichiometric ratio, indicative of the formation of denser (and therefore more efficient) patches.

4.3.2 Rate of aggregation of 2.1μm latex.

The residual singlet results discussed above again indicate that chitosan, as in the cases of the 85 and 400nm latices, flocculate the 2.1μm system via a charge neutralisation mechanism. However, again the rate of aggregation must be determined in order to distinguish between simple charge neutralisation and the electrostatic patch mechanism. Initial rates of aggregation were determined in order to clarify this point. A method using the Coulter Multisizer was employed. 0.5ml of latex was added to 9.5ml of 1M sodium chloride solution and the particle size distribution was determined after appropriate time intervals. As rapid aggregation is kinetically a second-order process, plotting $1/n_{TOTAL}$ against time should yield a straight line, in the early stages at least. Figure 4.50 shows the results of three such determinations. All three runs involve the coagulation of the 2.1μm latex with 1M NaCl. It can be seen that reproducibility is poor, with an error of 20% over just one standard deviation. Also carried out was a repeat of the method used by Matthews and Rhodes[282]. In this work, singlet population was determined (n_1) as well as initial singlet population, n_0 and a plot of $[(n_0 / n_1)^{1/2} - 1].T_{1/2}$ against time, where $T_{1/2}$ is the coagulation half-life, (the time required to reduce the total number of singlets by one half), produced a straight line with a slope equal to the reciprocal stability ratio, 1/W. Figure 4.51 shows several such plots for perikinetic coagulation, along with regressions for each. In this case,

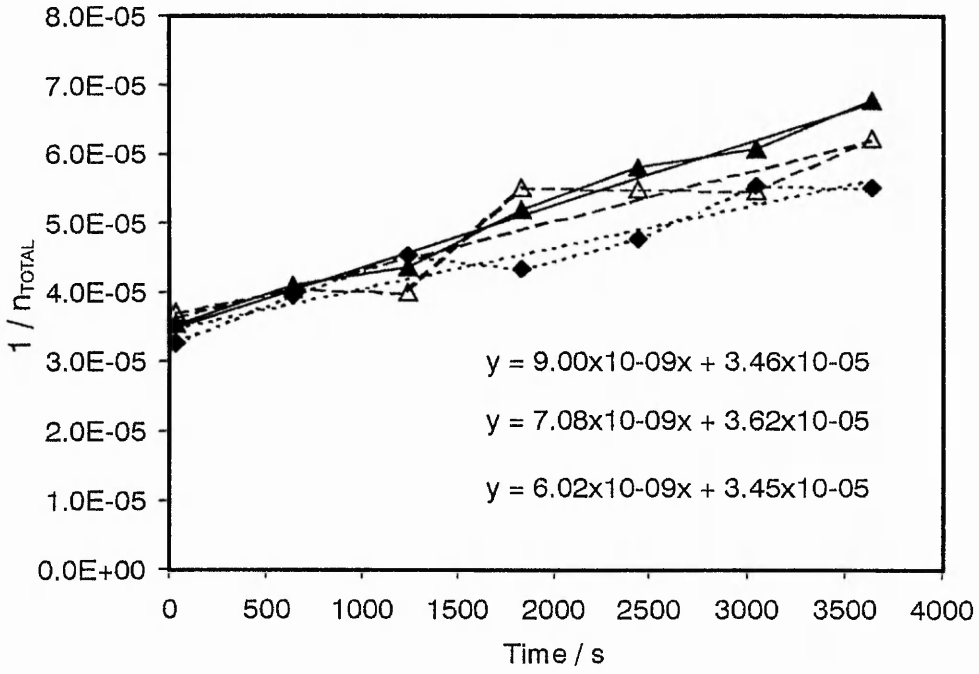

Figure 4.50 Plot of $1/n_{TOTAL}$ versus time for the coagulation of 2.1μm latex using 1M NaCl.

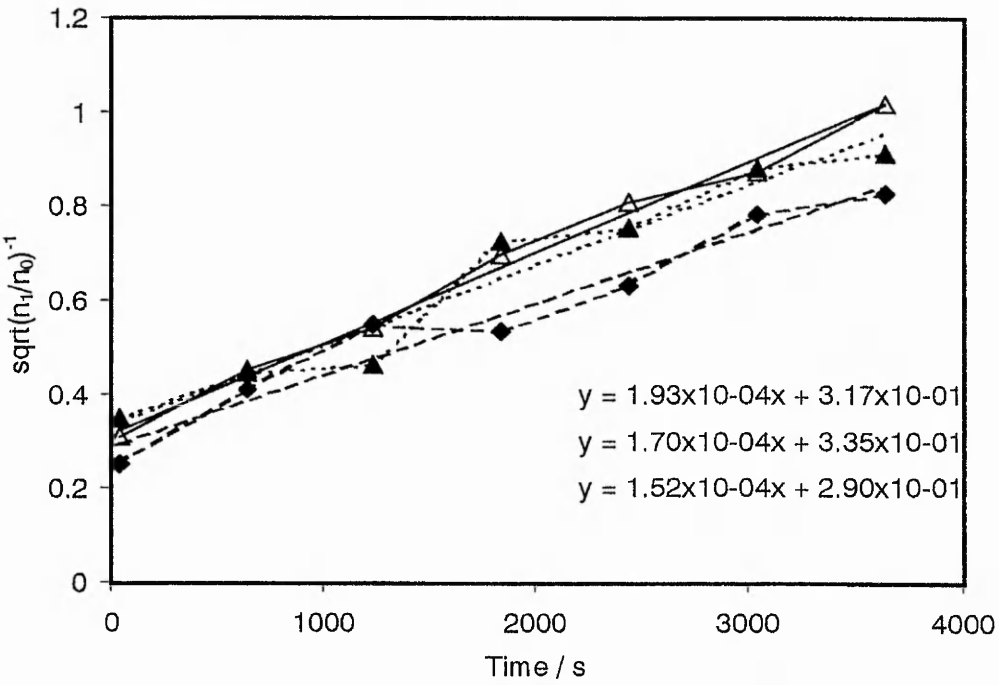

Figure 4.51 Plot of $[(n_0/n_1)^{1/2} - 1]$ versus time for the coagulation of 2.1μm latex using 1M NaCl.

for simplicity, the constant $T_{1/2}$ was omitted, the graph plotted gives a gradient proportional to W, an adequate figure for a simple comparison of aggregation rates. It can be seen that, whilst reasonably straight lines are produced, the gradient varies widely. The error over of all the runs was of the order of 30% over a single standard deviation, again suggesting that the reproducibility of the determination is not sufficiently great for the method to be used in this case.

In their studies on latex coagulation using a Coulter Counter, Matthews and Rhodes used smaller latex particles of 0.71μm diameter[282] but did mention that sedimentation was a problem[283] for latices of 1.87μm diameter and cited Johnson *et al*[343] using a slow rotating bath which was claimed to have no effect on the coagulation rate.

In an effort to measure aggregation rates more reproducibly, it was decided to subject the aggregating latex to a small amount of shear. This changed the regime from perikinetic (as with the other aggregating latices) to orthokinetic but, as all that was required was a simple comparison of coagulation and flocculation rates, such a change was deemed to be acceptable. Samples were subsequently rolled on a Denly Spiramix 5, which rotates and tilts the samples once per second, and measurements were made as in the case of the perikinetic determinations.

Figure 4.52 shows the graph of $1/n_{TOTAL}$ versus time and Figure 4.53 shows singlet population versus time for a range of F_A[0.02]M chitosan concentrations around the critical flocculation concentration, as well as two 1M sodium chloride coagulation runs in order to determine the second order rate constant k_2 under this new regime. It can be seen from Figure 4.52 that none of the determinations produce a particularly straight line, the coagulation runs in both figures especially point to the need for measurements over short time-scales that would be difficult to carry out using this method.

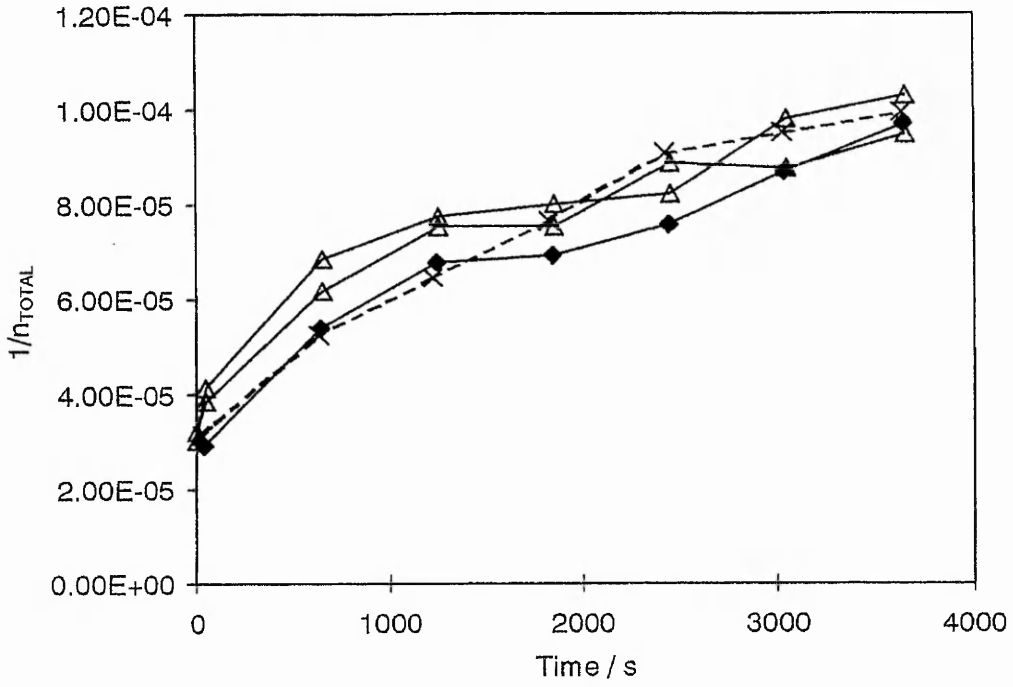

Figure 4.52 Plot of $1/n_{TOTAL}$ versus time for orthokinetic coagulation (△) and flocculation (by different concentrations of F_A[0.02]M chitosan, ◆, X) of 2.1μm latex.

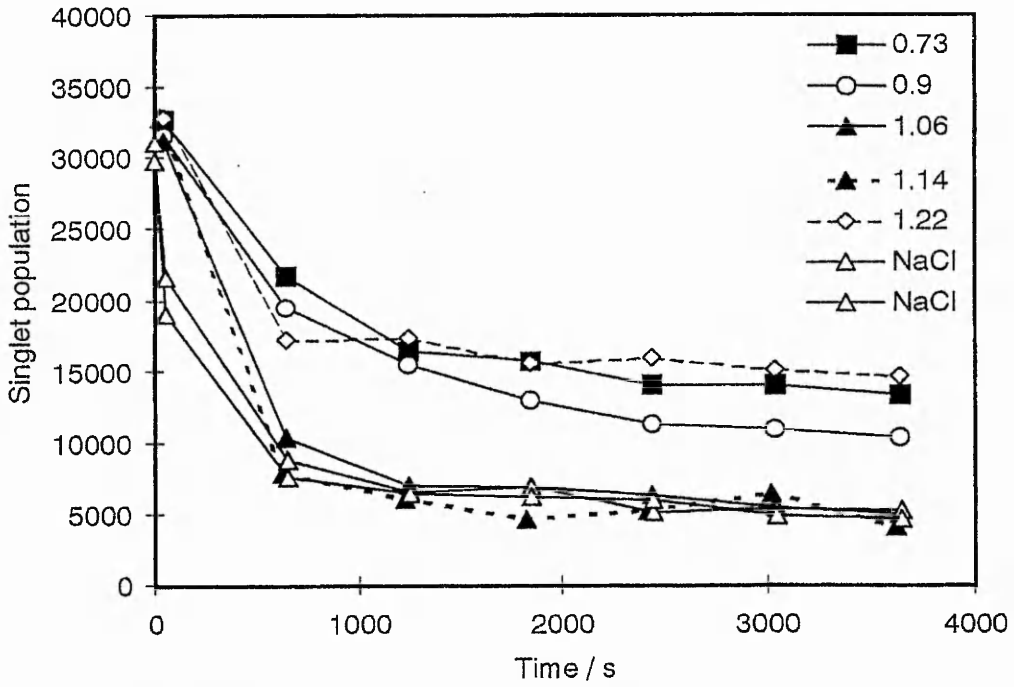

Figure 4.53 The disappearance of 2.1μm latex singlet particles with time for a range of coagulant and flocculant concentrations (expressed as ratios of amine:sulphate groups).

It is apparent that little quantitative data may be taken from this orthokinetic study, but the results seem to point towards the coagulation rate being in excess of the maximum flocculation rate.

The development of the flocculation may be observed more easily if data from Figure 4.53 for example is plotted to show singlet population versus amine : sulphate ratio at specific times (Figure 4.54). This apparent increase in optimum flocculant concentration (i.e. above a ratio of 1) may be due to a relatively long adsorption time. The latex may adsorb the required amount of flocculant from a solution with a flocculant concentration slightly higher than the notional (perikinetic) optimum concentration faster than from a solution of optimum concentration by simple virtue of the fact that there are more flocculant chains in solution. It may be shown[345], qualitatively at least, that under orthokinetic conditions the frequency of collision between two particles, may be significantly greater than the frequency of collision between particle and flocculant molecule. Therefore, in the case of flocculation, a particular particle may undergo several collisions with other particles before enough flocculant has adsorbed on its surface to bring about adherence during a collision. The rate of coagulation by contrast relies only on double layer compression by added electrolyte. This means that many of the earlier collisions, which in the flocculation experiment would not lead to adhesion due to lack of adsorbed flocculant, do result in aggregation and hence a much higher rate of aggregation is observed. Similarly, it can be seen in figure 4.53 that the extent of flocculation (singlet population reduction) at the first reading (t = 40 seconds) is greater at higher than optimum flocculant concentrations, and this may be explained using similar arguments.

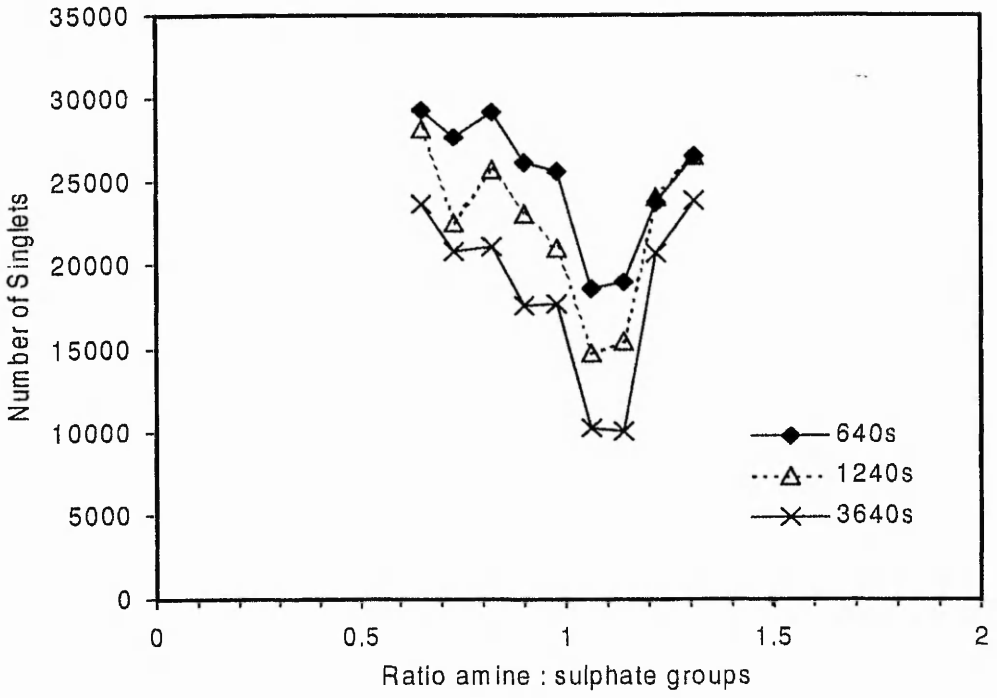

Figure 4.54 Singlet population versus flocculant concentration (in terms of amine : sulphate ratio) at various flocculation times for F_A[0.02]M.

In order to compare the rate of flocculation with coagulation (both perikinetic and orthokinetic) directly, it may be necessary to employ a "two step mixing" method to study the flocculation process, as employed previously in turbidity-rate determinations[270], in which the optimum amount of flocculant for a system is added to a *half* portion of the system, the flocculant is allowed a sufficient equilibration time, then the two halves are mixed (giving the optimum amount of flocculant overall) and the flocculation rate determined by the appropriate method. This two-step method would eliminate the time lag caused by polymer adsorption and hence allow the system to flocculate at its optimum rate from time, t = 0, and this rate could then be compared with the rapid coagulation rate of the system.

Flocculation experiments are necessarily carried at a higher number density than can be read directly in a Coulter counter since, for example Matthews and Rhodes[282]

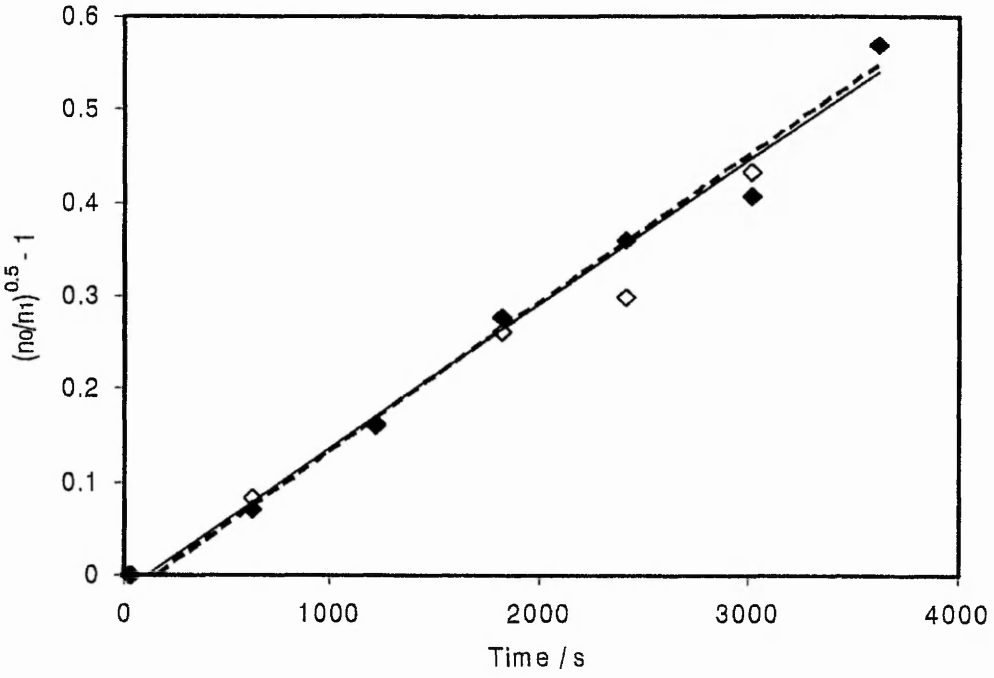

Figure 4.55 Matthews and Rhodes-type plot for the rapid coagulation of the 2.1μm latex under perikinetic conditions and using a 2mm wide pipette tip for sampling.

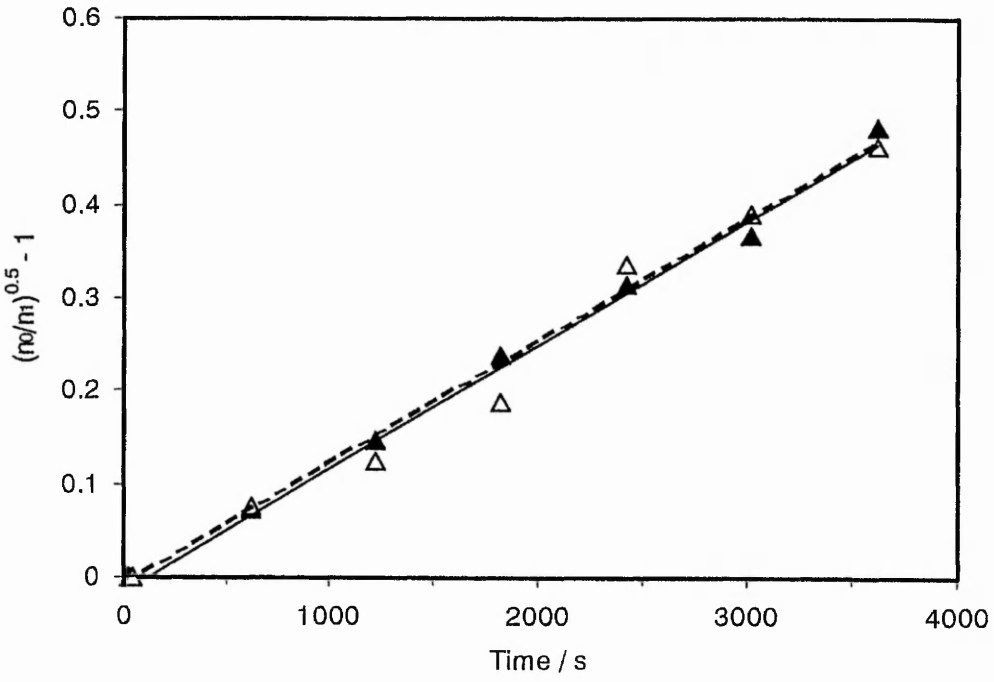

Figure 4.56 Matthews and Rhodes-type plot for the optimum flocculation rate of the 2.1μm latex under perikinetic conditions using F_A[0.02]M chitosan and a 2mm wide pipette tip for sampling.

showed that below $5x10^7$ particles per ml stability ratios were no longer constant. Sampling and dilution procedures are thus essential before Coulter counting and these procedures may introduce an element of orthokinetic aggregation into the system which could help to account for inconsistencies in observed rates. Adachi[344] for example has discussed the flocculation which can result upon each cycle of merely pouring the dispersion, in the presence of polyelectrolyte, from one beaker to another.

In a final effort to resolve this problem, the rates of coagulation and flocculation were again determined under perikinetic conditions. This time a two-step addition regime was used for the flocculation experiments and in order to reduce the influence of shear induced aggregation on sampling, samples from the aggregation vessel were removed using an auto pipette, the tip of which had been cut back so that the opening was approximately 2mm in diameter[348]. This resulted in a slight alteration in the exact volume dispensed, but this new volume was determined to be reproducible by gravimetric means using double distilled water.

Under this regime, Matthews and Rhodes-type plots of $[(n_0 / n_1)^{1/2} - 1]$ against time (t) were both linear and reproducible as displayed in Figures 4.55 and 4.56. The method gave concordant results for the apparent rate of rapid coagulation by 1M NaCl, the mean rate from the slope was $15.65x10^{-5}$ (Figure 4.55) and the mean rate for the optimum chitosan concentration was $13.24x10^{-5}$ (Figure 4.56).

Figure 4.57 compares the range of flocculation given by the residual singlets method with the rate of flocculation produced by different F_A[0.02]M chitosan concentrations in terms of ratio of flocculation to coagulation rate. Figure 4.57 shows that the ranges produced by the two methods overlap, with the maximum rate corresponding to the minimum singlet value. Also apparent is that the flocculation rate does not reach that of rapid coagulation, i.e. rather than enhancing the aggregation rate, chitosan produces a

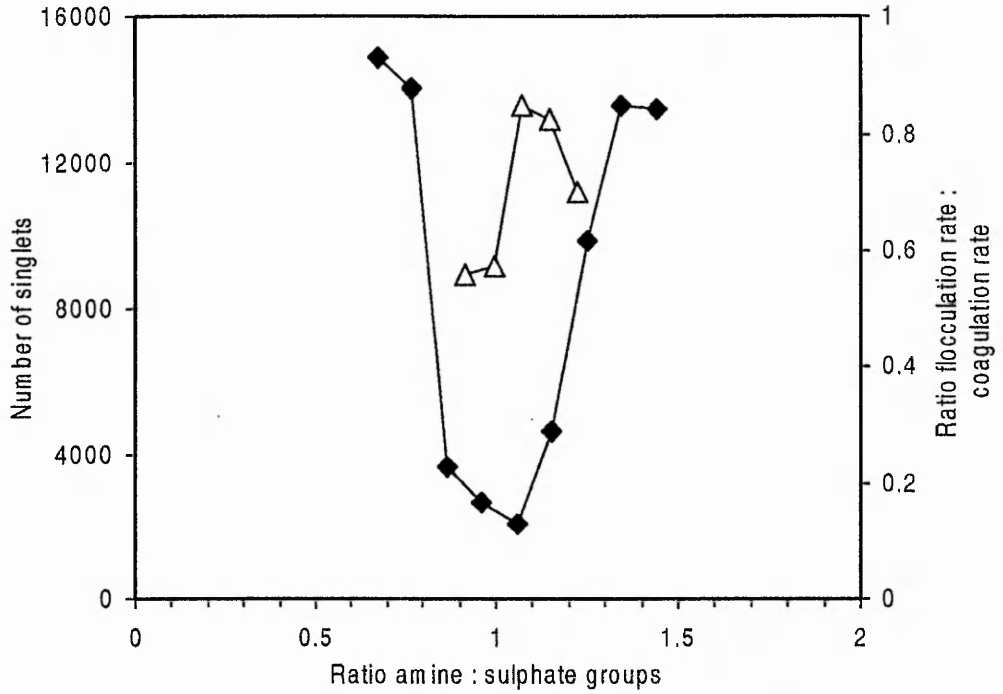

Figure 4.57 Flocculation ranges for the 2.1 μm Interfacial Dynamics latex produced by FA[0.02]M chitosan by the residual singlets method (◆) and by the Matthews and Rhodes[282] treatment of rate data (△).

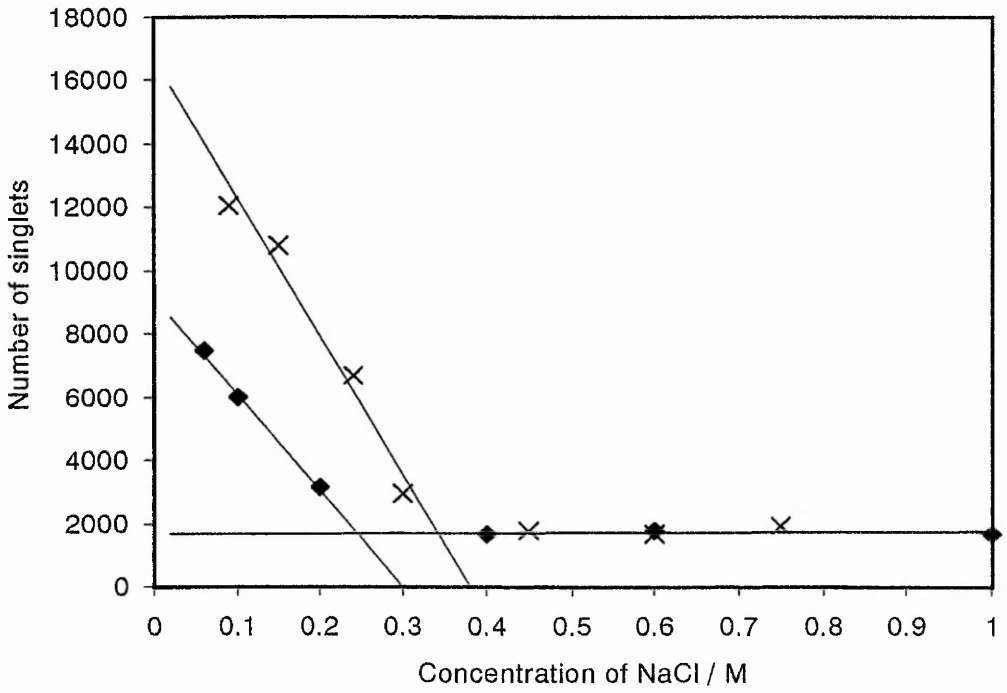

Figure 4.58 Comparison of the critical coagulation concentration of 2.1μm Interfacial dynamics latex with a sample of the same latex protected by F_A[0.17]H chitosan.

flocculation rate less than that of simple coagulation. Hydrodynamic interactions have been reported to influence rates of aggregation of latex particles >0.5μm[349, 350, 351, 352] in diameter, thus the effects of adsorbed chitosan on viscous drainage between particles may act to decrease the overall flocculation rate in the system.

4.3.3 Critical coagulation concentration

Figure 4.58 shows the effects of simple electrolyte (NaCl) on the latex system. The symbol ◆ represents the residual singlet populations after 24 hours upon the addition of various concentrations of NaCl. The second symbol, x, represents a similar study for a sample of the same latex which has been pre-treated with a sample of chitosan (F_A[0.17]H) equivalent to twice the critical flocculation concentration. Figures 4.59 and 4.60 show that only a small proportion of doublets (2.81% by number based on singlet population) are introduced when the 2.1 micron latex is converted from anionic to cationic.

It can be seen from Figure 4.58 that the stability of the latex is increased on the addition of sufficient chitosan, with a critical coagulation concentration of 0.34M NaCl rather than 0.25M, indicating that the chitosan covered latex carries a greater (cationic) charge density than the bare (anionic) latex. It is apparent from the magnitude of the indifferent electrolyte tolerance that this latex is electrostatically restabilised as tolerance to much higher electrolyte concentrations would be observed if steric stabilisation was in operation[347].

4.4 350nm latex

Figure 4.61 shows the results for the residual turbidity study of the 350nm latex. Comparing the flocculation range of F_A[0.02]M with the coagulation range of CTAB, plotted in terms of concentration of cations (-NH_3+ or CTA+) in the system, it can be seen that CTAB requires a somewhat higher concentration of cations to effect aggregation.

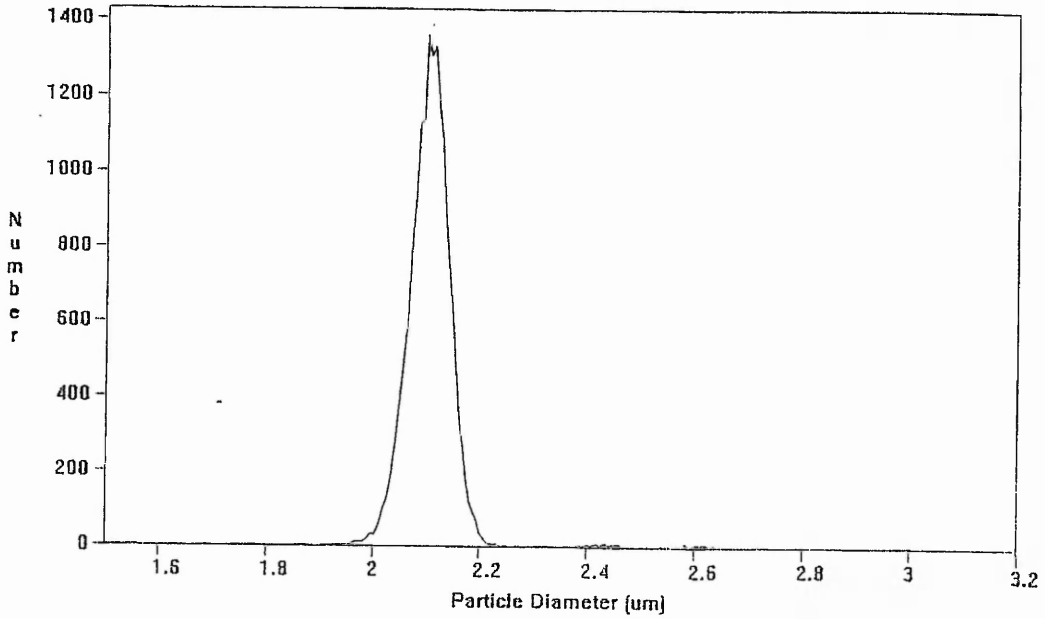

Figure 4.59 Particle size distribution for the original 2.1 micron latex using the Coulter Multisizer

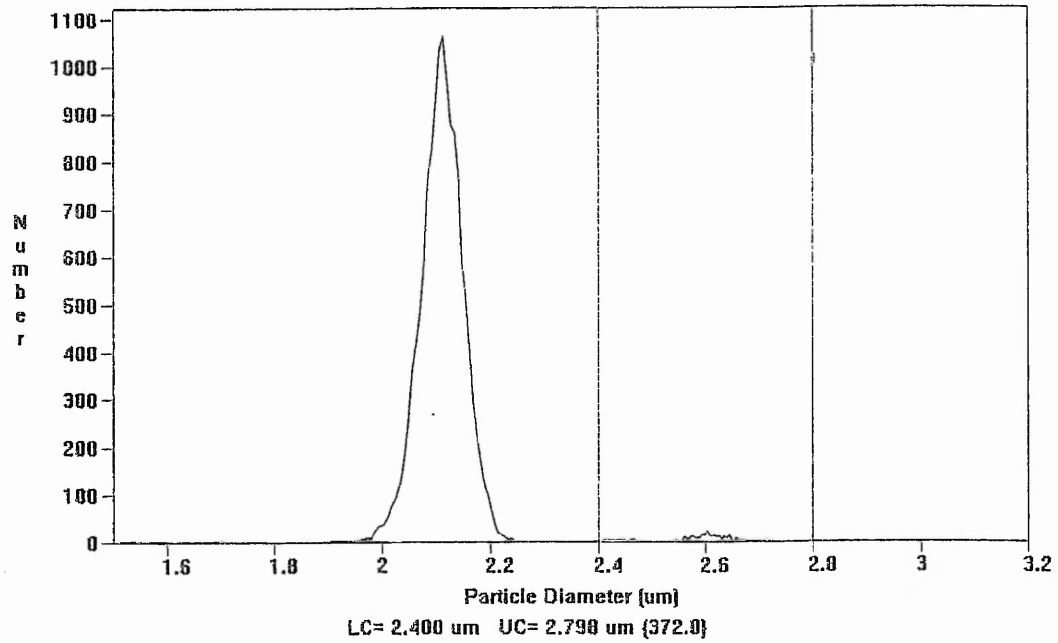

Figure 4.60 Particle size distribution for the FA[0.02]M protected 2.1 micron latex using the Coulter Multisizer showing a small increase in the doublet population.

However, if this data is re-plotted against ratio of amine : sulphate groups, based on the surface charge on the latex quoted by Interfacial Dynamics, Figure 4.62 is produced. It is observed that a significantly larger ratio than 1 is required by both F_A[0.02]M and CTAB, around 4.5 times as many amine groups than sulphate groups are required to flocculate the system with the chitosan sample, whilst 6 times as many CTA+ ions are required for flocculation. Considering the CTAB result, it may be conceivable that some partition of CTA+ ions occurs between the surface and the solution and the position of this equilibrium is effected by the low charge density on the latex, however a 6 fold excess still seems rather large. The range for F_A[0.02]M is, however more difficult to rationalise in this fashion as the polyelectrolyte should bind effectively to the surface through many points of contact; protonated amine groups, and hence chains should remain on the surfaces rather than in solution. Figure 4.63 re-presents the F_A[0.02]M residual turbidity data with data from an initial rate study for the system. It can be seen that the ranges coincide, and that there is a marked increase in the rate of flocculation over rapid coagulation.

Figure 4.64 shows the effects of CTAB on the electrophoretic mobility of the 350nm latex. The point at which the electrophoretic mobility of the particles is zero corresponds to a CTAB concentration of 3×10^{-7} mol dm^{-3}, much greater than that to be expected, considering the quoted surface charge on the latex, but in good agreement with the 2.9×10^{-7} mol dm^{-3} obtained from the flocculation experiment. While this in it self does not preclude the possibility of a large partition effect, it at least shows that the critical coagulation and flocculation points occur at approximately the point of charge neutralisation of the particles.

It may be suspected then that the surface charge density of the latex is somewhat higher than that originally certified. When queried, the stock latex was re-titrated and gave a higher value at 1.18 μEq g^{-1}, which is approximately double the original figure of

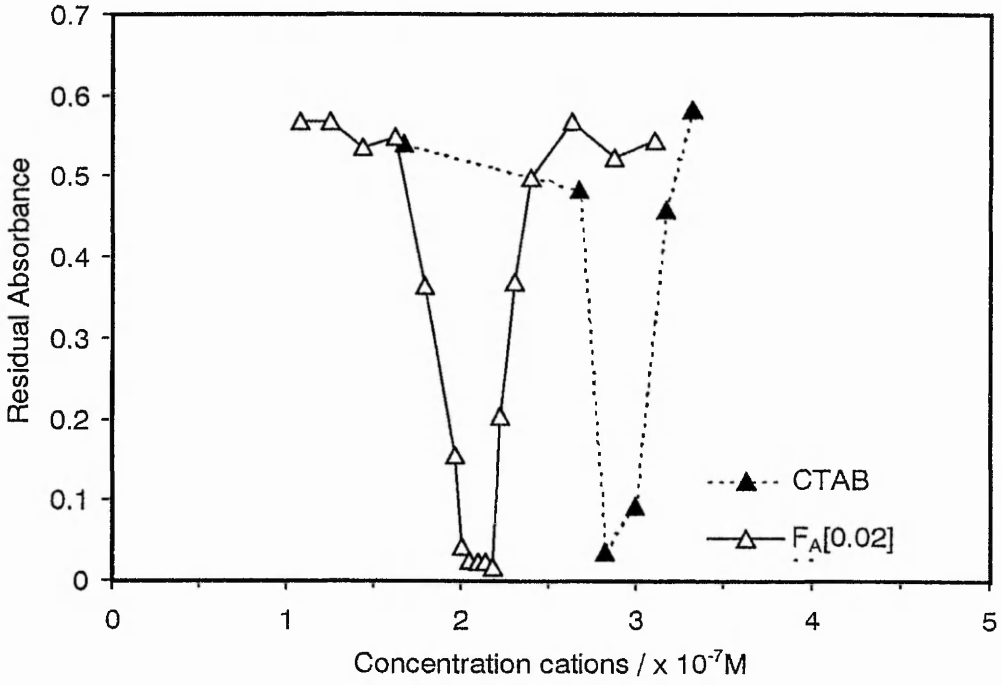

Figure 4.61 Residual Absorbance study of 350nm Interfacial Dynamics latex flocculated with F_A[0.02]M chitosan and coagulated with CTAB.

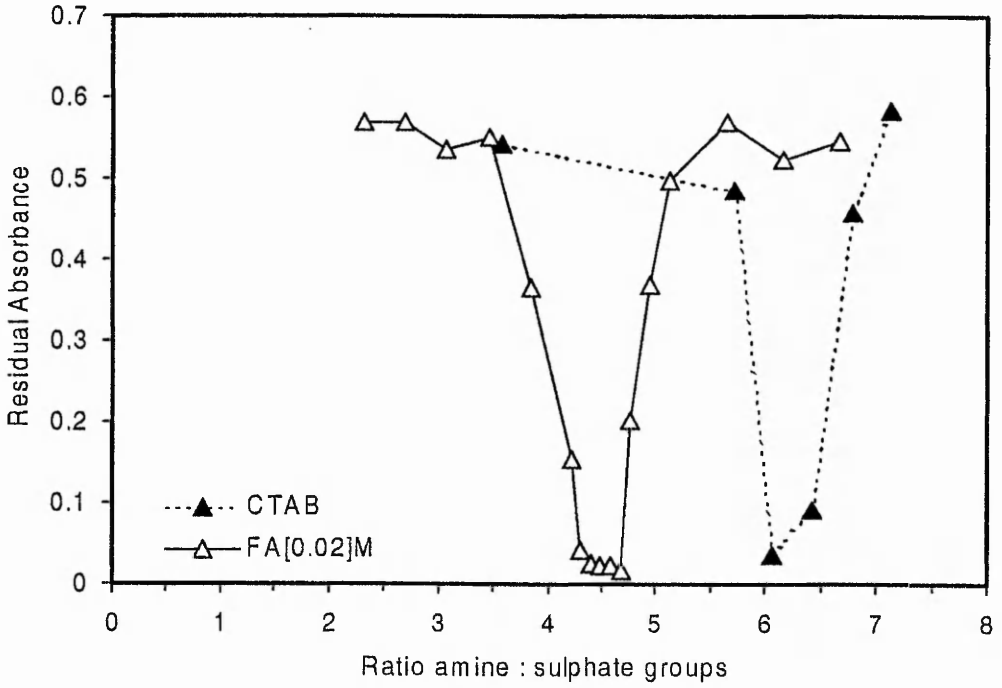

Figure 4.62 Residual Absorbance study of 350nm Interfacial Dynamics latex flocculated with F_A[0.02]M chitosan and coagulated with CTAB, expressed in terms of ratio of amine : sulphate groups.

0.57 μEq g^{-1}, but this is still some way short (a factor of at least 2) of the charge concentration suspected. The increase of charge density on a latex surface is unusual; one would normally expect a decrease in charge density due to hydrolysis of the sulphate groups. It has been suggested that some functional groups may be trapped in the sub surface layers of a latex upon preparation[353]. The possible slow diffusion of such end groups to the surface of the latex over time would be facilitated by a low surface charge density. Also the low surface charge density of the nuclei formed during a polymerisation reaction at low initiator concentration would lead to greater aggregation than usual and promote the burial of surface functional groups.

These results cannot be unequivocally interpreted. If the recent repeat titration data supplied by Interfacial Dynamics is correct then alternative reasons may be suggested for the observed results. Simply as a consequence of the exceptionally low surface charge density of this latex both chitosan and CTAB may be more partitioned towards the aqueous phase than was experienced with any of the other latices. The large excess shown by CTAB seems unlikely in view of the substantive nature of the CTAB and the ready access that the CTA+ ions would have to the surface on an individual basis. Alternatively the number of charges detected upon titration and the number of charged groups available on the samples used in the flocculation experiments could differ as a consequence of the use of ion exchange resins prior to the conductometric titration. The mixed bed ion-exchange resins could have either released low molecular weight cationic polyelectrolyte onto the titrated sample or could have adsorbed low molecular weight anionic materials from the latex surface. The use of ion exchange resins is known to be problematic and the effects would be exacerbated by the very low surface charge density of the latex. It is usually assumed that impurities derived from one component of the resin are adsorbed by the other component in the mixed bed situation but a latex is a third party capable of ion binding in

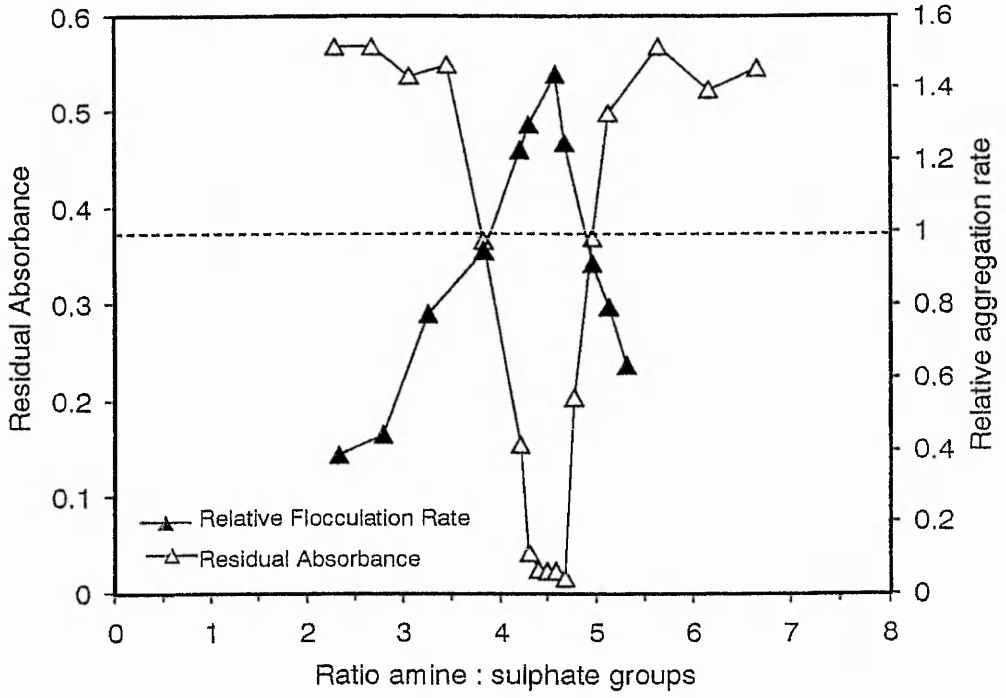

Figure 4.63 Comparison of flocculation ranges produced by residual Absorbance and initial rate experiments with 350nm latex.

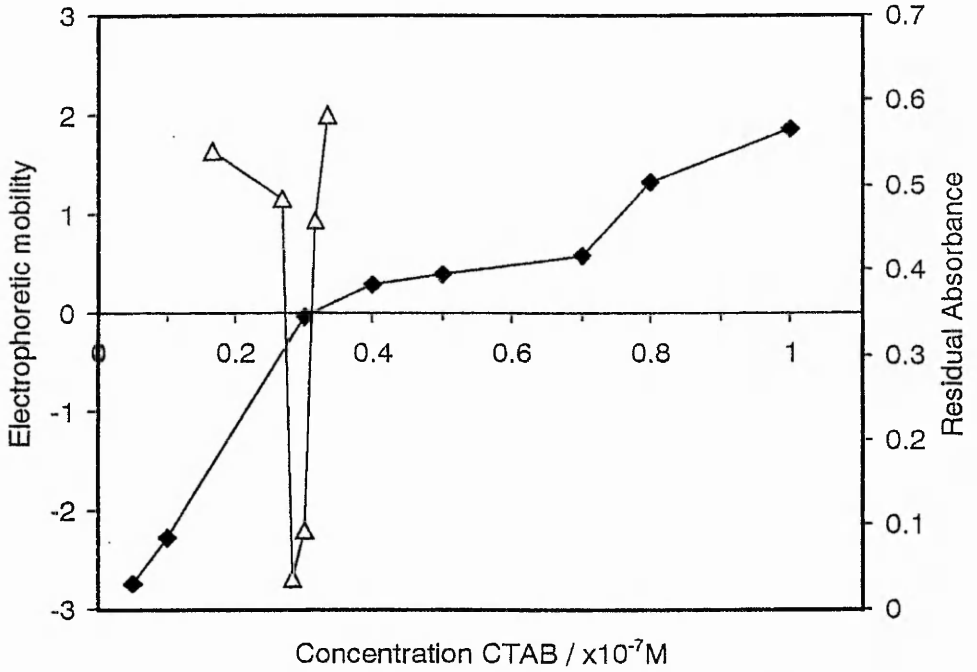

Figure 4.64 Comparison of CTAB coagulation range (△) and the point of charge reversal by electrophoretic mobility (◆) for the 350nm latex.

this situation. The evidence here strongly suggests that the latex as supplied does have a higher charge than stated.

Unfortunately time did not permit the preparation, cleaning and characterisation over a period of time of a very low surface charge density latex, in-house. Such a latex would provide considerable practical challenges since it would be inherently unstable and be susceptible to minor impurities having a large impact upon surface charge both during cleaning and upon conductometric titration. It would have helped to establish whether such a latex could be a valid model colloid.

4.5 Charge separation on latex and chitosan samples

The charge-patch mechanism relies upon an excess of charge on the flocculant chain compared to the particles surface in order to produce oppositely charged patches and hence illicit an increase in aggregation rate over rapid coagulation. Therefore important quantities to compare are the distances between adjacent charges on the polyelectrolyte and on the particles.

The distance between adjacent charges on latex particles may be calculated as in the following example for the 85nm latex.

From the original number density of the latex (1.97×10^{17} particles l^{-1}), and from the surface area of one particle;

$$\text{Area} = 4 \pi r^2 = 4 \times 3.14 \times (42.5 \times 10^{-9})^2 = 2.27 \times 10^{-14} \text{ m}^2\text{per particle}$$

The *surface area per litre* may then be calculated,

$$1.97 \times 10^{17} \times 2.27 \times 10^{-14} = \quad 4471.9 \text{ m}^2\text{l}^{-1}$$

Then from the titration data, the actual *number* of charges (sulphate groups) per litre may be calculated (1.56×10^{-3} eql^{-1} surface sulphate groups x Avagadro's number)

$= 9.39 \times 10^{20}$ charges l^{-1}

So, the area per charge,

$4471.9 / 9.39 \times 10^{20} = \quad 4.76 \times 10^{-18}$ m^2 $charge^{-1}$

This is the circular area per charge, so the radius may be calculated from Area = πr^2

$\pi r^2 = 4.76 \times 10^{-18}$

so, $r = (4.76 \times 10^{-18} / 3.14)^{1/2}$

$= 1.23 \times 10^{-9} m = 12.3$ Å

But, adjacent charges will be 2 radii apart,

$= 24.6$ Å

The Interfacial Dynamics latices are quoted as having the following areas per charge.

Latex Diameter / nm	Area / (Å^2)	Inter-charge distance / Å
350	4734	77.7
400	474	24.6
2100	186	15.4

Table 4.4 Areas and distances per charge for the Interfacial Dynamics latices

The results of this study however suggest that the 350nm latices possess approximately five times as much charge than that quoted which would suggest an inter-charge distance of approximately 34Å.

If these figures are compared with the distance between charges on chitosan chains, x-ray crystallography data suggests amide groups in chitin are approximately 15Å apart,

and therefore amine groups in chitosan F_A[0.0] should be the same distance. So, in chitosan F_A[0.02]M, the mean charge spacing would be a little greater than this (15.3Å). Therefore, in order to observe an enhancement in flocculation rate over coagulation rate, the surface charge separation on the particles should be greater than this, i.e. distance between adjacent charges must be greater than 15.3Å. Comparing this with the four latices, it can be seen that the 2100nm latex possesses an inter-charge distance of 15.4Å, and therefore very little, if any, rate enhancement will be due to the charge-patch mechanism, the flocculant should act predominantly via a simple charge neutralisation mechanism. The other latices possess greater inter-charge distances than 15.3Å, and therefore would be expected to display rate enhancement. Observing the rate of flocculation of each latex with F_A[0.02]M it can be seen that each does indeed show an enhancement in rate. The 350nm and 400nm latex test systems represent dispersions or similar particle size and number density but even the highest estimate of surface charge density on the 350nm shows a significant difference to that of the 400nm latex and hence a greater rate enhancement than that observed in the 400nm system may be expected due to the formation of, relatively, more positive polymer patches compared to the density of the surface negative charge. Comparing the flocculation rate of the 350nm latex with that of the 400nm latex, both flocculated by F_A[0.02]M, it can be seen that this is indeed the case with both the 350nm latex and the 400nm latex producing significant rate enhancements.

As the degree of acetylation increases, the average distance between charges increases. This being the case, it may be expected that the effectiveness of the patches produced is decreased. e.g. chitosan F_A[0.57]M will have a mean inter-charge distance of the order of 30Å, and hence greater than the inter-charge distance on the 400nm latex surface (24.6Å). The rate of flocculation may therefore be expected to be no greater than that of simple coagulation. Figure 4.28 shows the rate of flocculation of the 400nm latex

produced by F_A[0.57]M and it is apparent that the rate enhancement is minimal, any rate elevation observed may be due to an increased hydrophobic effects as in the case of CTAB coagulation (Figure 4.25). The apparent reduction in flocculation efficiency showed by a generally greater requirement of cationic charge to effect flocculation with increasing degree of acetylation may be due to inefficiency of packing on the surface of the latex, quaternary amine charges may ultimately lay shielded between surface sulphate charges, neither neutralising them or producing a excess of cationic charge and therefore a patch. In this way, the surface charge may be reduced and inter-particle collisions may be rendered less effective in producing adhesion, therefore failing to render the particle unstable. More chitosan would then be required to produce a patch effect (producing a much lower enhancement of rate). The situation may be compounded by some association of chitosan chains (increasing with increasing acetylation degree) perhaps rendering some of the cationic charges unavailable between chitosan chains.

The higher molecular weight samples have tended throughout to be more efficient irrespective of acetylation degree, with flocculation ranges generally produced around the point of charge neutralisation. This may in part be due to increased adsorption density[271] per patch, ensuring the formation of discrete, effective patches, there may also be a contribution of some degree of short range inter-particle bridging. Also, while chain association may act to reduce the effectiveness of some quaternary amine groups in lower molecular weight chitosan samples, in higher molecular weight samples chain association may serve to aid any tendency towards short range bridging.

4.6 Conclusions

Generally speaking, it may be concluded that chitosan flocculates model anionic polymer colloidal latex systems via a charge neutralisation mechanism. Further it may be added that, from evidence of enhancements of flocculation rate over rapid coagulation rate,

the 85, 350 and 400nm latices, chitosan flocculates these dispersions via the charge-patch mechanism. The reasons for these rate enhancements may be rationalised by considering the distance between charges on the latex surface compared with the distance between quaternary amine groups on the chitosan chain, the latter distance must be less than the former to produce an enhancement. A rate reduction compared to rapid coagulation has been observed for the 2100nm latex / F_A[0.02]M system. This may be explained via two observations. Similar inter-charge distances on chitosan and particle surface may lead to an expected rate very similar to that of rapid coagulation. Also, it has been previously observed[349, 350, 351, 352] that viscous drainage between large particles may act to retard the aggregation rate.

It has also been found that the efficiency of chitosan as a flocculant is affected by both the degree of acetylation and molecular weight. It would appear that there is a lessening of efficiency in flocculation for the medium molecular weight sample with greater acetylation degrees, perhaps due to changes in the physical properties of the chains making them less able to fit the 'template' provided by the surface charges. Even if the efficiency was comparable however, the actual concentration (in gl^{-1}) of chitosan required for flocculation increases dramatically with increasing degree of acetylation, due to the decrease in charge-content and the addition of acetyl groups.

The flocculation efficiency, in terms of amount of charge required, of higher molecular weight samples seemed less affected by the degree of acetylation, perhaps due to the increased polymer density within patches, and therefore charge density in the patches formed; however the above argument still applies to some extent, increasing acetylation degree necessarily implies an increase in optimum flocculant concentration (in gl^{-1}).

The dependence on its cationic charge (quaternary amine groups) for flocculation means that pH affects flocculation by chitosan, the decreased protonation at higher pHs

meaning that more polymer is required to provide the required charge for flocculation, and at high enough pHs flocculation may not be possible at all.

Overall then, it appears that the optimum chitosan sample to flocculate an anionic dispersion would be one of as low acetylation degree as possible, whilst retaining a high molecular weight, though even oligomeric samples of low acetylation degree would be expected to flocculate anionic dispersions adequately at the point of stoichiometric charge addition.

When chitosans are added at concentrations in excess of the optimum flocculation concentration, charge reversal results producing cationic latex particles having higher critical coagulation concentrations than the original anionic particles and which contain minimal numbers of aggregates. The cationic particles are charge stabilised rather than sterically stabilised confirming that chitosan adsorption is relatively flat on the particle surface.

4.7 Suggestions for Further Work

The in-house preparation of a very low surface charge density latices in sufficient quantities to be thoroughly cleaned and acid washed by microfiltration and then characterised by conductometric titration over a long period of time. This would establish the stability of the surface charge density and the suitability of such latices as model colloids.

A study of the flocculation of cationic latex particles by chitosans. In the like charge interactions it would be expected that a bridging mechanism would prevail and that high molecular weight samples would be needed together with the addition of some multivalent counter-ions. The techniques would be similar to those used in this thesis and it would again be instructive to investigate the effects of the degree of chitosan acetylation and the influence of the surface charge densities of latices.

References

(1) GAF Roberts, Chitin Chemistry, Macmillan Press Ltd, London, (1992) Page 1

(2) G Maresch; T Clausen; G Lang, *in* Chitin and Chitosan, Skjak-Braek, G. Anthonsen, T. Sandford, P. (Eds), Elsevier, London, (1989) Page 389

(3) LD Hall; M Yalpani, J. Chem. Soc. Chem. Comm., (1980) 1153

(4) J Ruiz-Herrera, Proceedings of the 1st International Conference on Chitin/Chitosan, Muzzarelli R A A, Pariser E R. (eds), (1977) Page 11

(5) M Falk; DG Smith; J McLachlan; AG McIness, Can. J. Chem., (1966), 44, 2269

(6) RH Hackman, Aust. J. Biol. Sci., (1960), 13, 568

(7) S Hunt, Polysaccharide-Protein Complexes in Invertebrates, Academic Press, London, (1970) Page 129

(8) GAF Roberts, ref.1, page 6

(9) GAF Roberts, ref.1, page 7

(10) GAF Roberts, ref.1, page 55

(11) GW Rigby, US Patent 2,040,879, (1934)

(12) Du Pont De Nemours & Co, UK Patent 458,839, (1936)

(13) CH Giles; ASA Hassan; M Laidlaw; RVR Subramanian, J. Soc. Dyers Colourists, (1958), 74, 645

(14) ACM Wu; WA Bough, *in* ref.4, Page 88

(15) RAA Muzzarelli; F Tanfani; M Emanualli; S Gentile, J. Appl. Biochem., (1980), 2, 380

(16) S Mima; M Miya; R Iwamoto; S Yosikawa, in Chitin and Chitosan, S Hirano; S Tokuras (eds), The Japanese Society of Chitin and Chitosan, (1982) page21

(17) K Shimahara; K Ohkouchi; M Ikedo, ref.16, Page 10

(18) RH Hackman, Aust. J. Biol. Sci., (1954), 7, 168

(19) RH Hackman; M Goldberg, Carbohydrate Res., (1974), 38, 35

(20) R Blumberg; CL Southall; NJ Van Rensberg; OB Volckman, J. Sci.Food. Agric., (1951), 2, 571

(21) P Broussignac, Chim. Ind. Genie. Chim., (1968), 99, 1241

(22) SA Karuppaswamy, ref 4, Page 437

(23) RL Whistler; JN BeMiller, J.Org.Chem., (1962), 27, 1161

(24) M Takeda; E Abe, Norisho Suisan Koshusho Hokoku, (1962), 11, 339

(25) GL Clark; AF Smith, J. Phys. Chem., (1936), 40, 863

(26) ST Horowitz; S Roseman; J Blumenthal, J. American. Chem. Soc., (1957), 79, 5046

(27) CG Anderson; N de Pablo; CR Romo, ref 4, Page 54

(28) MN Moorjani; V Achutha; DI Khasim, J. Food Sci. Technol., (1975), 12, 187

(29) AB Foster; RH Hackman, Nature, (1957), 180, 40

(30) M Takeda; K Katsuura, Suisan Daigaku Kankyu Kohoyu, (1964), 13, 109

(31) D Horton; DR Lineback, *in* Methods in Carbohydrate Chemistry, Whistler RL (ed), Academic Press, New York, (1965), vol 5, Page 403

(32) SA Barker; AB Foster; M Stacey; JM Webber, J. Chem. Soc. (1958), 2218

(33) E Winterstein, Ber., (1894), 27, 3113

(34) F Hoppe-Seyler, Ber., (1894), 27, 3329

(35) O von Furth; M Rosso, Beit. Chem. Physiol. Pathol., (1906), 8, 163

(36) E Lowey, Biochem. Zeit., (1909), 23, 47

(37) R Jeanloz; E Forchielli Helv. Chim. Acta., (1950), 33, 1690

(38) A Domard; M Rinaudo, Int. J. Biol. Macromol., (1983) 5, 49

(39) R Minke; J Blackwell, J. Mol. Biol., (1978), 120, 167

(40) J Blackwell; R Minke; KH Gardner, ref. 4, Page 108

(41) D Carlstrom, J. Biophys. Biochem. Cytol., (1957), 3, 669

(42) NE Dweltz, Biochem. Biophys. Acta., (1960), 44, 416

(43) NE Dweltz; JR Colvin; AG McInnes, Can. J. Chem., (1968), 46, 1513

(44) KH Gardner; J Blackwell, Biopolymers, (1975), 14, 1581

(45) KM Rudall, Adv. Insect. Physiol., (1963), 1, 257

(46) KM Rudall; W Kenchington, Biol. Rev., (1973), 49, 597

(47) J Blackwell, *in* Methods in Enzymology, WA Wood; ST Kellogg, (Eds) Academic Press, New York (1988), Vol.161, Page 435

(48) RJ Samuels, J. Pol. Sci., Phys. Ed., (1981), 19, 1081

(49) K Sakurai; M Takagi; T Takahashi, Sen-i Gakkaishi, (1984), 40, T-246

(50) K Sakurai; T Shibano; K Kimura; T Takahashi, Sen-i Gakkaishi, (1985), 41, T-361

(51) K Ogawa; S Hirano; T Miyanishi; T Yui; T Watanbe, Macromolecules (1984), 17, 973

(52) N Cartier; A Domard; H Chanzy, Int. J. Biol. Macromol., (1990), 12, 289

(53) FA Rutherford; PR Austin, ref. 4, Page 182

(54) GAF Roberts, ref.1, Page 278

(55) PP von Weimarn, Ind. Eng. Chem., (1927), 19, 109

(56) VF Lee, University Microfilms, (Ann Arbor) 74/29446, (1974)

(57) A Shirai; K Takahashi; R Rajiravanit; N Nishi; S Tohura, *in* Chitin and Chitosan : The Versatile, Environmentally Friendly Modern Materials, Mat B Zakaria, Wan Mohamed Wan Muda, Md Pauzi Abdulla (eds), Penerbit Universiti Kebansaan, Bangi, Malaysia (1995)

(58) M Vincendon; A Domard, *in* Advances in Chitin Science Vol. I, A Domard; C Jeuniaux; RAA Muzzarelli; GAF Roberts (Eds), Jacques Andre Publisher, Lyon, France, (1996), Page 340

(59) PR Austin, *in* Chitin, Chitosan and Related Enzymes, JP Zikakis (Ed), Academic Press, New York (1984), Page 227

(60) D Gagnaire; J Saint-Germain; M Vincendon, Makromol. Chem., (1982), 183, 593

(61) PR Austin, US Patent 3,892,731 (1975)

(62) GG Allen; PG Johnson; Y-z Lai; K.V Sarkanen, Chem. Ind., (1971), 127

(63) RC Capozza, German Patent 2,505,305, (1975)

(64) PR Austin, *in* ref. 47, vol.161, Page 403

(65) ER Hayes; DH Davies, in ref. 4, Page 406

(66) JG Domszy; GAF Roberts, Makromol. Chem., (1985), 186, 1671

(67) K Nagasawa; Y Inoue, Chem. Pharm. Bull., (1971), 19, 2617

(68) RAA Muzzarelli, Chitin, Pergamon, Oxford (1977), Page 104

(69) PR Austin; S Sennett, Amer. Chem. Soc. Pol. Preprints, (1977), 18(2), 279

(70) T Sannan; K Kurita; Y Iwakura, Makromol. Chem., (1975), 176, 1191

(71) T Sannen; K Kurita; Y Iwakura, Makromol. Chem., (1976), 177, 3589

(72) Lion Corporation, Japan Patent, 142,710 (1985)

(73) GK Moore; GAF Roberts, Int. J. Biol. Macromol., (1980), 2, 73

(74) LF Filar; MG Wirick, *in* ref.4, Page 169

(75) J Doczi, US Patent, 2,795,579, (1957)

(76) J Noguchi; K Arato; T Komai, Kogyu Kogaku Zasshi, (1969), 72, 796

(77) JW Park; K-H Choi; KK Park, Bull. Korean Chem. Soc., (1983), 4, 68

(78) A Katchalsky; P Spitinik, J. Pol. Sci., (1947), 2, 432

(79) A Domard, Int. J. Biol. Macromol., (1987), 9, 98

(80) BD Gummow; GAF Roberts, Makromol. Chem., (1985), 186, 1245

(81) H Bundenberg de Jong, *in* Colloid Science, Krurtz (Ed), Elsevier, Amsterdam (1949), vol.2, chapters 8, 9, 11

(82) AS Michaels, Ind. Eng. Chem., (1965), 57, 32

(83) A Katchalsky, Pure Appl. Chem., (1971), 26, 327

(84) H Terayama, J. Polym. Sci (1952) 8, 2, 243

(85) S Aiba, Int. J. Biol. Macromol., (1986) 8, 173

(86) M Vincendon in Chitin in Nature and Technology, RAA Muzzarelli; C Jeuniaux; GW Gooday (eds), Plenum Press, New York, (1986), page 343

(87) M Terbojevich; C Carraro; A Cosani; E Marsano, Carbohydr. Res., (1988), 180, 73

(88) H Saito; R Tabeta; Hirano S, in ref.16, Page 71

(89) PJ Van Duin; JJ Hermans, J. Polym. Sci., (1959) 36, 295

(90) S Ya Lyubina; I.A Strelina; LA Nud'ga; EA Plisko; IN Bogatova, Vysokomol. Soyed., (1983), A25, 1467

(91) CA Kienzle-Sterzer; D Rodriguez-Sanchez; C Rha, J. Appl. Pol. Sci., (1982), 27, 4467

(92) CA Kienzle-Sterzer; D Rodrigues-Sanchez; C Rha, in Chitin in Nature and Technology, RAA Muzzarelli; C Jeuniaux; GW Gooday (eds), Plenum Press, New York, (1986) Page 338

(93) NV Pogodina; GM Pavlov; SV Bushin; AB Mel'nikov; Ye. B. Kov, Vysokomol Seyed, (1986), A28, 232

(94) M Rinaudo; A Domard, ref.2, Page 71

(95) C Rha; D Rodriguez-Sanchez; CA Kienzle-Sterzer, in Biotechnology of Marine Polysaccharides, RR Colwell; ER Pariser; AJ Sinskey (eds), Hemisphere, New York, (1985) Page 283

(96) GAF Roberts, ref.1, Page 295

(97) A Elek; RA Harte, Ind. Eng. Chem., Anal. Ed., (1936) 8, 267

(98) F Niola; N Basora; E Chornet; P.F Vidal, Carbohyrate Research, (1993) 238, 1

(99) SE Darmon; KM Rudall, Disc. Faraday Soc., (1950) 9, 251

(100) GK Moore; GAF Roberts, ref.4, Page 421

(101) M Miya; R Iwamoto; S Yoshikawa; S Mima, Int. J. Biol. Macromol., (1980) 2, 323

(102) A Baxter; M Dillon; KDA Taylor; G.A.F Roberts, Int. J. Biol. Chem (1992) 14, 3, 166

(103) M Ratajska; MH Struszczyk; S Boryniec; M.G Peter; F Loth, Polymery, (1997) 42, 9, 572

(104) S Hirano; Yamaguchi R, Biopolymers, (1976) 15, 1685

(105) KM Varum; MW Anthonsen; H Grasdalen; O Smidsrod, Carbohydrate Research, (1991) 211, 17

(106) KM Varum; MW Anthonsen; H Grasdalen; O Smidsrod, Carbohydrate Research, (1991) 211, 19

(107) RAA Muzzarelli; R Rocchetti, Carbohydrate Polymers, (1985) 5, 461

(108) SC Tan; E Khor; TK Tan; SM Wong, Talanta, (1998) 45, 713

(109) A Domard, Int. J. Biol. Macromol (1987) 9, 333

(110) GG Maghami; GAF Roberts, Makromol. Chem., (1988) 189, 2239

(111) WA Neugbauer; E Neugebauer; R Brzezinski, Carbohydrate Research (1989) 189, 363

(112) GG Maghami; GAF Roberts, Makromol. Chem., (1988) 189, 195

(113) MW Anthonsen KM Varum;; AM Hermansson; O Smidsrod; DA Bandt, Carbohydrate Polymers, (1994) 25, 13 - 23

(114) GAF Roberts; JG Domszy, Int. J. Biol. Macromol(1982) 4, 374

(115) W Wang; Ph.D. Thesis, Nottingham Trent University (1997)

(116) A Domard; Rinaudo M, Polym. Comm., (1984) 25, 55

(117) RAA Muzzarelli; C Lough; M Emanuelli, Carbohydrate Research, (1987) 164, 433

(118) ACM Wu, in ref. 47, vol. 161, page 447

(119) A Denuzière; N Yagoubi; A Baillet; D Ferrier, S.T.P. Pharma Sciences, (1995) 5, 6, 481

(120) W Wang; S Bo; S Li; W Qin, Int. J. Biol. Macromol. (1991), 13, 281

(121) MW Anthonsen; KM Varum; O Smidsrod, Carbohydrate Polymers, 1993), (22, 193

(122) M Rinaudo; M Milas; P Le Dung, Int. J. Biol. Macromol., (1993), 15, 281

(123) JW Vanderhoff, ACS Division, Organic Coatings and Plastics, Preprints, (1964), 24, 2, 223

(124) RH Ottewill; JN Shaw, Disc. Faraday Soc., (1966), 42, 154

(125) A Watillon; AM Joseph Petit, Disc. Faraday Soc., (1966), 42, 143

(126) J Visser, Adv. Colloid Interface Sci. (1972), 3, 331

(127) CC Siegloff; J Mazur, J. Colloid and Interface. Sci., (1960),15, 437

(128) RH Ottewill; JN Shaw, J. Electroanal. Chem., (1972), 37, 133

(129) A Watillion; J Stone-Masui, Electroanal. Chem., (1972), 37, 143

(130) R C Backus; R C Williams, J. Appl. Phys. (1948), 19, 1186

(131) R C Backus; R C Williams, J. Appl. Phys. (1949) 20, 224

(132) T Alfrey; JR, E B Bradford; J W Vanderhoff and G Oster, J. Opt. Soc. Am. (1954), 44, 603

(133) E B Bradford; J W Vanderhoff, J. Appl. Phys. (1955), 26, 864

(134) CM Cheng; FK Micale; JW Vanderhoff; MS ElAasser, J. Polym. Sci., Part A Polymer Chem. (1992), 30, 235

(135) E Farber, Suspension Polymerisation, *in* Encyclopaedia of Polymer Science of Technology (13), Interscience, John Wiley & Sons, New York (1920)

(136) EB Bradford; JW Vanderhoff, J. Colloid Sci., (1956), 11, 135

(137) JW Vanderhoff; JF Vitkuska; EB Bradford; T Alfrey Jr., J. Polymer Sci., (1956), 20, 225.

(138) T Matsumoto; A Ochi, Kobunshi-Kagaku, (1965), 22, 481

(139) A Kotera; K Furusawa;Y Takeda, Kolloid-Z. u. Z. Polymere, (1970), 239, 677

(140) A Kotera; K Furusawa; K Kudo, Kolloid-Z. u. Z. Polymere, (1970), 240, 837

(141) RH Ottewill; J N Shaw, Kolloid-Z. u. Z. Polymere, (1967), 218, 34

(142) JW Goodwin; J Hearn; CC Ho; RH Ottewill, BR. Polymer J., (1973), 5, 347

(143) JW Goodwin; J Hearn; CC Ho; RH Ottewill, Colloid Polymer Sci, (1974), 252, 464

(144) Y Chung-li; JW Goodwin; RH Ottewill, Prog. Colloid Polymer Sci., (1976), 60, 163

(145) JW Goodwin; RH Ottewill; R Pelton; G Vionello; DE Yates, Br. Polym. J., (1978), 10, 173

(146) AR Goodall; MC Wilkinson; J Hearn, Polymer Colloids II, RM Fitch (ed), Plenum Press, (1989), Page 629

(147) JW Vanderhoff; EB Bradford, TAPPI, (1956), 39, 650

(148) JW Vanderhoff; FJ Micale; MS El-Aasser, "Production of Large-Particle-Size Monodisperse Latexes", proposal submitted in response to NASA A.O. No. OA-77-3, "Space Processing Investigation for STS Missions" April 1977

(149) JW Vanderhoff, Dow Chemical Co. (1959 – 1963) Unpublished Research

(150) E Trommsdorff; CE Schildknecht, *in* "Polmer Processes", CE Schildknecht (ed), Interscience, New York, (1956) ChIII

(151) FH Winslow; W Matareyek, Ind. Eng. Chem., (1951), 43, 1108

(152) E Vanzo, J. Appl. Polymer Sci., (1972), 16, 1867

(153) Y Almog; M Levy, J. Polymer. Sci. Polymer Chem. Ed., (1980), 18, 1

(154) Y Almog; M Levy, J. Polymer. Sci. Polymer Chem. Ed., (1981), 19, 115

(155) Y Almog; M Levy, J. Polymer. Sci. Polymer Chem. Ed., (1982), 20, 417

(156) Y Almog; M Levy, Ind. Eng. Chem. Pro. Res. Dev., (1982), 21, 163

(157) J Ugelstad, Makromol. Chem., (1978), 179, 815

(158) J Ugelstad; KH Kaggerud; FK Hansen; A Berge, Makromol. Chem., (1979), 180, 737

(159) J Ugelstad; PC Mork; KH Kaggerud; T Ellington; A Berge, Adv. Coll. Int. Sci., (1980), 13, 101

(160) J Ugelstad; KH Kaggerud; RM Fitch, *in* Polymer Colloids II, RM Fitch (ed), Plenum Press, New York, (1980), Page 83

(161) MC Wilkinson; J Hearn; PA Steward, Adv. In Colloid and Interface Sci., (1999), 81, 77

(162) WT McCarvell; RM Fitch, J. Colloid Interface Sci., (1978), 64, (3), 403

(163) SF Chen, PhD thesis, Bristol, England, (1974)

(164) IH Harding; TW Healy, J. Colloid Interface Sci., (1982), 89, (1), 185

(165) AR Goodall; J Hearn; MC Wilkinson, J. Polym. Sci. Polym. Chem. Ed., (1979), 17, 1019

(166) DH Everett; ME Gultepe; MC Wilkinson, J. Colloid Interface Sci., (1979), 71, (2), 336

(167) MA Barrett; DH Everett; ME Gultepe, *in* Polymer Colloids II, RM Fitch (ed), Plenum Press, New York, (1980), Page 313

(168) J Hearn; MC Wilkinson; ME Gultepe; P Cope, *in* Polymer Colloids II, RM Fitch (ed), Plenum Press, New York, (1980), Page 379

(169) AA Kamel; MS El-Aasser; JW Vanderhoff, J. Colloid Interface Sci., (1982), 87, (2), 537

(170) SM Ahmed; MS El-Aasser; GH Powli; GW Poehlein; JW Vanderhoff, J. Colloid Interface Sci., (1980), 73, (2), 388

(171) MC Wilkinson; J Hearn; P Cope; M Chainey; Br. Polym. J., (1981), 13, 82

(172) Y Chonde; IM Krieger, J. Colloid Interface Sci., (1980), 77, (1), 138

(173) ME Labib; AA Robertson, J. Colloid Interface Sci., (1978), 67, (3), 543

(174) J Zahka; L Min, Chem. Eng. Prog., (Decenber 1977), 53

(175) M Chainey, Unpublished Results, (1981)

(176) J Hearn; MC Wilkinson; AR Goodall, Adv. Colloid Interface Sci., (1981), 14, 173

(177) AR Goodall; MC Wilkinson; J Hearn; P Cope, Br. Polym. J., (1978), 10, 205

(178) MC Wilkinson; R Sherwood; J Hearn; AR Goodall, Br. Polym. J., (1979), 11, 1

(179) MS El-Aasser, NATO ASI Ser., 65 (Sci. Technol. Polym. Colloids), (1983), SER E, 442

(180) DH Everett; ME Gultepe, Surface Characterisation of Emulsifier Free Polystyrene Latices by Conductometric Titration in the presence of Electrolyte, NATO ASI, Trondheim, Norway, (1975)

(181) JW Vanderhoff; HF Van Den Hull; RJM Tausk; JTHG Overbeek, *in* Clean Surfaces; Their Preparation and Characterisation for Interfacial Studies, G Goldfinger (ed), Marcel Dekker, New York, (1970)

(182) DE Yates; RH Ottewill; JW Goodwin, J. Colloid Interface Sci., (1977), 62, (2), 356

(183) HR Kruyt (ed), Colloid Science, Elsevier Press, New York, (1952), vol.1, 68

(184) J Hearn; RH Ottewill; JN Shaw, Br. Polym. J., (1970), 2, 116

(185) LS Su; S Jayasurya; RM Fitch, Polym. Int., (1993), 30, (2), 221

(186) JS Rutt, J. Polym. Sci., Part A Polym. Chem., (1994), 32, 777

(187) MC Davies, RAP Lynn; SS Davies; J Hearn; FF Watts; JC Vickerman; D Johnson, J. Colloid Interface Sci., (1993), 156, (1), 229

(188) M Antonietti; L Vorwerg, Colloid and Polym. Sci., (1997), 275, (9), 883

(189) HF Van Den Hull; JW Vanderhoff, J. Colloid Interface Sci., (1969), 28, (2), 336

(190) JW Vanderhoff, Morphology in Emulsion Polymers, Pro. Water Bourne and High Solids Coating Symp., University Southern Mississippi, (1976), Page 1

(191) JW Vanderhoff, *in* Characterisation of Metal and Polymer Surfaces, LH Lee (ed), Academic Press, New York, (1977), vol 2, 365

(192) SM Ahmed; MS El-Aasser; FJ Micale; GW Poehlein; JW Vanderhoff, *in* Solution Chemistry of Surfactants, KL Mittal (ed), Plenum Press, New York, (1979), vol2, 853

(193) GD McCann; EB Bradford; HJ Van den Hull; JW Vanderhoff, *in* Polymer Colloids, RM Fitch (ed), Plenum Press, New York, (1971), Page 29

(194) GD McCann; EB Bradford; HJ Van den Hull; JW Vanderhoff, J. Colloid Interface Sci., (1971), 36, (1), 159

(195) WC Wu; MS El-Aasser; FJ Micale; JW Vanderhoff, *in* Emulsions, Latices and Dispersions, P Becher; MN Yudenfreund (eds), Marcel Dekker, New York, (1978) Page 71

(196) AA Kamel; MS El-Aasser; JW Vanderhoff, J. Dispersion Sci. Technol., (1981) 2 (2 and 3), 183

(197) JW Vanderhoff; HJ Van den Hull, J. Macromol. Sci. Chem., (1973), A7, (3), 677

(198) JW Vanderhoff, Pure & Appl. Chem., (1980), 52, 1263

(199) JW Vanderhoff, Proc. 4th Int. Conf. Organic Coatings Sci. and Technology, Athens, (1978), 447

(200) HJ Van den Hull; JW Vanderhoff, *in* Polymer Colloids, RM Fitch (ed), Plenum Press, New York, (1971), Page 1

(201) JH Schenkel; JA Kitchener, Nature, (1958), 182, 131

(202) RH Ottewill, Private Communication, (1980)

(203) FJ Delasnieves; ES Daniels; MS El-Aasser, Colloids and Surfaces, (1991), 60, 107

(204) MS El-Aasser; SM Ahmed; GW Poehlein; JW Vanderhoff; X Rovira; JI Tabernero; P De La Moremna, *in* Polymer Colloids II, RM Fitch (ed), Plenum Press, New York, (1980), Page 361

(205) P Bagchi; BV Gray; SM Birnbaum, J. Colloid Interface Sci., (1979), 63, (3), 502

(206) HJ Van den Hull; JW Vanderhoff, Desorption of Emulsifiers from Polystyrene Latexes, Proc Vth Int. Congress on Surface Active Substances, Barcelona, (1968), Sect. BII, 31

(207) S Nishida; MS El-Aasser; A Klein; JW Vanderhoff, in Emulsion Polymers and Emulsion Polymerisation, DR Bassett; AE Hamielec (eds), ASC Symp. Series No. 165, Washington DC, (1981), Page 291

(208) BR Paulke; PM Moglich; A Budde; R Nitzsche; RH Muller, Langmuir, (1995), 11, (1), 70

(209) HR Dicke; W Heitz, Colloid Polym. Sci., (1982), 260, 3

(210) JC Brodnyan; EL Kelley, J. Polym. Sci., Part C, (1969), (No,27), 263

(211) BW Greene, J. Colloid Interface Sci., (1973), 43, (2), 449

(212) DA House, Chem. Rev., (1962), 62, 185

(213) SR Palit, Pure Appl. Chem., (1962), 4, 451

(214) SR Palit, Chemistry & Industry, (1960), Page 1531

(215) G Roy; BM Mandel; SR Palit, in Polymer Colloids, , RM Fitch (ed), Plenum Press, New York, (1971)

(216) SR Palit; GK Saxena, Nature, (1966), 209, 1127

(217) SR Palit; P Ghosh, (1962), 58, 1225

(218) SR Palit, Anal. Chem., (1961), 33, 1441

(219) SH Maron; ME Elder, J. Colloid Interface Sci., (1963), 18, 199

(220) PE Pierce; SH Maron, J. Colloid Interface Sci., (1964), 19, 658

(221) P Conner; RH Ottewill; J. Colloid Interface Sci., (1971), 37, 642

(222) JN Shaw; MC Marshall, J. Polym. Sci., 91968), (A1), 6, 449

(223) HJ van den Hull; JW Vanderhoff, Br. Polym. J., (1970), 2, 121

(224) JN Shaw, J. Polym. Sci., (1969), Part C, 27, 237

(225) J Laaksonen; JC Bell; P Stenious, J. Electroanal. Chem., (1975), 64, 207

(226) DE Yates, NATO ASI Polymer Colloids, Norway, (1975)

(227) EB Bradford; JW Vanderhoff, J. Polym. Sci., (1963), C3, 41

(228) JThG Overbeek, in Colloid Science, HR Kruyt (ed), (1951), vol. 1, Page 240

(229) SA Rice; M Nagasawa, Polyelectrolyte Solutions, Academic Press, (1961)

(230) F Oosawa, Polyelectrolytes, Dekker, New York, (1971)

(231) AR Goodall, PhD Thesis, C.N.A.A., (1976)

(232) AR Goodall; J Hearn; MC Wilkinson, Br. Polym. J.,(1978), 10, 141

(233) HTS Briton, Conductometric Analysis, Chapman & Hall, London, (1934), Page 78

(234) HTS Briton, Conductometric Analysis, Chapman & Hall, London, (1934), Page 60

(235) RO James; JA Davis; JO Leckie, J. Colloid Interface Sci., (1978), 65, (2), 331

(236) J Stone-Masui; A Watillion, J. Colloid Interface Sci., (1975), 52, 429

(237) LG Sillen, Warnquist Arkiv Kev, (1968), 31, 315, 341

(238) LT Weng; P Bertrand; JH Stone-Masui, Surface Interface Anal., (1994), 21, 387

(239) M Chainey; MC Wilkinson; J Hearn, J. Colloid Interface Sci., (1987), 117, 477

(240) JE Seeburgh; JC Berg, Colloids Surf. A. Physicochem. Eng. Aspects, (1995), 100, 139

(241) D Bastos-Gonzalez; R Hidalgo-Alvarez; FJ De Las Nieves, J. Colloid Interface Sci., (1996), 177, 372

(242) BJ Marlow; RL Rowell, Langmuir, (1991), 7, 2970

(243) J Zhao; W Brown, Langmuir, (1996), 12, 1141

(244) RH Ottewill, *in* An Introduction to Polymer Colloids, F Candau; RH Ottewill (Eds), Kluwer Academic Publishers, Netherlands (1990)

(245) EJW Verwey; JThG Overbeek, Theory of the Stability of Lyophobic Colloids, Elsevier, Amsterdam, (1948)

(246) RW O'Brien; LR White, J. Chem. Soc. Faraday Trans. II, (1978), 74, 1607

(247) RJ Hunter, Zeta Potential in Colloid Science, Academic press, London, (1981)

(248) JN Israelachvili, Intermolecular and Surface Forces, Academic Press, London, (1985)

(249) SD Lubetkin; SR Middleton; RH Ottewill, Phil. Trans. R. Soc. London, (1984), A311, 353

(250) S Tolansky, Multiple Beam Interferometry of Surfaces and Films, Oxford University Press, Oxford, (1948)

(251) JS Lyons; DN Fulong; TW Healy, Aust. J. Chem., (1981), 34, 1177

(252) H Reerink; JThG Overbeek, Discuss. Faraday Soc., (1954), 18, 74

(253) RH Ottewill; I Piirma, Emulsion Polymerisation, Academic Press Inc., (1982)

(254) E Dickinson; L Eriksson, Adv. Colloid and Interface Sci., (1991), 34, 1

(255) J Lyklema, in Proceedings of the NATO Advanced Study Institute on The Scientific Basis of Flocculation, Cambridge, UK, (1977) Page3

(256) AA Bibeau; E Matejevic, J. Colloid and Interface Sci. (1973),43, 330

(257) J Gregory, in ref.136, Page101

(258) MJ Vold, J. Colloid and Interface Sci (1961),16, 1

(259) DWJ Osmond; B Vincent; FA Waite, J. Colloid and Interface Sci (1973),42, 262

(260) DH Napper, J. Colloid and Interface Sci (1977), 58, 390

(261) R Evans; JB Smitham; DH Napper, Colloid and Polymer Science (1977), 255, 161

(262) A Doroszkowski; R Lambourne, J. Colloid and Interface Sci., (1973), 43, 97

(263) DH Napper, J. Colloid and Interface Sci., (1973), 45, 557

(264) RH Ottewill; T Walker, JCS Faraday I, (1973), 70, 917

(265) VK La Mer, Disc. Faraday. Soc., (1966),42, 248

(266) WP Shyluk; FS Stow, J. Appl. Polym. Sci., (1969), 13, 1023

(267) DH Napper, Polymeric Stabilization of Colloidal Dispersions, Academic Press, London (1983)

(268) B Vincent, Adv. Colloid and Interface Sci., (1974), 4, 193

(269) J Gregory, J. Colloid and Interface Sci., (1973), 42 (2), 448

(270) J Gregory, J. Colloid and Interface Sci., (1976), 55 (1), 35

(271) DR Kasper, Ph.D. Thesis, California Institute of Technology, (1971)

(272) DH Napper, in The Effect of Polymers on Dispersion Properties, ThF Thadros (ed), Academic Press, London (1982)

(273) RA Ruehrwein; DW Ward, Soil Science, (1952), 73, 485

(274) AS Michaels, Ind.Eng.Chem., (1954), 46, 1485

(275) JA Kitchener, British Polym. J., (1972), 4, 217

(276) GJ Fleer, Thesis, Agricultural University, Wageningen (1971)

(277) S Sandell; P Luner, J. App. Polym. Sci., (1974),18, 2075

(278) N Sarker; NS Teot, J. Colloid and Interface Sci., (1973), 43, 370

(279) VK LaMer, J. Colloid and Interface Sci., (1964), 19, 291

(280) DH Napper; RJ Hunter; *in* M.T.I. Review of Science, Physical Chemistry, Surface Chemistry and Colloids, M Kerker (ed), Ser.1, Vol.7, Butterworths, London, (1972)

(281) WP Schyluk; RW Smith, J. Polym. Sci., Part A2(1969), 7, 27

(282) BA Matthews; CT Rhodes, J. Pharm. Sci. (1968), 574, 557

(283) BA Matthews; CT Rhodes, J. Colloid and Interface Sci., (1970), 32, 339

(284) DJ Shaw, Introduction to Colloid and Surface Chemistry, 4th Edition, Butterworth-Heinmann, (1992) Page 54

(285) J Gregory, NATO Advanced Workshop on Nanoparticles in Solids and Solutions, Szeged, Hungary, March (1996)

(286) FA Uriarte, Thesis, Univ. Carnegie Mellon, Diss. Abstr., (1971), 32, 1541

(287) DJ Shaw, ref.166, Page 61

(288) Malvern, Zetasizer III reference manual

(289) G Bolle; C Cametti; P Codastefano; P Tartaglia, Phys. Rev., A., (1987), 35, 837

(290) TM Herrington; BR Midmore, J. Chem. Soc., Faraday Trans. I, (1989), 85, 3529

(291) Z Zhou; P Wu; B Chu, J. Colloid and Interface. Sci., (1991), 146, 541

(292) TM Herrington; BR Midmore, Colloids and Surfaces A, (1993), 70, 199

(293) VK La Mer; TW Healy, Rev. Pure Appl. Chem., (1963), 13, 112

(294) VK La Mer; RH Smellie; PK Lee, J. Colloid Sci., (1957), 12, 506

(295) ID Ratee; MM Breuer, The Physical Chemistry of Dyes, Academic Press, London, (1974)

(296) GG Allen; GD Crosby; KV Sarkanen, Int. Paper Phys. Conf., (1975), 109

(297) JG Domszy; GK Moore; GAF Roberts, *in* Cellulose and its Derivatives JF Kennedy; GO Phillips; DJ Wedlock; PA Williams (eds), Ellis Horwood, Chichester, (1985), Page 463

(298) JA Rippon, J. Soc. Dyers Colourists, (1984), 100, 298

(299) JG Domszy; Roberts GAF, *in* Chitin in Nature and Technology, RAA Muzzarelli; C Jeuniaux; GW Gooday (eds), Plenum Press, NewYork, (1986), Page 331

(300) A Domard; M Rinaudo; C Terrassin, J. Applied Polym. Sci., (1989), 38, 1799

(301) Per M Claesson; BW Ninham, Langmuir, (1992), 8, 1406

(302) WA Bough, Poultry Sci., (1975), 54, 612

(303) WA Bough; DR Landes, J. Dairy Sci., (1976), 59, 1874

(304) Allied Colloids, Personal Communication

(305) S Kawamura, J.American Water Works Association, (1991), 83, (10,) 88

(306) Y Zhuo; H Liu; S Du; W Zhang; G Zhuang, Wuli Huaxue Xuebao, (1993), 9, (1), 77

(307) C Huang; Y Chen, J.Chem.Tech.Biotechnol., (1996), 66, 227

(308) S Dermarger-Andre; A Domard, Carbohydrate Polymers, (1993), 22, 117

(309) S Dermarger-Andre; A Domard, Carbohydrate Polymers, (1994), 24, 177

(310) A Domard; S Dermarger-Andre, Macromolecular Reports, (1994), A31, (Suppls. 6&7), 849

(311) LA Tsar'kova; LI Lopatina, Colloid J., (1998), 60, (5), 644

(312) BD Gummow; GAF Roberts, Makromol. Chem.,(1986), 187, 99

(313) J Gregory; I Sheiham, Br. Polym. J. (1974), 6, 47

(314) WH Coulter, Proc. Natl. Electron. Conf., (1956), 12, 1034

(315) Coulter Electronics Ltd, Fine Particle Application Notes for Coulter Instruments, Issue E, (1988)

(316) BV Miller; RW Lines, CRC Critical Reviews in Analytical Chemistry, (1988), 20, (2), 75

(317) T Allen, *in* Particle Size Analysis, Proc. 1st Conf. On Particle Size Analysis, Society for Analytical Chemistry, London, (1967)

(318) T Allen, Particle Size Measurement, 3rd Edition, Powder Technology Series, Chapman & hall, London, (1981)

(319) CFT Mattern; FS Bracket; BJ Olson, J. Appl. Physiol, (1957), 10, 50

(320) G Pfieffer, Z. Med. Labortechnik, (1962), 3, 2, 5, 57

(321) LH Princen; WF Kwolek, Rev. Scient. Instrum., (1965), 36, 646

(322) JF Pisani; GM Thomson, J. Phys. E., (1971), 4, 359

(323) NB Grover; J Naaman; S Ben-Sasson F Doljanski; E Nadav, Biophys. J., (1969), 9, 1398, 1415

(324) DA Elkington; R Wilson, *in* Particle Size Analysis 1985, PJ Lloyd (ed), Wiley, Chichester, England, (1987)

(325) JG Harfield, Current Awareness in Particle Technology, (1987), 20, 211

(326) JG Harfield; RA Wharton, Part. Part. Syst. Charact., (1988), 5, 29

(327) Coulter Electronics Ltd., Reference Manual for the Coulter Multisizer, Issue J, (1990)

(328) Coulter Electronics Ltd., Operators Handbook for the Coulter Multisizer, Issue E, (1989)

(329) MC Wilkinson; J Hearn; FH Karpowicz; M Chainey, Particulate Science and Technology, (1987), 5, 65

(330) M Smoluchowski, Z. Physik Chem., (1917), 92, 129

(331) B A Matthews; CT Rhodes, J. Colloid Interface Sci., (1968), 28, 71

(332) Rank Bros. Mk II Particle Micro-Electrophoresis manual.

(333) LJ Poiseulle, Comptes Rendus (1840), 11, 961

(334) Coulter Delsa Manual

(335) DC Henry, Proc. Royal Soc., (1931), A133, 106

(335) MC Wilkinson; J Hearn; F Karpowicz; M Chainey, Particle Characterisation 3, (1986), 56

(337) PH Wiersema; AL Loeb; JThG Overbeek, J. Colloid Interface Sci., (1966), 22, 78

(338) J Gregory, Trans. Faraday Soc., (1969), 65, 2260

(339) W Heller, Pure Appl. Chem., (1966), 12, 249

(340) GAF Roberts, Personal Communication

(341) V Shubin; Y Samoshina; A Menshikova; T Evseeva, Colloid Polym. Sci., (1997), 134, 217

(342) Shinoda Nakajima, Bull. Inst. Chem. Res. Kyoto Univ. 53(1975)392

(343) GA Johnson; SMA Lecchini; EG Smith; J Clifford; BA Pethica, Disc. Faraday Soc., (1966), 42, 120

(344) Y Adachi; MA Cohen-Stuart; R Fokkink, J. Colloid Interface Sci., (1994), 165, 310

(345) J Gregory, *in* The Effect of Polymers on Dispersion Properties, Th F Thadros (ed), Academic Press (1982), page 301

(346) J Gregory, Trans. Faraday Soc., (1969), 65, 2260

(347) R Buscall, in Polymer Colloids, R Buscall; T Corner; JF Stageman (eds), Elsevier Applied Science, London (1985), page 197

(348) RJ Gibbs, J. Sediment. Petrol., (1982), 52(2), 657

(349) WI Higuchi; R Okada; GA Stelter; PA Lemberger, J. Pharm. Sci., (1963), 52, 49

(350) DL Smith; SK Friedlander, J. Colloid Interface Sci., (1964), 19, 621

(351) JWTh Lichtenbelt; HJMC Ras; PH Wiersema, J. Colloid Interface Sci., (1974), 46, 522

(352) JWTh Lichtenbelt; C Patmanoharan; PH Wiersema, J. Colloid Interface Sci., (1974), 49, 281

(353) DH Everett, ME Gultepe, MC Wilkinson, J. Colloid Interface Sci., (1997), 71, 336

(354) A Pinotti; A Bevilacqua; N Zaritzky, J. Food Eng., (1997), 32, 69